CARDE TECHNICAL LETTER No. 1091/58

Copy No. 35

FIFTH PROGRESS REPORT

on

CF-105 WEAPON SYSTEM ASSESSMENT

Compiled by

R.S. Mitchell and C.J. Wilson

CANADIAN ARMAMENT RESEARCH AND DEVELOPMENT ESTABLISHMENT

Valcartier, Quebec

January, 1958

58-01988

#298448

Technical Letter No. 1091
P.C.C. No. D46-9736-21

PROJECT
CF-105 ASSESSMENT

FIFTH PROGRESS REPORT

Period 1 Aug. 57 to 31 Dec. 57

Compiled by

R.S. Mitchell &
C.J. Wilson

CANADIAN ARMAMENT RESEARCH AND DEVELOPMENT ESTABLISHMENT
VALCARTIER, QUE.

Enclosure (1) to CNO Serial 004955 P92

January 1958

6517005-01

SUMMARY

This technical letter is a progress report on work being done at C.A.R.D.E. in connection with the CF-105 Weapon System Assessment, recording work done in the period August to December 1957.

The main work of this period has been the completion of REAC placement charts for three dimensional attacks. The raw data is given herein. Effort has been directed to methods of homing when the A.I. is jammed. Preliminary results are given herein. The remaining data on these investigations will be given in the next progress report.

A final report on the complete study is in the planning stage.

TABLE OF CONTENTS

FIFTH PROGRESS REPORT

on

CF 105 WEAPON SYSTEM ASSESSMENT

---

1. INTRODUCTION

The engagement of high speed targets by supersonic interceptors armed with air-to-air missiles introduces a variety of new problems which cannot be assessed by extrapolation of data arising from experience with conventionally armed subsonic aircraft.

For this reason, CARDE has been requested by the RCAF to carry out an evaluation study of the effectiveness of a supersonic interceptor weapon system based on the AVRO CF-105 aircraft armed with Sparrow II or Sparrow III air-to-air missiles.

The primary objectives of the study as stated by the RCAF are:

(i) To evaluate the combat effectiveness of the system with different types of armament, beginning with the Sparrow series, for probable bomber threats including the Bison, Badger and Bear.

(ii) To investigate the effect of variation in fire control parameters such as A.I. radar range and look angle.

(iii) To establish the minimum acceptable level of aerodynamic performance and to investigate the effect of possible design changes in the aircraft and engine parameters, insofar as these changes affect combat performance.

(iv) To determine the effect of variations in G.C.I. placement accuracy.

(v) To explore possible tactics and suggest optimum modes of attack.

In order to arrive at an accurate assessment of the overall combat effectiveness of this weapon system, the many inter-dependent sub-systems of which it is composed require analysis, first individually and then collectively, so that the relative importance of the principal parameters can be established. Naturally, an exploratory study of this nature is quite involved and certainly time-consuming, if it is to be sufficiently exhaustive to achieve the above-stated objectives. Further, the task is rendered difficult in that very little primary information is available on which to base investigations, as it is evident that the establishment of such data is perhaps the primary object of the study.

The general approach then has been to adopt a range of parameters which should encompass final characteristics, then to conduct an analysis based on these and thus establish their validity and importance in the particular sub-system, as well as their influence on the effectiveness of the system as a whole. In this way overall effectiveness can be established as a function of the parameters of individual sub-systems and optimum design values indicated.

Although this method is elongated and somewhat tedious, an important compensatory feature lies in the fact that the most critical areas requiring further study are highlighted.

2. PROGRESS OF STUDY

CARDE Technical Letter N-47-3, May 1956, gives a review of the general interceptor-weapon problem with particular reference to the proposed CF-105 system, and sets out in some detail a proposal for the prosecution of studies to attain the objectives enumerated by the RCAF. Progress of the work is detailed in CARDE Technical Letters N-47-8, N-47-12, N-47-18, and 1012/57. A digest of the first year's results is contained in CARDE Technical Memorandum 150/57.

The work to date on the second year's portion is mainly concentrated on three-dimensional problems, fire control and ECM considerations and missile lethality. The main body of the raw data of this phase of the work is contained in this report. One more progress report will give the remaining data on a few specialized problems which are presently in progress. A summary report on the whole study is to be written; work on the first draft is to start immediately.

3. EFFORT ALLOTTED TO THE STUDY

The work is being carried out by specialist sections within the Wings of CARDE, under the coordination and direction of the Systems Group, which is generally responsible for the task.

During the period under review, a total of ten professional personnel have been engaged in the programme. The degree of participation including contractors' personnel was as follows:-

	Full Time	Part Time
Systems Group	1	3
"B" Wing	0	1
"C" Wing	0	2
"G" Wing	8	1
TOTAL	9	7

The total complement of contractors' personnel was available by September. This number will diminish beginning 1 January and, under present plans, all contractors will be released by 1 April.

4. ACTIVITIES - August - December 1957

4.1 General

The main activity of the quarter under review has been the completion of the basic three-dimensional placement work and concentration on minimum information studies relating to the A.I. phase under ECM conditions. Work on missile lethality has also progressed.

4.2 Placement Studies

The basic three-dimensional placement studies as outlined on pages 14 and 15 of CARDE Technical Letter 1012/57 have been completed. This work surveyed the kinematic aspects of placement and fire control modes. The basic results are given in Appendix "A". Work on analysis of these results is in progress and will appear in the final summary report of the project.

4.3 Fire Control

The fire control problem was detailed in Appendix "P", page 39, of Technical Letter 1012/57. Herein some 10 or 12 topics were

summarized. The main effort has been placed on the minimum information studies, which are essentially concerned with homing and ranging under ECM. These investigations are reported in Appendices "B" and "C". Appendices "E" and "U" deal with other topics in the fire control studies. The remaining problems are either under study or awaiting further REAC work.

4.4 Missile Studies

The main effort in the missile field was concentrated on an extended visit to Douglas Aircraft Company to review the existing simulation results that were available in the field. This trip is summarized in Appendix "D". A detailed visit report is presently being written. Because of reduction in staff, and also in the light of the information obtained from Douglas, it is not thought advisable to embark on an extended missile study at present. It would seem that the most profitable information in this area will come from a combination of trial results and simulator studies in connection with the C.E.P.E. evaluation programme.

4.5 Lethality

The engagement simulator has been placed in operation and some three to four months work has been done on the geometrical aspects of the impact phase. A range of approach trajectories for the Sparrow missile vs the Bear has been studied. Hit patterns for fragmenting and continuous rod warheads have been determined for more than 3000 burst points.

4.6 E.C.M.

The main work on ECM has been in connection with the minimum information studies of the fire control programme. These are outlined in Appendices "B" and "C". A visit on this subject was made to RCA in connection with Project End Run. A report on this visit is given in Appendix "K".

4.7 Long Range Rockets

A visit to RCA was made on this subject. It is not thought that extensive analysis will be needed in this area; however, information has been obtained both from RCA and from the Explosives Physics Section at CARDE, and will be reported on under separate cover with the final report.

4.8 Low Altitude

No work has been done on this problem.

4.9 I.R.

The tactical studies under way on minimum information are applicable to the I.R. situation as well as the radar, ECM situation. (See Appendix "B".)

The technical characteristics of the I.R. system have been discussed with RCA, the RCAF and the I.R. group of "G" Wing.

4.10 Information Sources

Outside contact has been with RCA, Waltham, Douglas Aircraft Company, and AVRO Aircraft. The highlights of these liaison visits are given in Appendices "K", "D", and "F".

5. PRESENT INDICATIONS

Apart from scattered comments given in the Appendices on trends, no detailed analysis is at present available. Work in this area is in progress, and it is hoped that an overall picture can be given in the final report.

APPENDIX 'A'

RESULTS OF THE THREE-DIMENSIONAL PLACEMENT STUDY

by C.J. Wilson

1.0 INTRODUCTION

The programme scheduled for the three-dimensional placement study has been completed. The capability of the CF-105 interceptor against high altitude targets has been studied when the approach is made with an altitude disadvantage.

This appendix contains a resume of the analogue computer method used and those results of the work which have not been published previously. Combined-plane and snap-up attacks have both been studied and comparison of the results is now possible.

Placement diagrams showing the allowable placement zones under various conditions are reproduced here, together with placement probability curves for values of A.I. radar range and G.C.I. accuracy which might occur with the CF-105 system.

2.0 METHOD

Attacks by individual interceptors against single high-flying, high-speed targets have been considered during the phase between detection of the target by the A.I. radar and firing of the missile. During this phase the interceptor is under the control of its own radar and fire control system. An analogue computer simulation of this part of the attack has been made; some descriptions of this work have already appeared in previous progress reports (Ref. 1, 2, 3 and 4) and a complete descriptionof the equations assumed and the computer circuit diagrams is now being prepared (Ref. 7). For convenience, however, the more important details of the work are reviewed here. Figure A-0 is a block diagram of the system simulated; the component blocks are described under the sub-headings below.

2.1 Geometry

The interceptor's position and velocity were specified in target coordinates; that is to say, they were measured relative to the target. Only simple target motions were considered, so that, fortunately, there was a simple relation between target coordinates and space coordinates.

2.2 Target

The target was assumed to fly at constant speed at constant altitude. The manoeuvring target was assumed to begin a circular turn from its initial bearing when A.I. contact was made; that is, at the same time as the interceptor began to manoeuvre into a launch position. This turn was maintained until either the interceptor was behind the target or the attack was completed.

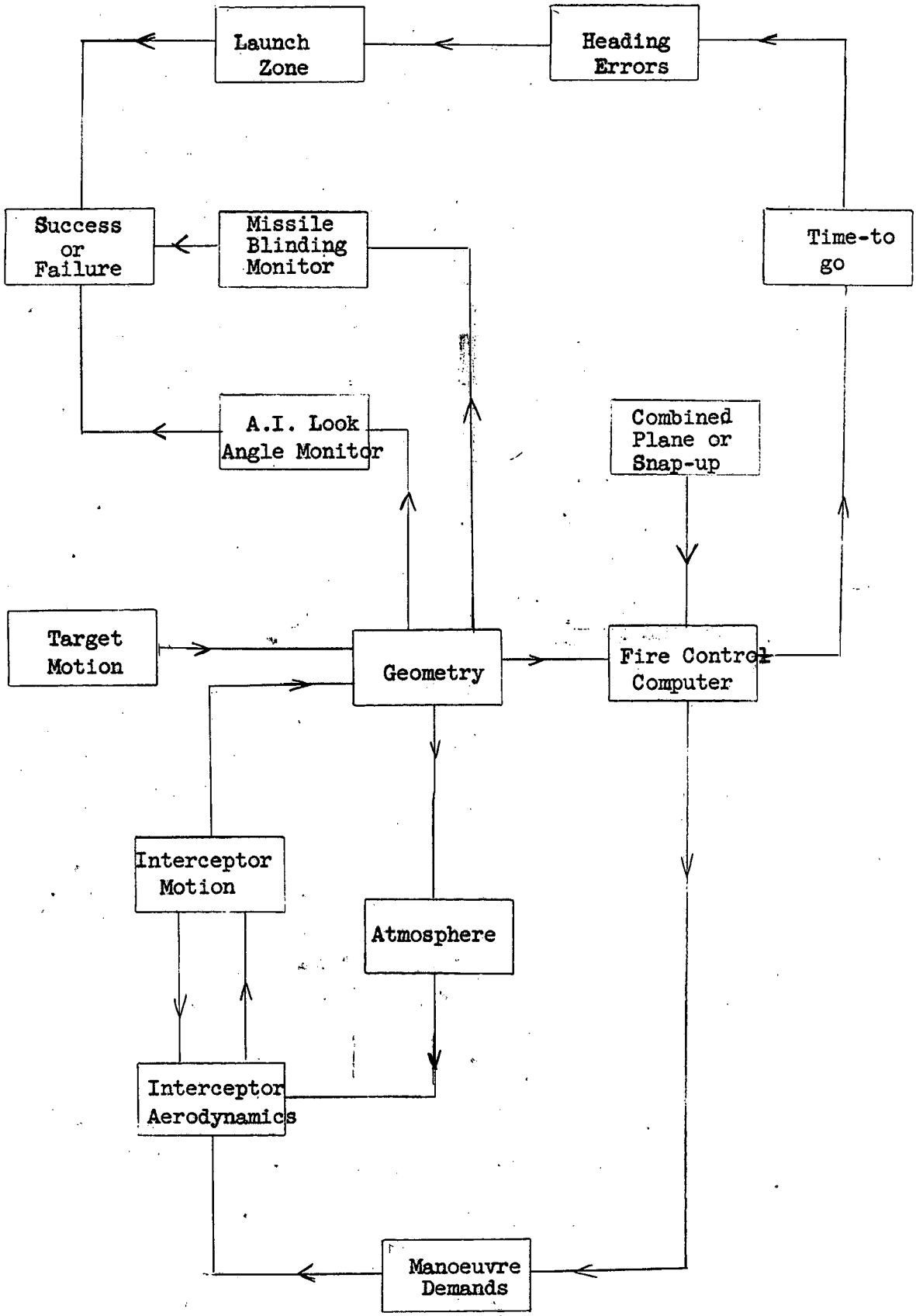

Figure A-0 Block Diagram

2.3 Interceptor Aerodynamics

Performance estimates for the CF-105 with Iroquois engines (Ref. 5 and 6) were used as the basis of the simulation, thrust, drag and aerodynamic lift limits being represented as functions of altitude, Mach number and load factor. The thrust estimate used included the improvement in engine performance at high Mach numbers due to compressor rematching. Consequently the interceptor model accelerated or decelerated according to the balance between thrust and drag as the real aircraft will. Maximum throttle setting with full afterburning was assumed throughout the attacks except where the interceptor would have accelerated beyond Mach 2.0. A Mach number upper limit of 2.0 was used in this work.

An arbitrary upper limit to load factor of 4.0 g's was imposed even when the aerodynamic limits would allow tighter manoeuvres. When the aerodynamic limit (a function of speed and altitude) was below 4.0 g's it was the dominating factor, of course.

Attacks were regarded as failures if the interceptor's Mach number fell below 1.2. This arbitrary limit must be considered in relation to the high target speeds used (not less than Mach 1.5) and the decreased capability of the CF-105 at high altitudes and low Mach numbers.

The dynamic behaviour of the interceptor was not represented. That is to say, the assumption was made that there would be an immediate manoeuvre to correct any heading errors indicated by the fire control computer without delays for such things as pilot reaction, time to roll and pitch time constant.

2.4 The Fire Control System

Lead collision steering was used with constants chosen to be compatible with the missile characteristics assumed. Conversion to lead pursuit within the launch zone or any similar procedure was not necessary in the computer model because of the launch zone conditions used.

Combined-plane attacks were compared with snap-up attacks in those cases where the interceptor has an initial altitude disadvantage. In the former mode a lead-collision course in three-dimensions was established as early as possible and, if possible, followed up to the missile launch point. In the snap-up mode the interceptor corrected horizontal errors at constant altitude, ignoring any vertical error, until the last allowable moment when the snap-up occurred to correct this error. Snap-up was mechanised by isolating the vertical error from the steering controls until a given time-to-go, chosen as a function of target altitude and of altitude difference.

Time delays in the radar system and fire control computer were neglected in the simulation. Components of heading error in azimuth and elevation were computed immediately from the geometry and it was assumed that the aircraft will turn towards a lead-collision course at a rate proportional to the errors. Since aerodynamic delays were also neglected the interceptor in the simulation responded immediately to any geometrical errors.

Neglecting all time delays in the system made it possible to ensure that the control loop was stable without great difficulty. Stabilisation of the control loop in the real interceptor system is a practical problem of profound importance, but it was assumed that this problem will be solved. The object of the present work was to determine the effectiveness of the system with a stable control loop. With all time delays neglected it was possible to use a value of loop gain higher than any which could be used in practice. In this work a value of 4 degrees per second per degree of heading error has been used, in practice 2 degrees per second per degree may be the highest allowable.

It has been stated above that the simulated interceptor turned at a rate proportional to the errors. This was true only when the errors were small; when the errors were large the interceptor turned in the right direction at maximum permitted load factor.

2.5 Look Angle Limits

The azimuth and elevation gimbal deflections of the AI and missile antennae were determined continuously throughout interceptions. The attitude of the interceptor, its roll position and angle of attack were all taken into account. The actual deflections were compared with the maximum allowable A.I. antenna deflections to determine any loss of target by the interceptor's radar and with the allowable missile antenna deflections, including limitations due to airframe screening, to determine any missile blinding. Failure was assumed to result from loss of the target by the A.I. at any point of the attack and also from missile blinding at the time of launch.

2.6 Missile Launch Conditions

Complete representation of the missile launch zones proved to be impossible because of incomplete information and shortage of analogue computing equipment. However, simple launch zone assumptions were used in this work and tests made to confirm that the placement diagrams obtained do not differ substantially from those which would be obtained with more complete representation of launch zones. These tests have shown that it is more important for the fire-control and missile models assumed to be completely compatible than for either to be an exact representation of the real system in every way.

The missile model assumed for this study had better high altitude characteristics than the present Sparrow II. The following relationship between launch altitude and allowable heading error was used:

Altitude of Launch	Allowable Heading Error
40,000 ft.	23°
50,000 ft.	14°
60,000 ft.	8°
70,000 ft.	5°

and it has been assumed that these figures are independent of interceptor speed and of aspect at launch and of target altitude. These figures may not be too optimistic for coaltitude attacks, but they are certainly optimistic for attacks against 70,000 ft. and 80,000 ft. targets.

In practice a guided missile may be launched successfully between maximum and minimum range limits which may be widely separated and the time of flight of the missile may vary correspondingly. In this work it was assumed that the missile would be launched by the interceptor when the indicated time-to-go was 8 seconds so that the time of flight of the missile was always about 8 seconds. Ideal heading at launch was determined from the assumption that the missile would fly 7,000 ft relative to the interceptor during this time before hitting the target.

3.0 RESULTS

3.1 Cases Studied

This placement study has been divided into a number of separate problems, each problem number defining a set of attack parameters, shown in Table I.

Problems 0 and I were introductory in nature and a variety of aerodynamics, launch zones and look angle limits were used. Only the results of problems II to IX are of real significance. Each of these problems has been subdivided according to initial course difference and interceptor altitude. Table II is given to make quick reference to the results possible.

TABLE I

Problem Number	Target			Initial Interceptor	Comments
	Mach No.	Altitude	Evasion (Load Factor)	Mach No.	
0	2.0	60,000	None	2.0	Some results publishied in ref. 3, pp. 362 to 367.
I	2.0	60,000	None	2.0	Designed to provide a link between problem 0 and subsequent work. Results not published.
II	2.0	60,000	None	2.0	Some results published in ref. 4, pp. 16 to 38; remainder published here.
III	2.0	60,000	1.25	2.0	
IV	2.0	70,000	None	2.0	All results of this work published in this appendix. In problem IX the interceptor Mach no. was not allowed to rise above 1.5.
V	3.5	70,000	None	2.0	
VI	3.5	80,000	None	2.0	
VII	1.5	60,000	None	2.0	
VIII	2.0	70,000	1.1	2.0	
IX	2.0	60,000	None	1.5	

TABLE II

Number Identifying Placement Diagram	Target Parameters			Interceptor Parameters		
	Mach No.	Altitude (ft)	Evasion Load Factor	Initial Mach No.	Initial Altitude	Initial Course Difference
II A	2.0	60,000	None	2.0	60,000	180°
II B	2.0	60,000	None	2.0	50,000	180°
II C	2.0	60,000	None	2.0	40,000	180°
II D	2.0	60,000	None	2.0	60,000	135°
II E	2.0	60,000	None	2.0	50,000	135°
II F	2.0	60,000	None	2.0	40,000	135°
II G	2.0	60,000	None	2.0	60,000	110°
II H	2.0	60,000	None	2.0	50,000	110°
II K	2.0	60,000	None	2.0	40,000	110°
II L	2.0	60,000	None	2.0	60,000	75°
II M	2.0	60,000	None	2.0	50,000	75°
II N	2.0	60,000	None	2.0	40,000	75°
III A	2.0	60,000	1.25	2.0	60,000	180°
III B	2.0	60,000	1.25	2.0	50,000	180°
III C	2.0	60,000	1.25	2.0	40,000	180°
III D	2.0	60,000	1.25	2.0	60,000	135°
III E	2.0	60,000	1.25	2.0	50,000	135°
III F	2.0	60,000	1.25	2.0	40,000	135°
III G	2.0	60,000	1.25	2.0	60,000	110°
III H	2.0	60,000	1.25	2.0	50,000	110°
III K	2.0	60,000	1.25	2.0	40,000	110°
III L	2.0	60,000	1.25	2.0	60,000	75°
III M	2.0	60,000	1.25	2.0	50,000	75°
III N	2.0	60,000	1.25	2.0	40,000	75°
IV A	2.0	70,000	None	2.0	60,000	180°
IV B	2.0	70,000	None	2.0	50,000	180°
IV C	2.0	70,000	None	2.0	40,000	180°
IV D	2.0	70,000	None	2.0	60,000	135°
IV E	2.0	70,000	None	2.0	50,000	135°
IV F	2.0	70,000	None	2.0	40,000	135°
IV G	2.0	70,000	None	2.0	60,000	110°
IV H	2.0	70,000	None	2.0	50,000	110°
IV K	2.0	70,000	None	2.0	40,000	110°
IV L	2.0	70,000	None	2.0	60,000	75°
IV M	2.0	70,000	None	2.0	50,000	75°
IV N	2.0	70,000	None	2.0	40,000	75°

TABLE II (cont'd)

Number Identifying Placement Diagram	Target Parameters			Interceptor Parameters		
	Mach No.	Altitude (ft)	Evasion Load Factor	Initial Mach No.	Initial Altitude	Initial Course Difference
V A	3.5	70,000	None	2.0	60,000	180°
V B	3.5	70,000	None	2.0	40,000	180°
V C	3.5	70,000	None	2.0	60,000	135°
V D	3.5	70,000	None	2.0	40,000	135°
VI A	3.5	80,000	None	2.0	40,000	180°
VI B	3.5	80,000	None	2.0	40,000	135°
VII A	1.5	60,000	None	2.0	60,000	180°
VII B	1.5	60,000	None	2.0	50,000	180°
VII C	1.5	60,000	None	2.0	40,000	180°
VII D	1.5	60,000	None	2.0	60,000	135°
VII E	1.5	60,000	None	2.0	50,000	135°
VII F	1.5	60,000	None	2.0	40,000	135°
VII G	1.5	60,000	None	2.0	60,000	110°
VII H	1.5	60,000	None	2.0	50,000	110°
VII K	1.5	60,000	None	2.0	40,000	110°
VII L	1.5	60,000	None	2.0	60,000	75°
VII M	1.5	60,000	None	2.0	50,000	75°
VII N	1.5	60,000	None	2.0	40,000	75°
VIII A	2.0	70,000	1.1	2.0	60,000	180°
VIII B	2.0	70,000	1.1	2.0	40,000	180°
VIII C	2.0	70,000	1.1	2.0	60,000	135°
VIII D	2.0	70,000	1.1	2.0	40,000	135°
IX A	2.0	60,000	None	1.5	60,000	180°
IX B	2.0	60,000	None	1.5	50,000	180°
IX C	2.0	60,000	None	1.5	40,000	180°
IX D	2.0	60,000	None	1.5	60,000	110°
IX E	2.0	60,000	None	1.5	50,000	110°
IX F	2.0	60,000	None	1.5	40,000	110°

3.2 Method of Obtaining Placement Probabilities

The placement diagrams show the region relative to the target from which successful attacks can be made. For a given target there are different placement diagrams for different approach altitudes as well as for different approach course differences.

In computing placement probabilities it has beenassumed that the interceptor can be sent to the prescribed altitude with a high degree of accuracy and that the placement errors occur in the horizontal plane of the placement diagram only. It has been assumed that A.I. radar detection ranges will not be changed by altitude differences between target and interceptor. In the cases studied the horizontal separation at detection is much greater than the vertical separation and the approximation is close.

The "ideal" approach line which is used by G.C.I. has also been assumed independent of altitude difference. It is probable that this line could be redefined in the light of the results to optimize placement probability, but this has not been attempted at present.

4.0 REFERENCES

1. CARDE Technical Letter N-47-8 "First Quarterly Report on CF-105 Weapon System Assessment " Appendix G (SECRET).

2. CARDE Technical Letter N-47-12 "Second Quarterly Report on CF-105 Weapon System Assessment" Appendix D (SECRET).

3. CARDE Technical Letter N-47-18 "Third Quarterly Report on CF-105 Weapon System Assessment" Appendix G (SECRET).

4. CARDE Technical Letter 1012/57 "Fourth Progress Report on CF-105 Weapon System Assessment" Appendix A (SECRET).

5. AVRO Report "CF-105 Periodic Performance Report No. 9" (SECRET).

6. AVRO Report "CF-105 Periodic Performance Report No. 10" (SECRET).

7. CARDE Technical Letter 1084/57 "CF-105 Aircraft Interceptor Placement Problem - 3 Dimensional REAC Simulation" (SECRET).

PROB II ABC CLIMBING

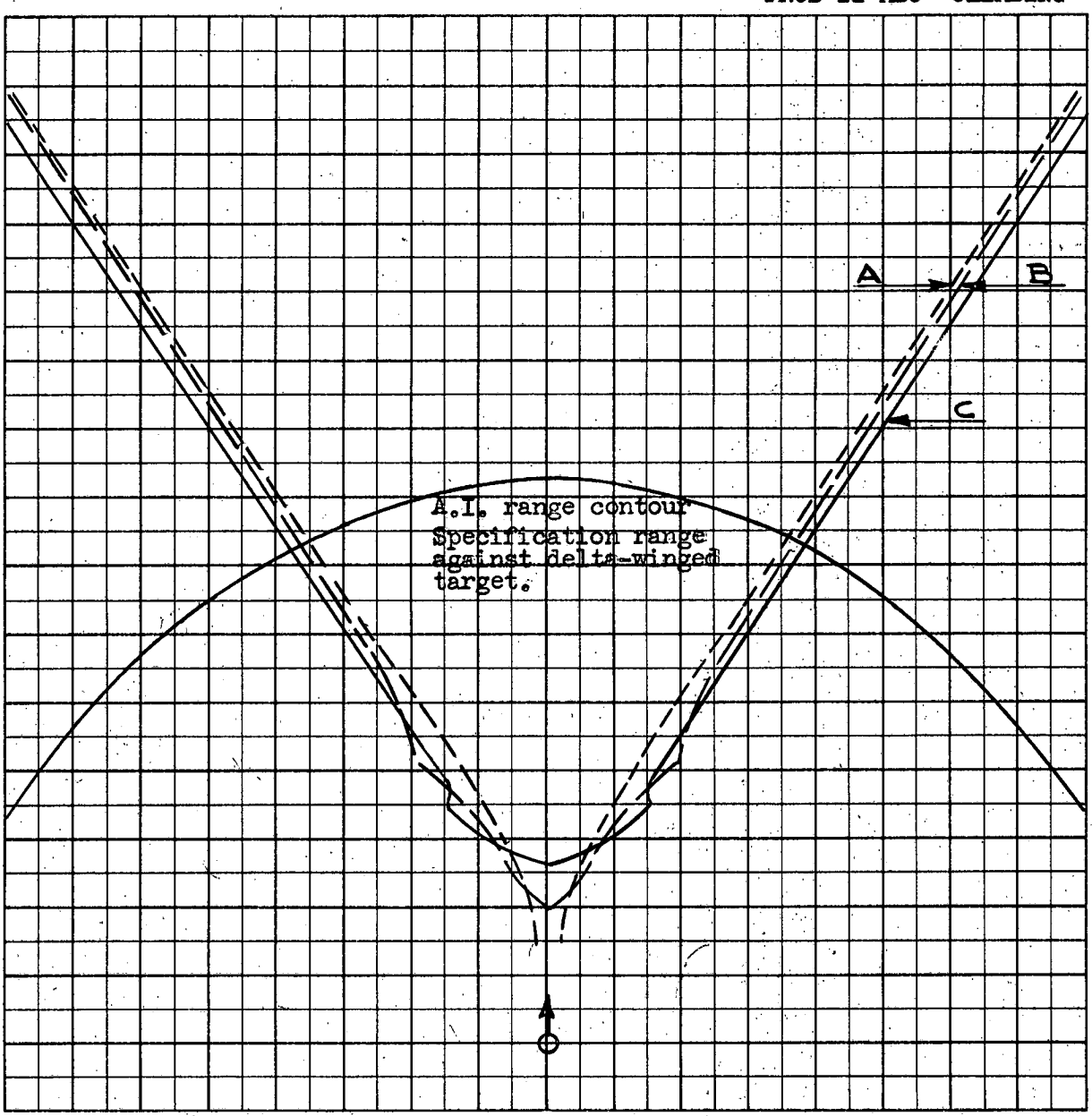

M_t = 2.0

h_t = 60 K

M_{fo} = 2.0

h_{fo} A = 60 K
B = 50 K
C = 40 K

Γ_o = 180°

Scale 25,000 ft/cm

A-1

PROB II B

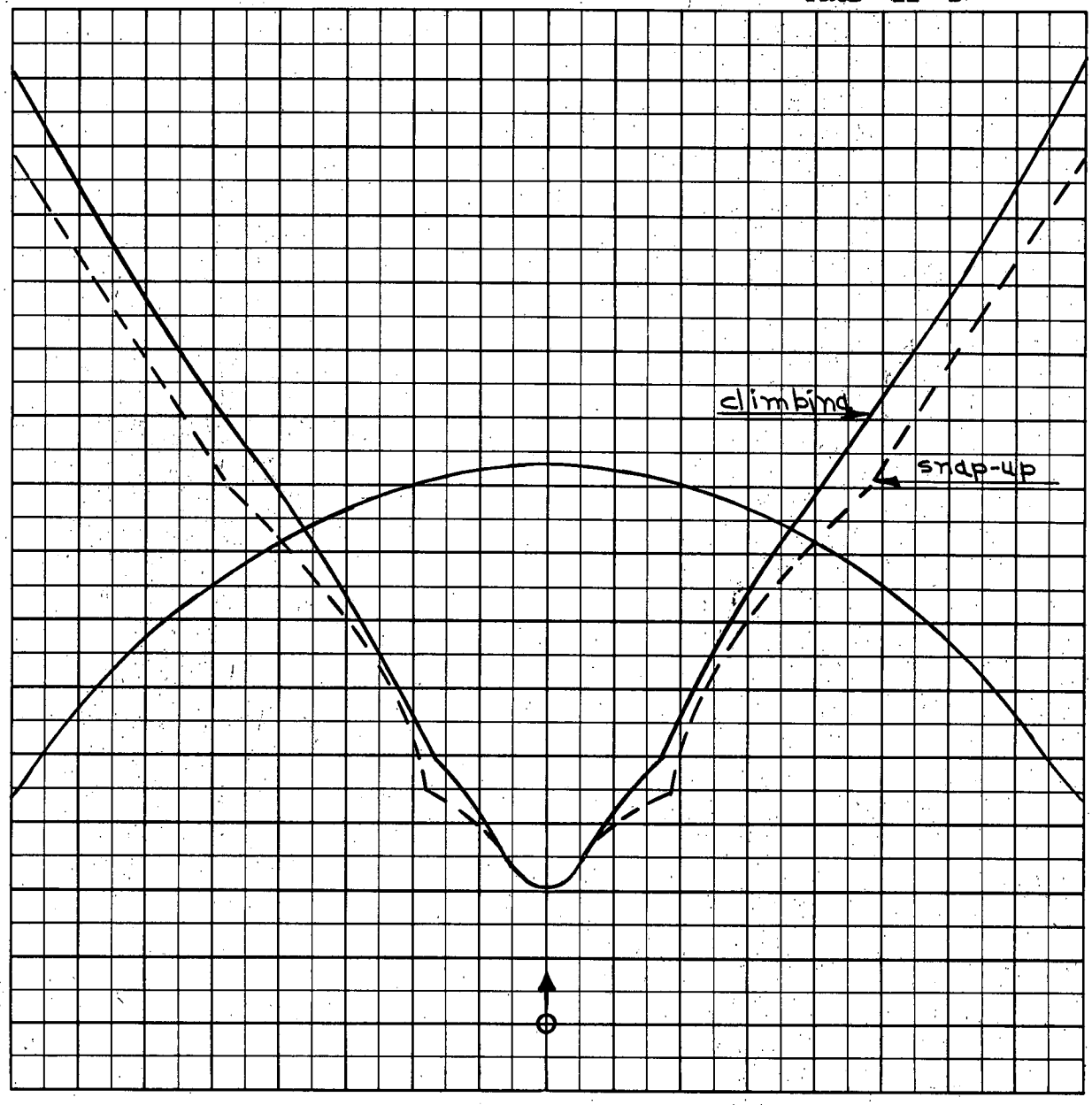

M_t = 2.0
h_t = 60 K
M_{fo} = 2.0
h_{fo} = 50 K
Γ_o = 180°

Scale 25,000 Ft/cm

A-2

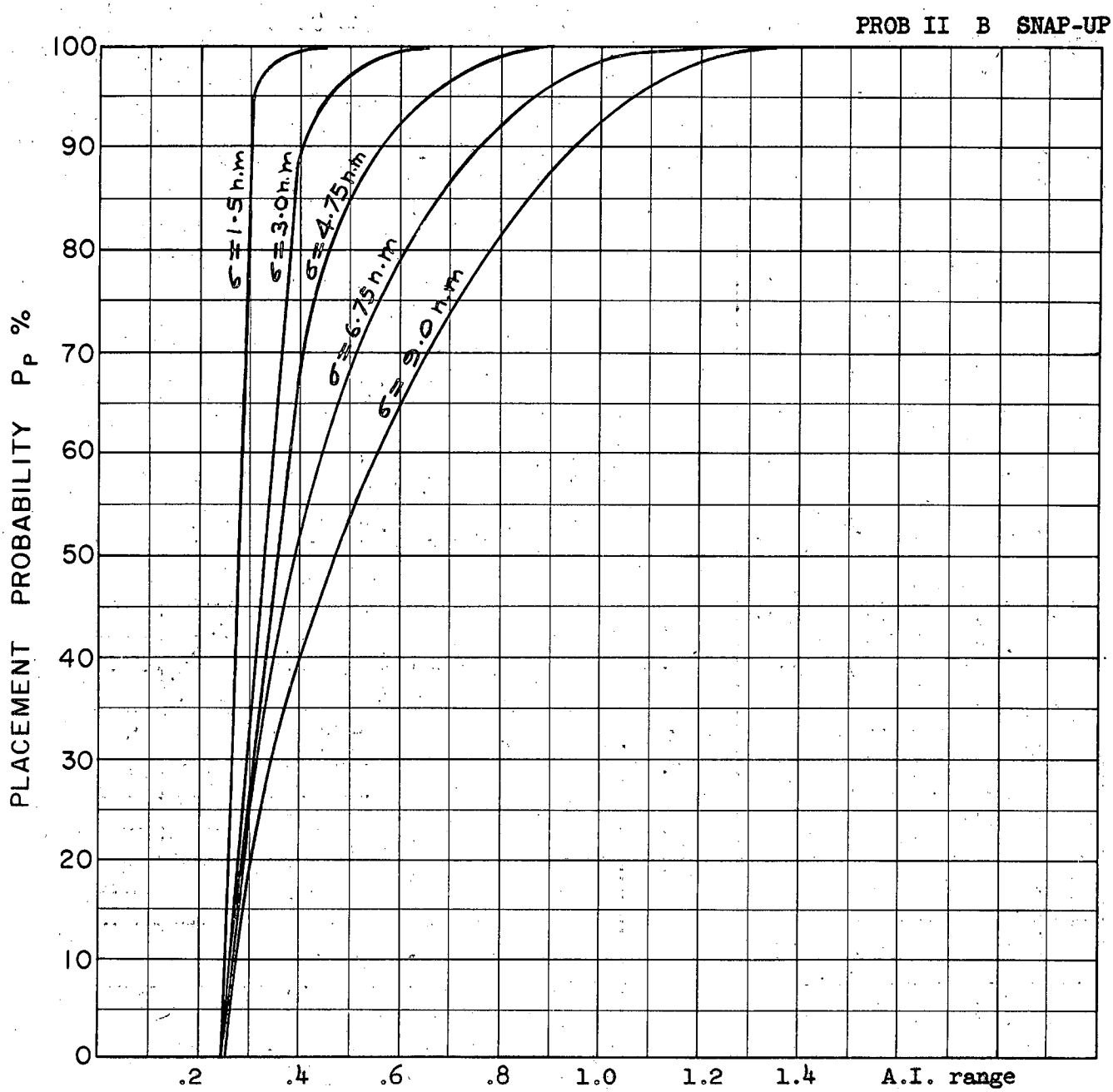

A-3

COURSE DIFFERENCE: 180°
TARGET EVASION: 0
TARGET MACH NO.: 2.0
INTERCEPTOR LATERAL G's: Avro 3.3
INTERCEPTOR MACH NO.: 2.0
σ OF G.C.I. ACCURACY: 5 values
A.I. DETECTION RANGE AS FRACTION OF SPECIFICATION RANGE, S: Abscissa
A.I. DETECTION RANGE CONTOUR: Delta
ALTITUDE: H_t = 60 K
H_{fo} = 50 K

PROB II C

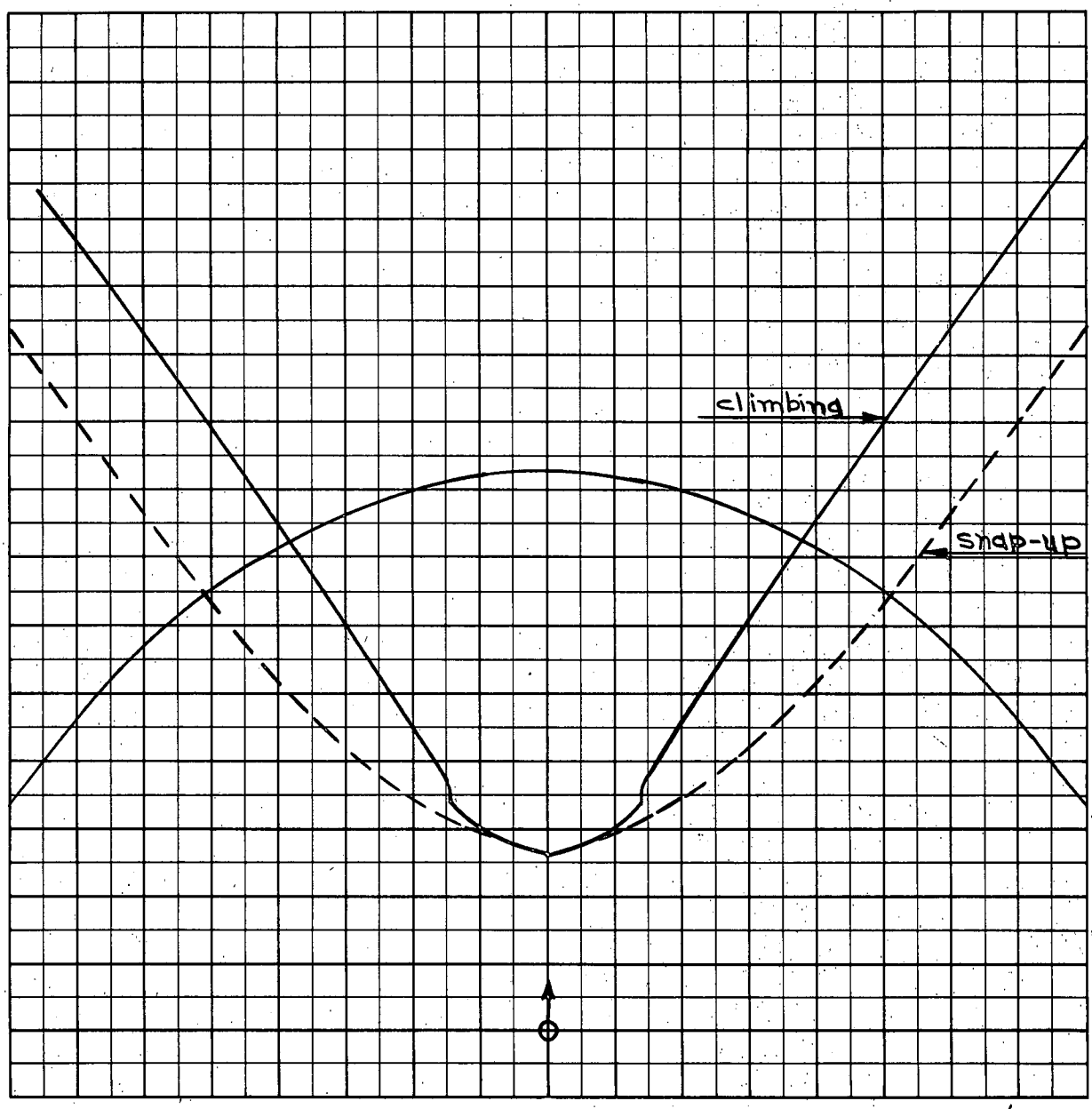

M_t = 2.0

h_t = 60 K

M_{fo} = 2.0

h_{fo} = 40 K

Γ_o = 180°

Scale 25,000 ft/cm

A-4

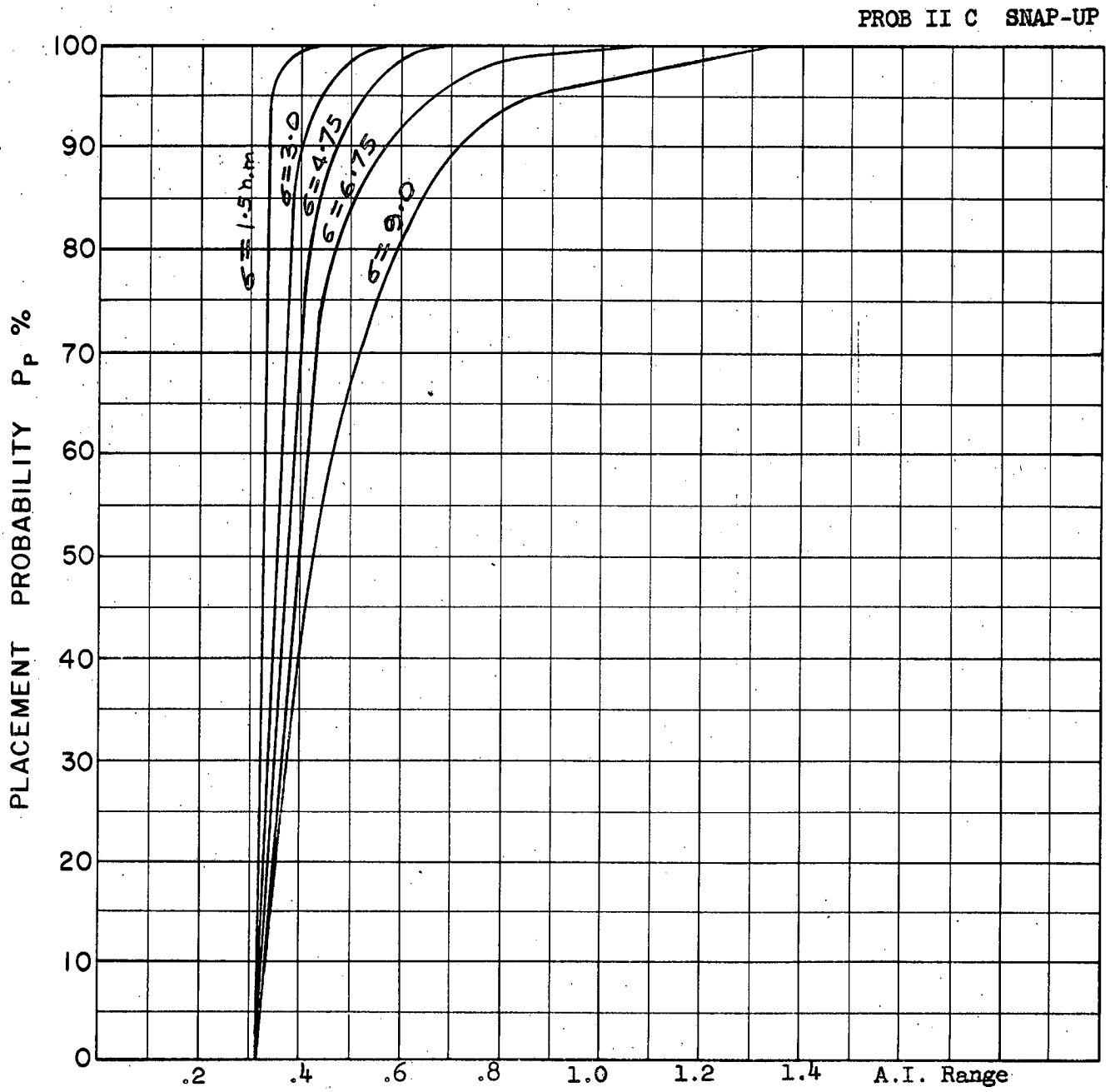

A-5

COURSE DIFFERENCE: 180°
TARGET EVASION: 0
TARGET MACH NO.: 2.0
INTERCEPTOR LATERAL G's: Avro 3.3
INTERCEPTOR MACH NO.: 2.0
σ OF G.C.I. ACCURACY: 5 values
A.I. DETECTION RANGE AS FRACTION OF SPECIFICATION RANGE, S: Abscissa
A.I. DETECTION RANGE CONTOUR: Delta
ALTITUDE: H_t = 60K
H_{fo} = 40K

PROB II DEF CLIMBING

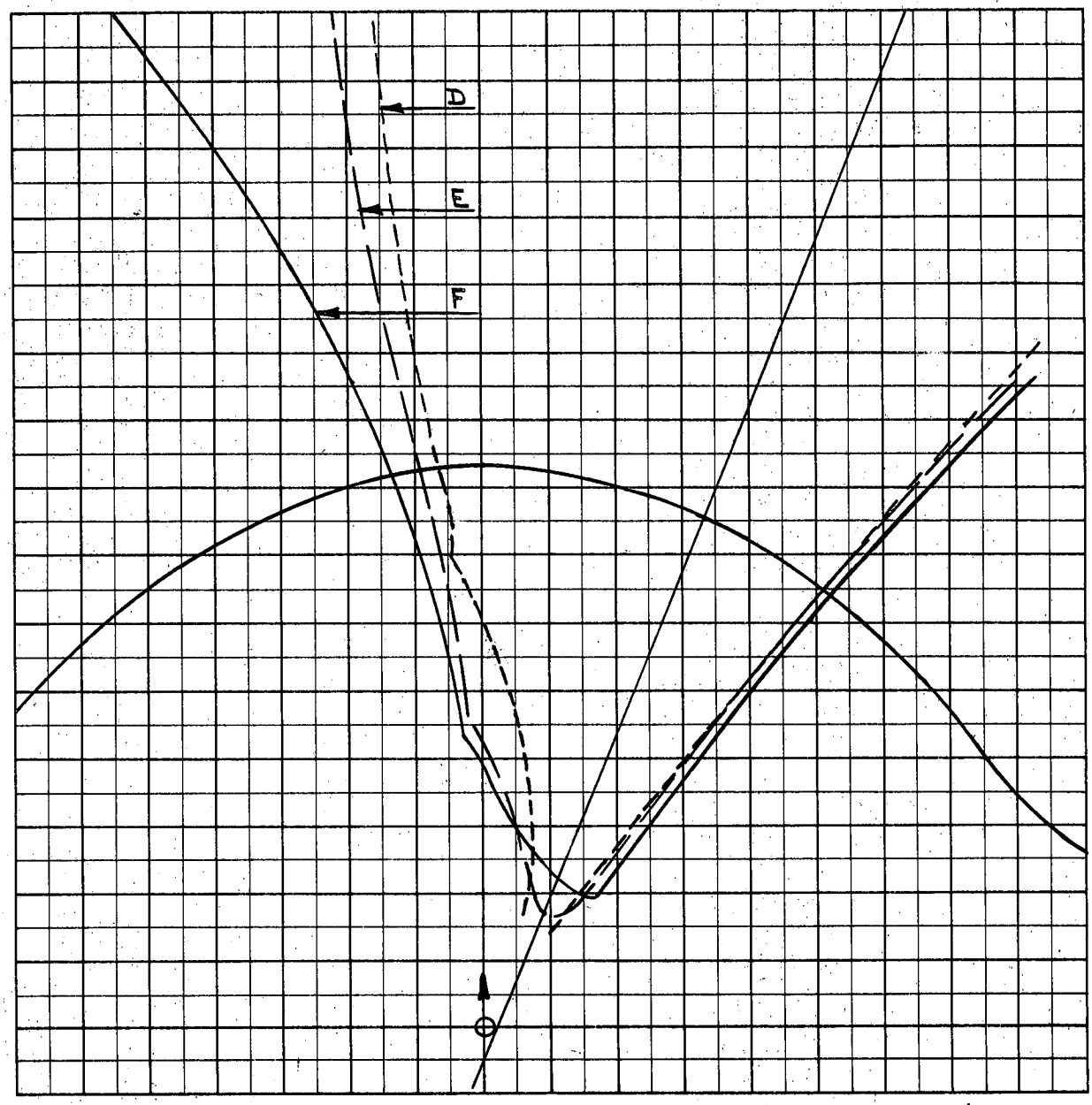

Scale 25,000 ft/cm

A-6

M_t = 2.0

h_t = 60 K

M_{fo} = 2.0

h_{fo} D = 60 K
E = 50 K
F = 40 K

Γ_o = 135°

PROB II E

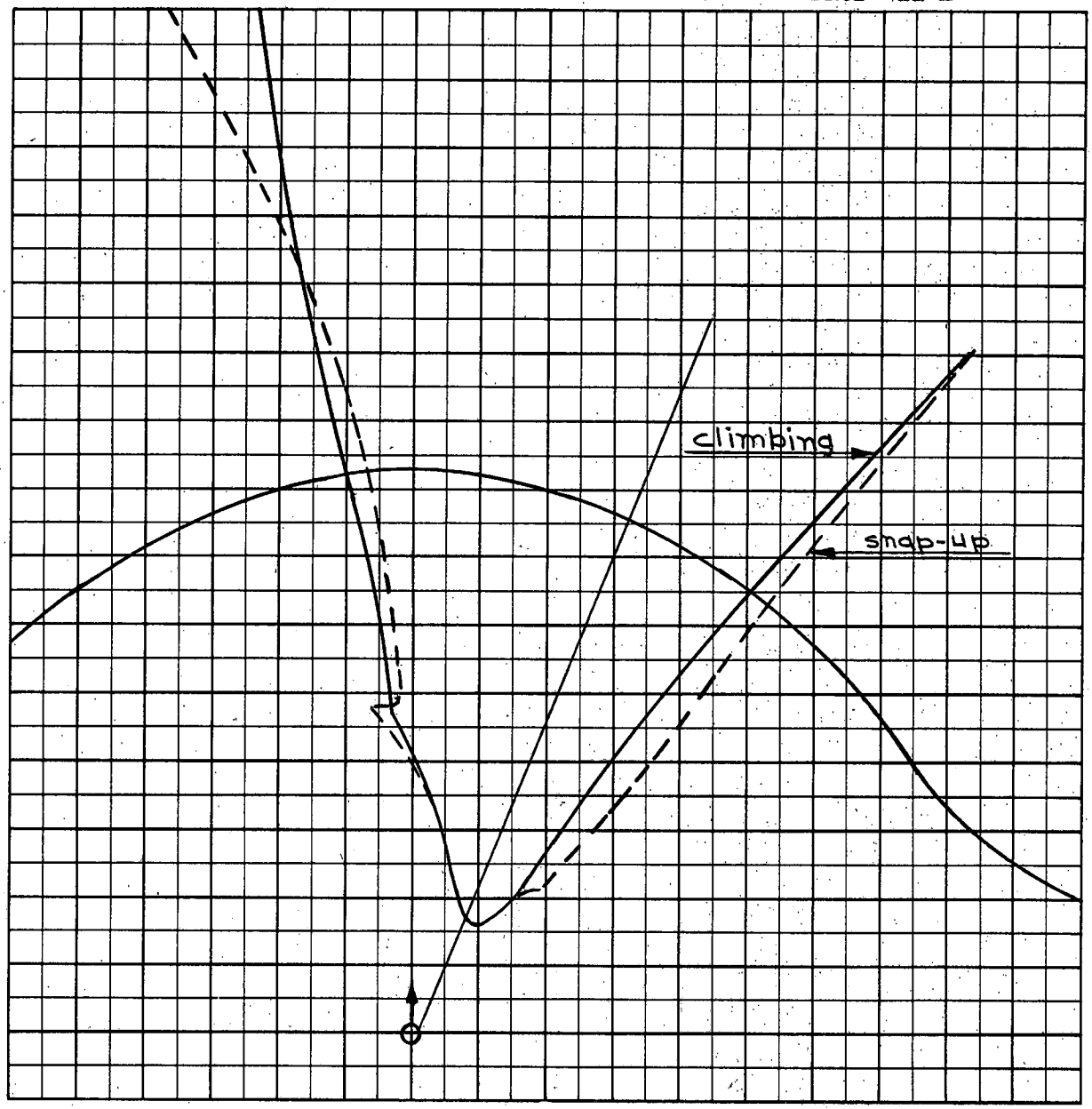

Scale 25,000 ft/cm

M_t = 2.0

h_t = 60 K

M_{fo} = 2.0

h_{fo} E = 50 K

Γ_o = 135°

A-7

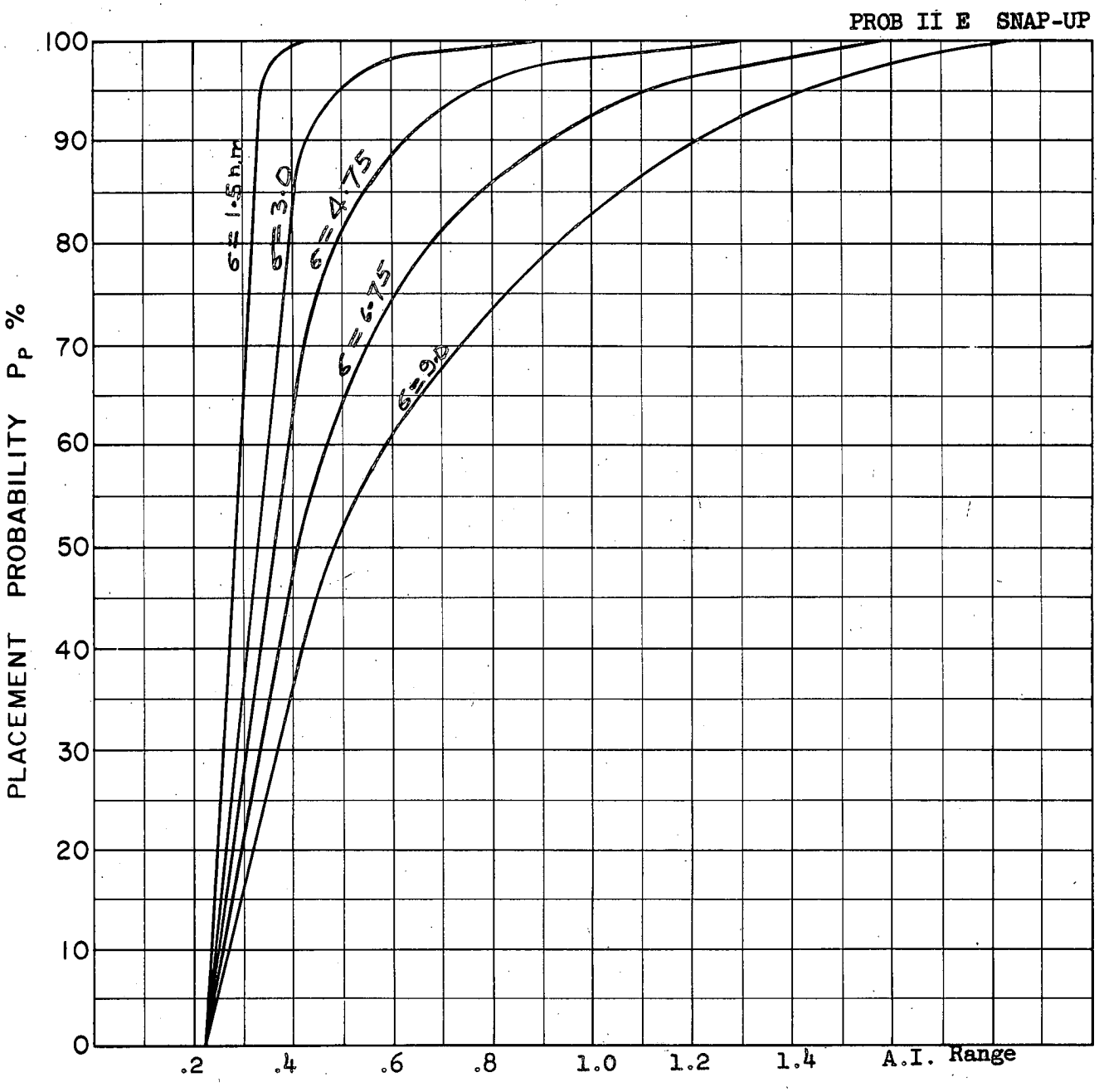

A-8

COURSE DIFFERENCE: 135°
TARGET EVASION: 0
TARGET MACH NO.: 2.0
INTERCEPTOR LATERAL G's: Avro 3.3
INTERCEPTOR MACH NO.: 2.0
σ OF G.C.I. ACCURACY: 5 Values
A.I. DETECTION RANGE AS FRACTION OF SPECIFICATION RANGE, S: Abscissa
A.I. DETECTION RANGE CONTOUR: Delta
ALTITUDE: H_t = 60 K
H_{fo} = 50 K

PROB II F

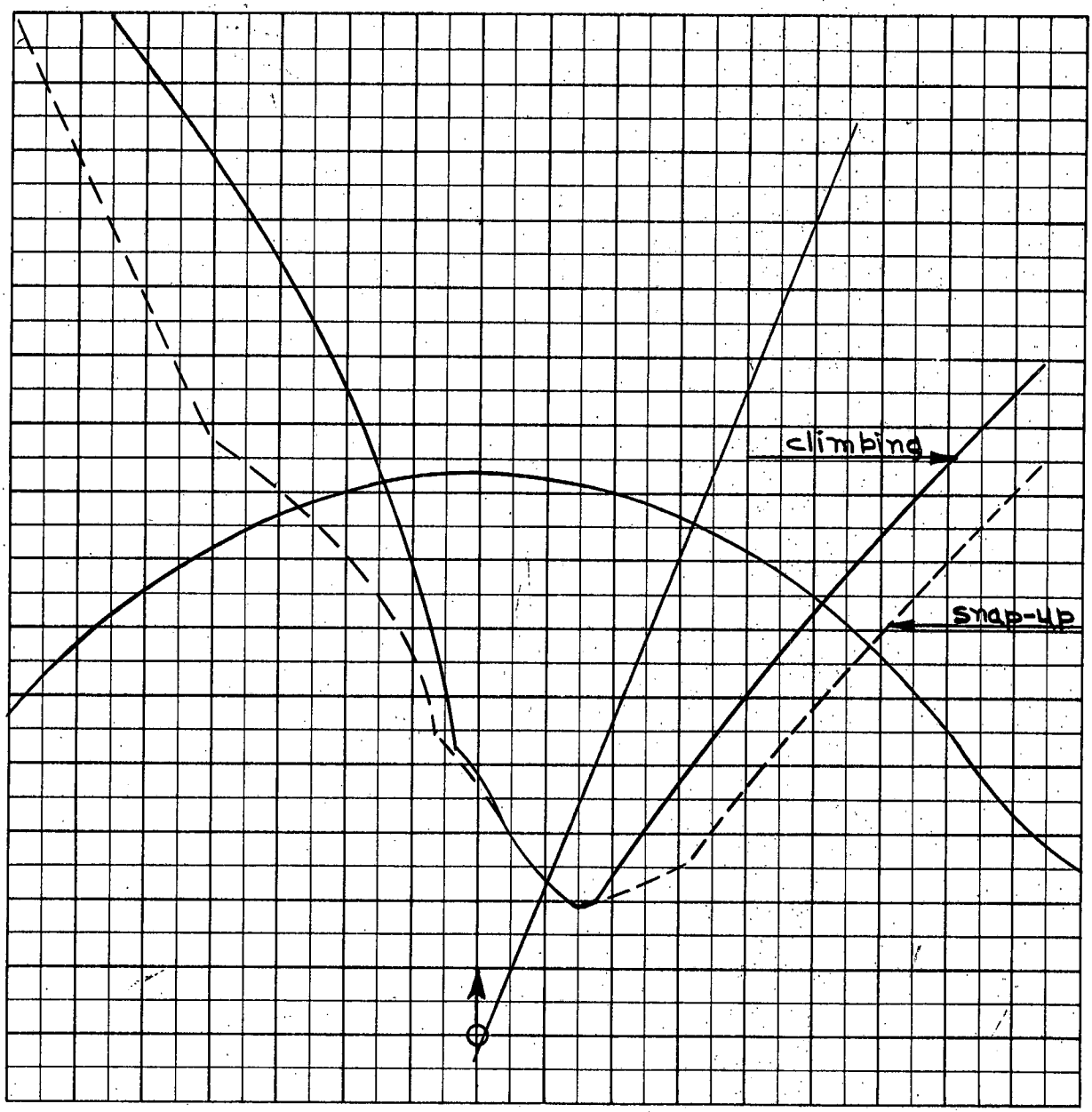

Scale 25,000 ft/cm

A-9

M_t = 2.0

h_t = 60 K

M_{fo} = 2.0

h_{fo} F = 40 K

Γ_o = 135°

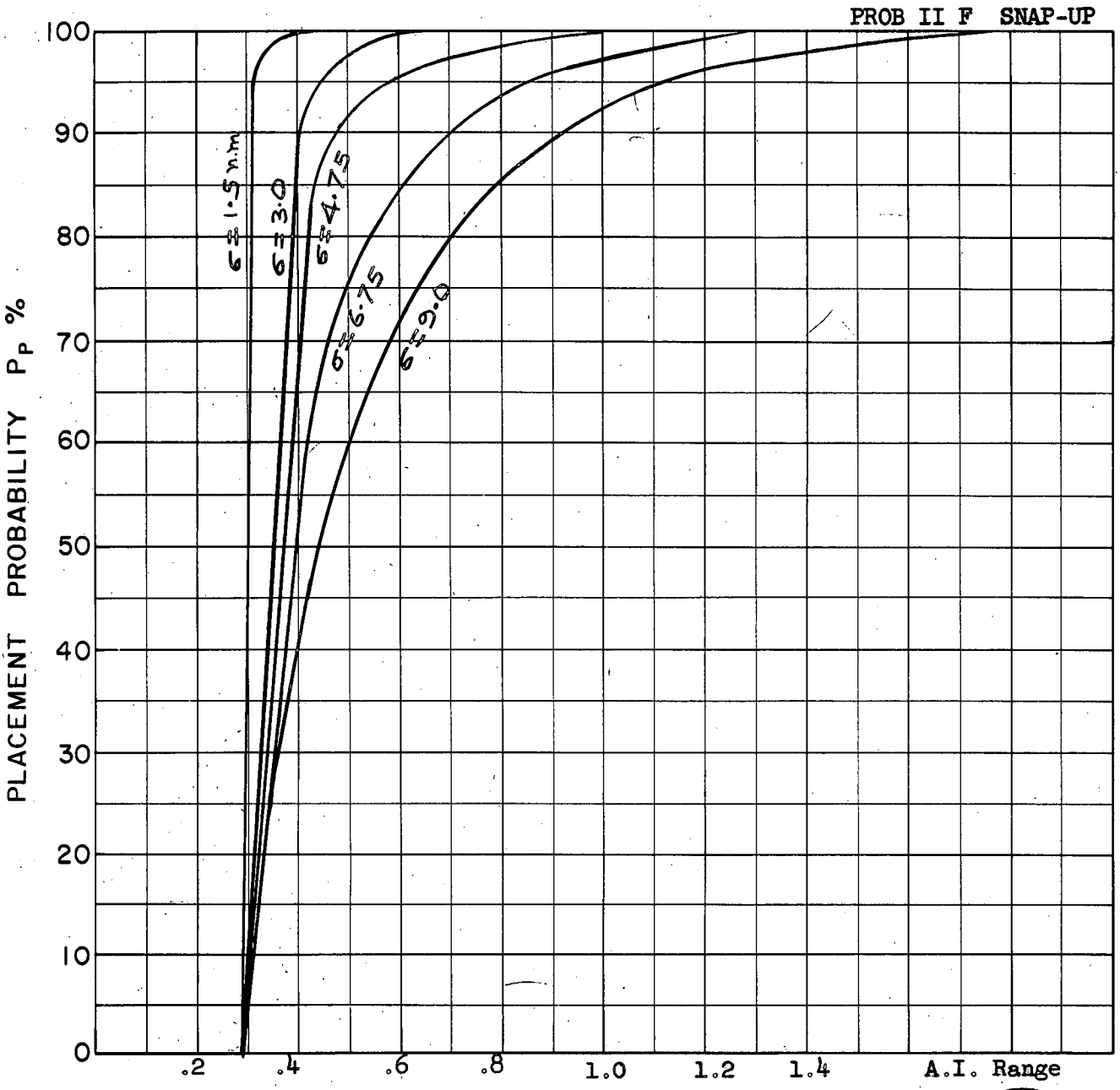

A-10

COURSE DIFFERENCE: 135°
TARGET EVASION: 0
TARGET MACH NO.: 2.0
INTERCEPTOR LATERAL G's: Avro 3.3
INTERCEPTOR MACH NO.: 2.0
σ OF G.C.I. ACCURACY: 5 values
A.I. DETECTION RANGE AS FRACTION OF SPECIFICATION RANGE, S: Abscissa
A.I. DETECTION RANGE CONTOUR: Delta
ALTITUDE: H_t = 60 K
H_{fo} = 40 K

PROB II GHK CLIMBING

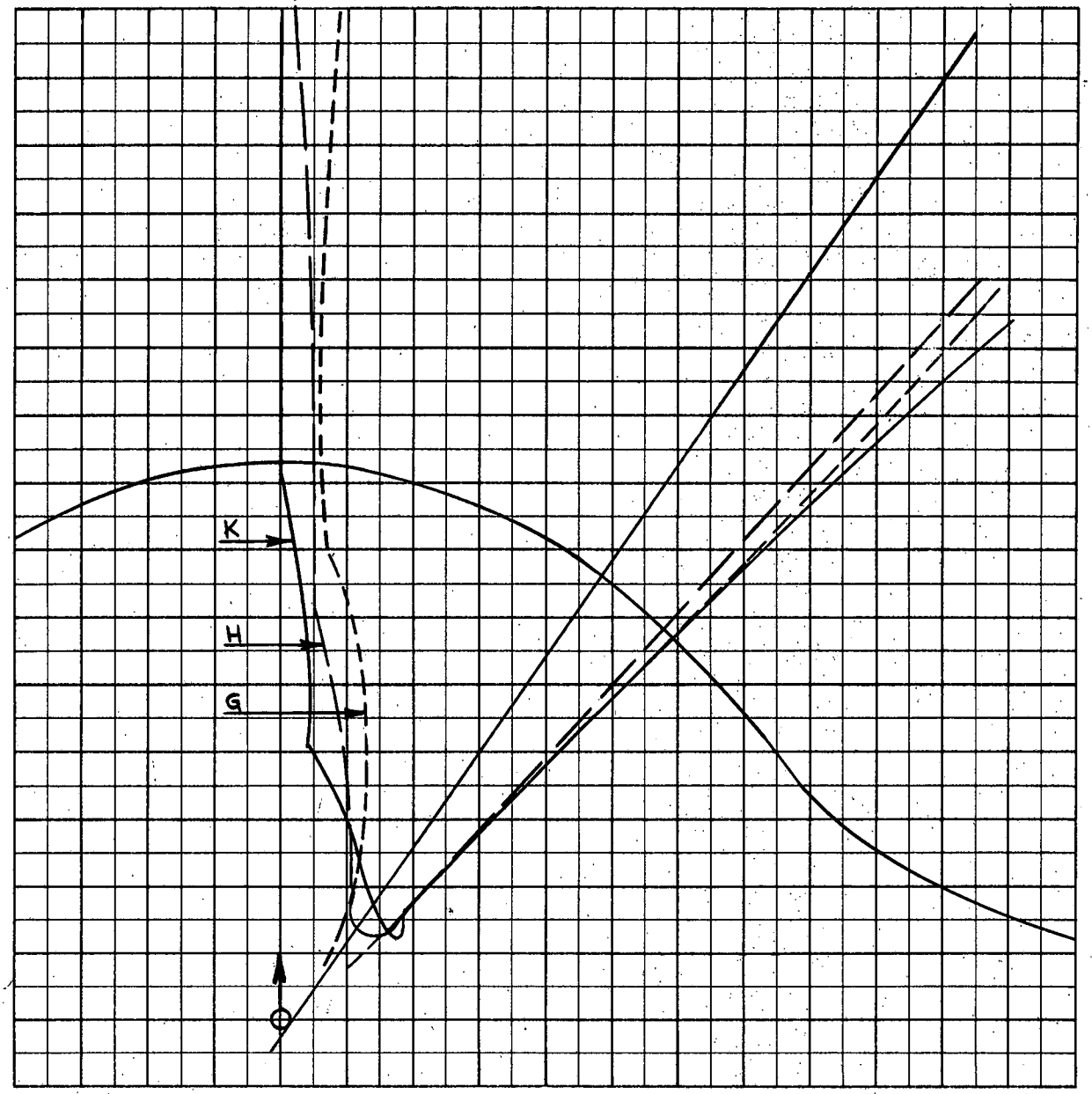

Scale 25,000 ft/cm

M_t = 2.0
h_t = 60 K
M_{fo} = 2.0
h_{fo} G = 60 K
H = 50 K
K = 40 K
Γ_o = 110°

A-11

PROB II H

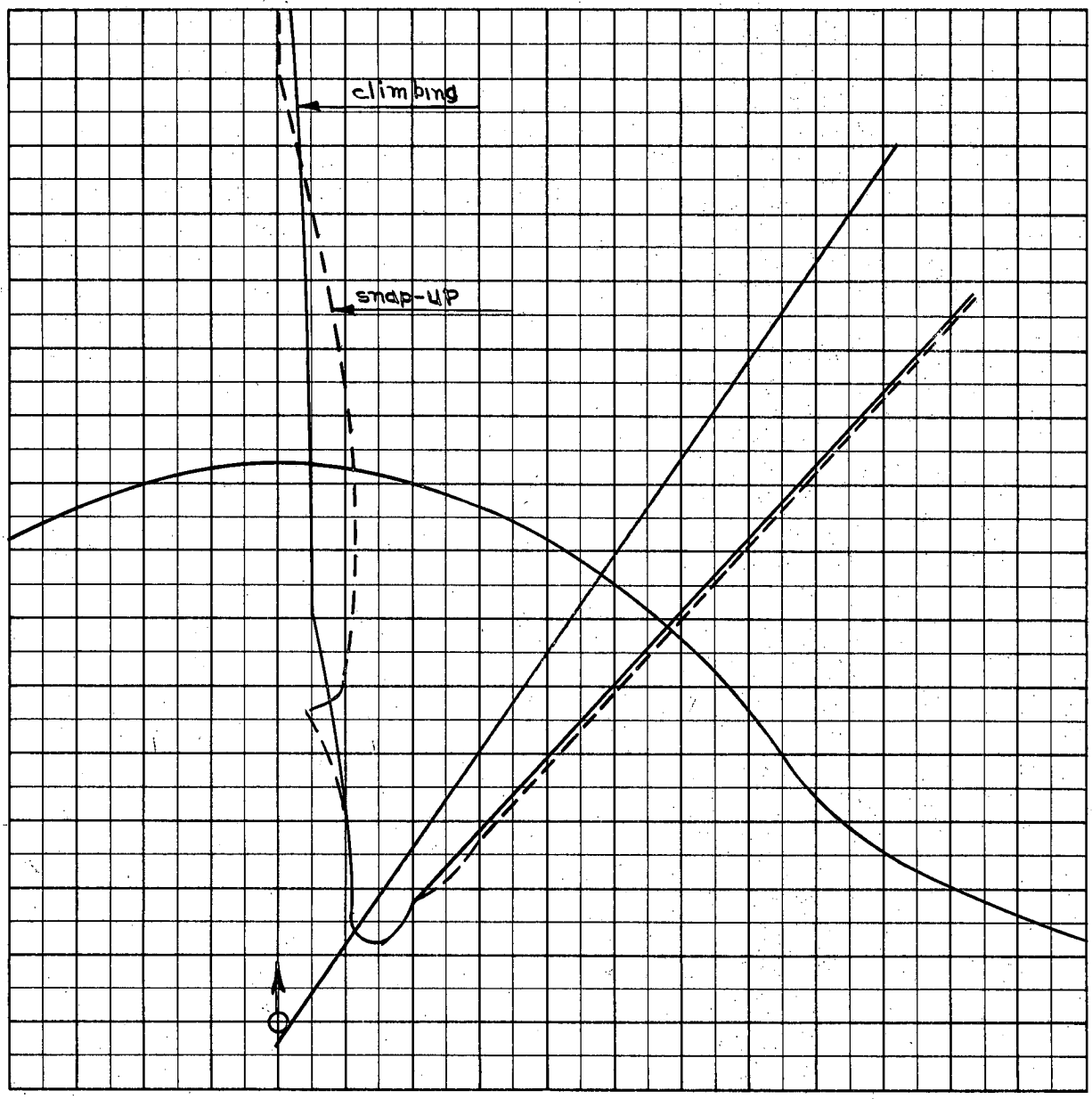

Scale 25,000 ft/cm

M_t = 2.0
h_t = 60 K
M_{fo} = 2.0
h_{fo} H = 50 K
Γ_o = 110°

A-12

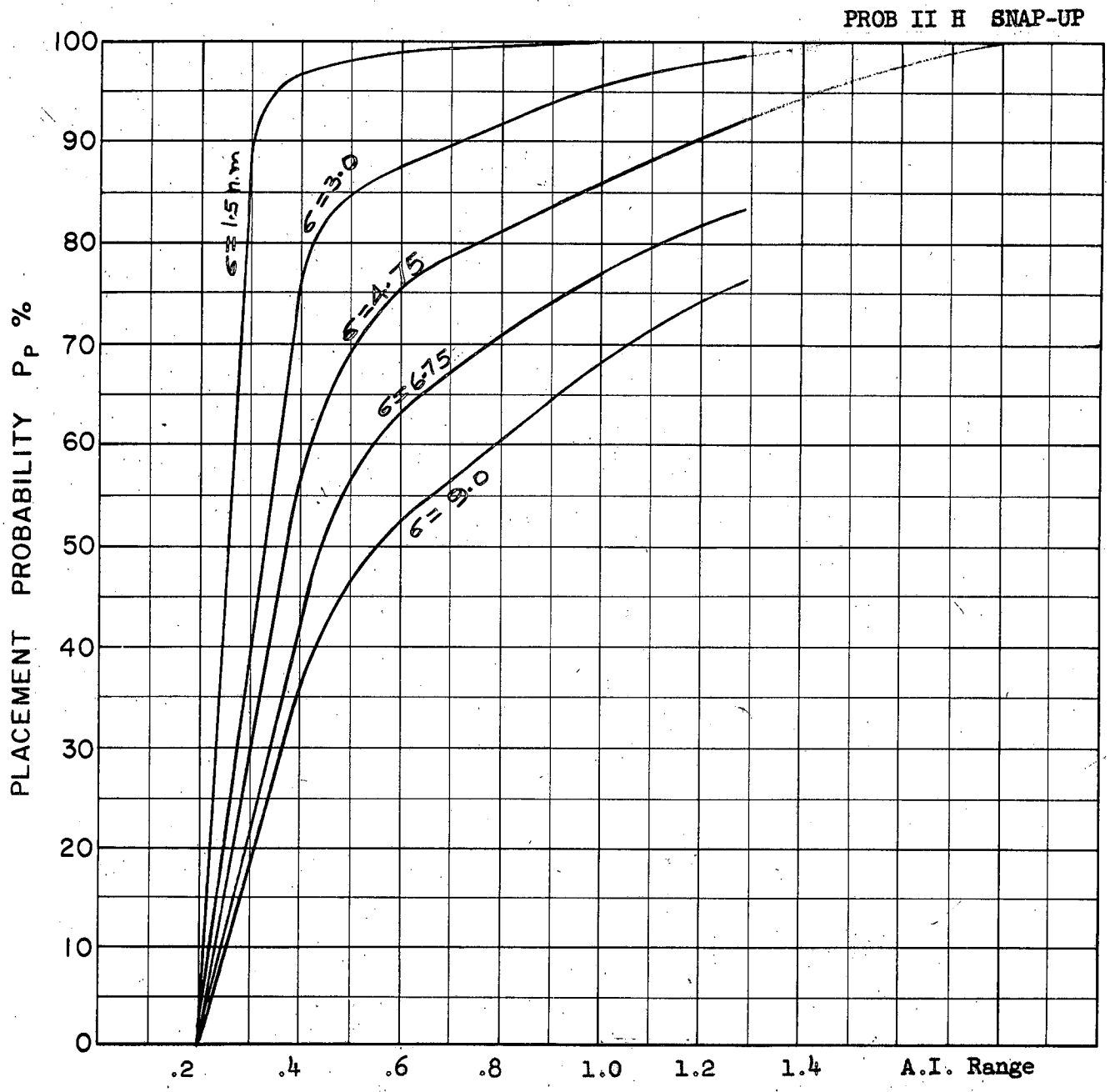

A-13

COURSE DIFFERENCE: 110°
TARGET EVASION: 0
TARGET MACH NO.: 2.0
INTERCEPTOR LATERAL G's: Avro 3.3
INTERCEPTOR MACH NO.: 2.0
σ OF G.C.I. ACCURACY: 5 Values
A.I. DETECTION RANGE AS FRACTION OF SPECIFICATION RANGE, S: Abscissa
A.I. DETECTION RANGE CONTOUR: Delta
ALTITUDE: H_t = 60 K
H_{fo} = 50 K

PROB II K

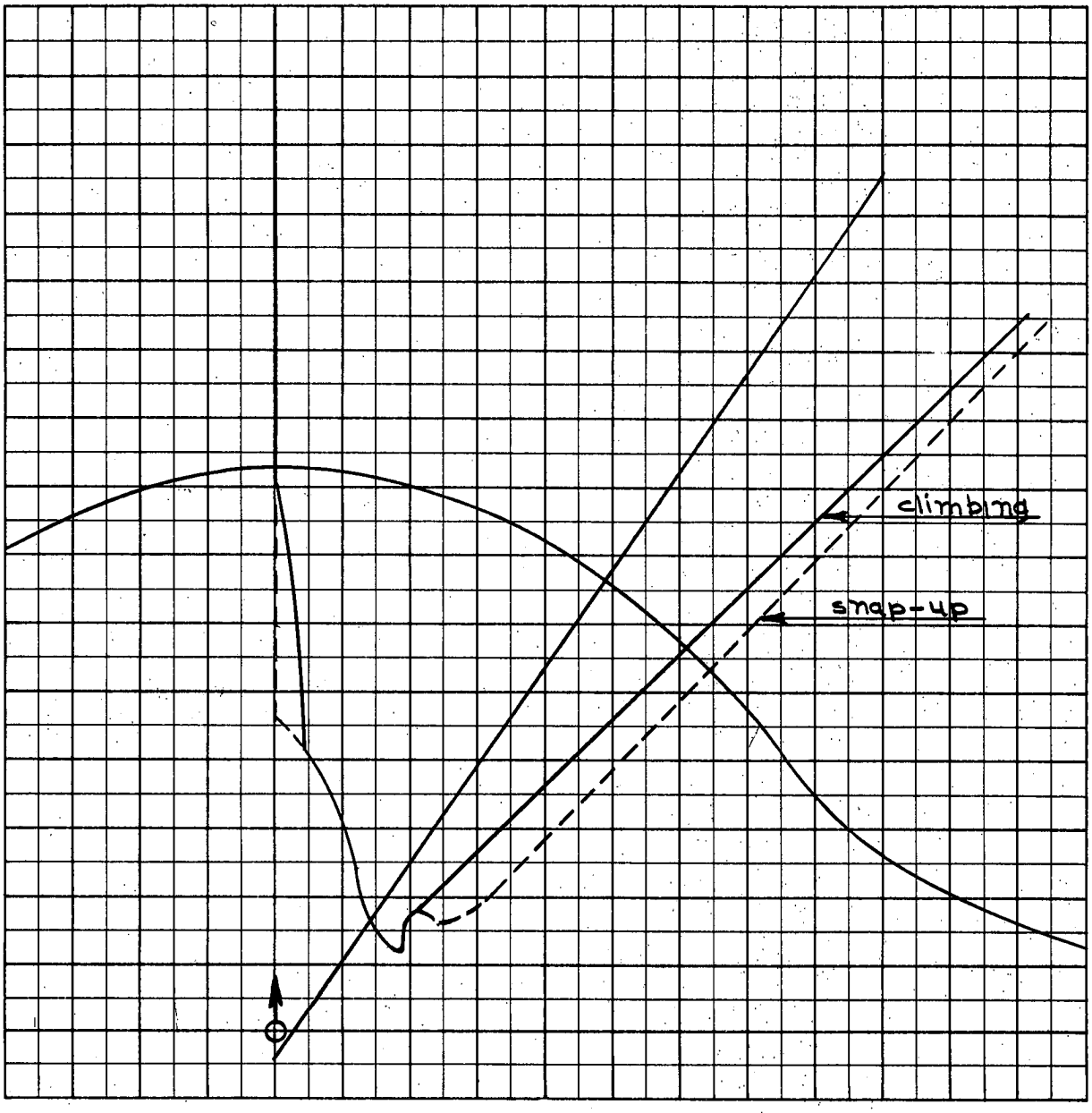

SCALE 25,000 ft/cm

A-14

M_t = 2.0

h_t = 60 K

M_{fo} = 2.0

$h_{fo\ K}$ = 40 K

Γ_o = 110°

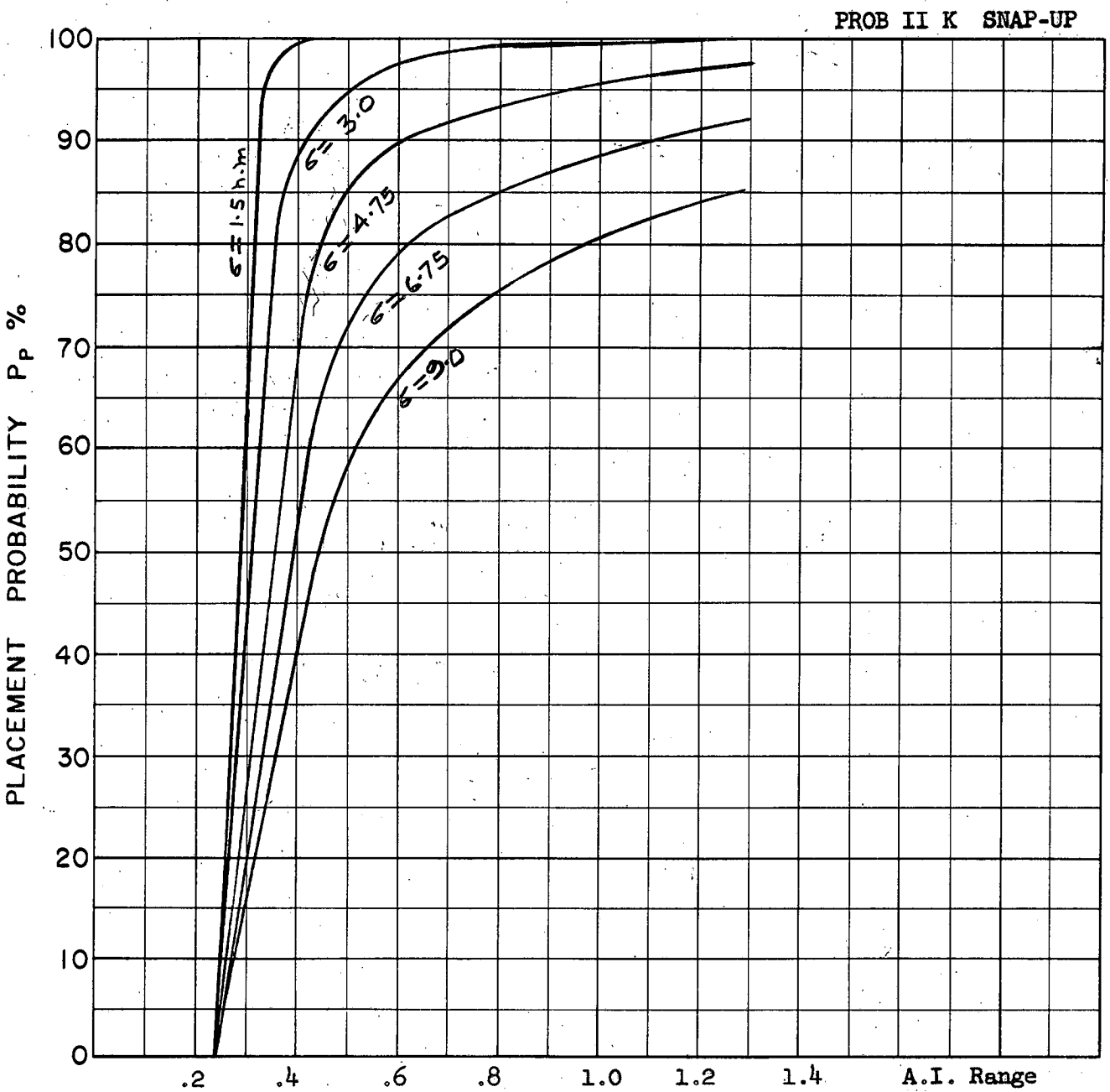

A-15

COURSE DIFFERENCE: 110°
TARGET EVASION: 0
TARGET MACH NO.: 2.0
INTERCEPTOR LATERAL G's: Avro 3.3
INTERCEPTOR MACH NO.: 2.0
σ OF G.C.I. ACCURACY: 5 Values
A.I. DETECTION RANGE AS FRACTION OF SPECIFICATION RANGE, S: Abscissa
A.I. DETECTION RANGE CONTOUR: Delta
ALTITUDE: H_t = 60 K
H_{fo} = 40 K

PROB II LMN CLIMBING

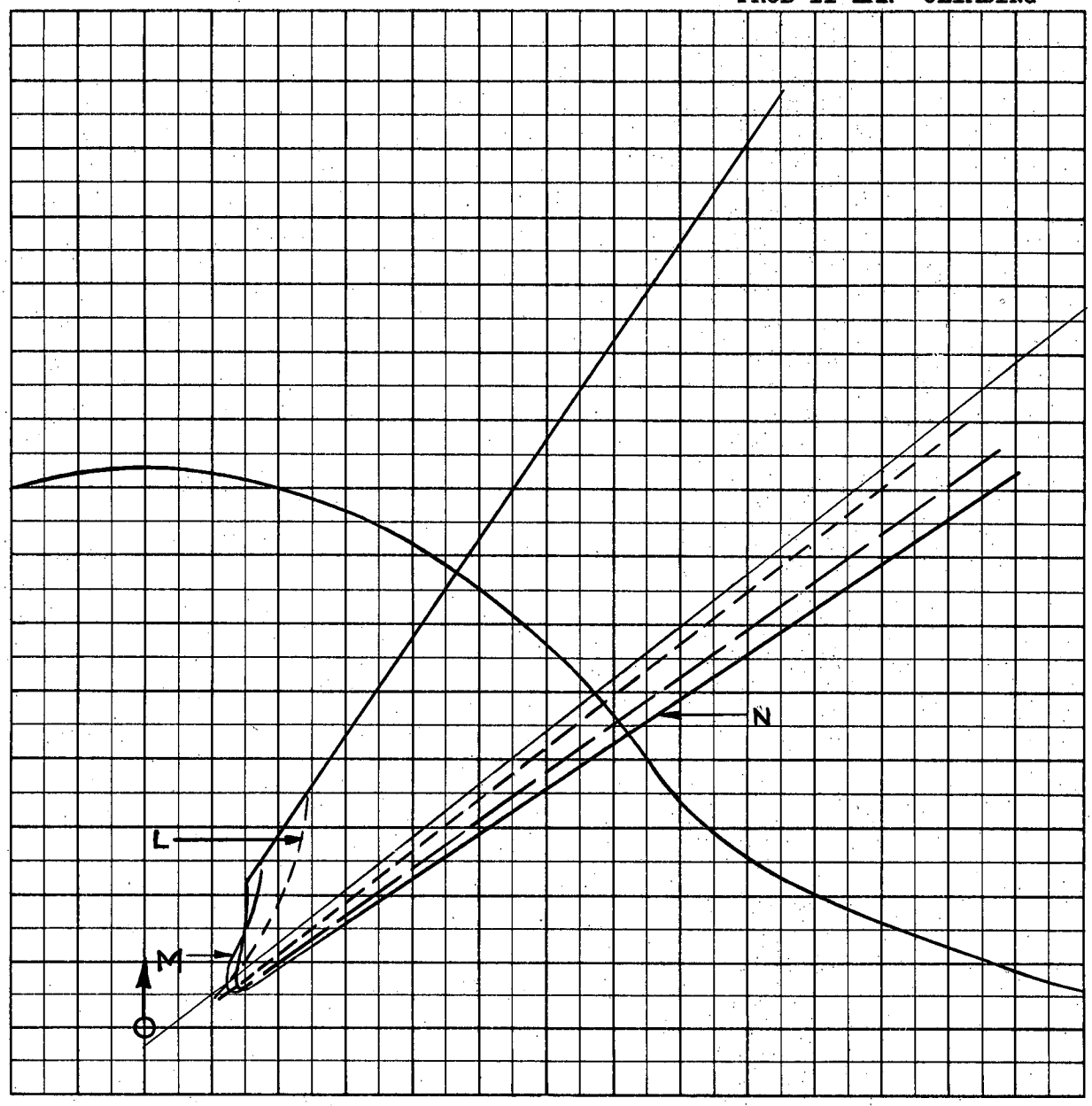

Scale 25,000 ft/cm

M_t = 2.0
h_t = 60 K

M_{fo} = 2.0

h_{fo} L = 60 K
M = 50 K
N = 40 K

Γ_o = 75°

A-16

PROB II M

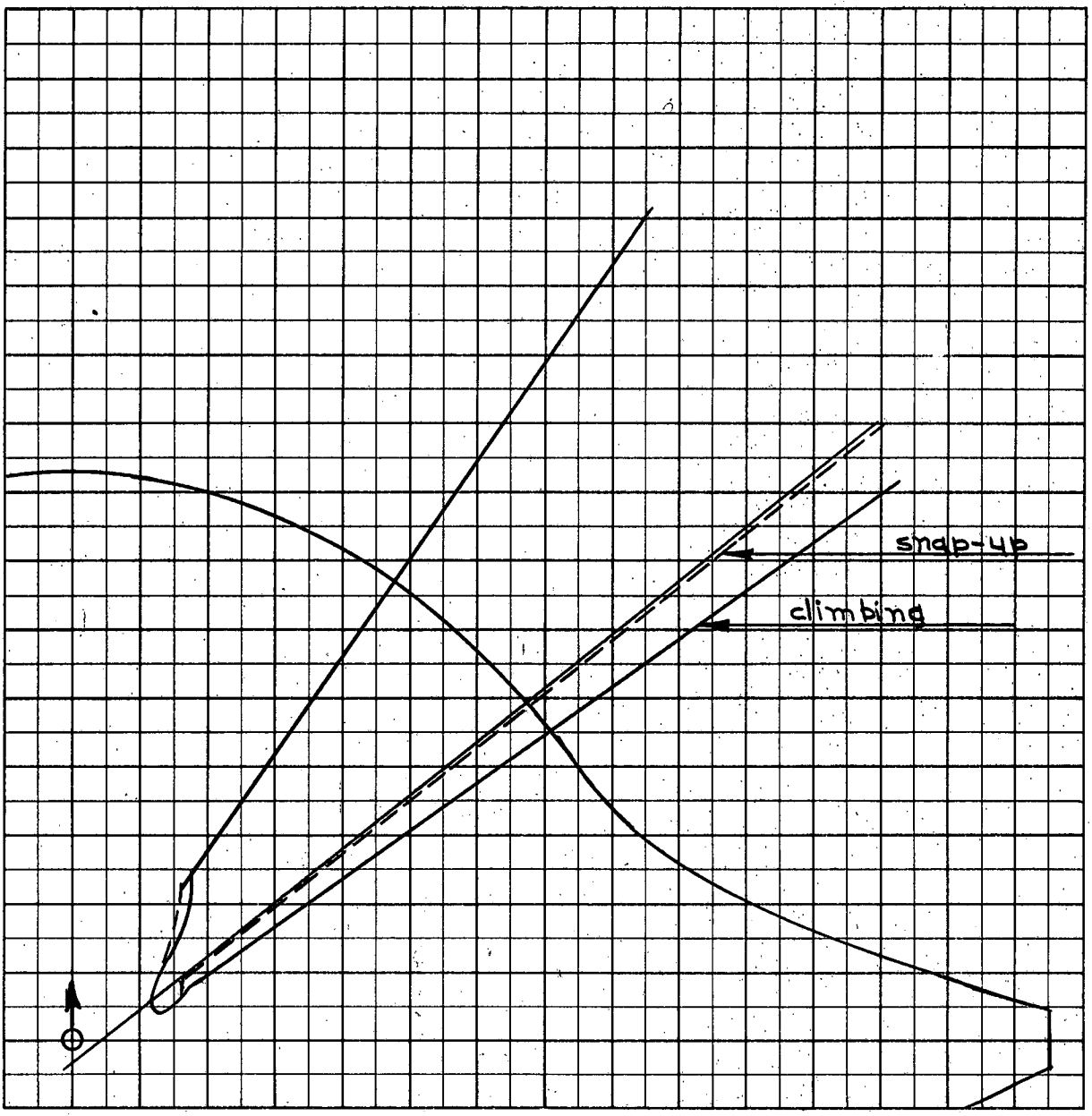

Scale 25,000 ft/cm

M_t = 2.0
h_t = 60 K
M_{fo} = 2.0
$h_{fo\ M}$ = 50 K
Γ_o = 75°

A-17

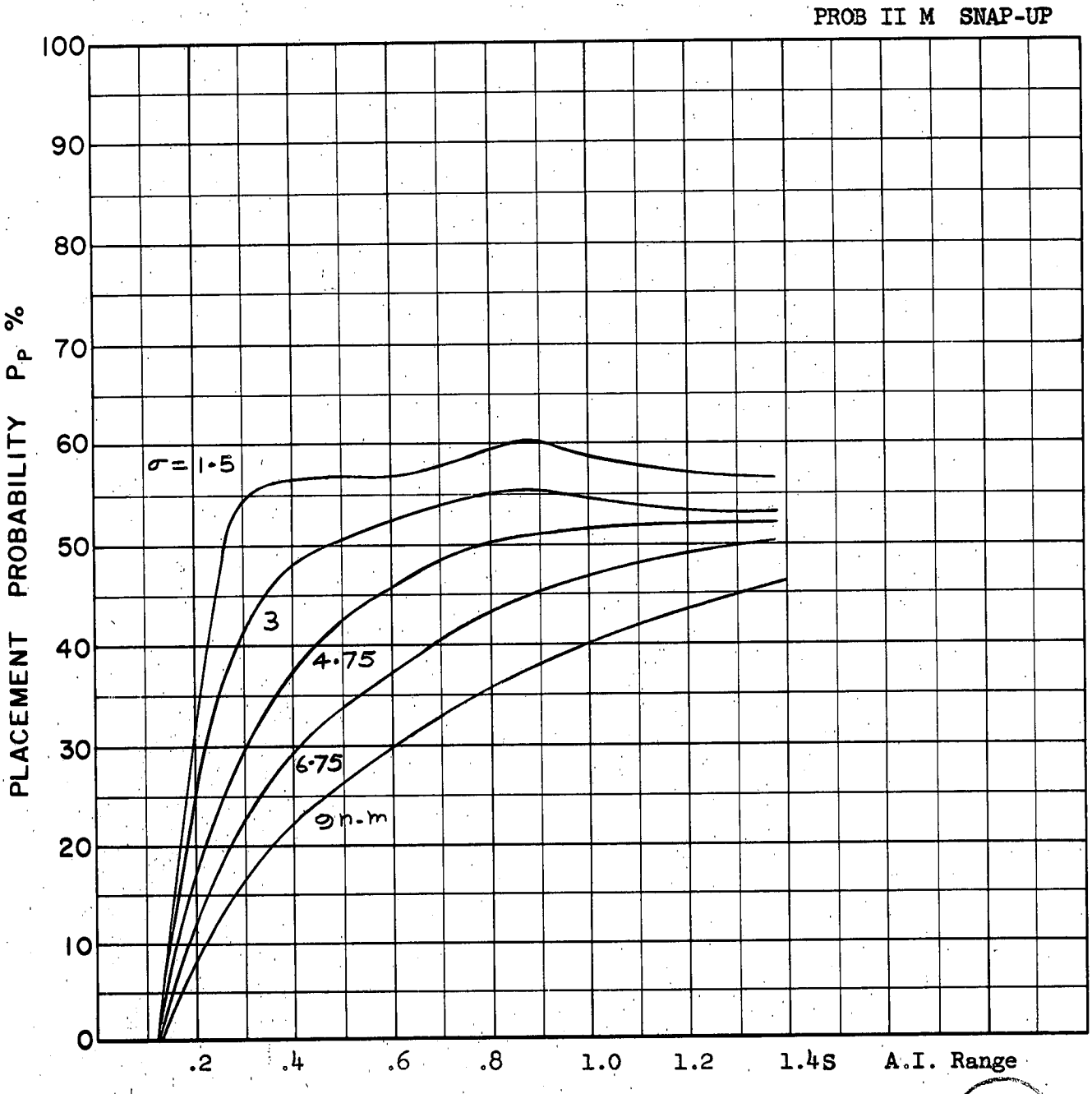

A-18

COURSE DIFFERENCE: 75°
TARGET EVASION: 0
TARGET MACH NO.: 2.0
INTERCEPTOR LATERAL G's: Avro 3.3
INTERCEPTOR MACH NO.: 2.0
σ OF G.C.I. ACCURACY: 5 Values
A.I. DETECTION RANGE AS FRACTION OF SPECIFICATION RANGE, S: Abscissa
A.I. DETECTION RANGE CONTOUR: Delta
ALTITUDE: H_t = 60 K
H_{fo} = 50 K

PROB II N

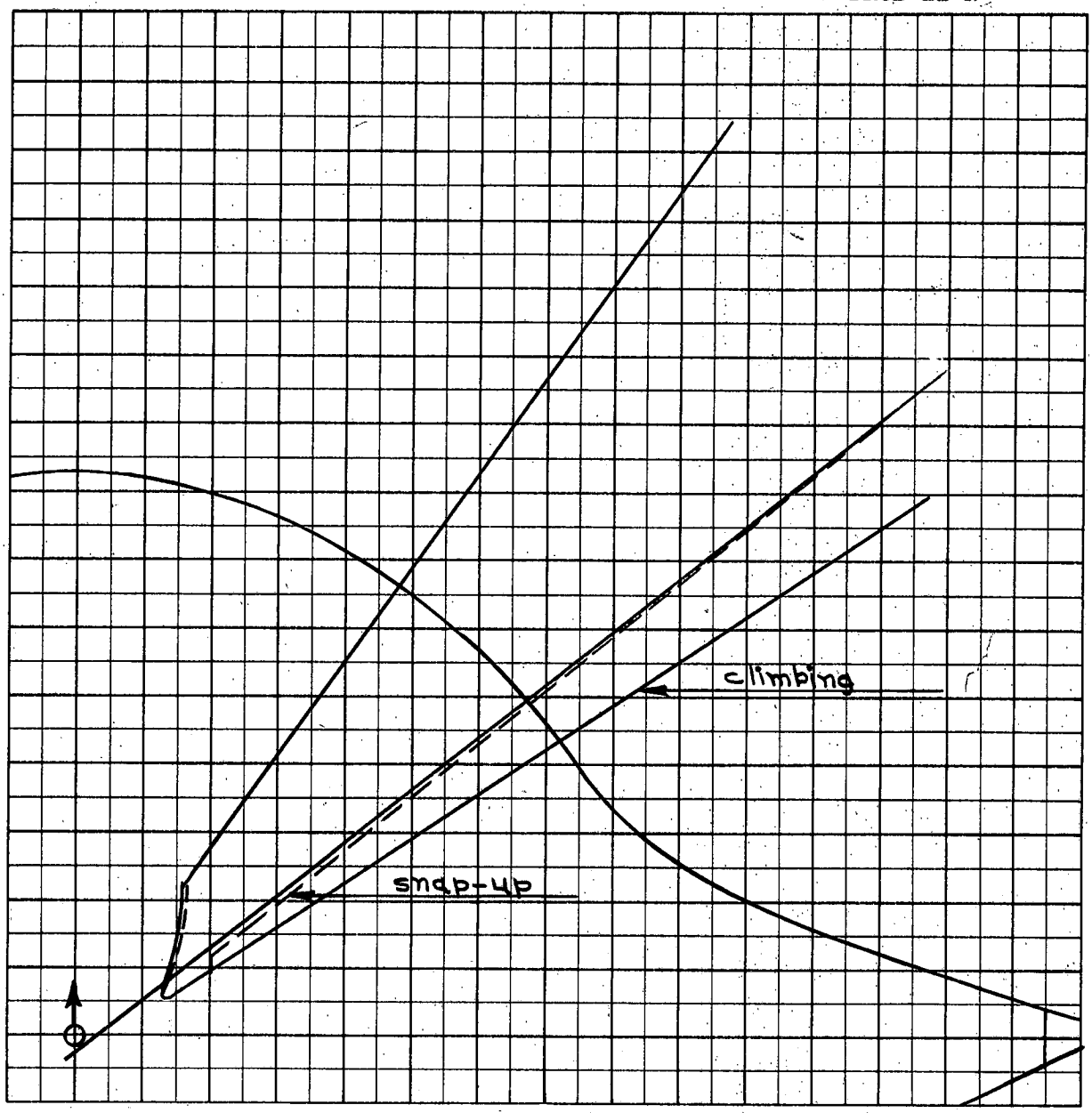

Scale 25,000 ft/cm

A-19

M_f = 2.0

h_t = 60 K

M_{fo} = 2.0

$h_{fo\ N}$ = 40 K

Γ_o = 75°

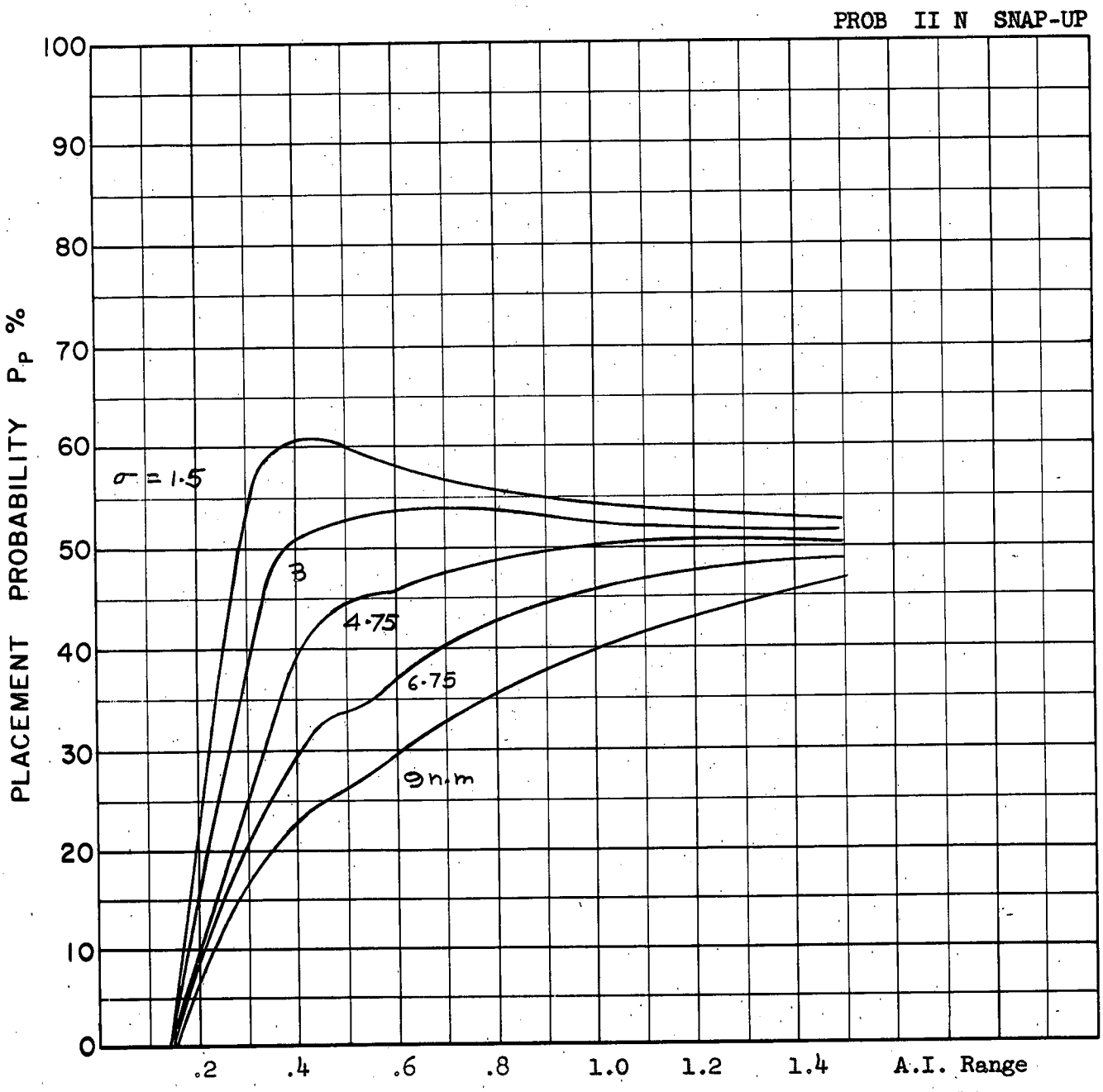

A-20

COURSE DIFFERENCE: 75°
TARGET EVASION: 0
TARGET MACH NO.: 2.0
INTERCEPTOR LATERAL G's: Avro 3.3
INTERCEPTOR MACH NO.: 2.0
σ OF G.C.I. ACCURACY: 5 Values
A.I. DETECTION RANGE AS FRACTION OF SPECIFICATION RANGE, S: Abscissa
A.I. DETECTION RANGE CONTOUR: Delta
ALTITUDE: H_t = 60 K
H_{fo} = 40 K

PROB III ABC CLIMBING

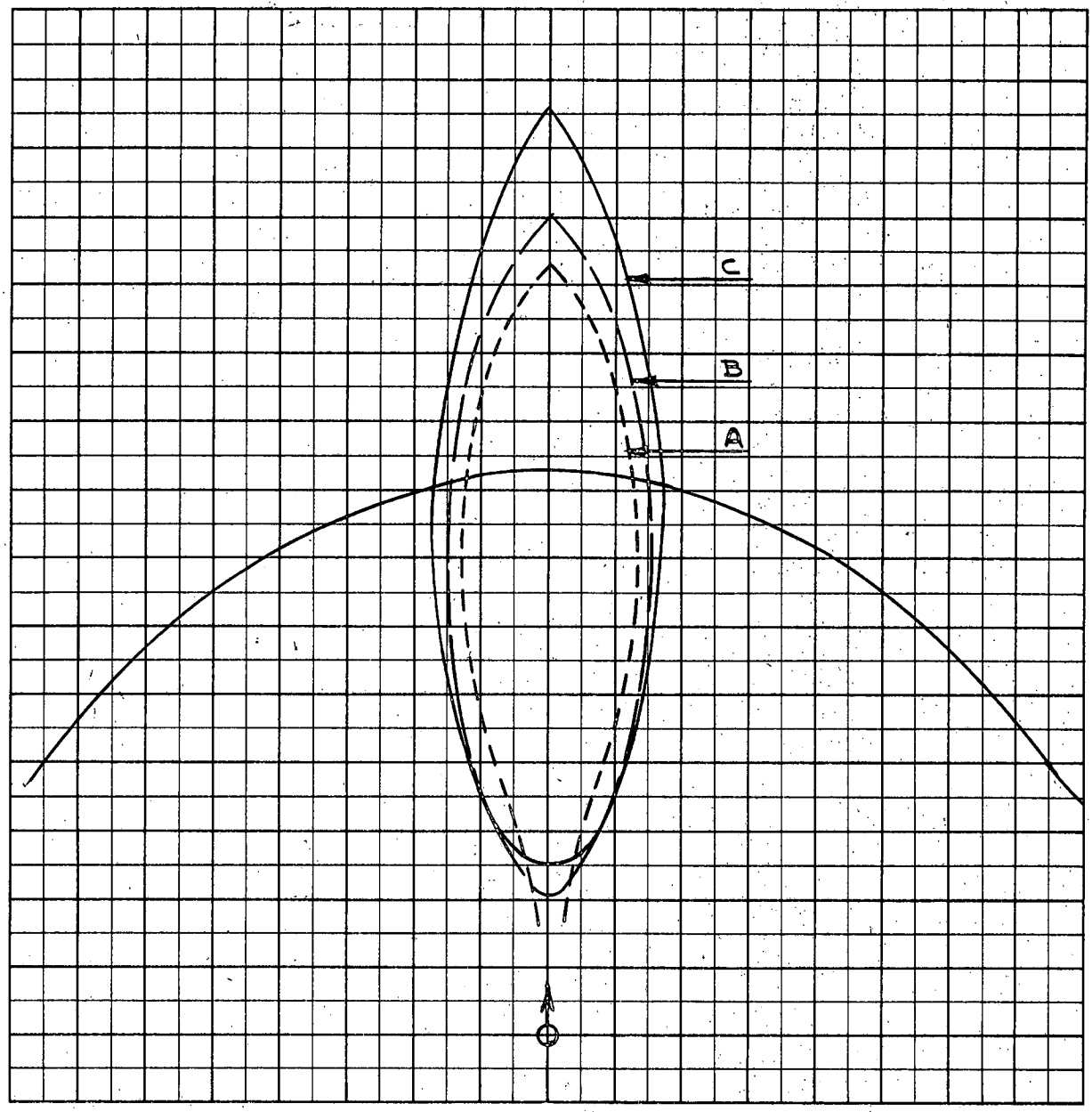

Scale 25,000 ft/cm

A-21

M_t = 2.0
h_t = 60 K
M_{fo} = 2.0
h_{fo} A = 60 K
B = 50 K
C = 40 K
$V_t R_t$ = 0.75 g
Γ_o = 180°

Area common to + and - evasion zones.

PROB III A COALTITUDE

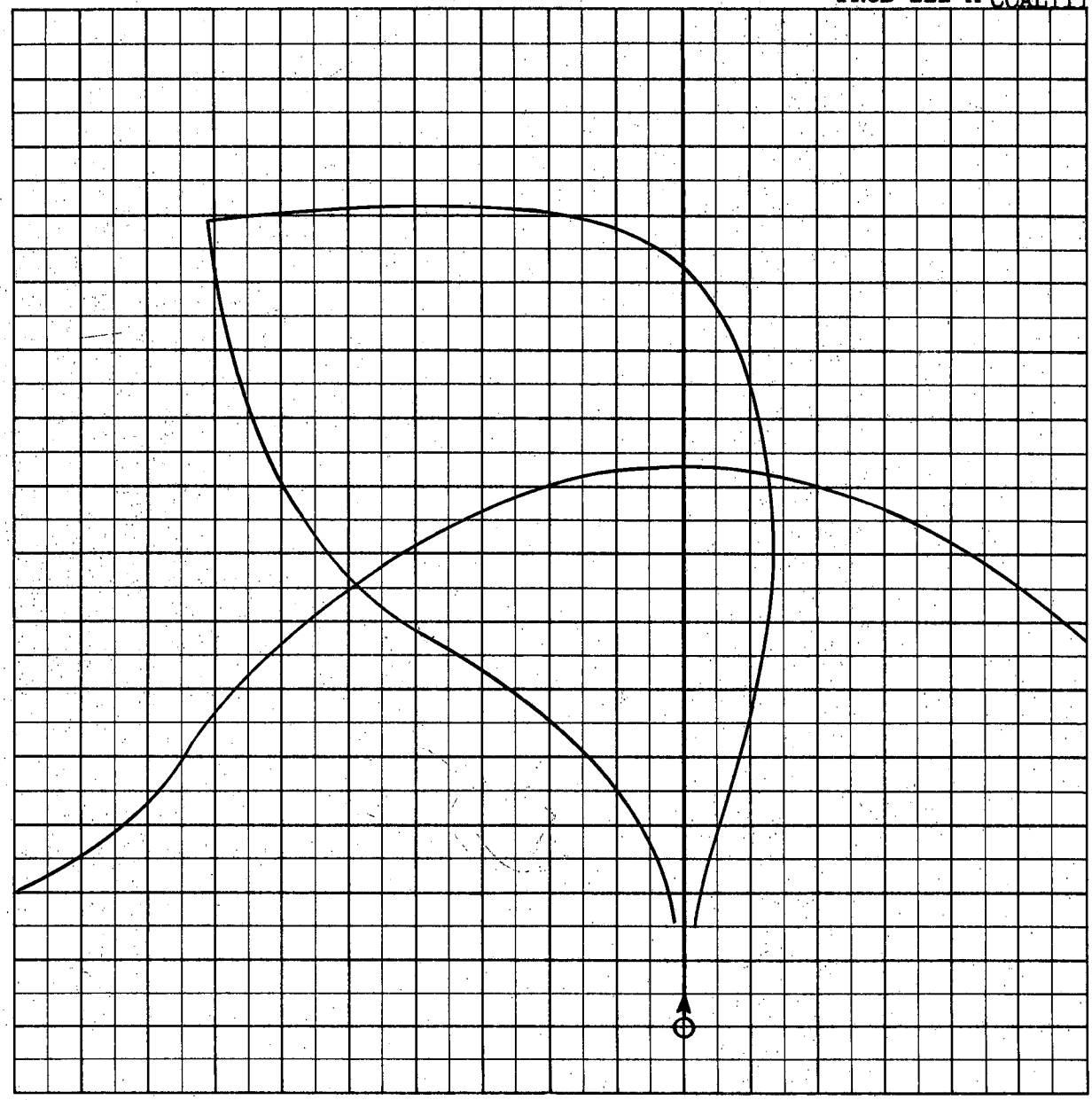

Scale 25,000 ft/cm

A-22

M_t = 2.0
h_t = 60 K
M_{fo} = 2.0
$h_{fo\ A}$ = 60 K
$V_t R_t$ = 0.75g
Γ_o = 180°

Target turning to the left.

PROB III B

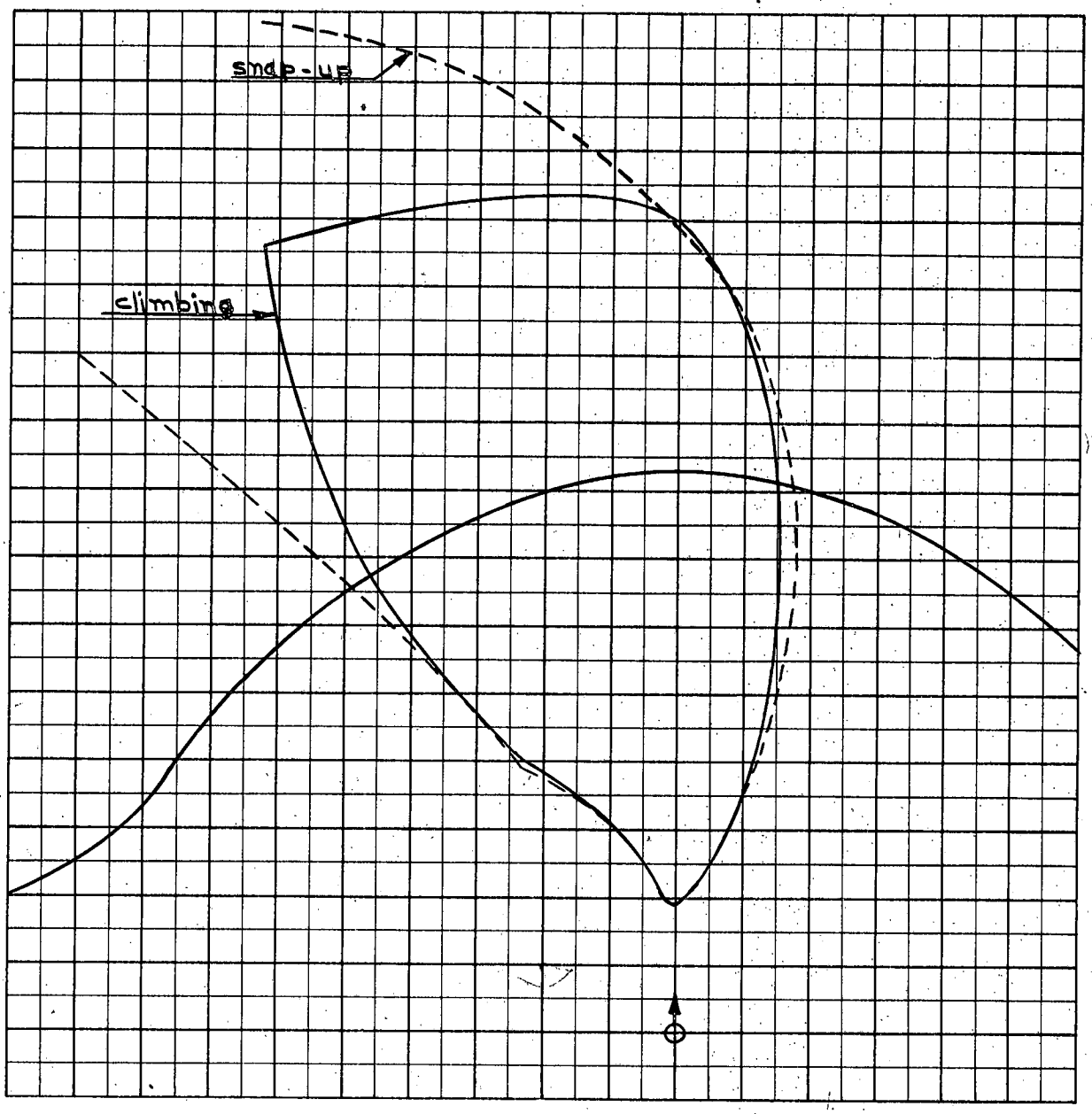

Scale 25,000 ft/cm

M_t = 2.0
h_t = 60 K
M_{fo} = 2.0
$h_{fo\ B}$ = 50 K
$V_t R_t$ = 0.75g
Γ_o = 180°

A-23

Target turning to the left.

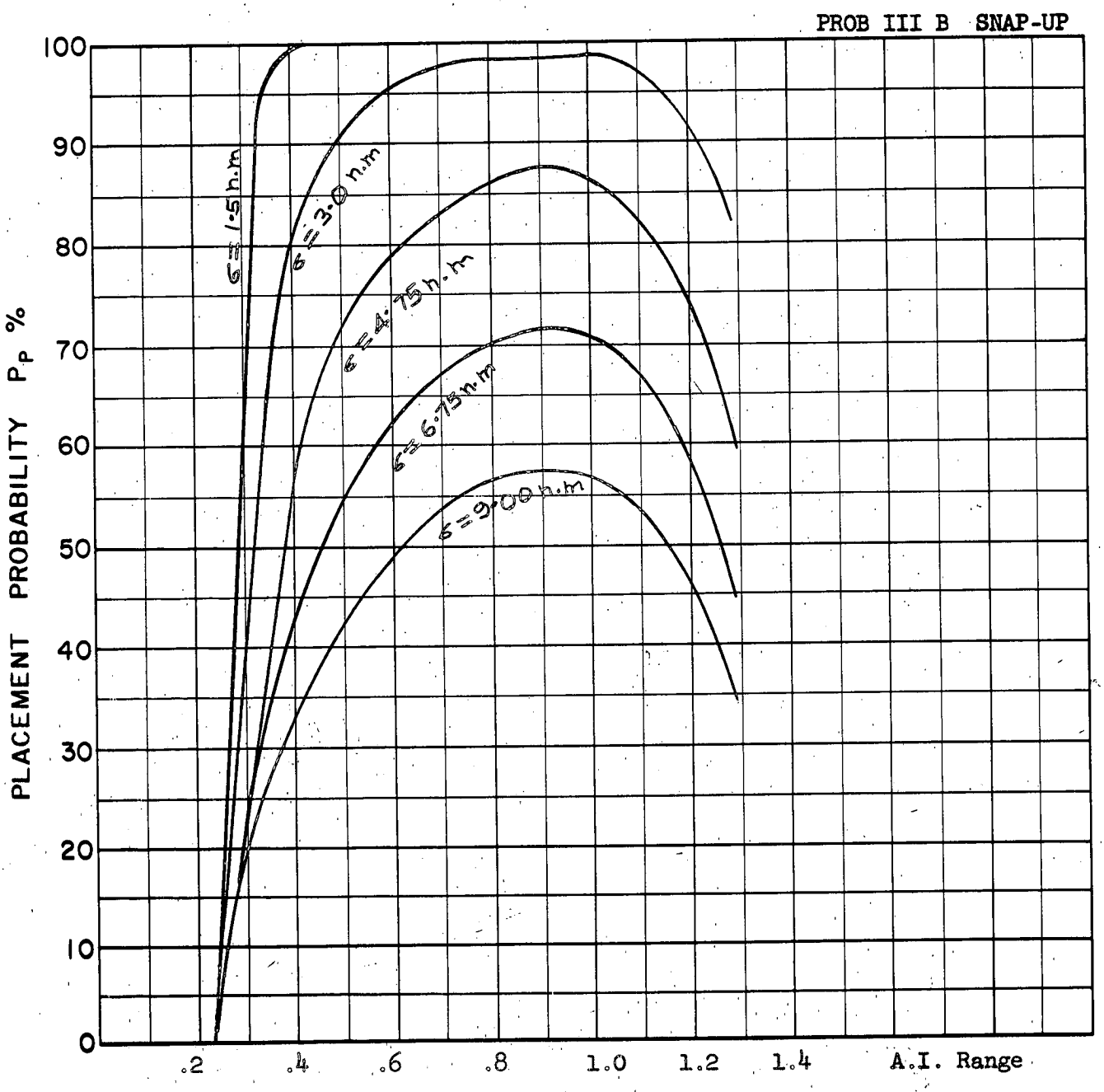

A-24

COURSE DIFFERENCE : 180°
TARGET EVASION : 0.75g lateral
TARGET MACH NO. : 2.0
INTERCEPTOR LATERAL G's : Avro 3.3
INTERCEPTOR MACH NO. : 2.0
σ OF G.C.I. ACCURACY : 5 Values
A.I. DETECTION RANGE AS FRACTION OF SPECIFICATION RANGE, S : Abscissa
A.I. DETECTION RANGE CONTOUR : Delta
ALTITUDE : H_t = 60 K
H_{fo} = 50 K

Probability values calculated from the placement zone common to the positive and negative evasion cases.

PROB III C

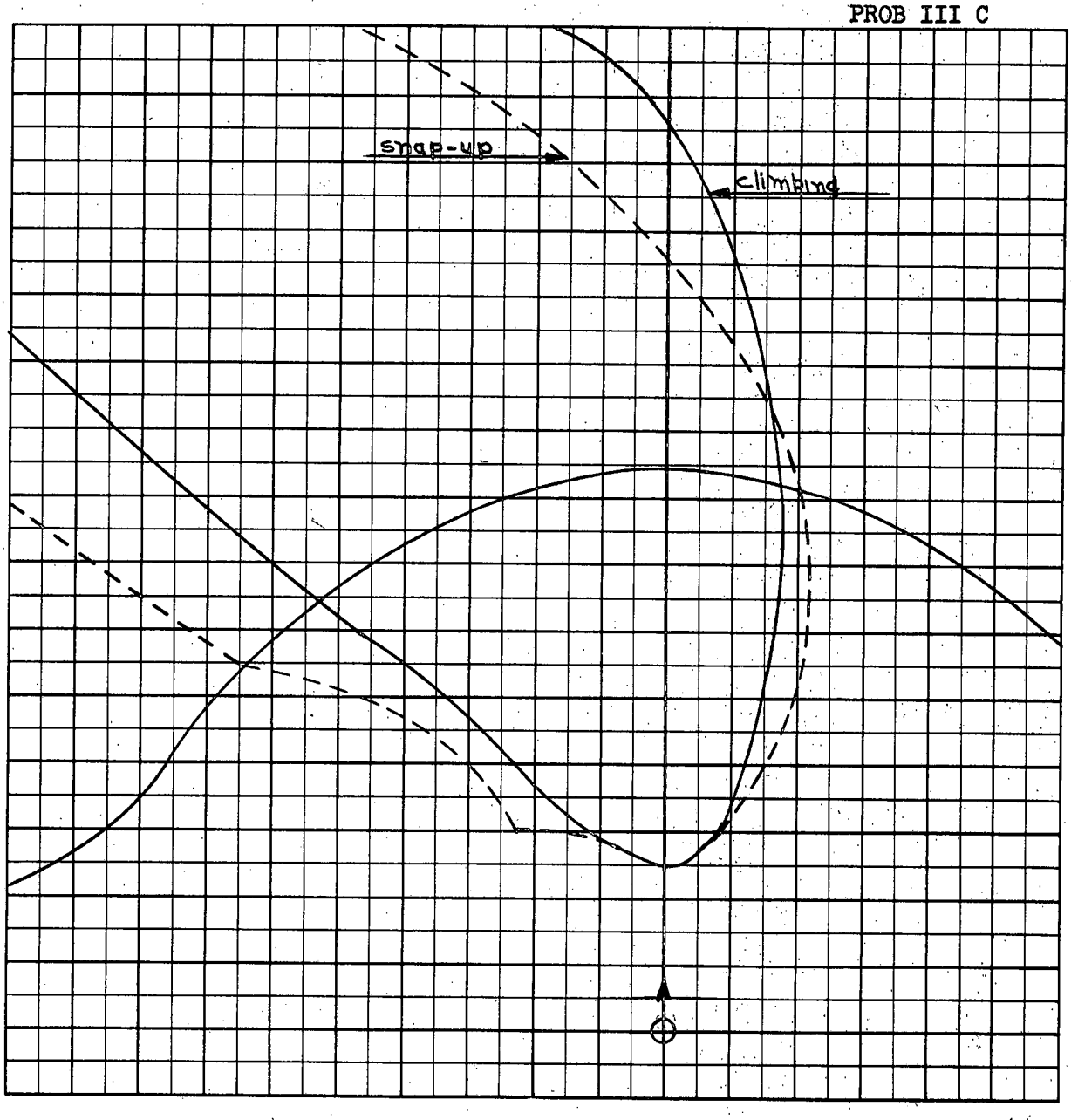

Scale 25,000 ft/cm

M_t = 2.0
h_t = 60 K
M_{fo} = 2.0
$h_{fo\ C}$ = 40 K
$V_t R_t$ = 0.75g
Γ_o = 180°

A-25

Target turning to the left.

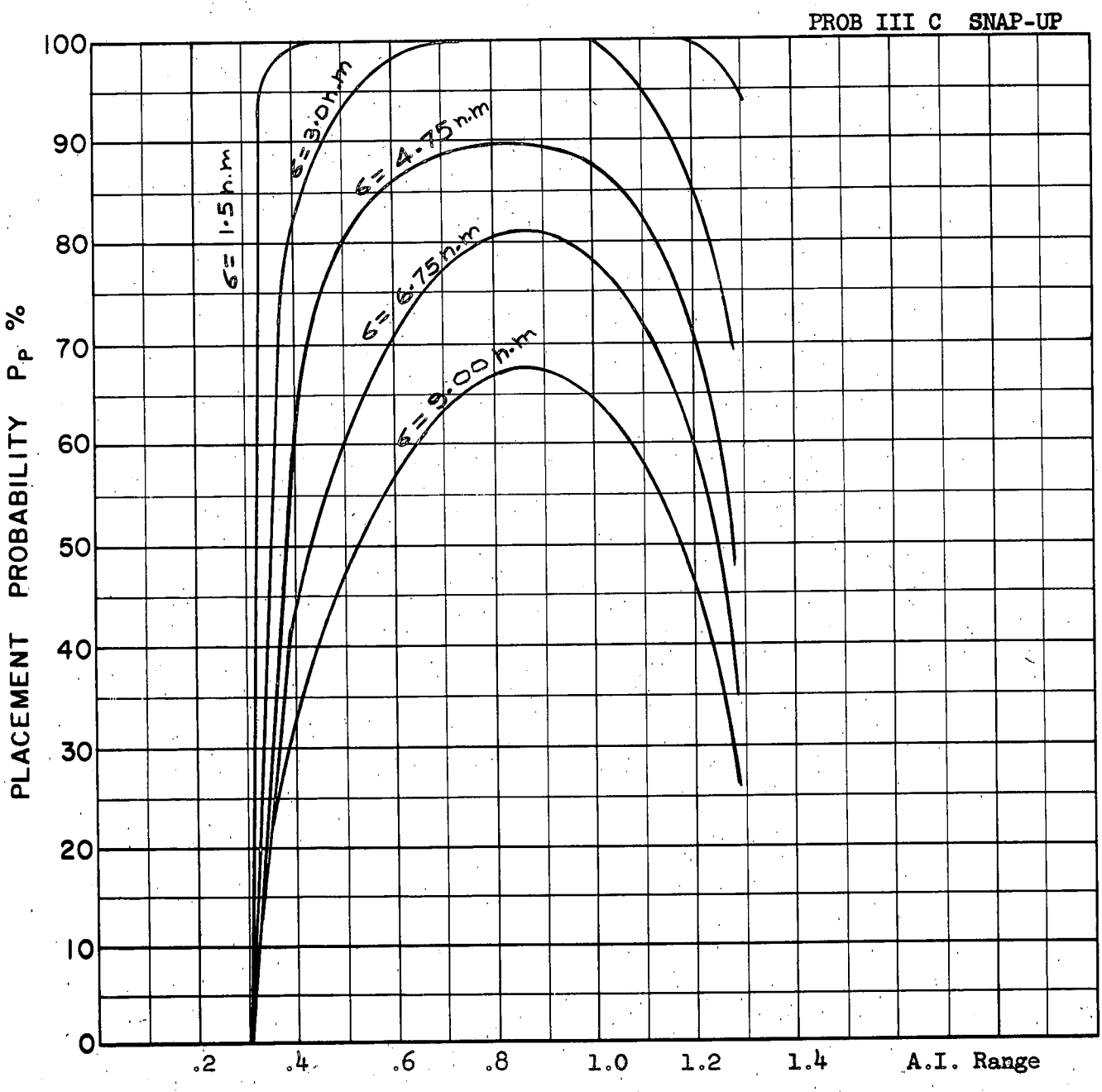

A-26

COURSE DIFFERENCE: 180°
TARGET EVASION: 0.75g
TARGET MACH NO.: 2.0
INTERCEPTOR LATERAL G's: Avro 3.3
INTERCEPTOR MACH NO.: 2.0
σ OF G.C.I. ACCURACY: 5 Values
A.I. DETECTION RANGE AS FRACTION OF SPECIFICATION RANGE, S: Abscissa
A.I. DETECTION RANGE CONTOUR: Delta
ALTITUDE: H_t = 60 K
H_{fo} = 40 K

Probability values calculated from the placement zone common to the positive and negative evasion cases.

Prob III DEF CLIMBING

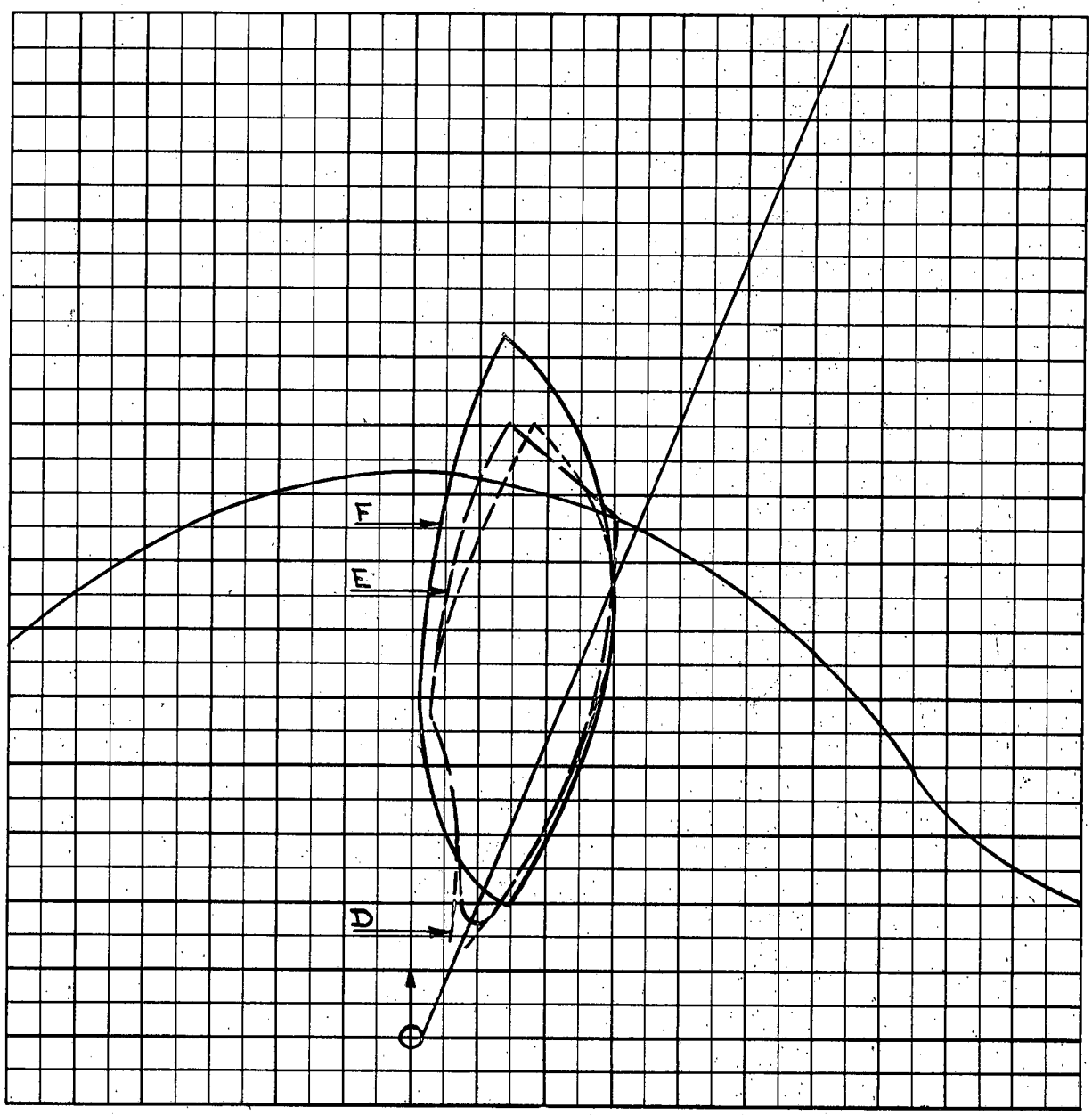

Scale 25,000 ft/cm

M_t = 2.0

h_t = 60 K

M_{fo} = 2.0

h_{fo} D = 60 K

E = 50 K

F = 40 K

$V_t R_t$ = 0.75 g

Γ_o = 135°

Area common to + and - evasion zones

A-27

PROB III D COALTITUDE

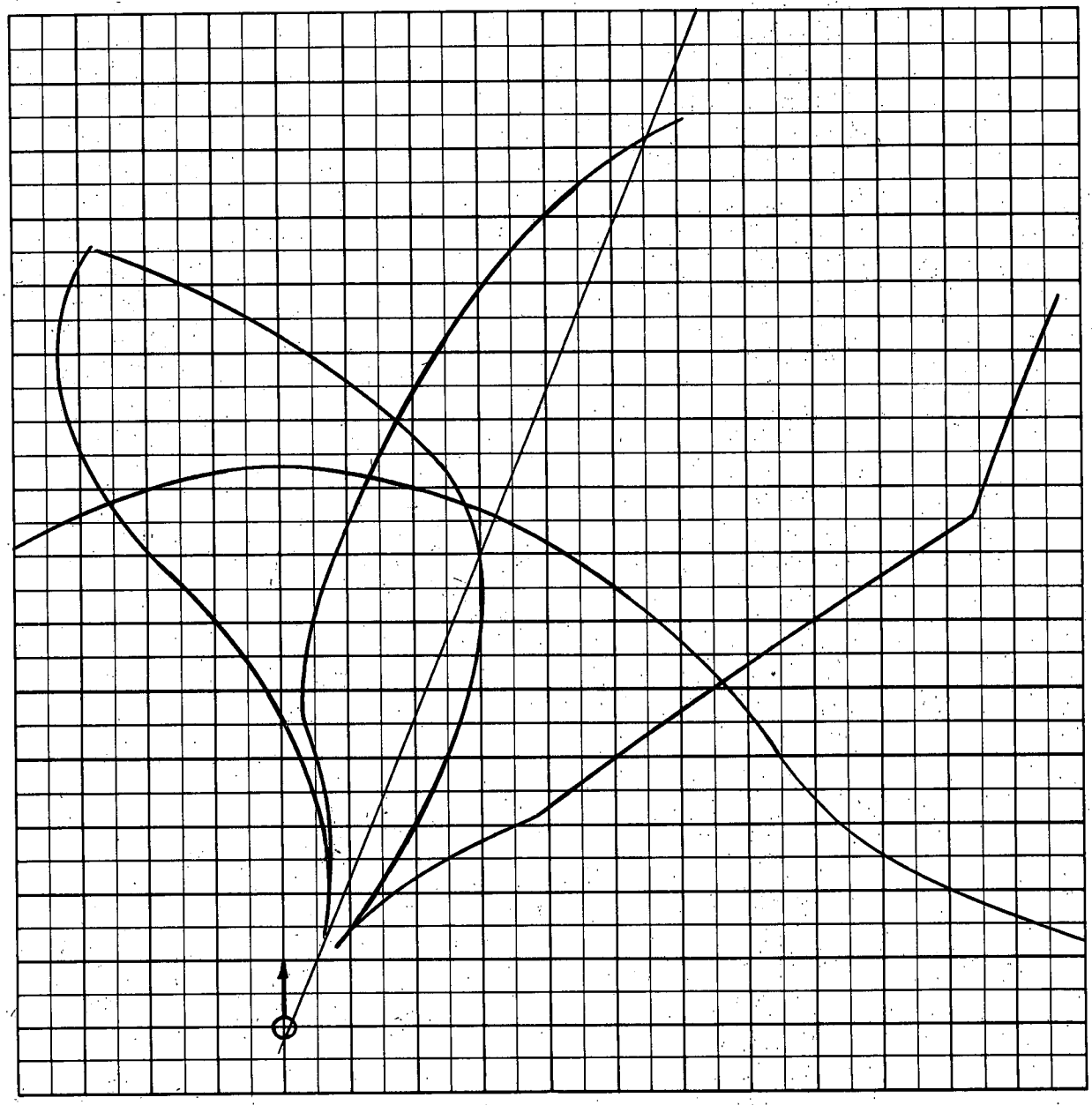

Scale 25000 ft/cm

M_t = 2.0
h_t = 60 K
M_{fo} = 2.0
$h_{fo\ D}$ = 60 K
$V_t R_t$ = 0.75 g
Γ_o = 135°

A-28

Zones for target turns to the left and right both shown.

PROB III E

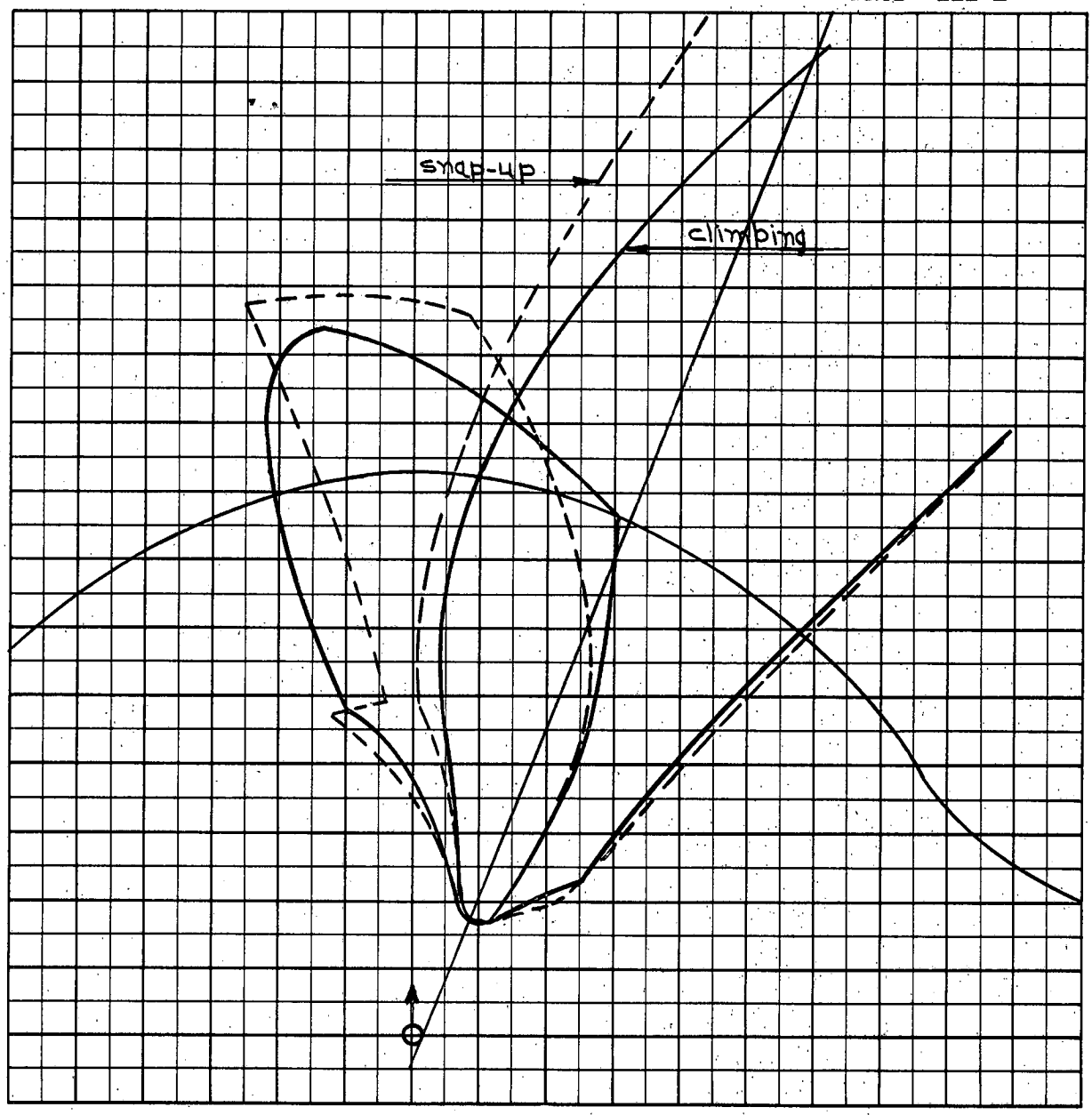

Scale 25,000 ft/cm

M_t = 2.0
h_t = 60 K
M_{fo} = 2.0
$h_{fo\ E}$ = 50 K
$V_t R_t$ = 0.75g
Γ_o = 135°

A-29

Zones for target turns to the left and right both shown.

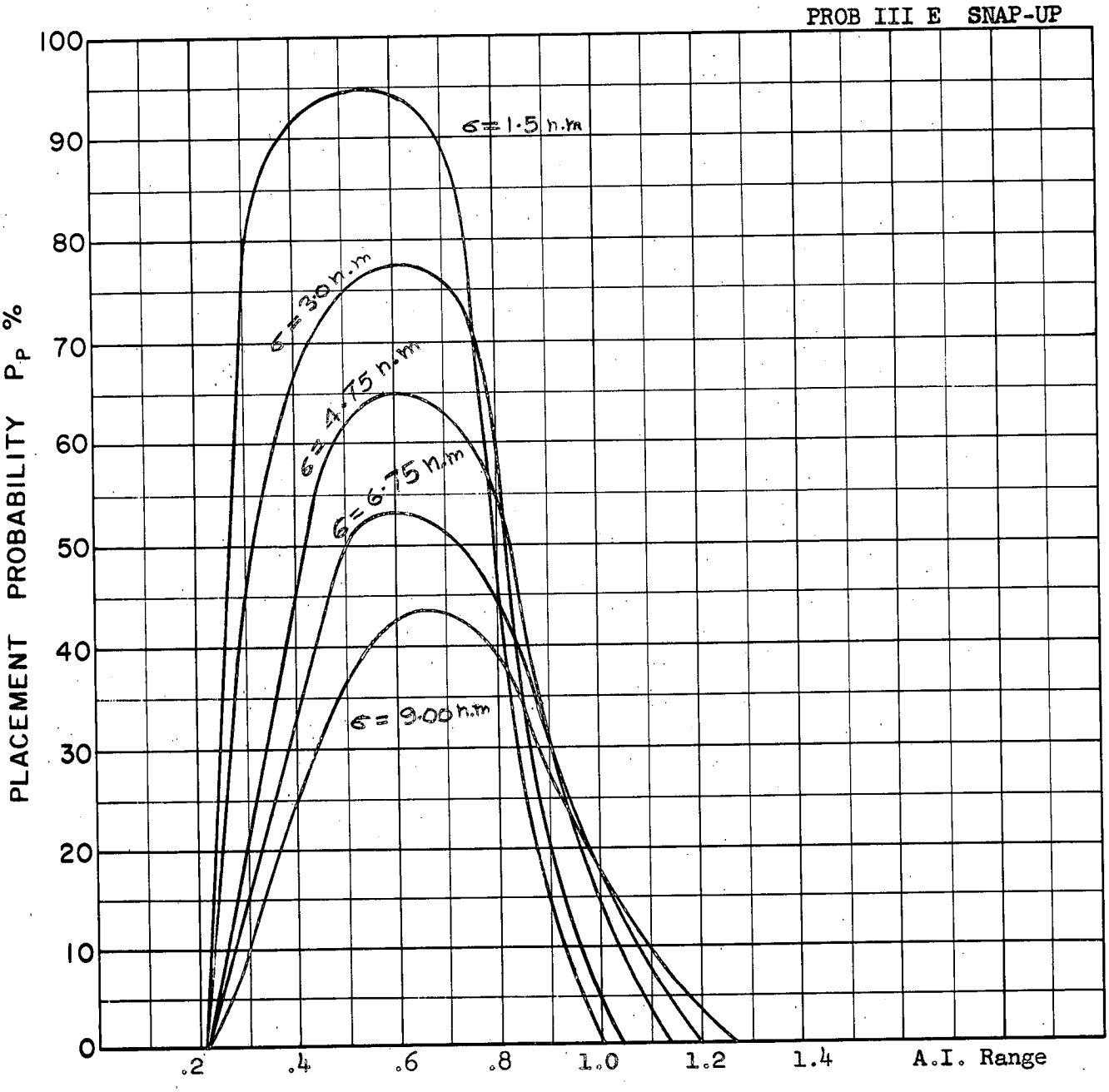

A-30

COURSE DIFFERENCE: 135°
TARGET EVASION: 0.75g
TARGET MACH NO.: 2.0
INTERCEPTOR LATERAL G's: Avro 3.3
INTERCEPTOR MACH NO.: 2.0
σ OF G.C.I. ACCURACY: 5 Values
A.I. DETECTION RANGE AS FRACTION OF SPECIFICATION RANGE, S: Abscissa
A.I. DETECTION RANGE CONTOUR: Delta
ALTITUDE: H_t = 60 K
H_f = 50 K

Probability values calculated from the placement zone common to the positive and negative evasion cases.

PROB III F

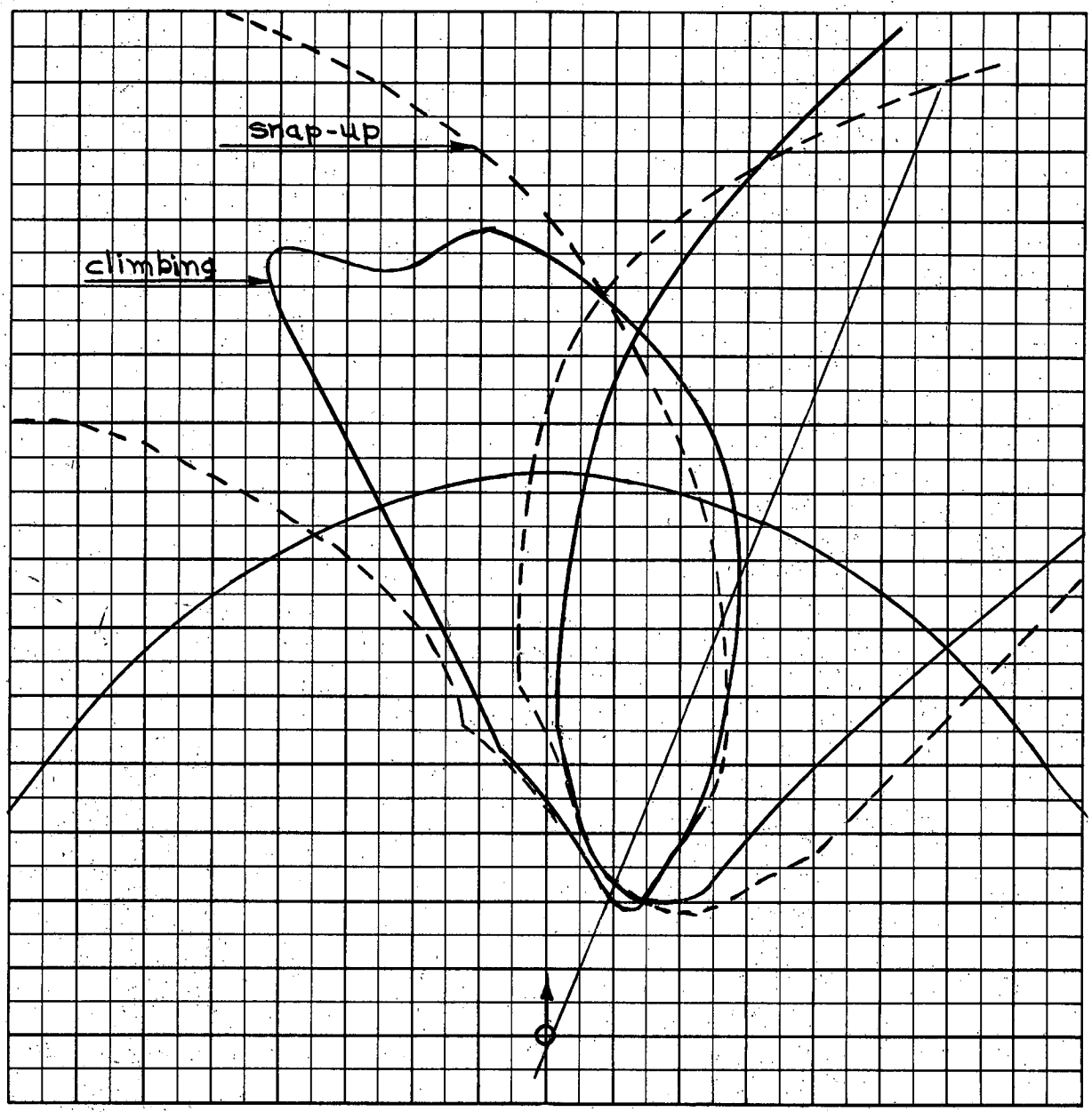

Scale 25,000 ft/cm

M_t = 2.0
h_t = 60 K
M_{fo} = 2.0
$h_{fo\ F}$ = 40 K
$V_t R_t$ = 0.75 g
= 135°

A-31

Zones for target turns to the left and right both shown.

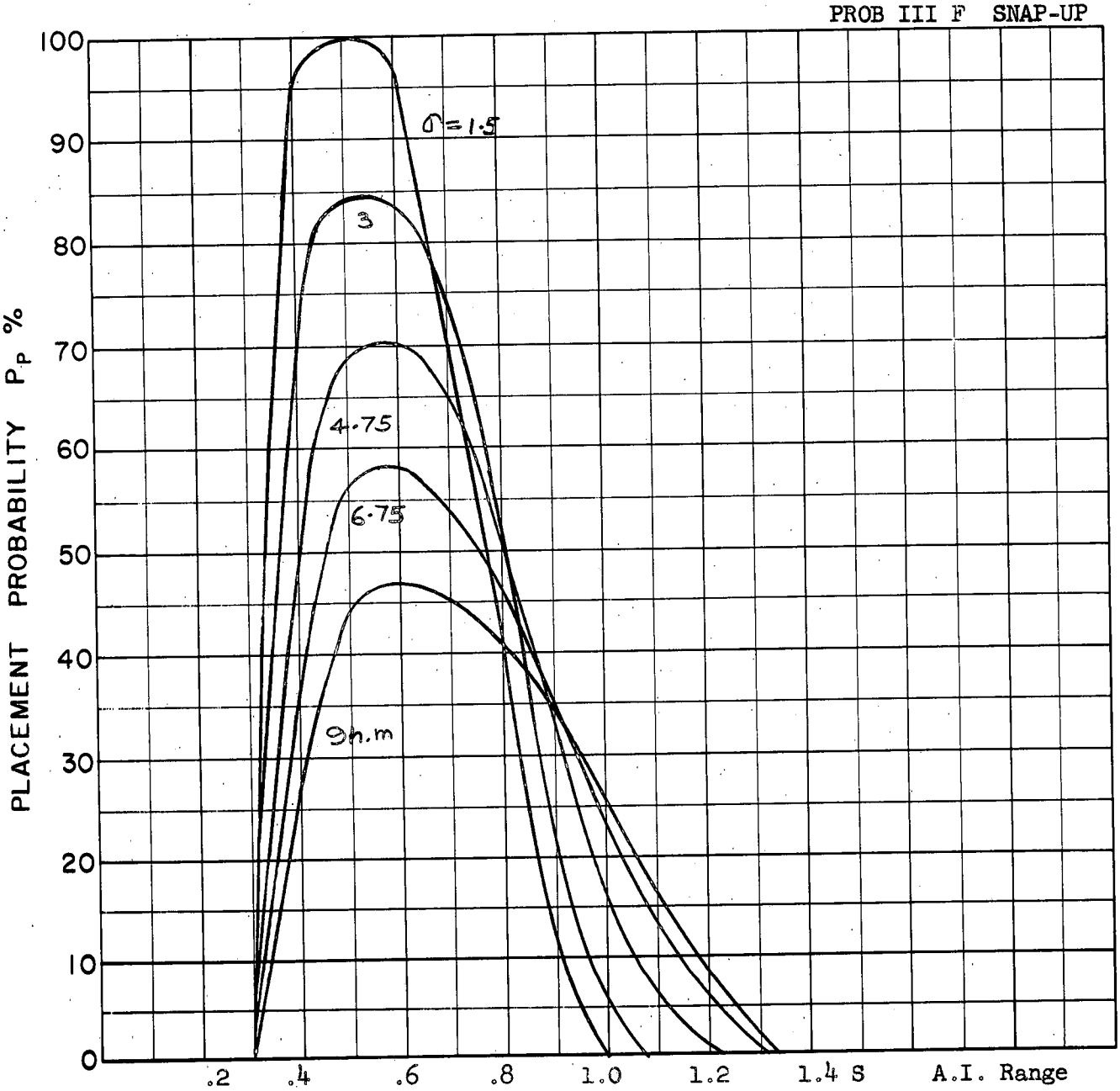

A-32

COURSE DIFFERENCE: 135°
TARGET EVASION: 1.25g Load Factor
TARGET MACH NO.: 2.0
INTERCEPTOR LATERAL G's: Avro 3.3
INTERCEPTOR MACH NO.: 2.0
σ OF G.C.I. ACCURACY: 5 Values
A.I. DETECTION RANGE AS FRACTION OF SPECIFICATION RANGE, S: Abscissa
A.I. DETECTION RANGE CONTOUR: Delta
ALTITUDE: H_t = 60 K
H_{fo} = 40 K

Probability values calculated from the placement zone common to the positive and negative evasion cases.

PROB III GHK CLIMBING

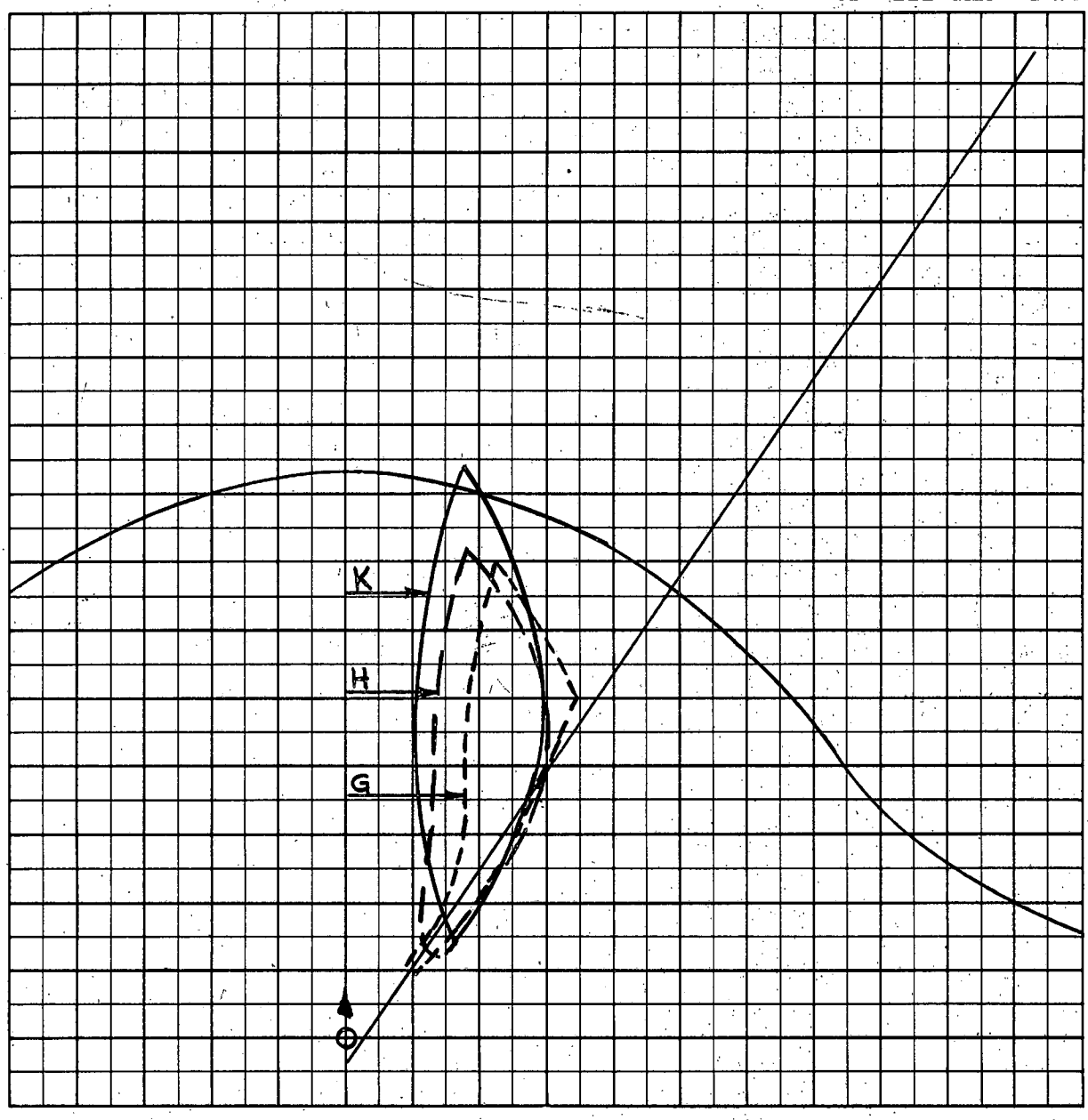

Scale 25,000 ft/cm

M_t = 2.0
h_t = 60 K
M_{fo} = 2.0
h_{fo} G = 60 K
H = 50 K
K = 40 K
V_tR_t = 0.75 g
= 110°

Area common to + and - evasion zones.

A-33

PROB III G COALTITUDE

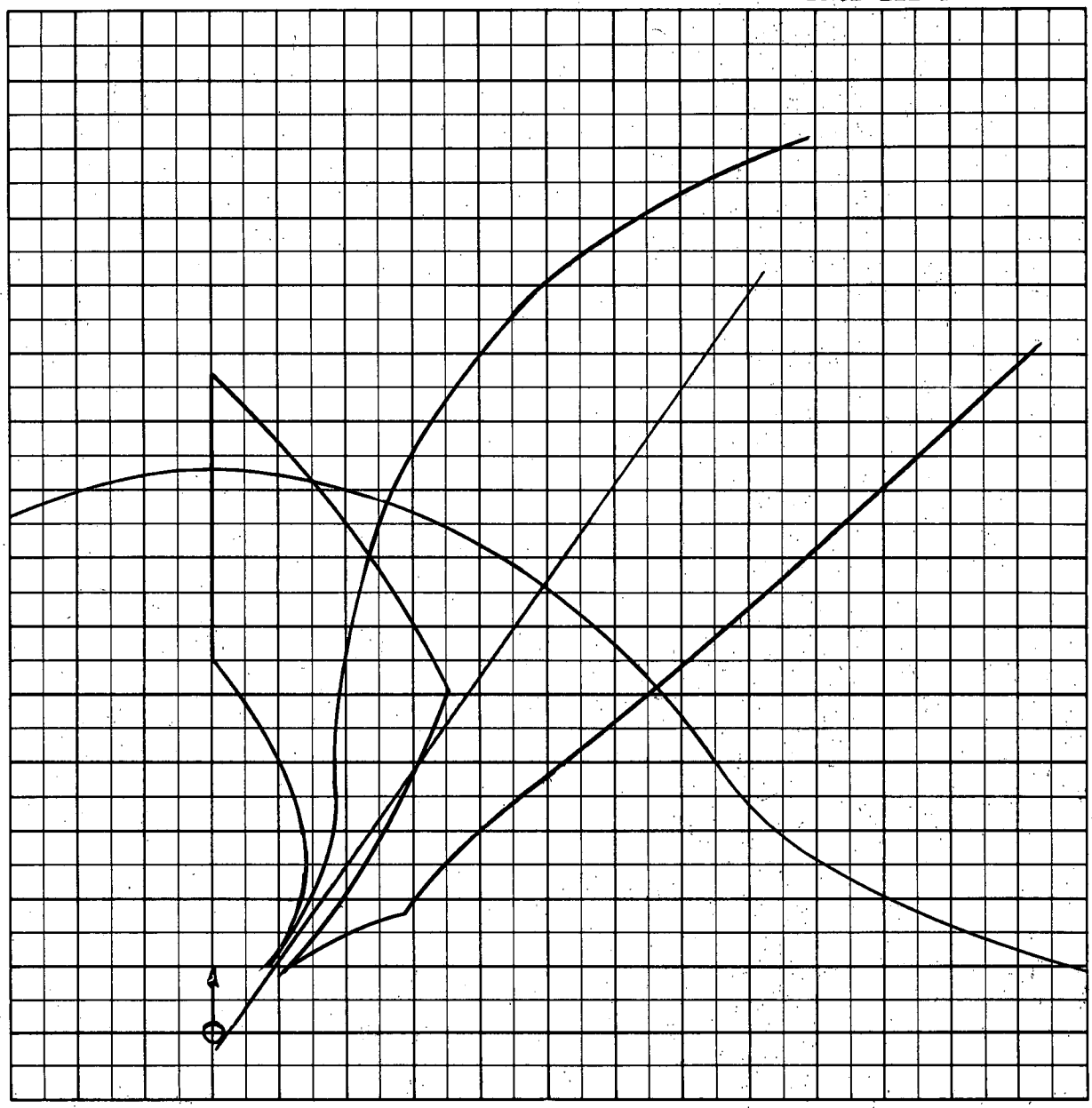

Scale 25000 ft/cm

M_t = 2.0
h_t = 60 K
M_{fo} = 2.0
$h_{fo\ G}$ = 60 K
$V_t R_t$ = 0.75 g
Γ_o = 110°

A-34

Zones for target turns to the left and right both shown.

PROB III H

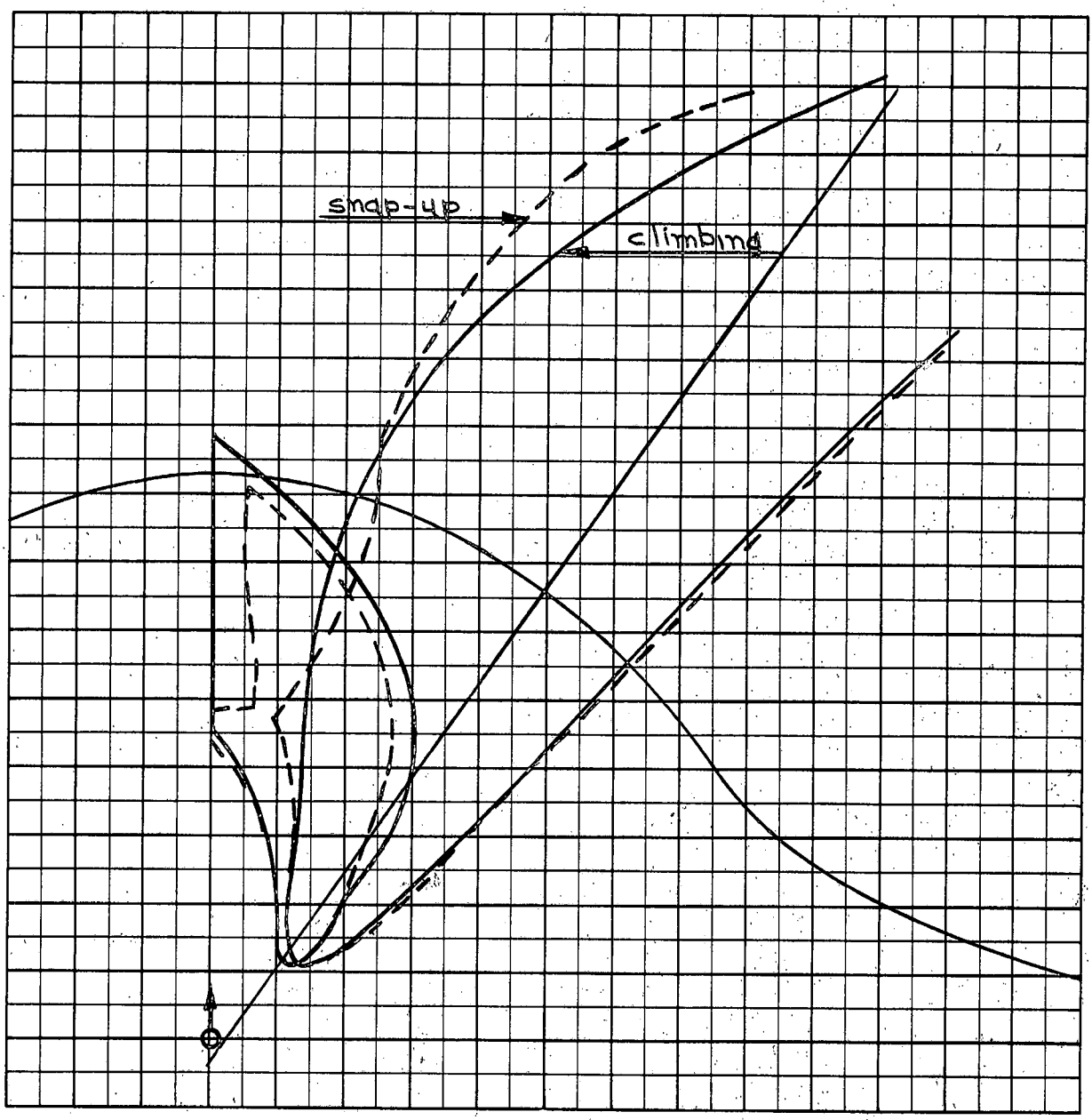

Scale 25000 ft/cm

M_t = 2.0
h_t = 60 K
M_{fo} = 2.0
$h_{fo\ H}$ = 50 K
$V_t R_t$ = 0.75 g
= 110°

A-35

Zones for target turns to the left and right both shown.

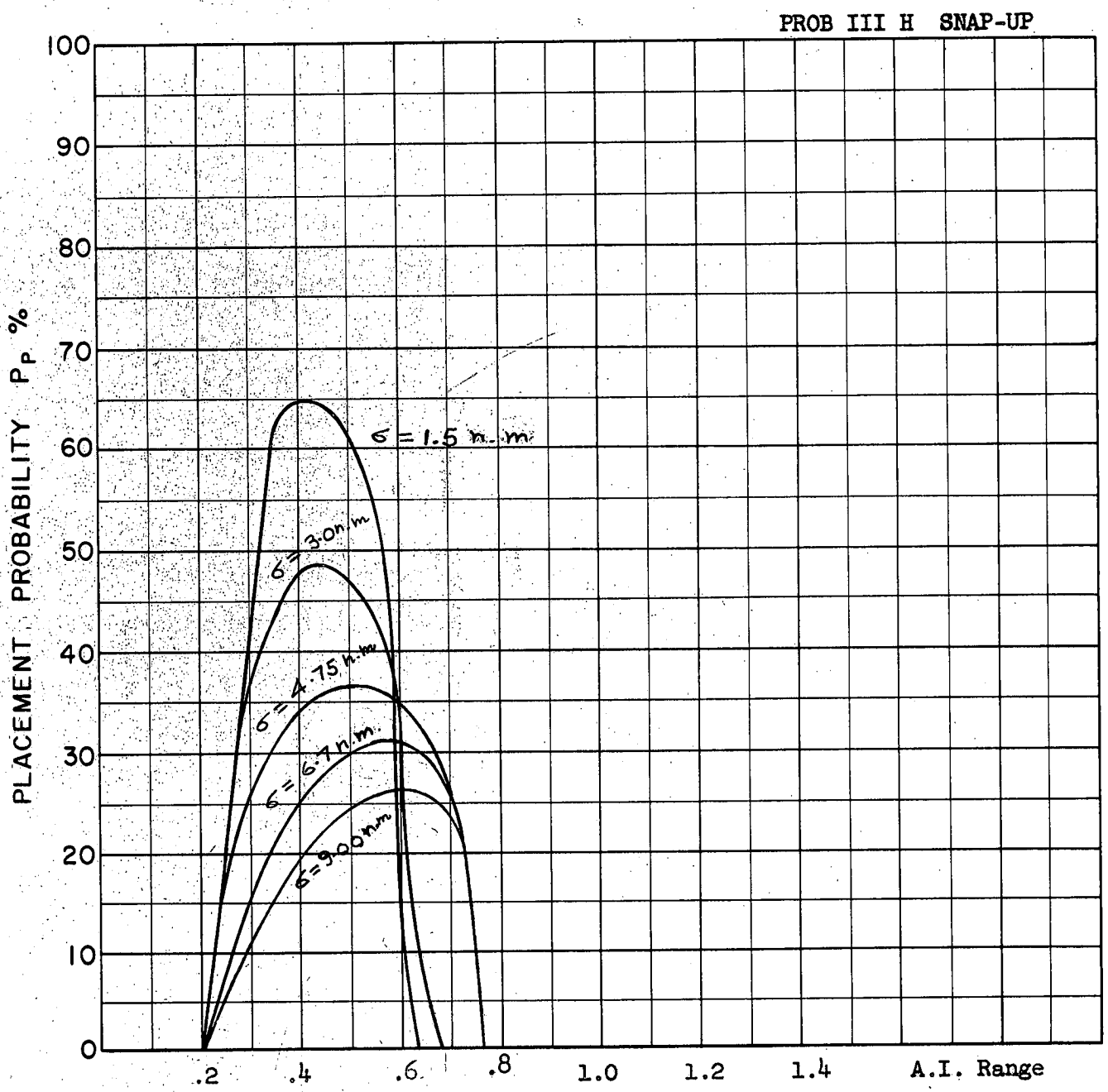

A-36

COURSE DIFFERENCE: 110°
TARGET EVASION: 0.75g
TARGET MACH NO.: 2.0
INTERCEPTOR LATERAL G's: Avro 3.3
INTERCEPTOR MACH NO.: 2.0
σ OF G.C.I. ACCURACY: 5 Values
A.I. DETECTION RANGE AS FRACTION OF SPECIFICATION RANGE, S: Abscissa
A.I. DETECTION RANGE CONTOUR: Delta
ALTITUDE: H_t = 60 K
H_{fo} = 50 K

Probability values calculated from the placement zone common to the positive and negative evasion cases.

PROB III K

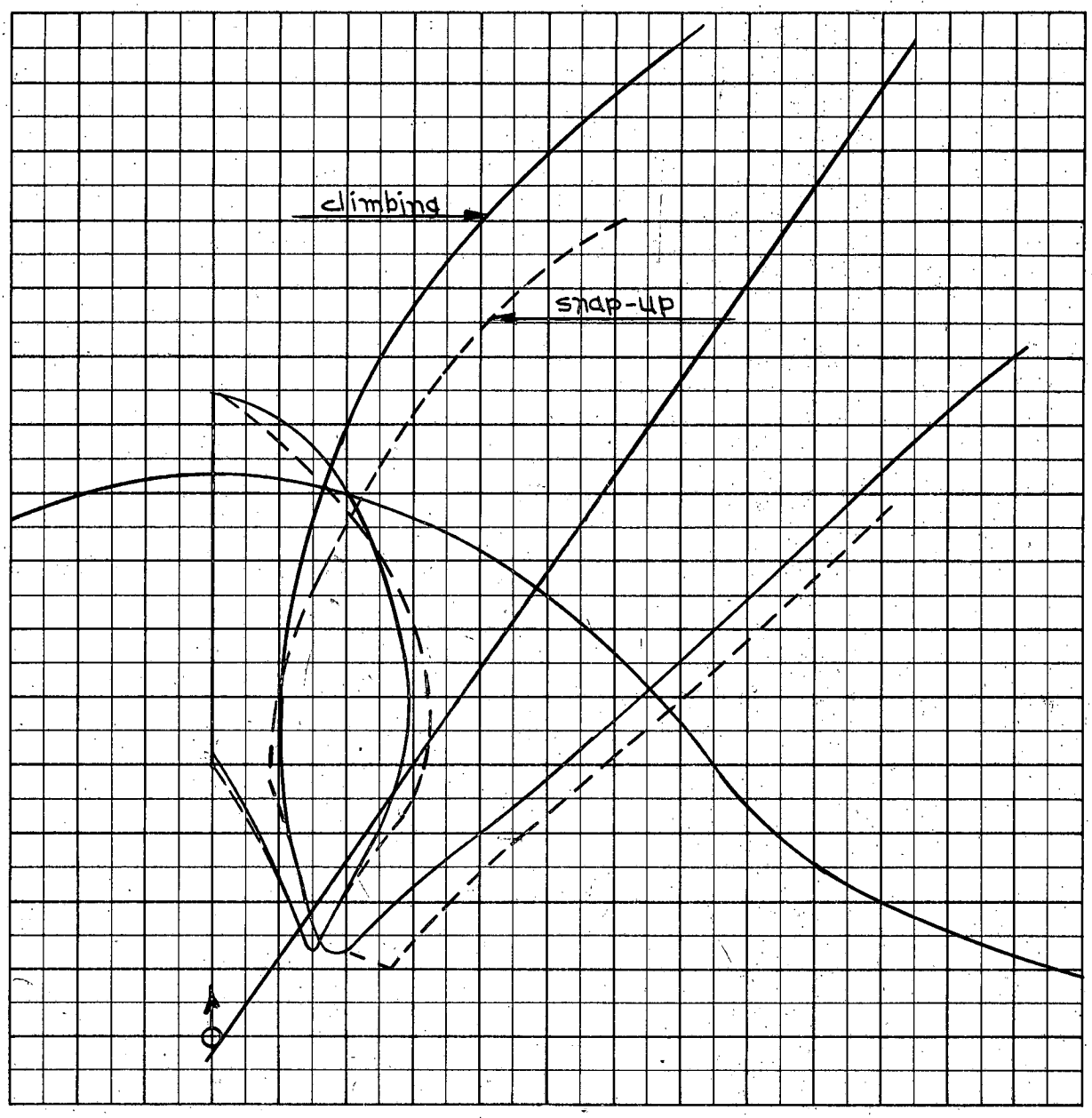

Scale 25,000 ft/cm

M_t = 2.0
h_t = 60 K
M_{fo} = 2.0
$h_{fo\ K}$ = 40 K
$V_t R_t$ = 0.75 g
Γ_o = 110°

A-37

Zones for target turns to the left and right both shown.

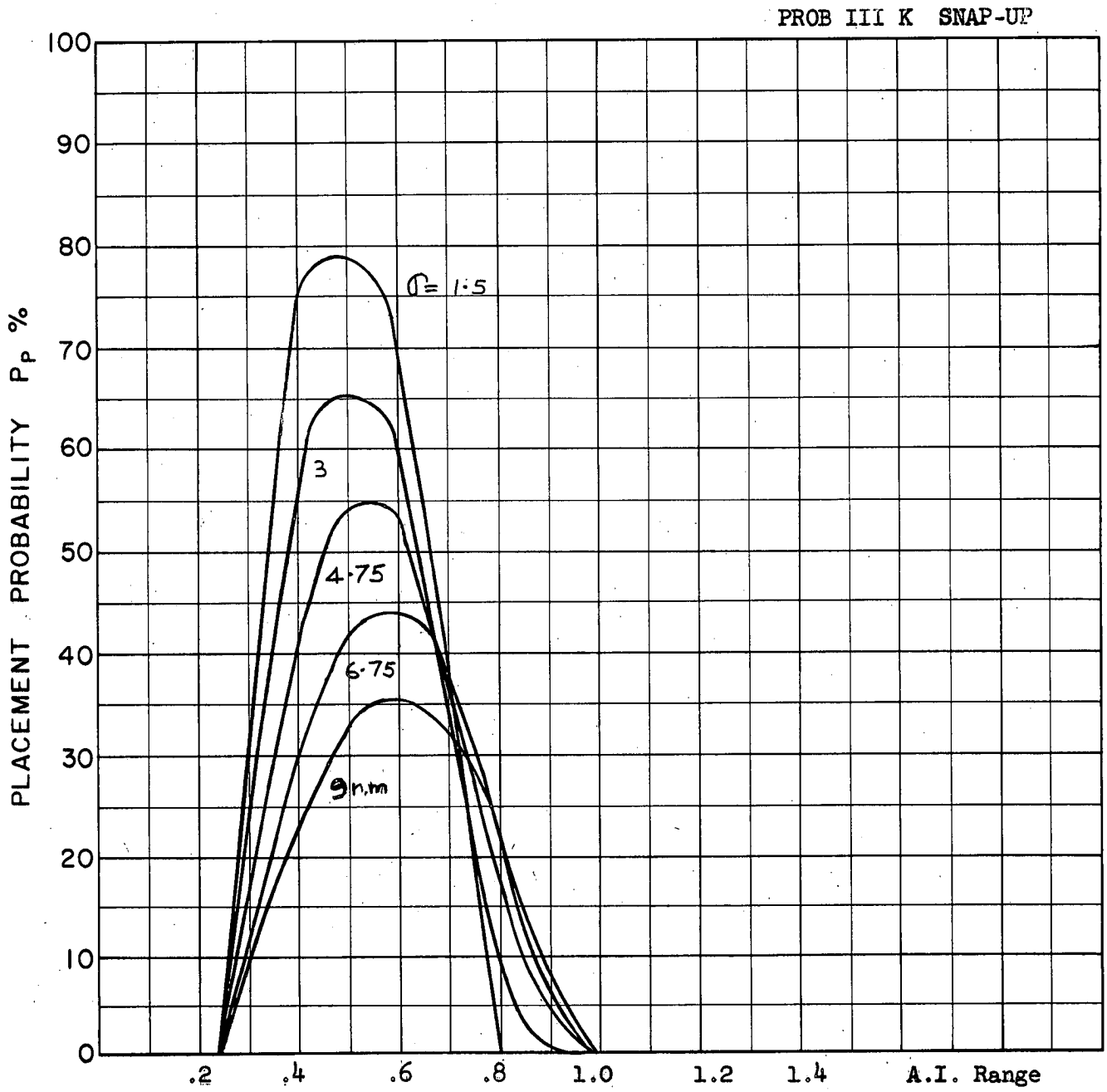

A-38

COURSE DIFFERENCE: 110°
TARGET EVASION: 1.25g Load Factor
TARGET MACH NO.: 2.0
INTERCEPTOR LATERAL G's: Avro 3.3
INTERCEPTOR MACH NO.: 2.0
σ OF G.C.I. ACCURACY: 5 Values
A.I. DETECTION RANGE AS FRACTION OF SPECIFICATION RANGE, S: Abscissa
A.I. DETECTION RANGE CONTOUR: Delta
ALTITUDE: H_t = 60 K
H_{fo} = 40 K

Probability values calculated from the placement zone common to the positive and negative evasion cases.

PROB III LMN CLIMBING

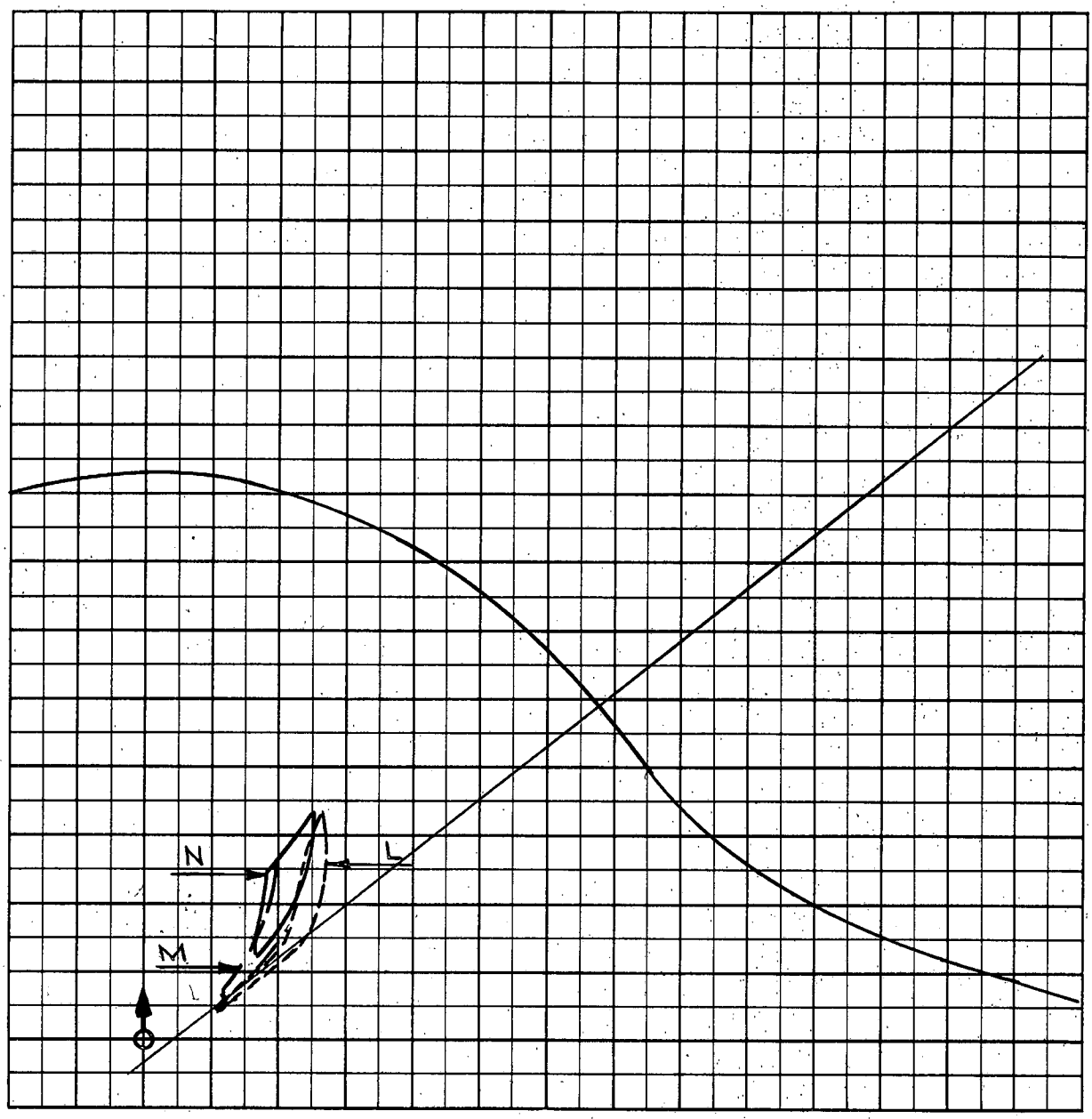

Scale 25,000 ft/cm

M_t = 2.0
h_t = 60 K
M_{fo} = 2.0
h_{fo} L = 60 K
M = 50 K
N = 40 K
$V_t R_t$ = 0.75 g
Γ_a = 75°

Area common to + and - evasion zones.

A-39

Placement probability values are very small for all A.I. ranges. Curves have not been down in this case.

PROB III L COALTITUDE

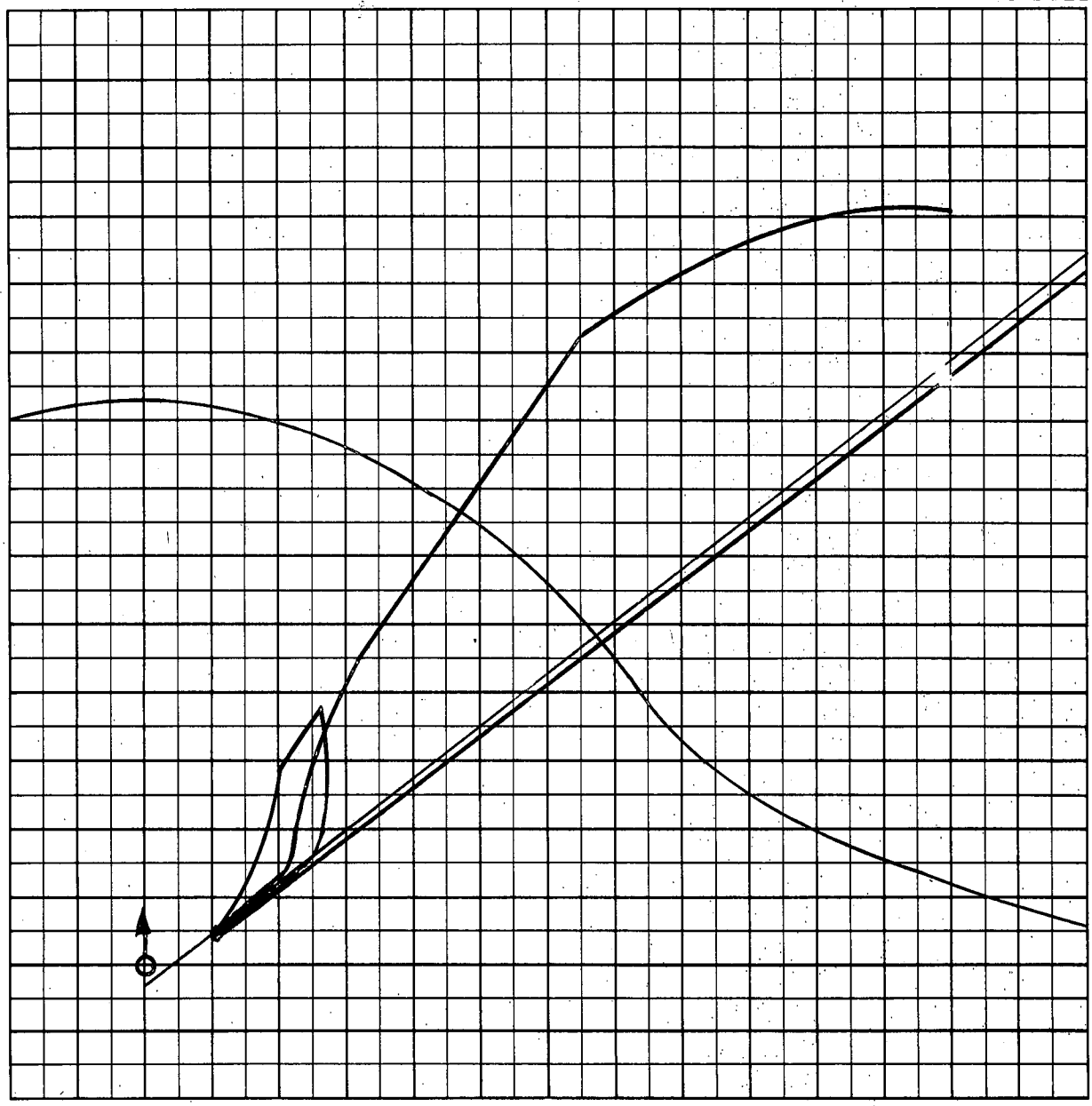

Scale 25,000 ft/cm

M_t = 2.0
h_t = 60 K
M_{fo} = 2.0
$h_{fo\ L}$ = 60 K
$V_t R_t$ = 0.75 g
Γ_o = 75°

A-40

Zones for target turns to the left and right both shown.

Placement probability values are very small for all A.I. ranges. Curves have not been down in this case.

PROB III M

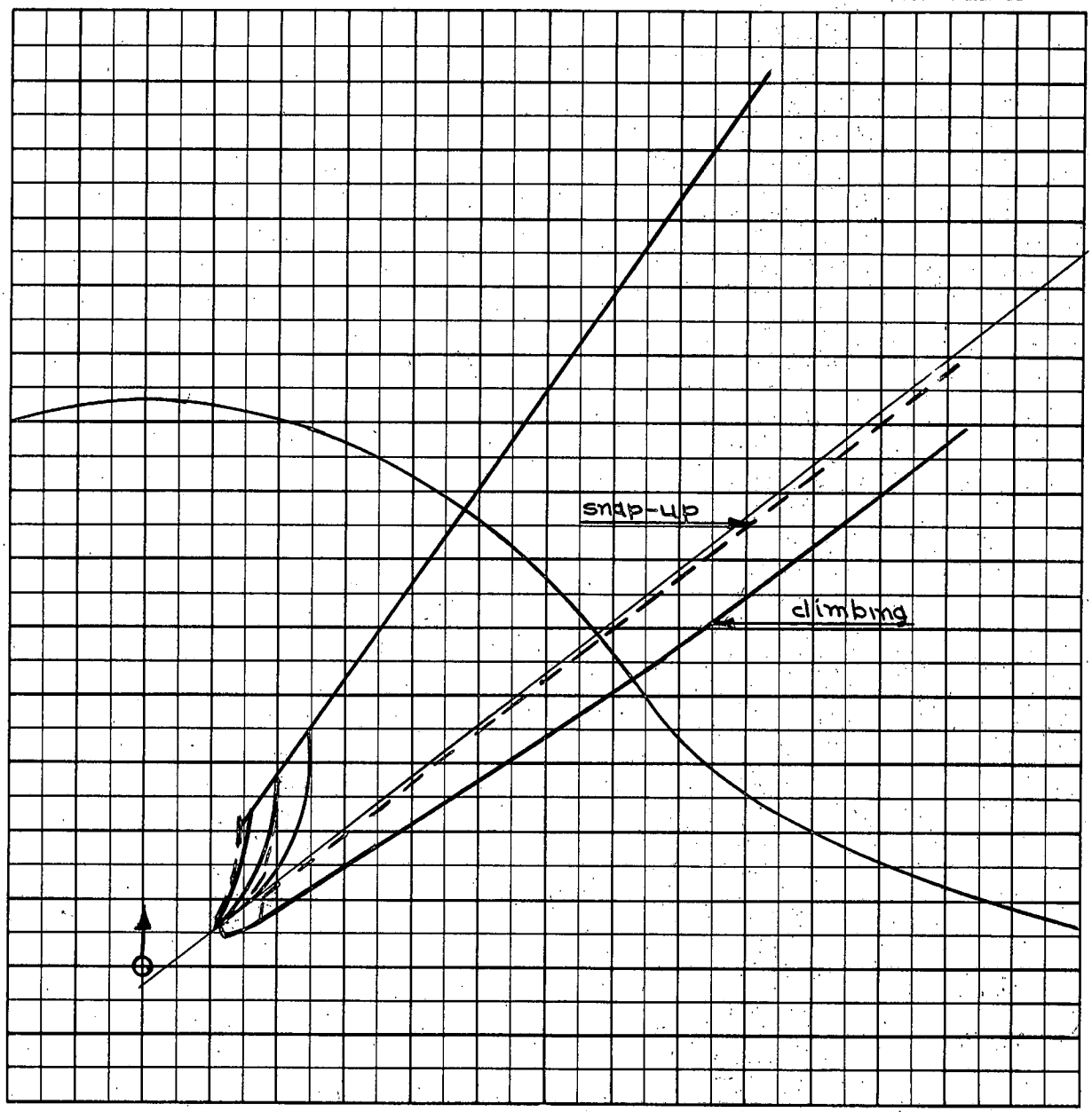

Scale 25,000 ft/cm

M_t = 2.0

h_t = 60 K

M_{fo} = 2.0

$h_{fo\ M}$ = 50 K

$V_t R_t$ = 0.75 g

Γ_o = 75°

A-41

Zones for target turns to the left and right both shown.

Placement probability values are very small for all A.I. ranges. Curves have not been down in this case.

PROB III N

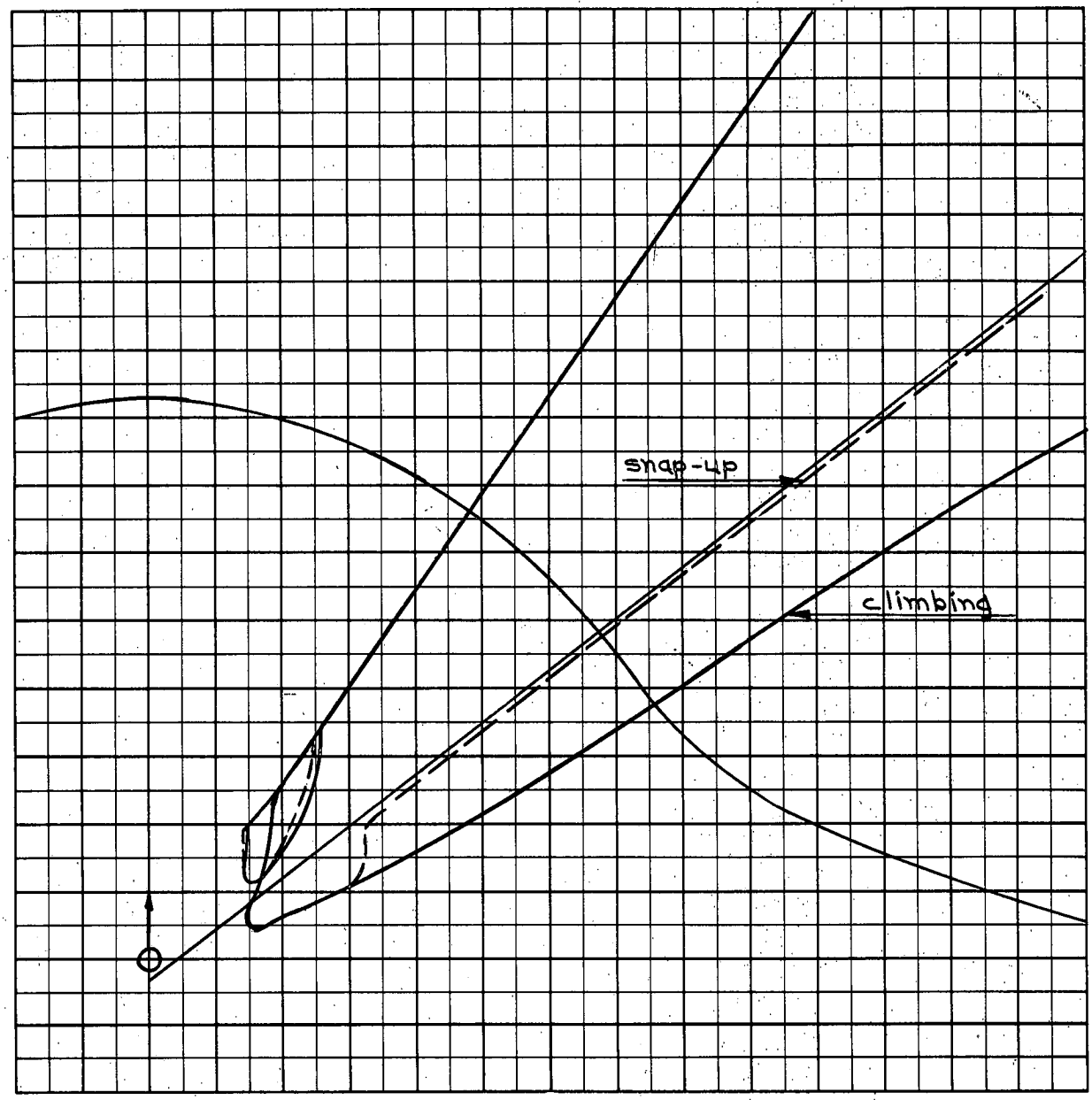

Scale 25,000 ft/cm

M_t = 2.0

h_t = 60 K

M_{fo} = 2.0

$h_{fo\ N}$ = 40 K

V_tR_t = 0.75 g

Γ_o = 75°

A-42

Zones for target turns to the left and right both shown.

Placement probability values are very small for all A.I. ranges. Curves have not been down in this case.

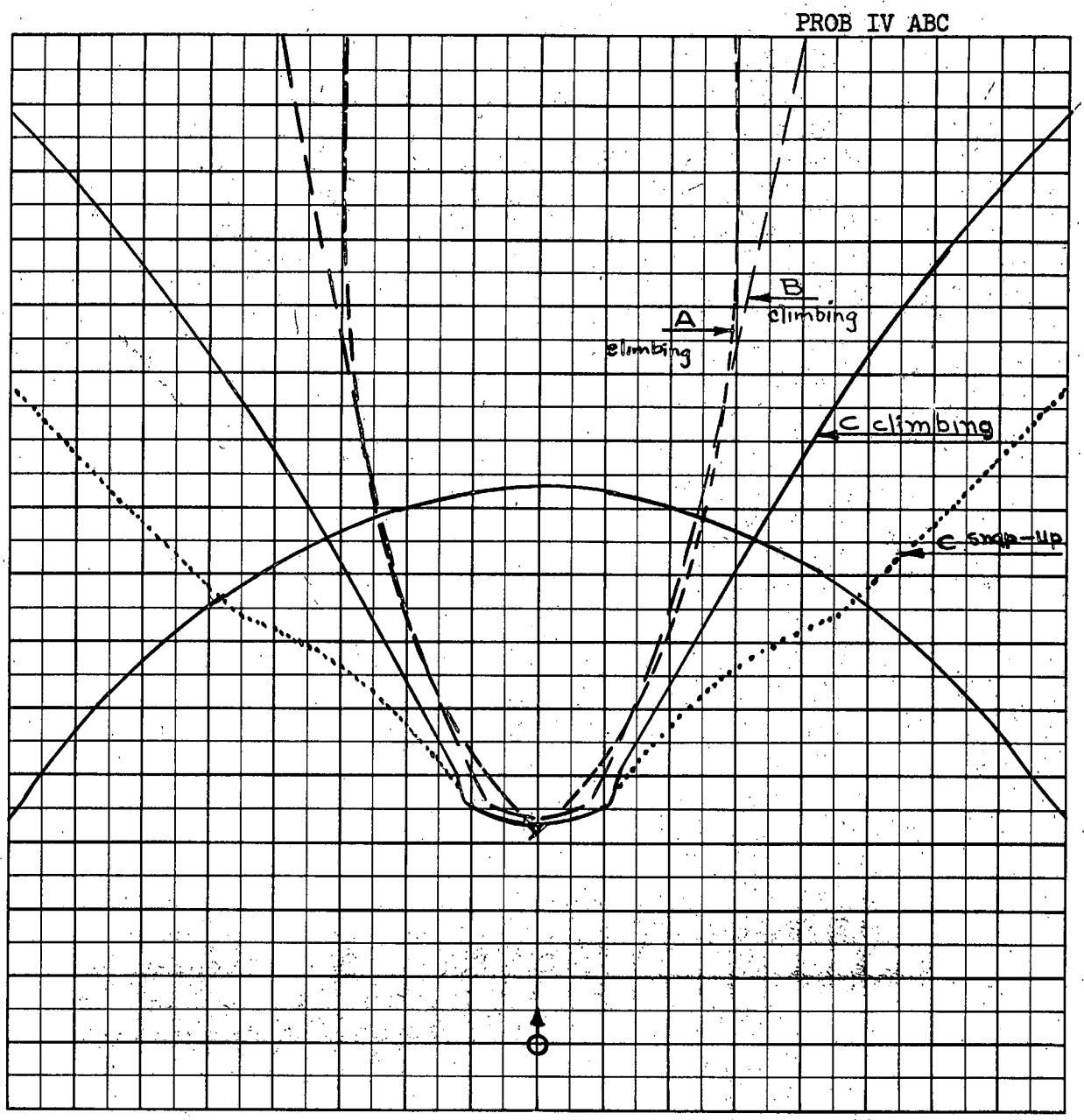

Scale 25,000 ft/cm

M_t = 2.0

h_t = 70 K

M_{fo} = 2.0

h_{fo} A = 60 K

B = 50 K

C = 40 K

Γ_o = 180°

A-43

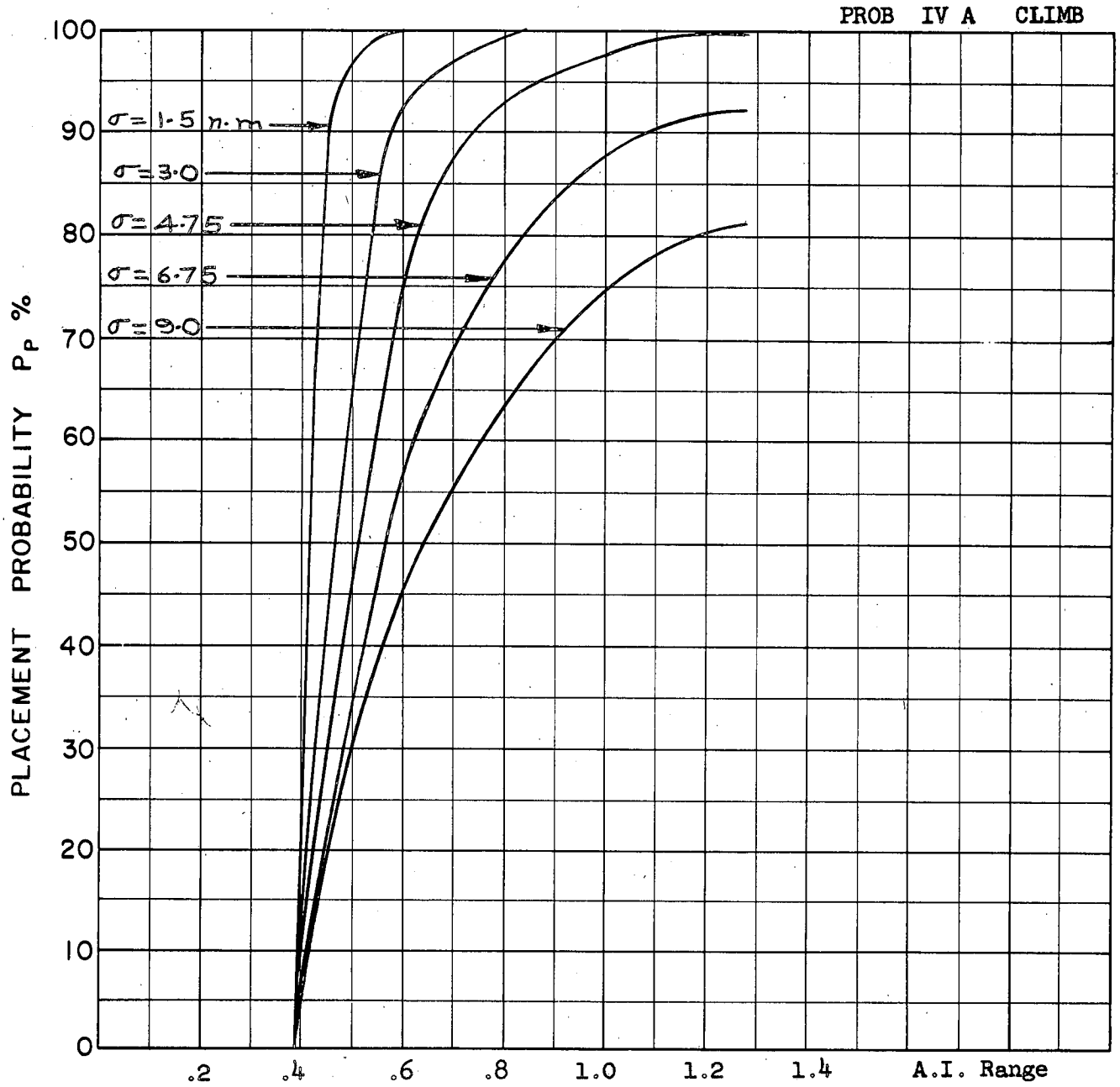

A-44

COURSE DIFFERENCE: 180°
TARGET EVASION: Nil
TARGET MACH NO.: 2.0
INTERCEPTOR LATERAL G's: Avro 3.3
INTERCEPTOR MACH NO.: 2.0
σ OF G.C.I. ACCURACY: 5 Values
A.I. DETECTION RANGE AS FRACTION OF SPECIFICATION RANGE, S: Abscissa
A.I. DETECTION RANGE CONTOUR: Delta
ALTITUDE: H_t = 70 K
H_f = 60 K

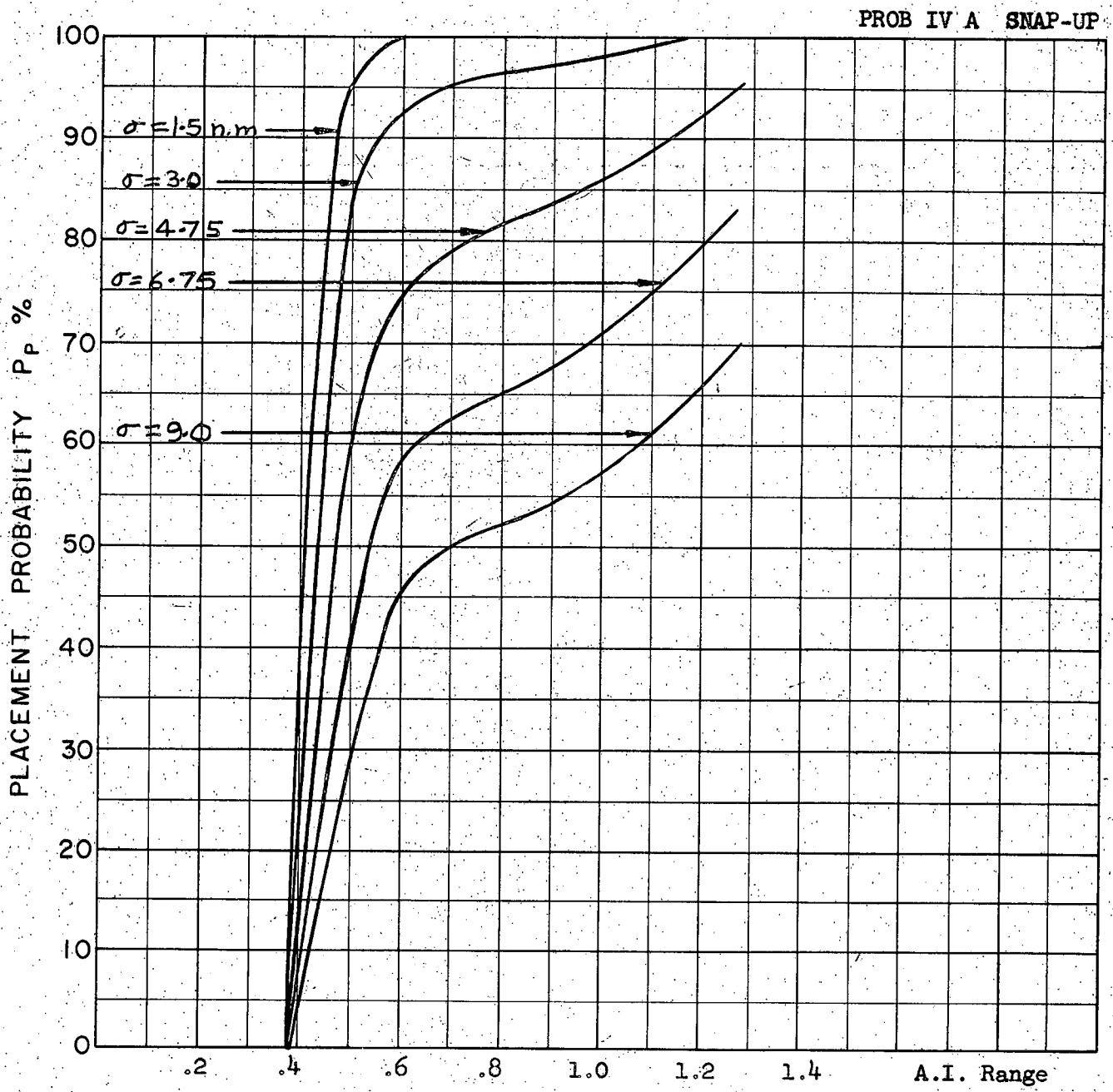

A-45

COURSE DIFFERENCE: 180°
TARGET EVASION: Nil
TARGET MACH NO.: 2.0
INTERCEPTOR LATERAL G's: Avro 3.3
INTERCEPTOR MACH NO.: 2.0
σ OF G.C.I. ACCURACY: 5 Values
A.I. DETECTION RANGE AS FRACTION OF SPECIFICATION RANGE, S: Abscissa
A.I. DETECTION RANGE CONTOUR: Delta
ALTITUDE: H_t = 70 K
H_f = 60 K

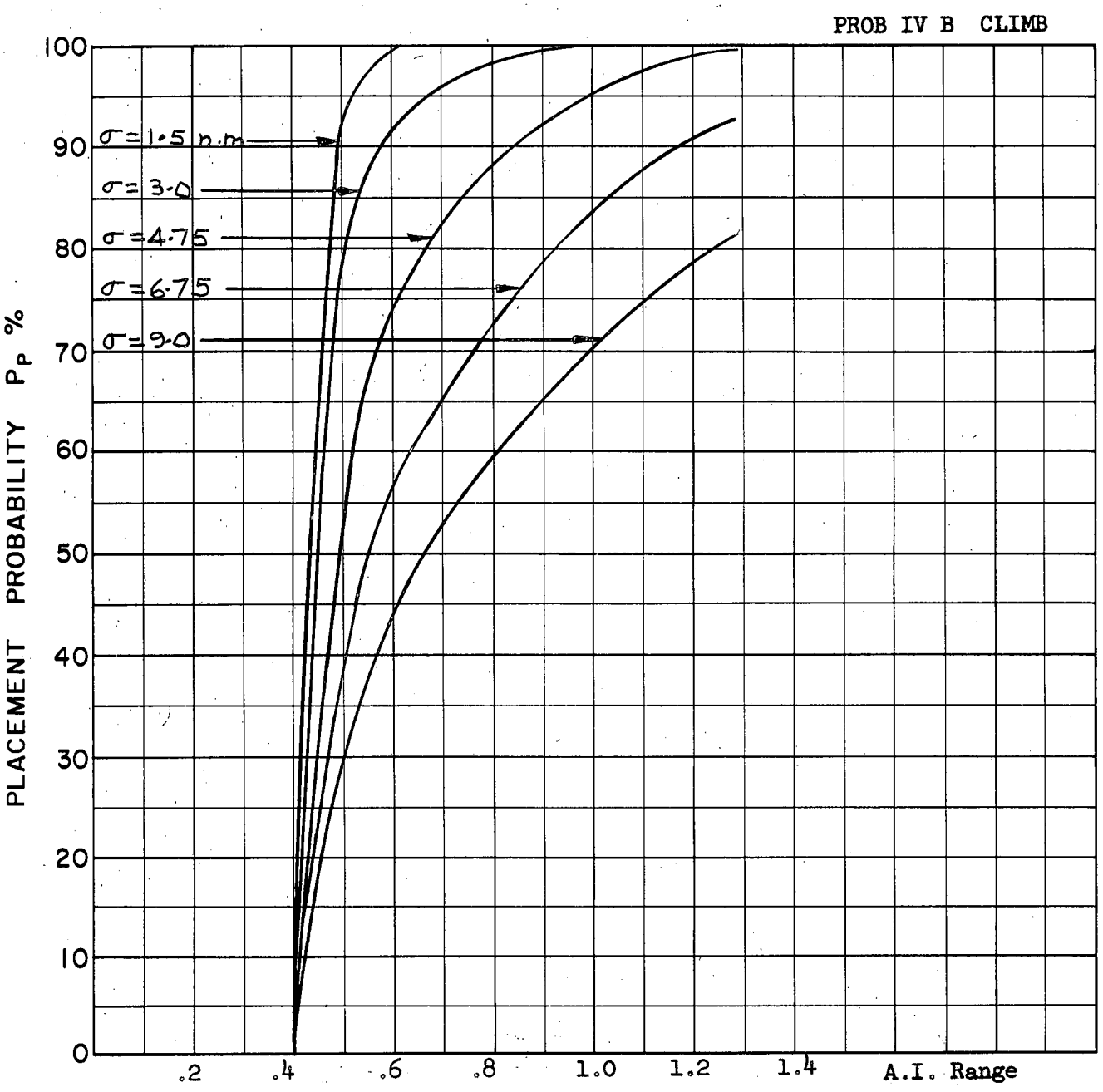

A-46

COURSE DIFFERENCE: 180°
TARGET EVASION: Nil
TARGET MACH NO.: 2.0
INTERCEPTOR LATERAL G's: Avro 3.3
INTERCEPTOR MACH NO.: 2.0
σ OF G.C.I. ACCURACY: 5 Values
A.I. DETECTION RANGE AS FRACTION OF SPECIFICATION RANGE, S: Abscissa
A.I. DETECTION RANGE CONTOUR: Delta
ALTITUDE: H_t = 70 K
H_f = 50 K

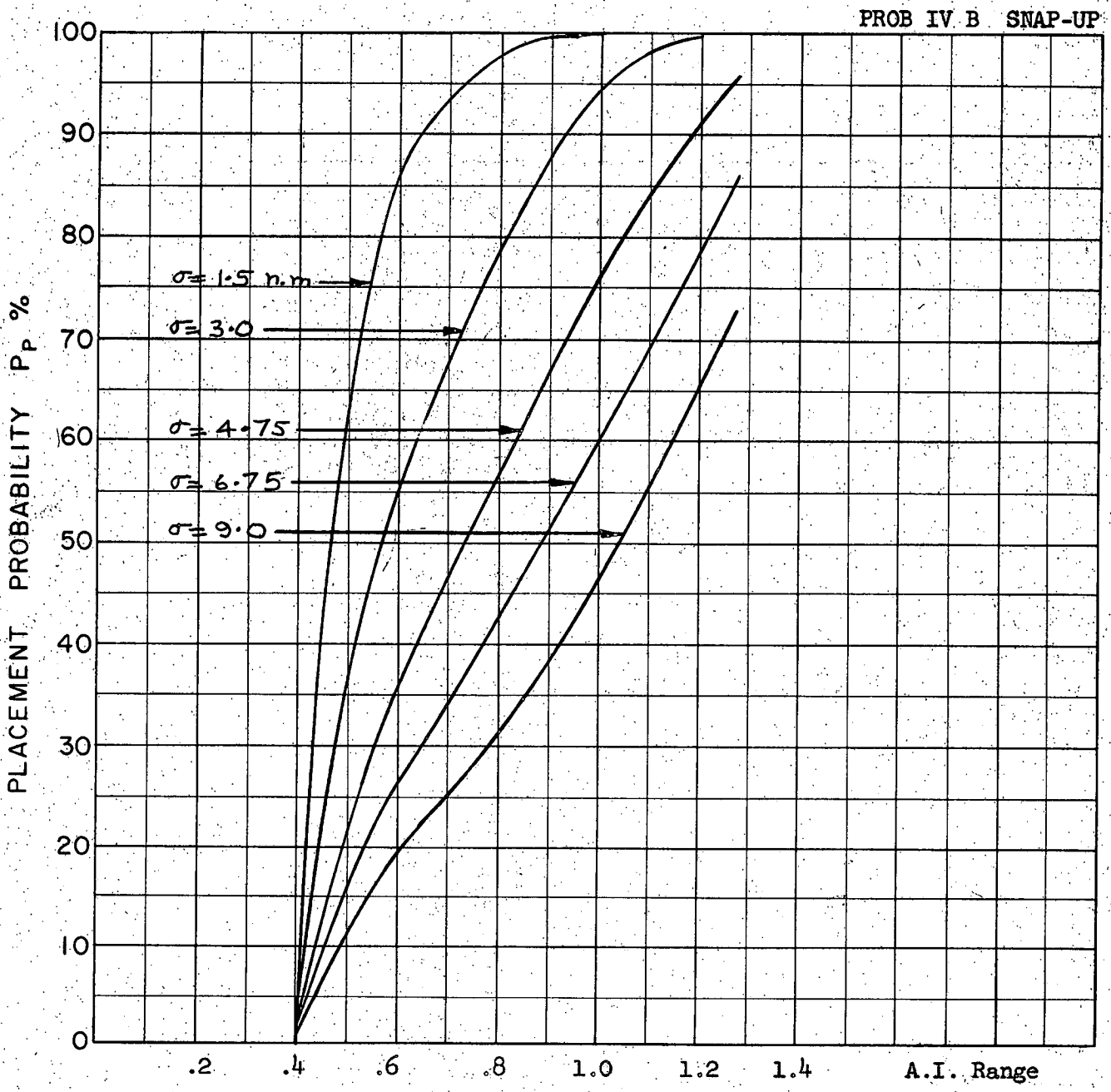

A-47

COURSE DIFFERENCE: 180°
TARGET EVASION: Nil
TARGET MACH NO.: 2.0
INTERCEPTOR LATERAL G's: Avro 3.3
INTERCEPTOR MACH NO.: 2.0
σ OF G.C.I. ACCURACY: 5 Values
A.I. DETECTION RANGE AS FRACTION OF SPECIFICATION RANGE, S: Abscissa
A.I. DETECTION RANGE CONTOUR: Delta
ALTITUDE: H_t = 70 K
H_f = 50 K

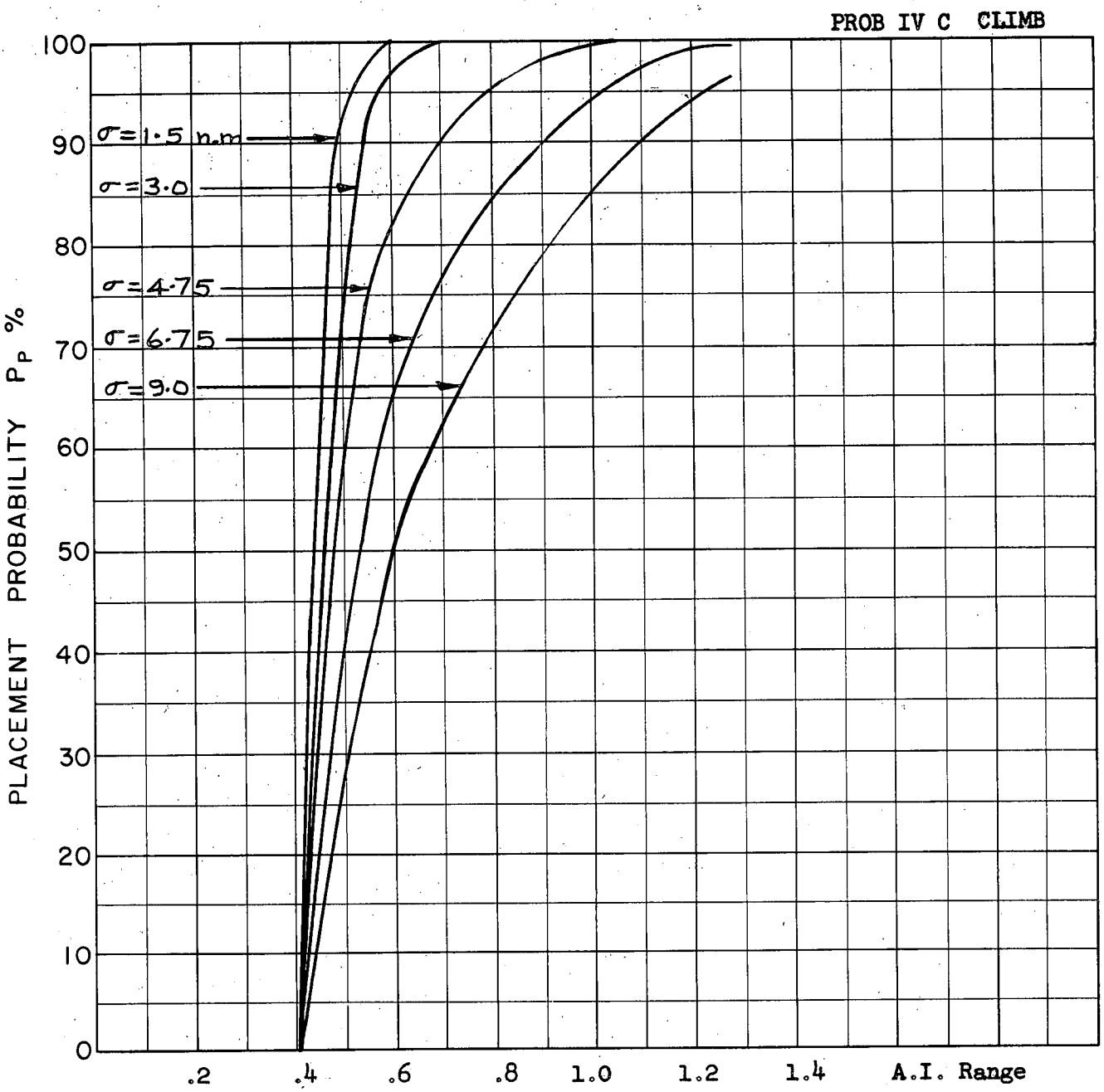

A-48

COURSE DIFFERENCE: 180°
TARGET EVASION: Nil
TARGET MACH NO.: 2.0
INTERCEPTOR LATERAL G's: Avro 3.3
INTERCEPTOR MACH NO.: 2.0
σ OF G.C.I. ACCURACY: 5 Values
A.I. DETECTION RANGE AS FRACTION OF SPECIFICATION RANGE, S: Abscissa
A.I. DETECTION RANGE CONTOUR: Delta
ALTITUDE: H_t = 70 K
H_f = 40 K

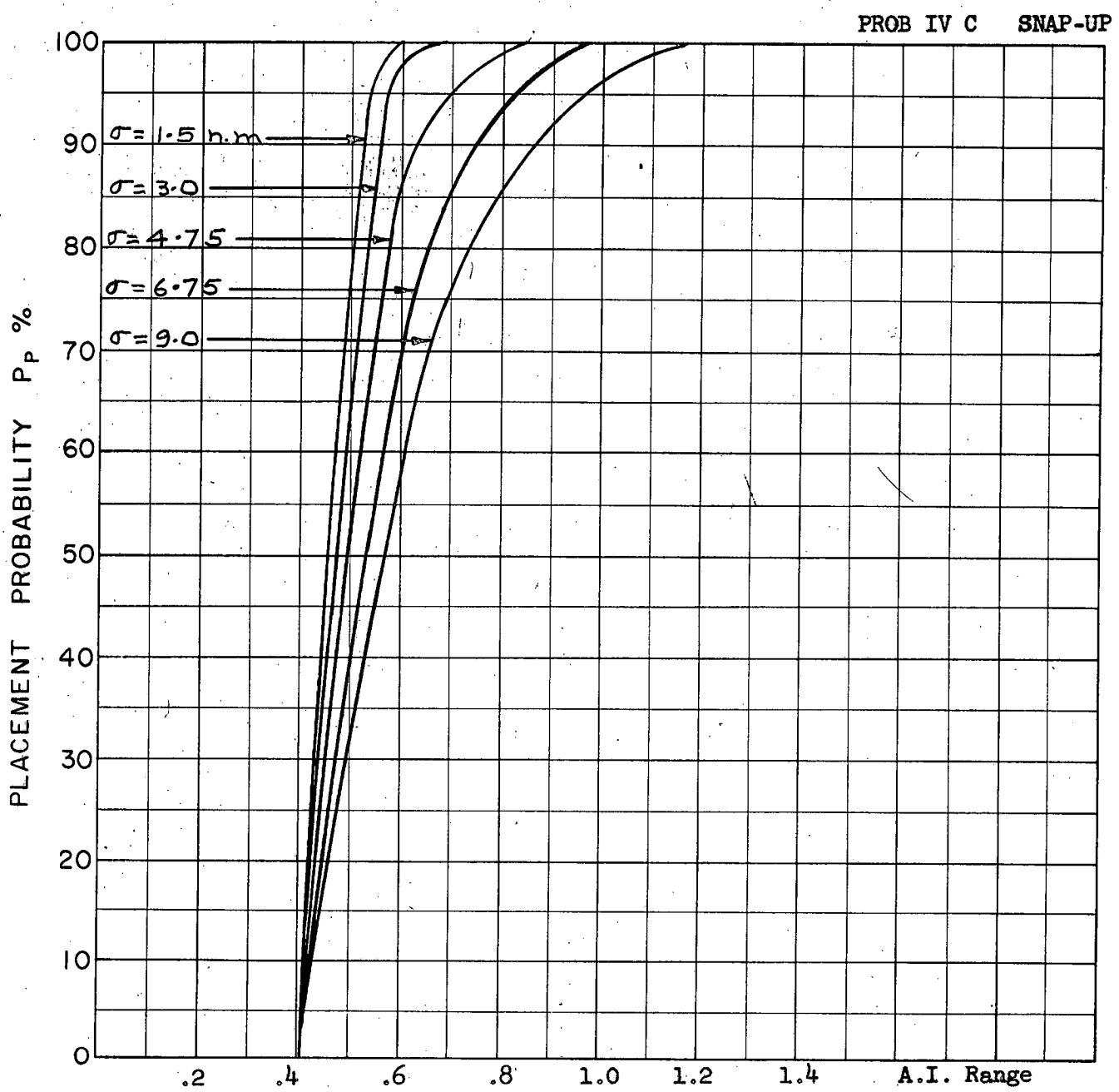

A-49

COURSE DIFFERENCE: 180°
TARGET EVASION: Nil
TARGET MACH NO.: 2.0
INTERCEPTOR LATERAL G's: Avro 3.3
INTERCEPTOR MACH NO.: 2.0
σ OF G.C.I. ACCURACY: 5 Values
A.I. DETECTION RANGE AS FRACTION OF SPECIFICATION RANGE, S: Abscissa
A.I. DETECTION RANGE CONTOUR: Delta
ALTITUDE: H_t = 70 K
H_f = 40 K

PROB IV DEF

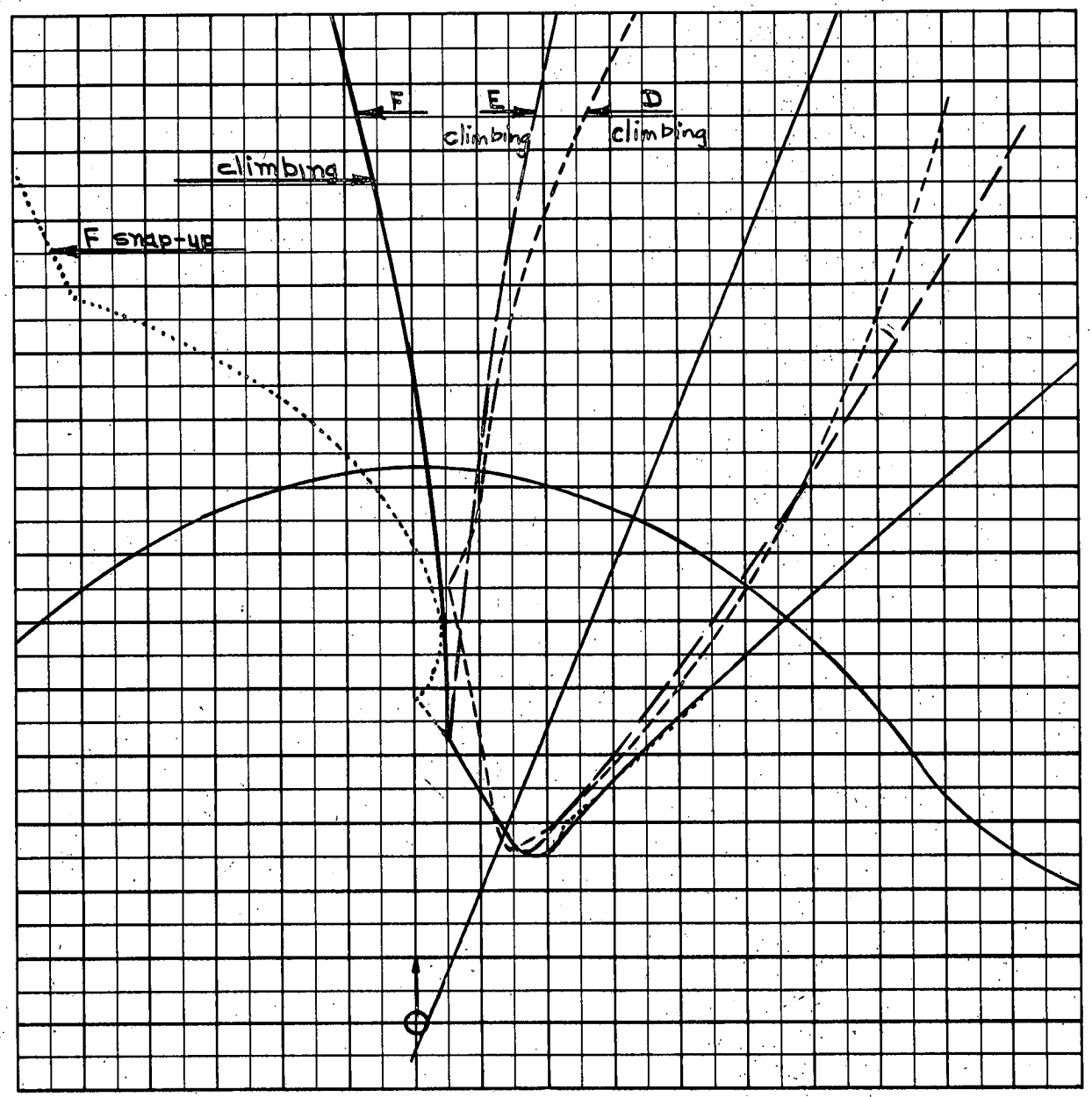

Scale 25,000 ft/cm

A-50

M_t = 2.0

h_t = 70 K

M_{fo} = 2.0

h_{fo} D = 60 K

E = 50 K

F = 40 K

Γ_o = 135°

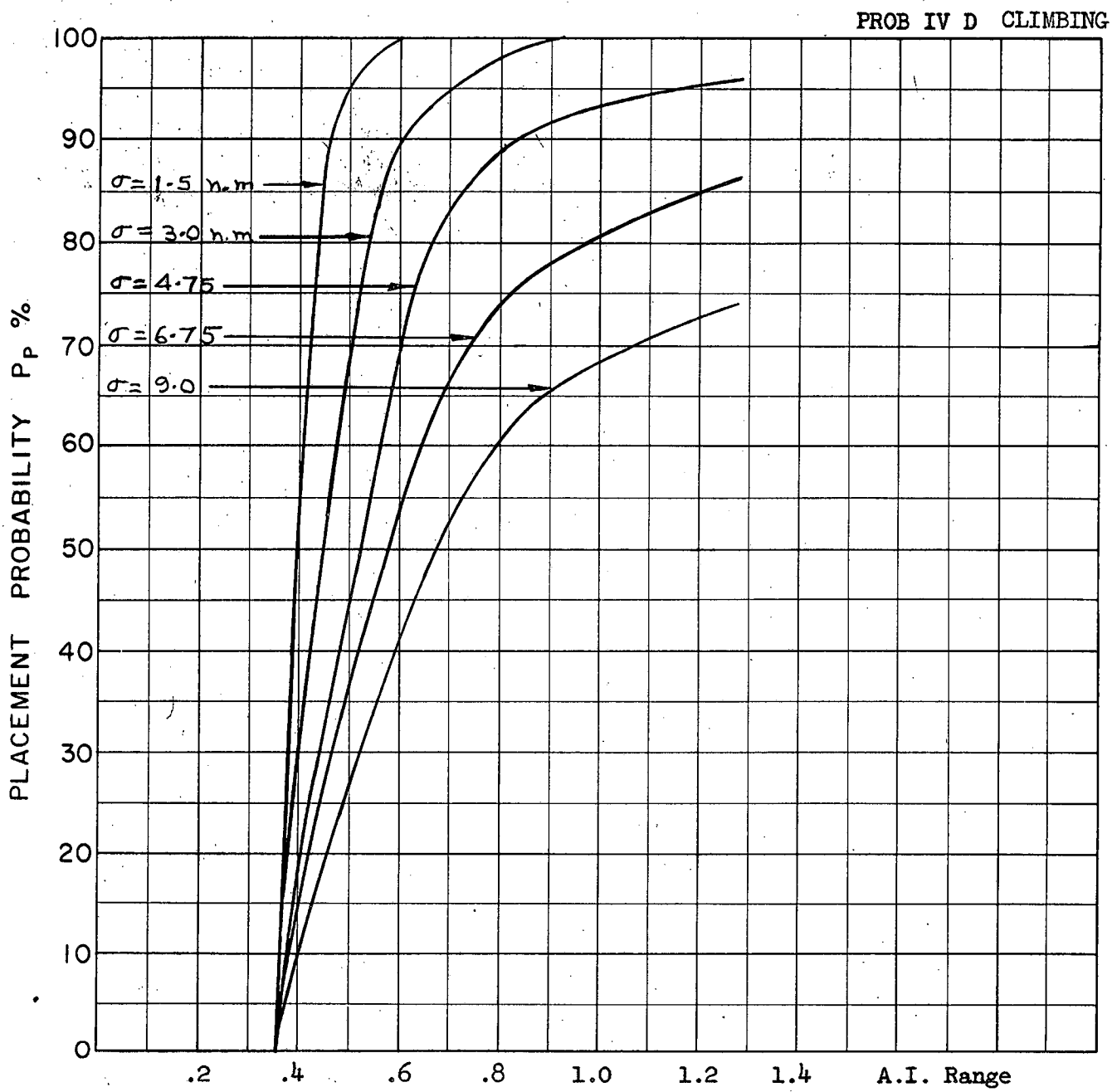

A-51

COURSE DIFFERENCE: 135°
TARGET EVASION: Nil
TARGET MACH NO.: 2.0
INTERCEPTOR LATERAL G's: Avro 3.3
INTERCEPTOR MACH NO.: 2.0
σ OF G.C.I. ACCURACY: 5 Values
A.I. DETECTION RANGE AS FRACTION OF SPECIFICATION RANGE, S: Abscissa
A.I. DETECTION RANGE CONTOUR: Delta
ALTITUDE: H_t = 70 K
H_f = 60 K

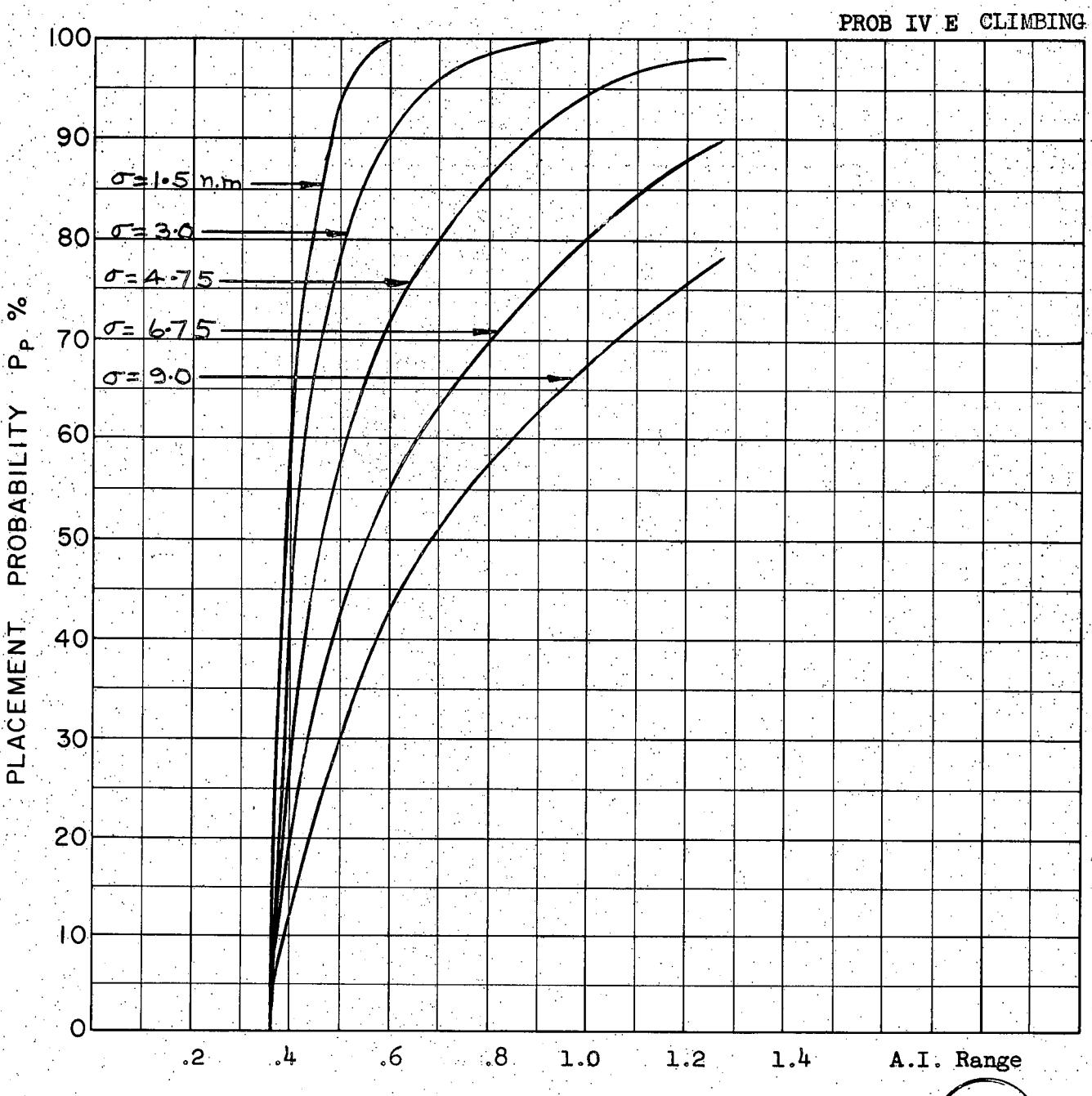

A-52

COURSE DIFFERENCE: 135°
TARGET EVASION: Nil
TARGET MACH NO.: 2.0
INTERCEPTOR LATERAL G's: Avro 3.3
INTERCEPTOR MACH NO.: 2.0
σ OF G.C.I. ACCURACY: 5 Values
A.I. DETECTION RANGE AS FRACTION OF SPECIFICATION RANGE, S: Abscissa
A.I. DETECTION RANGE CONTOUR: Delta
ALTITUDE: H_t = 70 K
H_f = 50 K

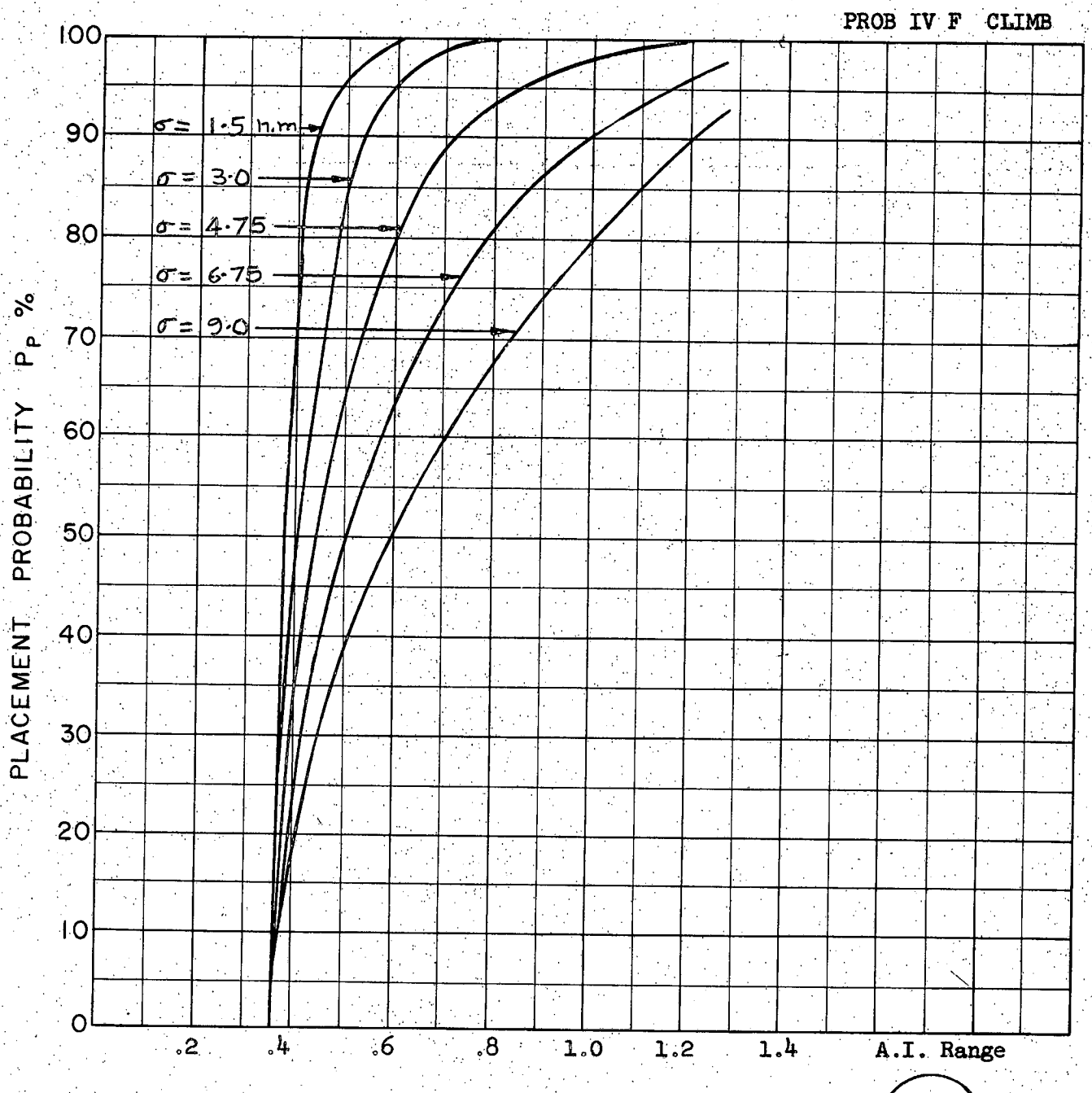

A-53

COURSE DIFFERENCE: 135°
TARGET EVASION: Nil
TARGET MACH NO.: 2.0
INTERCEPTOR LATERAL G's: Avro 3.3
INTERCEPTOR MACH NO.: 2.0
σ OF G.C.I. ACCURACY: 5 Values
A.I. DETECTION RANGE AS FRACTION OF SPECIFICATION RANGE, S: Abscissa
A.I. DETECTION RANGE CONTOUR: Delta
ALTITUDE: H_t = 70 K
H_f = 40 K

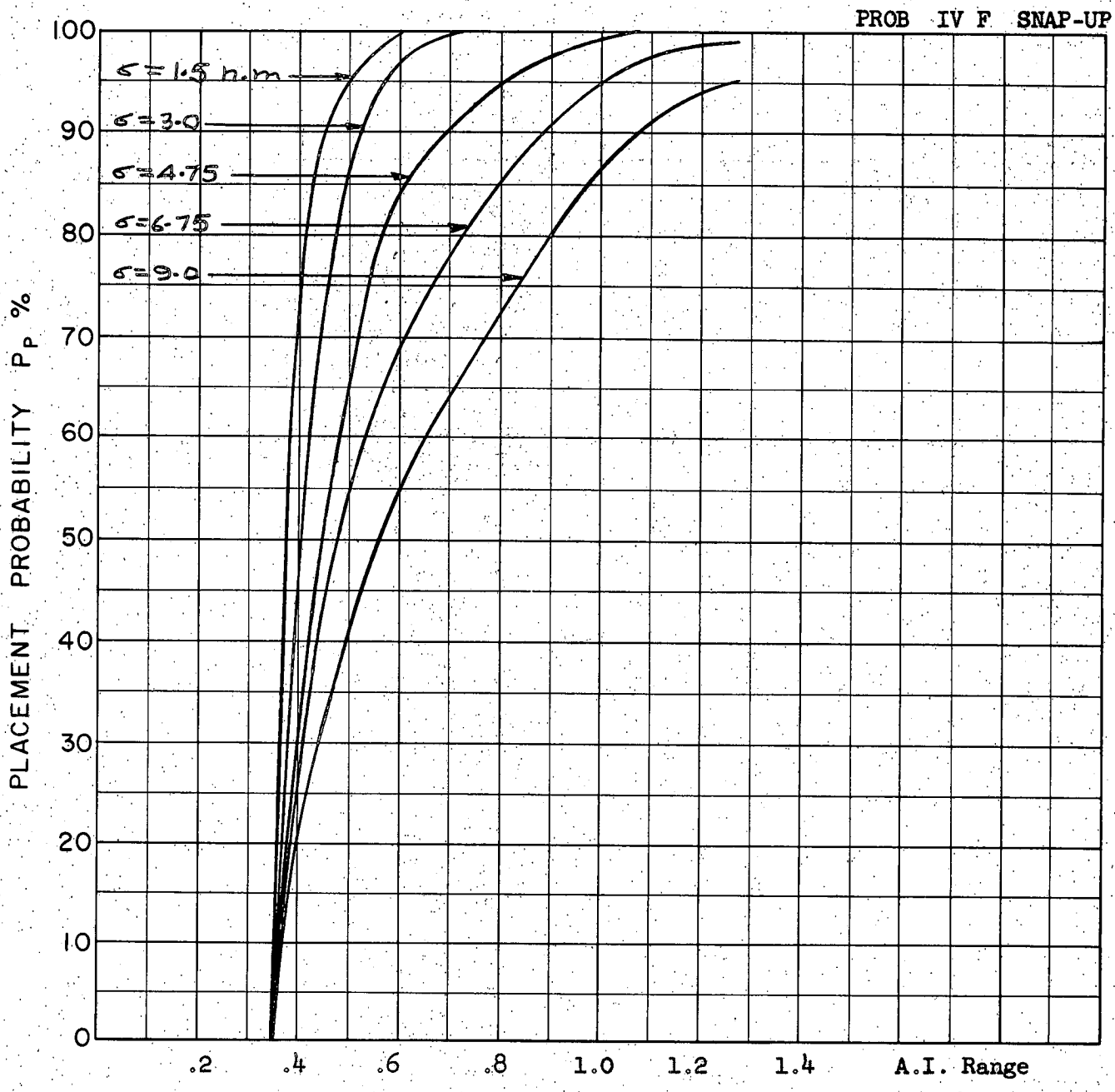

A-54

COURSE DIFFERENCE: 135°
TARGET EVASION: Nil
TARGET MACH NO.: 2.0
INTERCEPTOR LATERAL G's: Avro 3.3
INTERCEPTOR MACH NO.: 2.0
σ OF G.C.I. ACCURACY: 5 Values
A.I. DETECTION RANGE AS FRACTION OF SPECIFICATION RANGE, S: Abscissa
A.I. DETECTION RANGE CONTOUR: Delta
ALTITUDE: H_t = 70 K
H_f = 40 K

PROB IV GHK

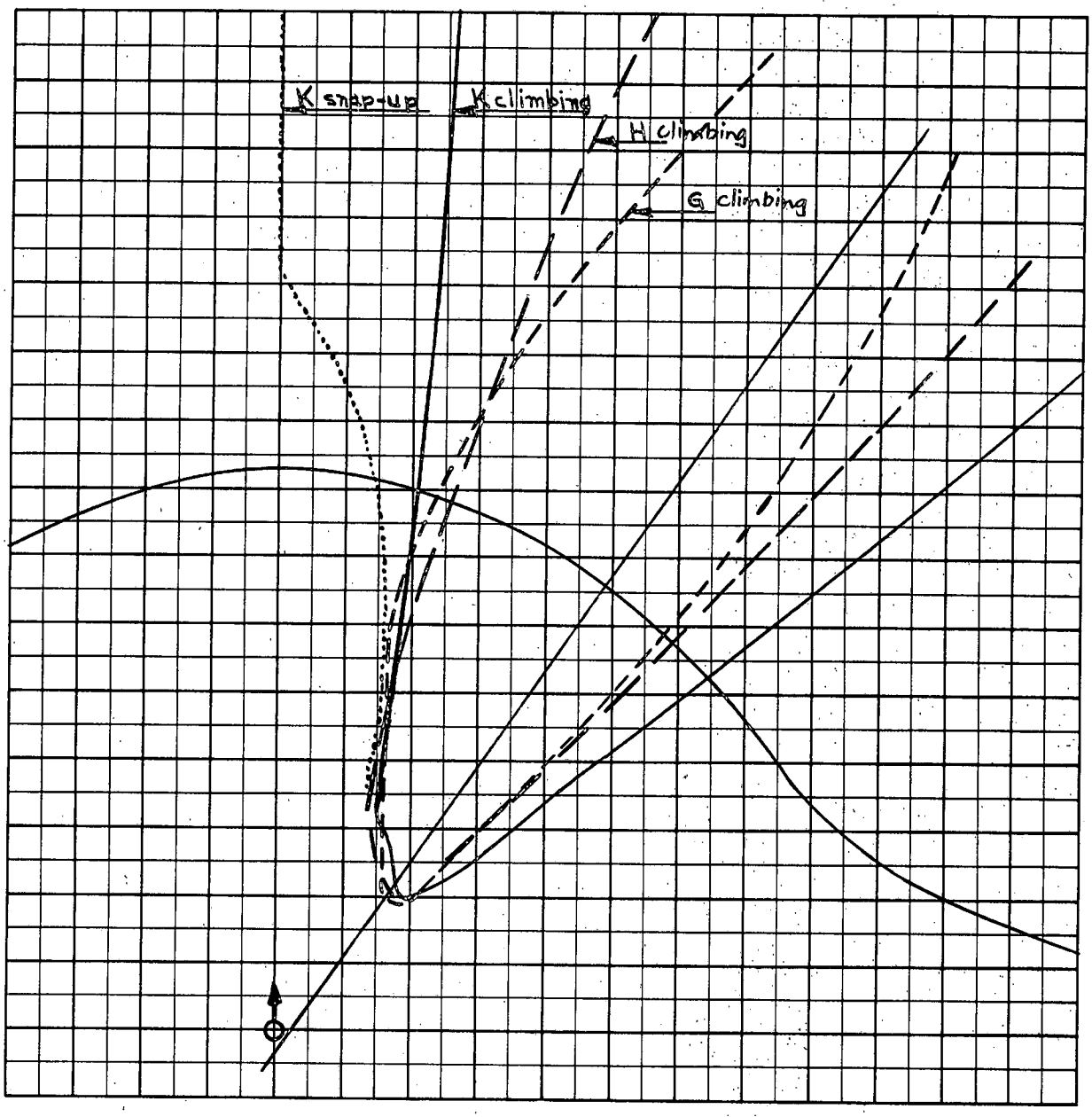

Scale 25,000 ft/cm

M_t = 2.0

h_t = 70 K

M_{fo} = 2.0

h_{fo} G = 60 K

H = 50 K

K = 40 K

Γ_o = 110°

A-55

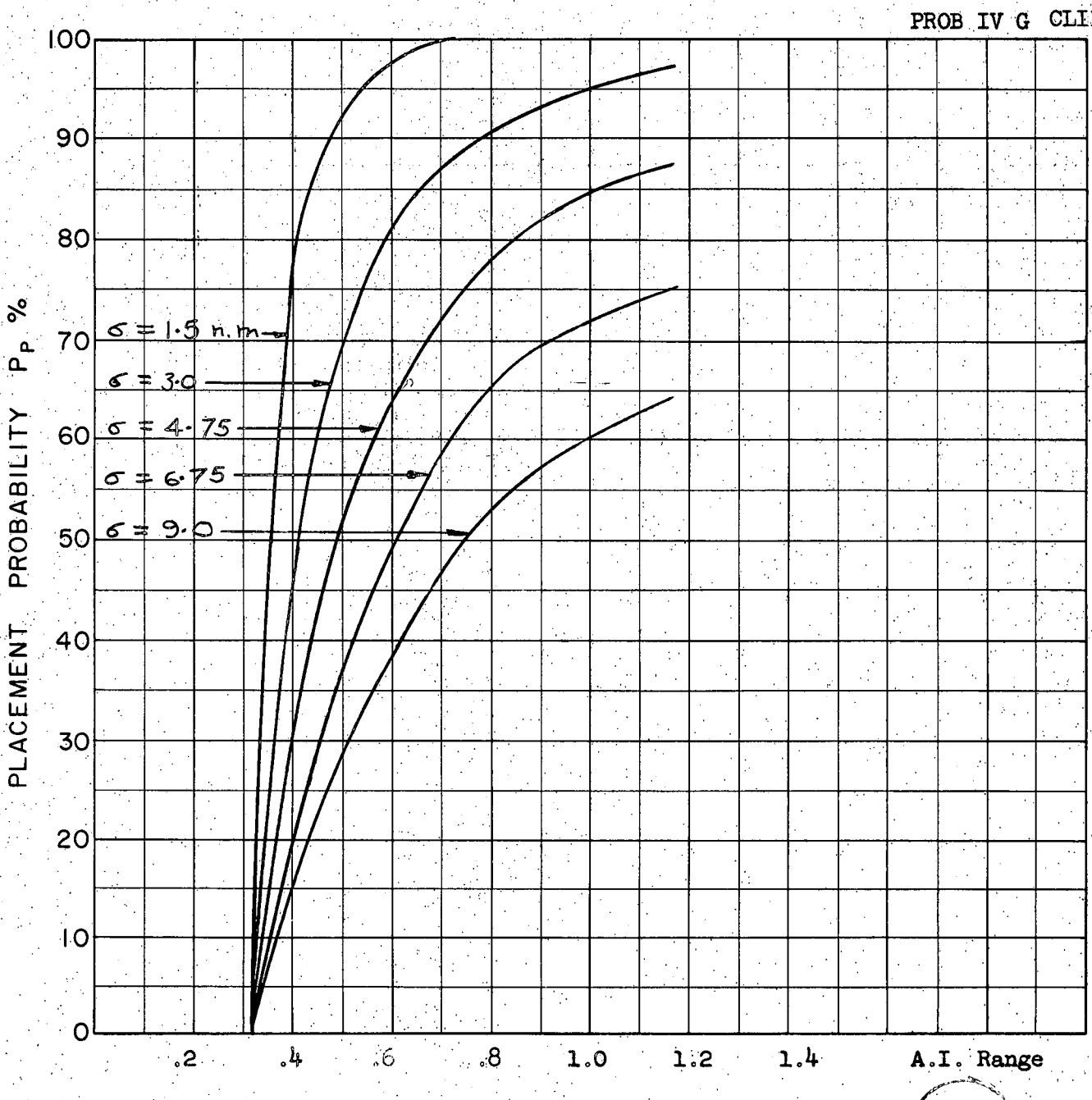

A-56

COURSE DIFFERENCE: 110°
TARGET EVASION: Nil
TARGET MACH NO.: 2.0
INTERCEPTOR LATERAL G's: Avro 3.3
INTERCEPTOR MACH NO.: 2.0
σ OF G.C.I. ACCURACY: 5 Values
A.I. DETECTION RANGE AS FRACTION OF SPECIFICATION RANGE, S: Abscissa
A.I. DETECTION RANGE CONTOUR: Delta
ALTITUDE: H_t = 70 K
H_f = 60 K

PROB IV H CLIMBING

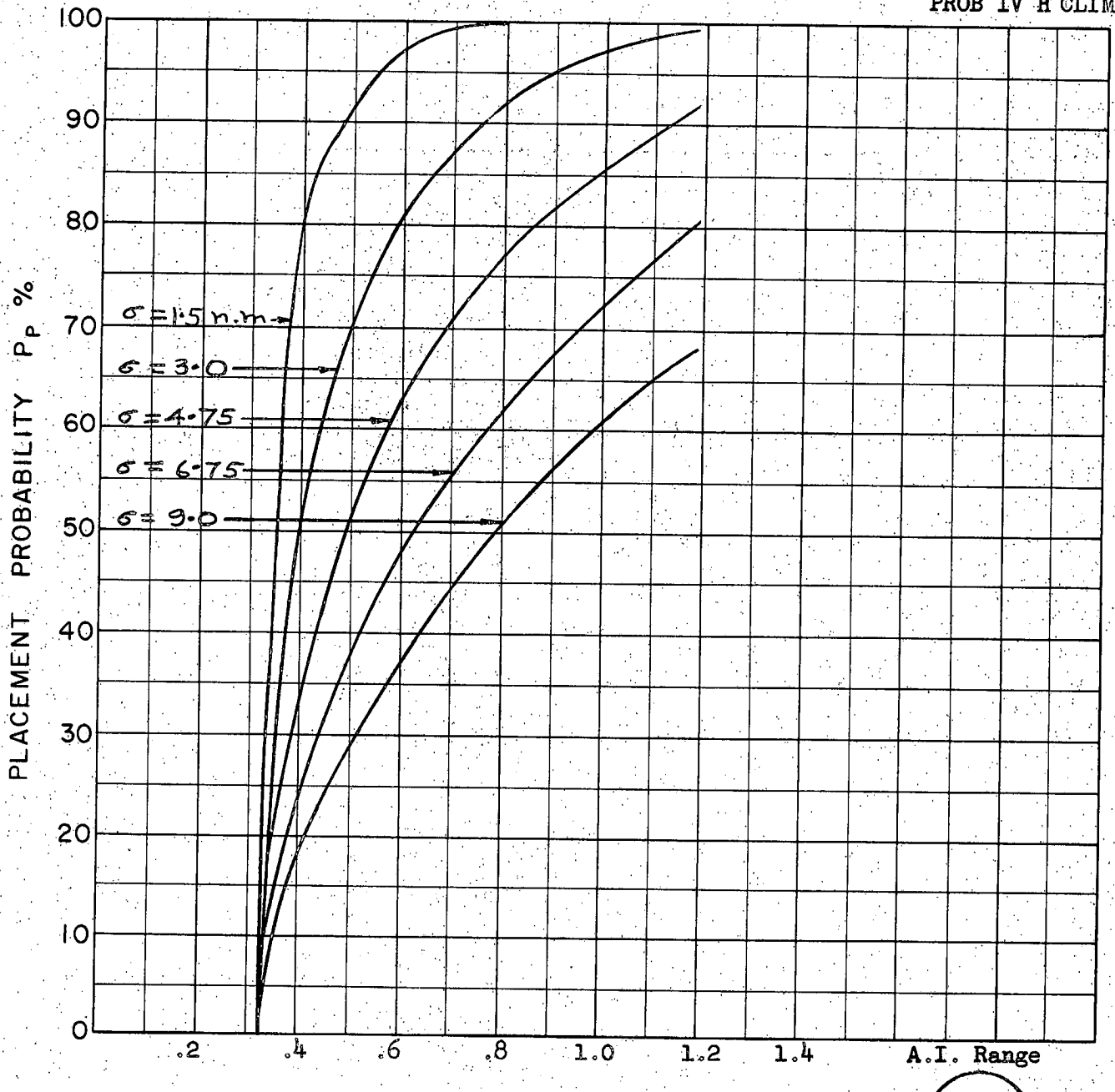

A-57

COURSE DIFFERENCE: 110°
TARGET EVASION: Nil
TARGET MACH NO.: 2.0
INTERCEPTOR LATERAL G's: Avro 3.3
INTERCEPTOR MACH NO.: 2.0
σ OF G.C.I. ACCURACY: 5 Values
A.I. DETECTION RANGE AS FRACTION OF SPECIFICATION RANGE, S: Abscissa
A.I. DETECTION RANGE CONTOUR: Delta
ALTITUDE: H_t = 70 K
H_f = 50 K

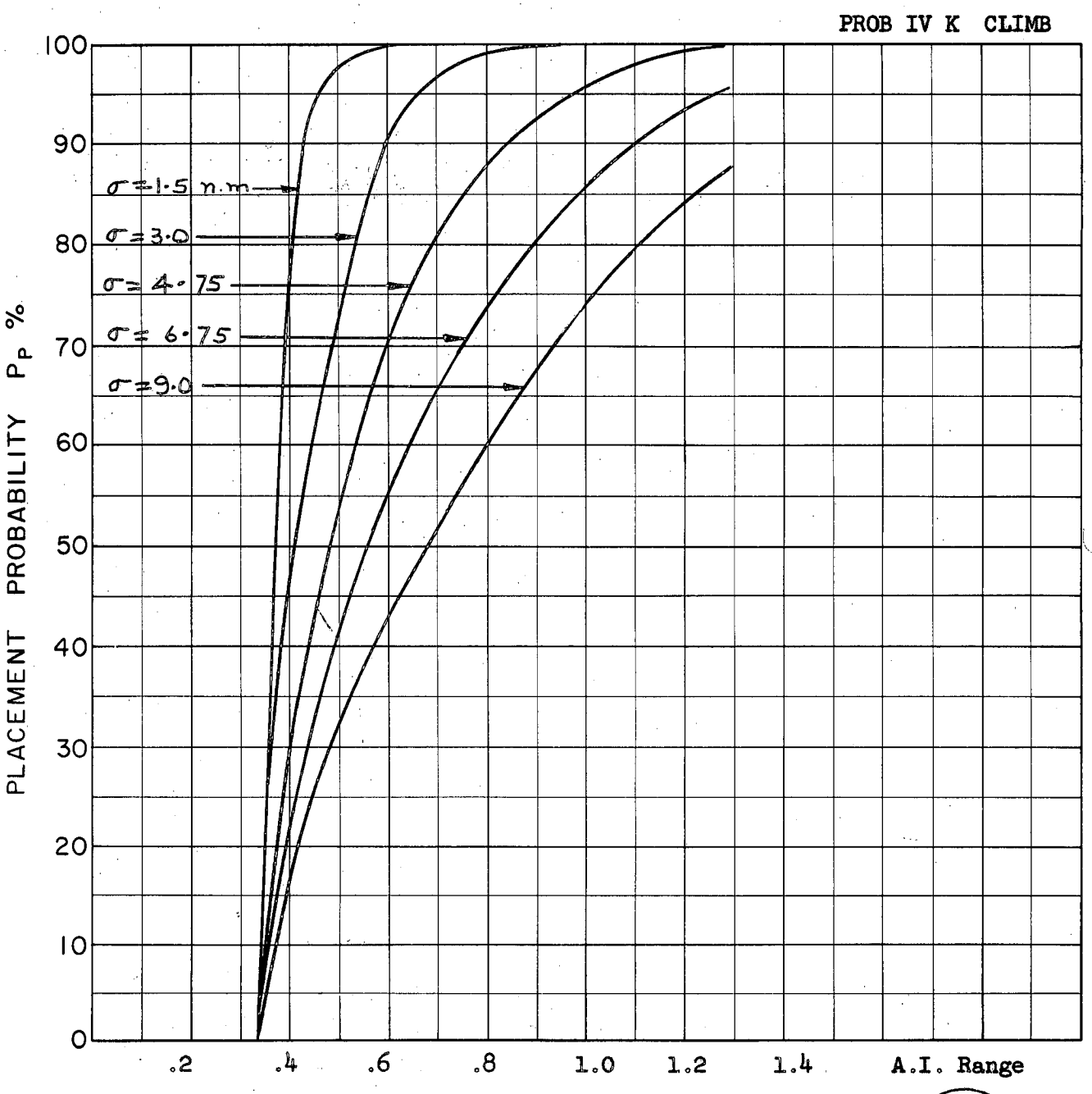

A-58

COURSE DIFFERENCE: 110°
TARGET EVASION: Nil
TARGET MACH NO.: 2.0
INTERCEPTOR LATERAL G's: Avro 3.3
INTERCEPTOR MACH NO.: 2.0
σ OF G.C.I. ACCURACY: 5 Values
A.I. DETECTION RANGE AS FRACTION OF SPECIFICATION RANGE, S: Abscissa
A.I. DETECTION RANGE CONTOUR: Delta
ALTITUDE: H_t = 70 K
H_f = 40 K

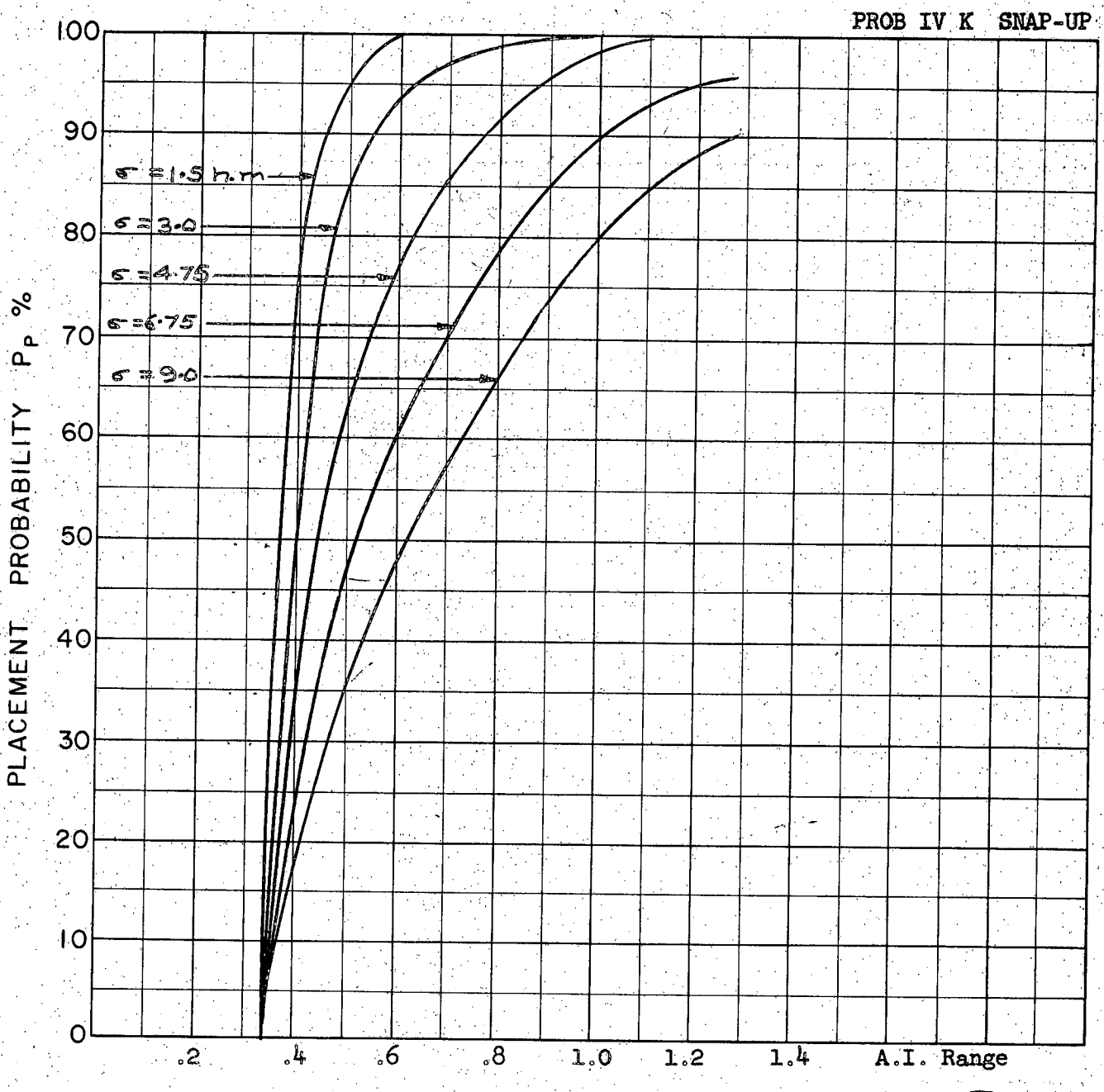

A-59

COURSE DIFFERENCE: 110°
TARGET EVASION: Nil
TARGET MACH NO.: 2.0
INTERCEPTOR LATERAL G's: Avro 3.3
INTERCEPTOR MACH NO.: 2.0
σ OF G.C.I. ACCURACY: 5 Values
A.I. DETECTION RANGE AS FRACTION OF SPECIFICATION RANGE, S: Abscissa
A.I. DETECTION RANGE CONTOUR: Delta
ALTITUDE: H_t = 70 K
H_f = 40 K

PROB IV LMN

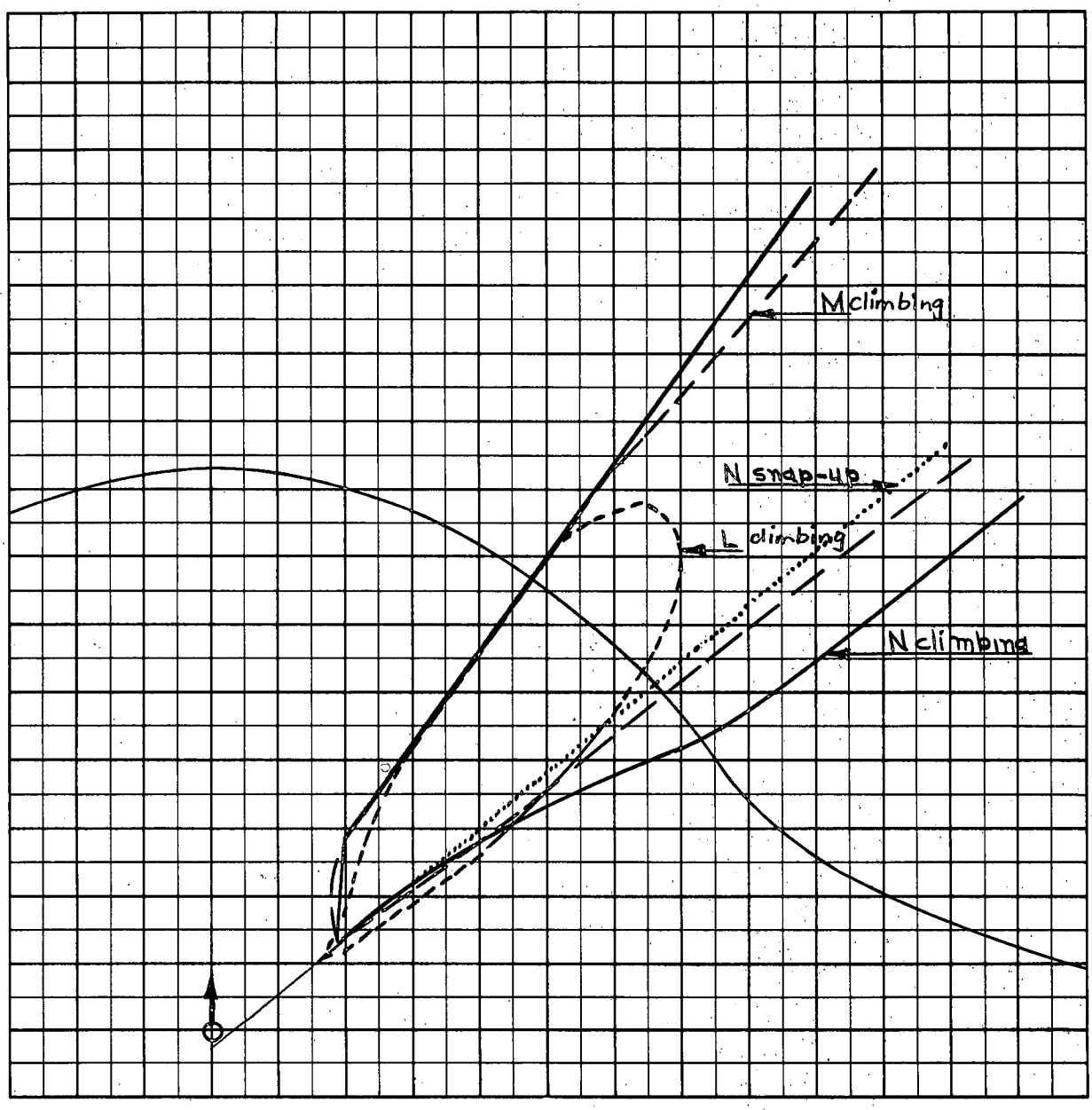

Scale 25,000 ft/cm

A-60

M_t = 2.0

h_t = 70 K

M_{fo} = 2.0

h_{fo} L = 60 K

M = 50 K

N = 40 K

Γ_o = 75°

PROB IV L CLIMBING

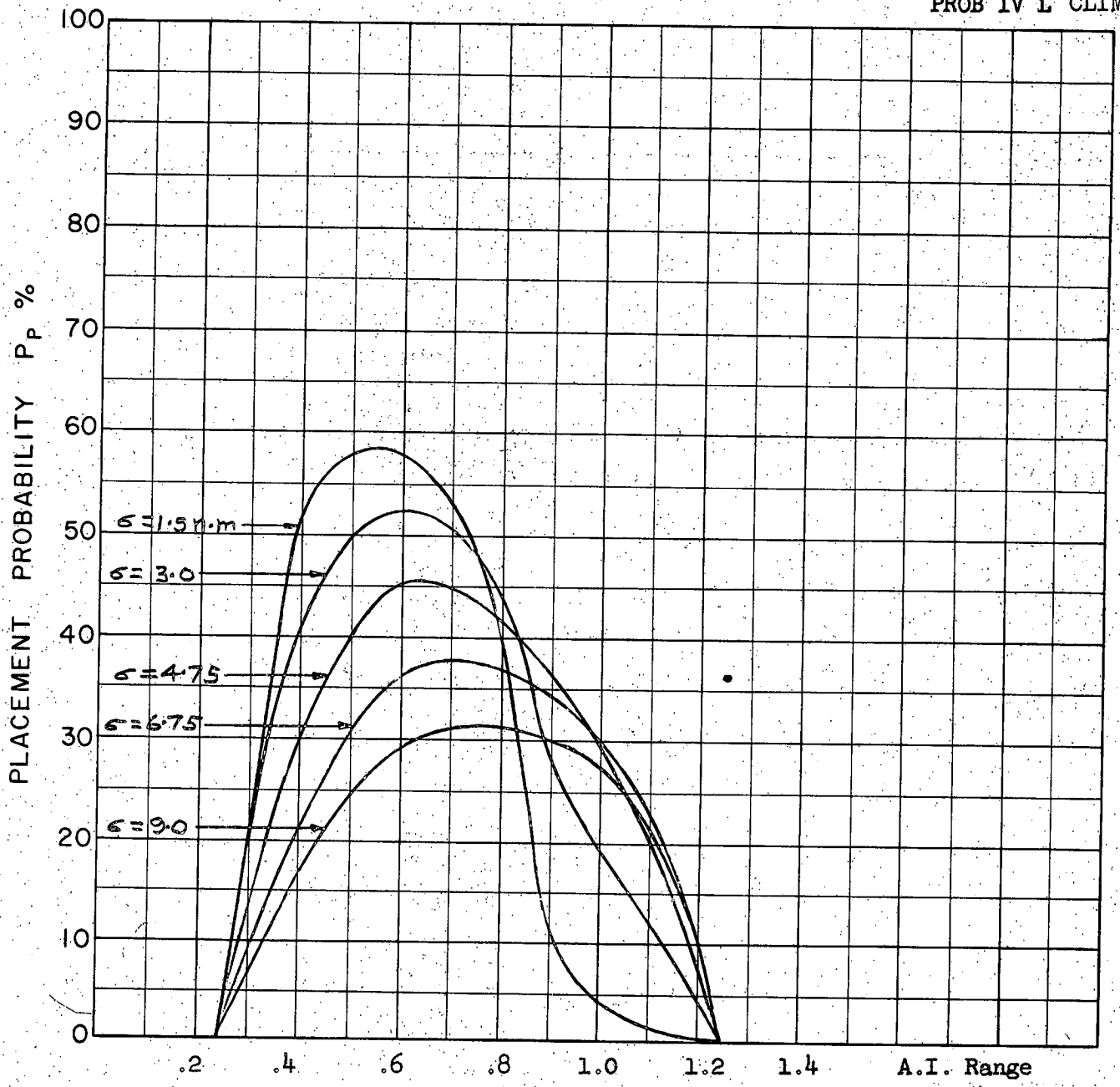

A-61

COURSE DIFFERENCE: 75°
TARGET EVASION: Nil
TARGET MACH NO.: 2.0
INTERCEPTOR LATERAL G's: Avro 3.3
INTERCEPTOR MACH NO.: 2.0
σ OF G.C.I. ACCURACY: 5 Values
A.I. DETECTION RANGE AS FRACTION OF SPECIFICATION RANGE, S: Abscissa
A.I. DETECTION RANGE CONTOUR: Delta
ALTITUDE: H_t = 70 K
H_f = 60 K

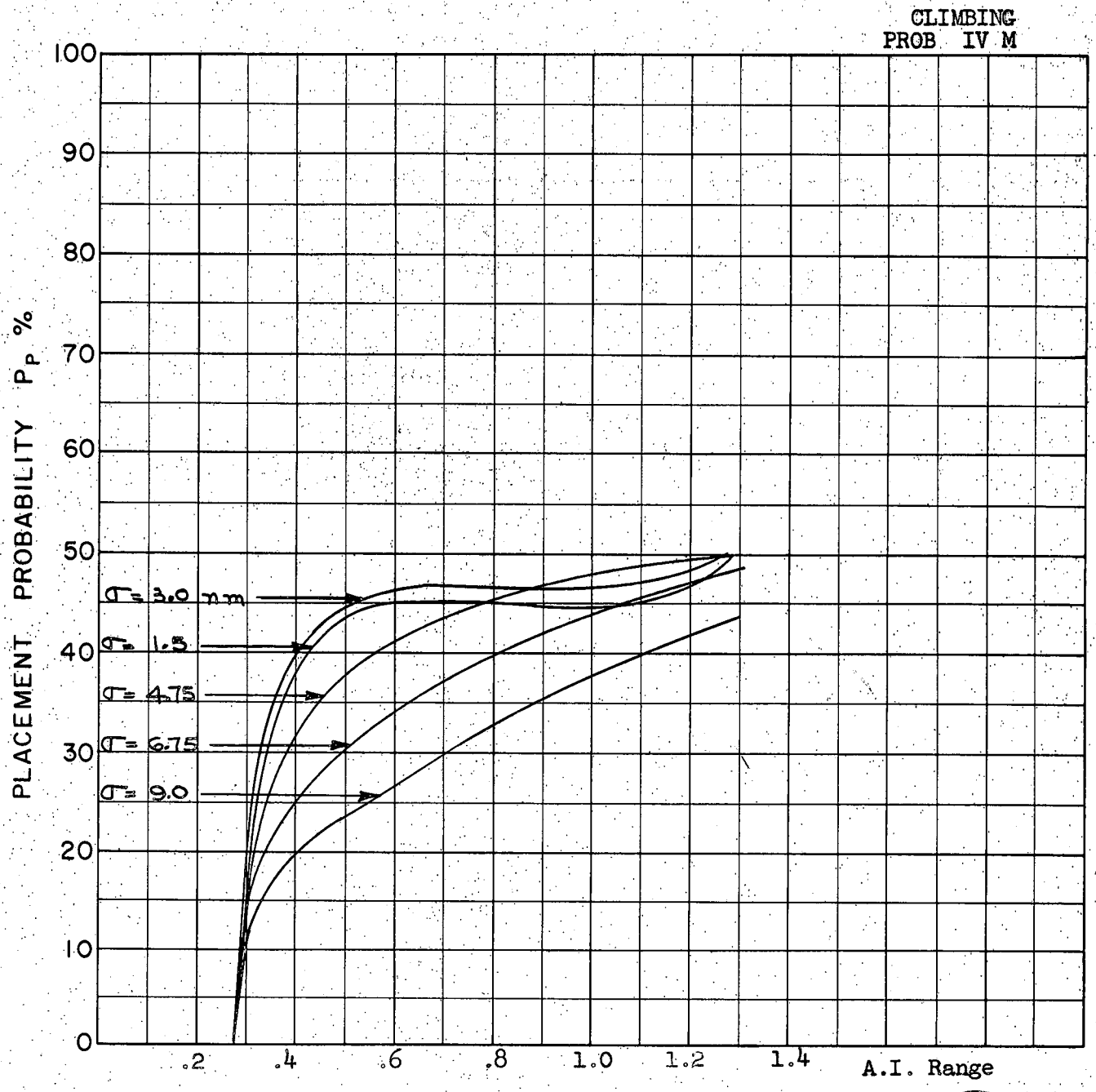

A-62

COURSE DIFFERENCE: 75°
TARGET EVASION: Nil
TARGET MACH NO.: 2.0
INTERCEPTOR LATERAL G's: Avro 3.3
INTERCEPTOR MACH NO.: 2.0
σ OF G.C.I. ACCURACY: 5 Values
A.I. DETECTION RANGE AS FRACTION OF SPECIFICATION RANGE, S: Abscissa
A.I. DETECTION RANGE CONTOUR: Delta
ALTITUDE: H_t = 70 K

H_f = 50 K

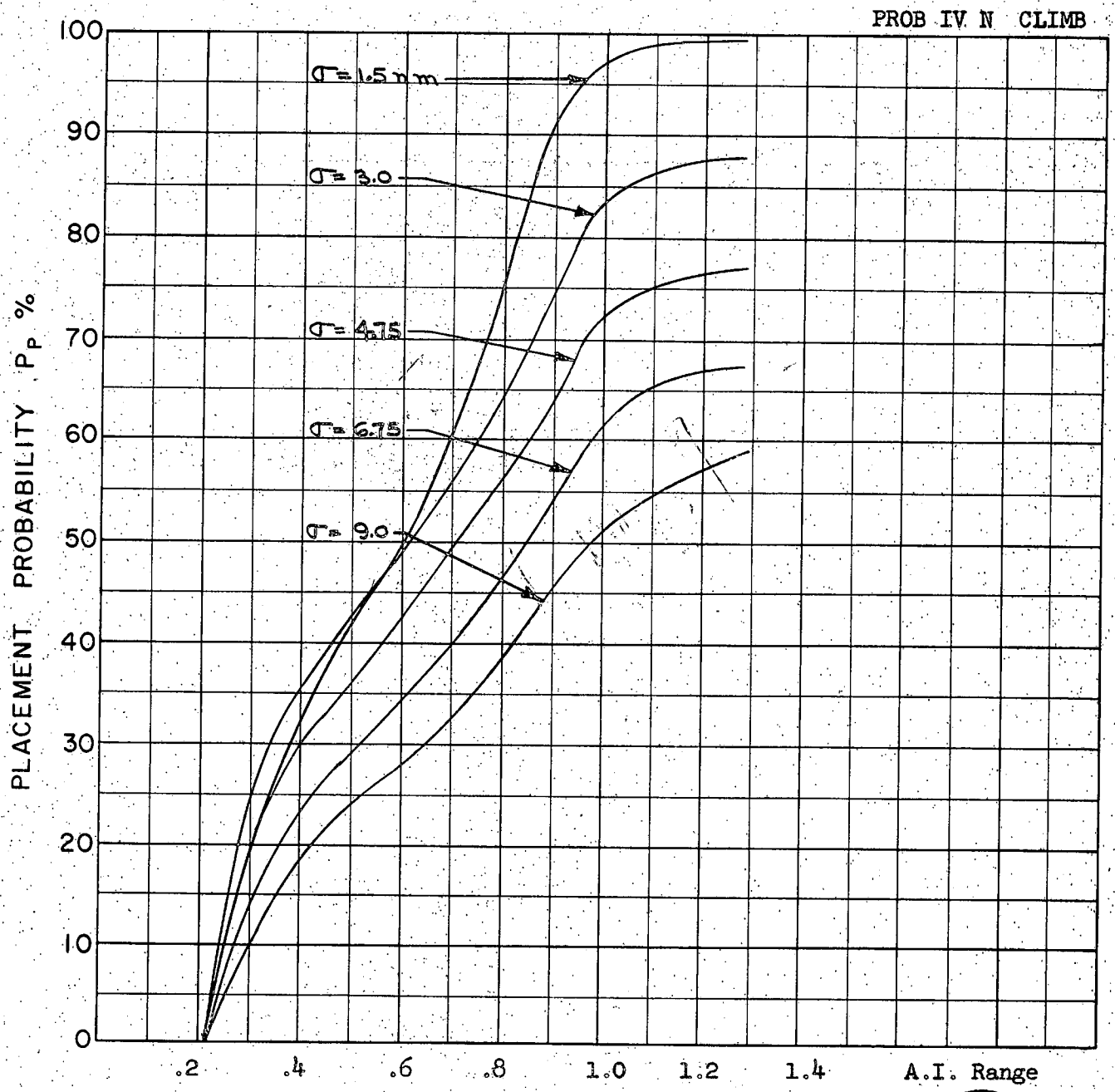

A-63

COURSE DIFFERENCE: 75°
TARGET EVASION: Nil
TARGET MACH NO.: 2.0
INTERCEPTOR LATERAL G's: Avro 3.3
INTERCEPTOR MACH NO.: 2.0
σ OF G.C.I. ACCURACY: 5 Values
A.I. DETECTION RANGE AS FRACTION OF SPECIFICATION RANGE, S: Abscissa
A.I. DETECTION RANGE CONTOUR: Delta
ALTITUDE: H_t = 70 K
H_f = 40 K

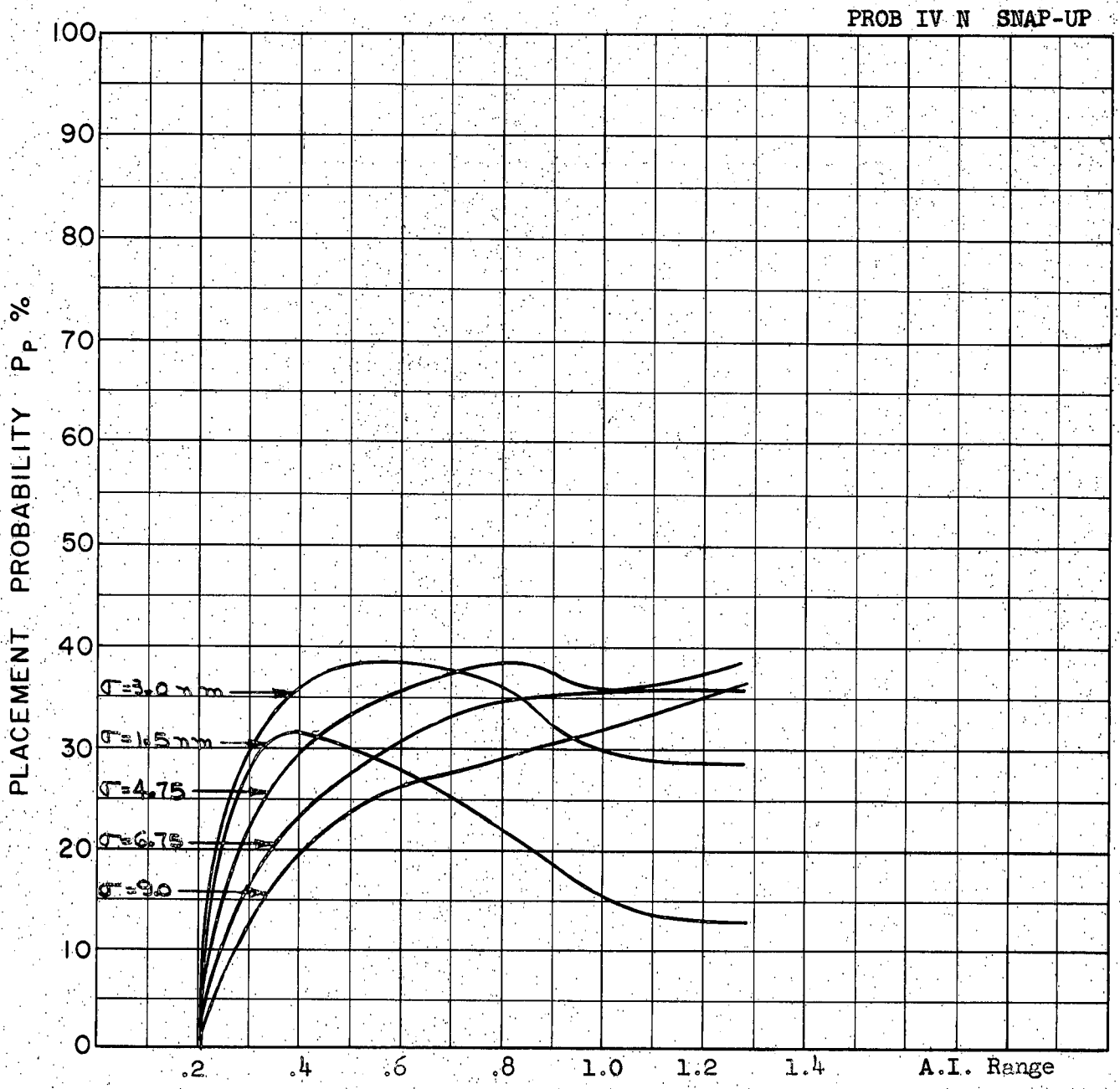

A-64

COURSE DIFFERENCE: 75°
TARGET EVASION: Nil
TARGET MACH NO.: 2.0
INTERCEPTOR LATERAL G's: Avro 3.3
INTERCEPTOR MACH NO.: 2.0
σ OF G.C.I. ACCURACY: 5 Values
A.I. DETECTION RANGE AS FRACTION OF SPECIFICATION RANGE, S: Abscissa
A.I. DETECTION RANGE CONTOUR: Delta
ALTITUDE: H_t = 70 K
H_f = 40 K

PROB V AB

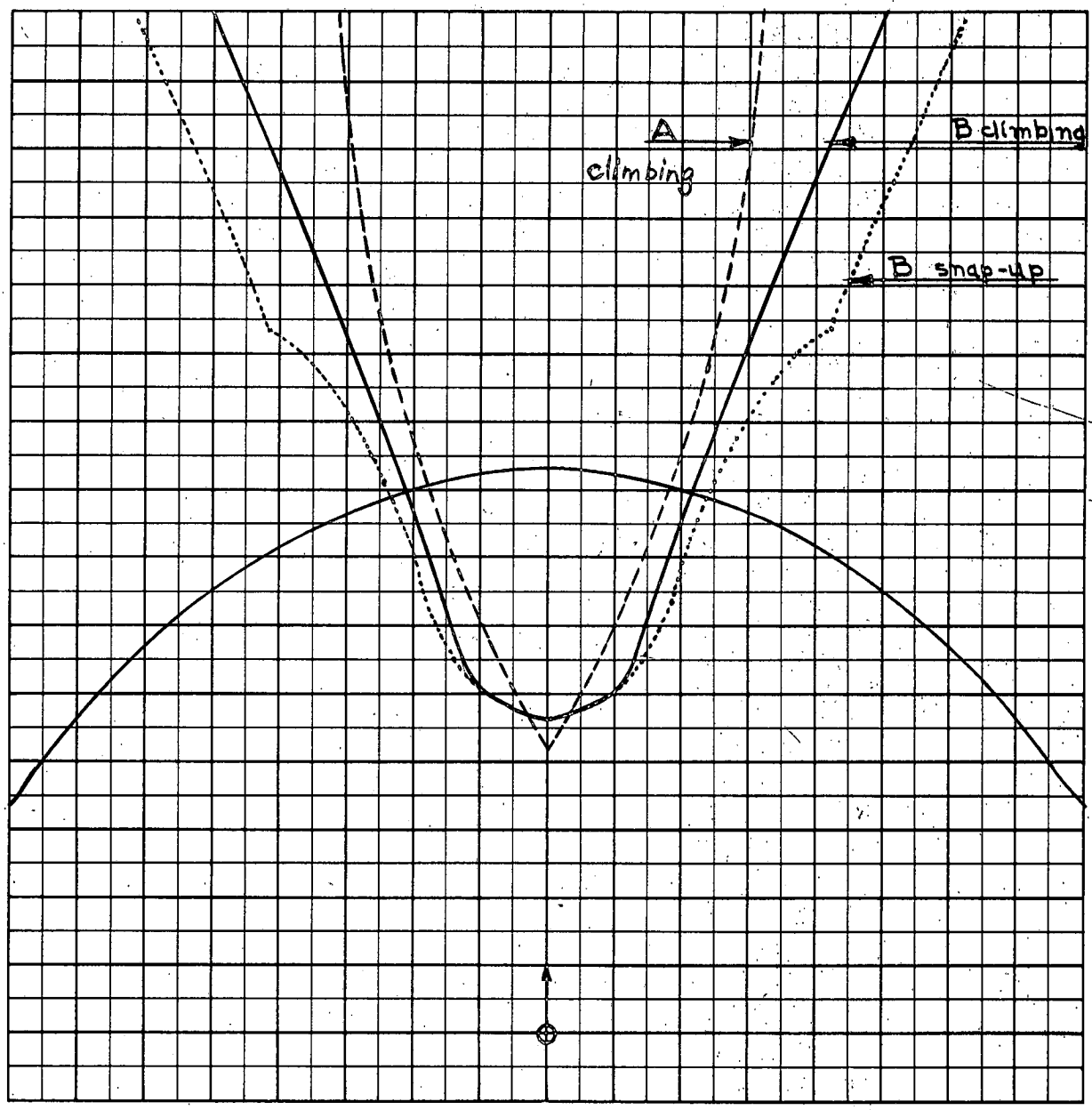

Scale 25,000 ft/cm

A-65

M_t = 3.5

h_t = 70 K

M_{fo} = 2.0

$h_{fo\ A}$ = 60 K

B = 40 K

Γ_o = 180°

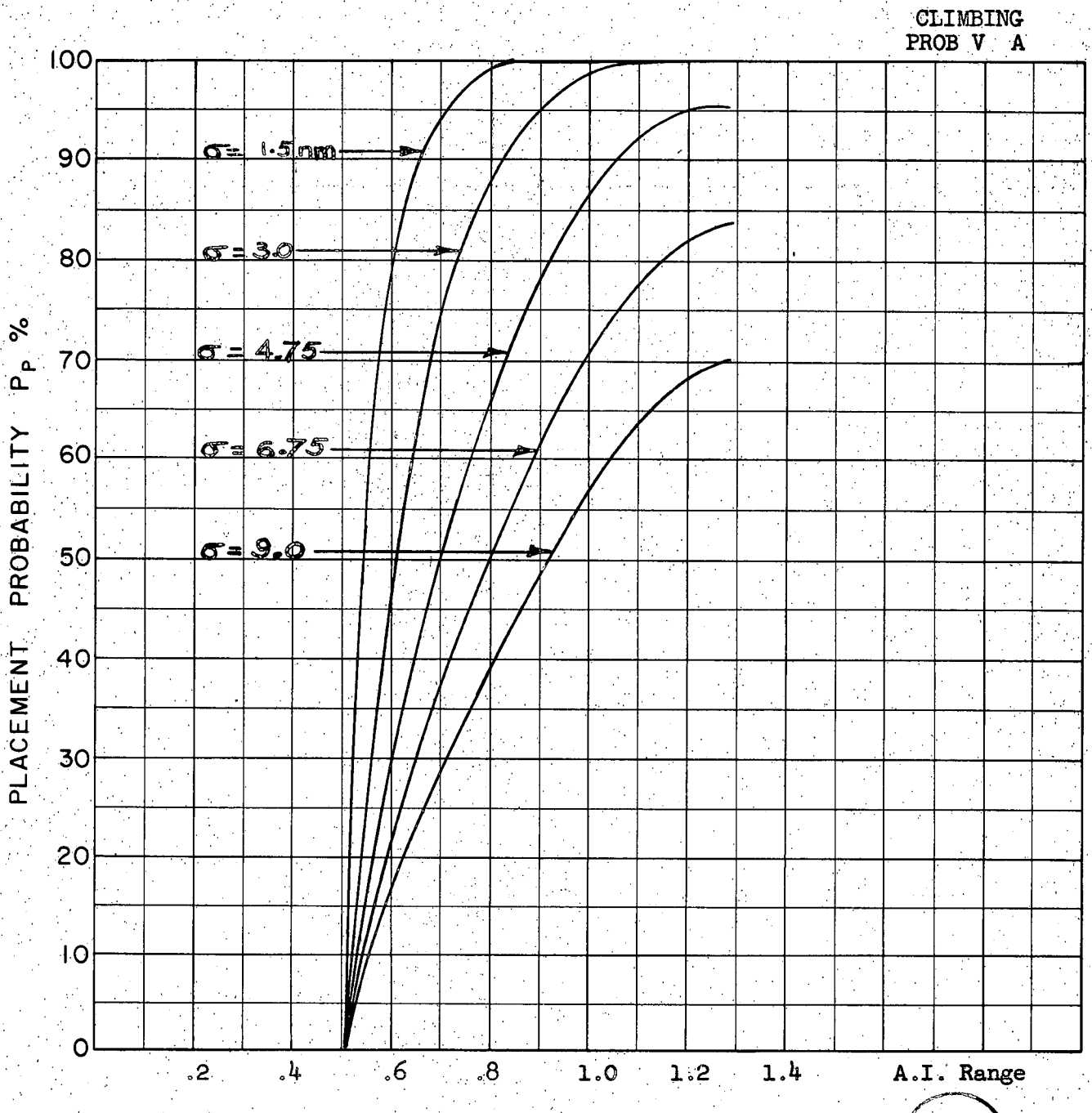

A-66

COURSE DIFFERENCE: 180°
TARGET EVASION: Nil
TARGET MACH NO.: 3.5
INTERCEPTOR LATERAL G's: Avro 3.3
INTERCEPTOR MACH NO.: 2.0
σ OF G.C.I. ACCURACY: 5 Values
A.I. DETECTION RANGE AS FRACTION OF SPECIFICATION RANGE, S: Abscissa
A.I. DETECTION RANGE CONTOUR: Delta
ALTITUDE: H_t = 70 K
H_f = 60 K

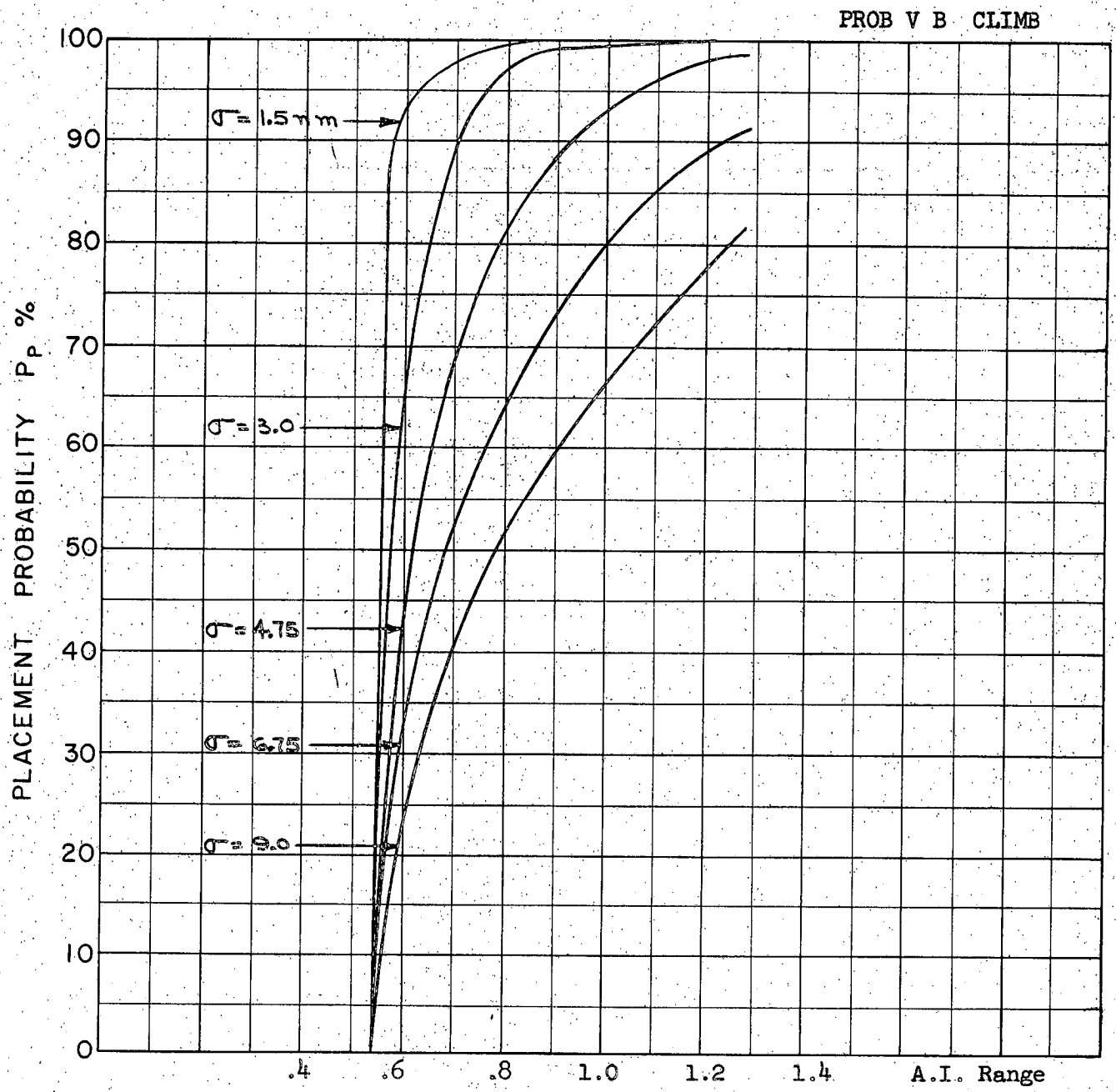

A-67

COURSE DIFFERENCE: 180°
TARGET EVASION: Nil
TARGET MACH NO.: 3.5
INTERCEPTOR LATERAL G's: Avro 3.3
INTERCEPTOR MACH NO.: 2.0
σ OF G.C.I. ACCURACY: 5 Values
A.I. DETECTION RANGE AS FRACTION OF SPECIFICATION RANGE, S: Abscissa
A.I. DETECTION RANGE CONTOUR: Delta
ALTITUDE: H_t = 70 K
H_f = 40 K

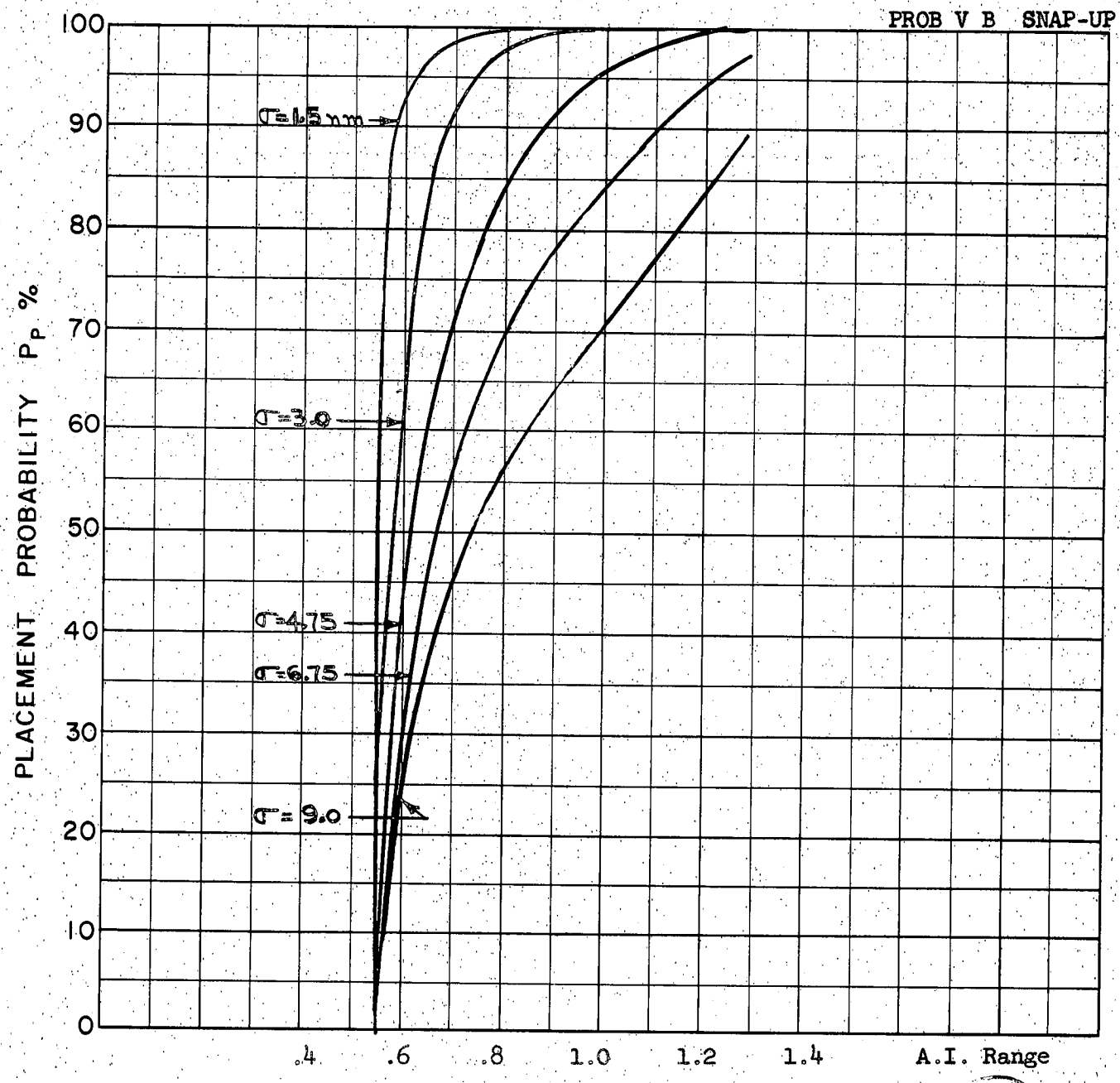

A-68

COURSE DIFFERENCE: 180°
TARGET EVASION: Nil
TARGET MACH NO.: 3.5
INTERCEPTOR LATERAL G's: Avro 3.3
INTERCEPTOR MACH NO.: 2.0
σ OF G.C.I. ACCURACY: 5 Values
A.I. DETECTION RANGE AS FRACTION OF SPECIFICATION RANGE, S: Abscissa
A.I. DETECTION RANGE CONTOUR: Delta
ALTITUDE: H_t = 70 K
H_f = 40 K

PROB V CD

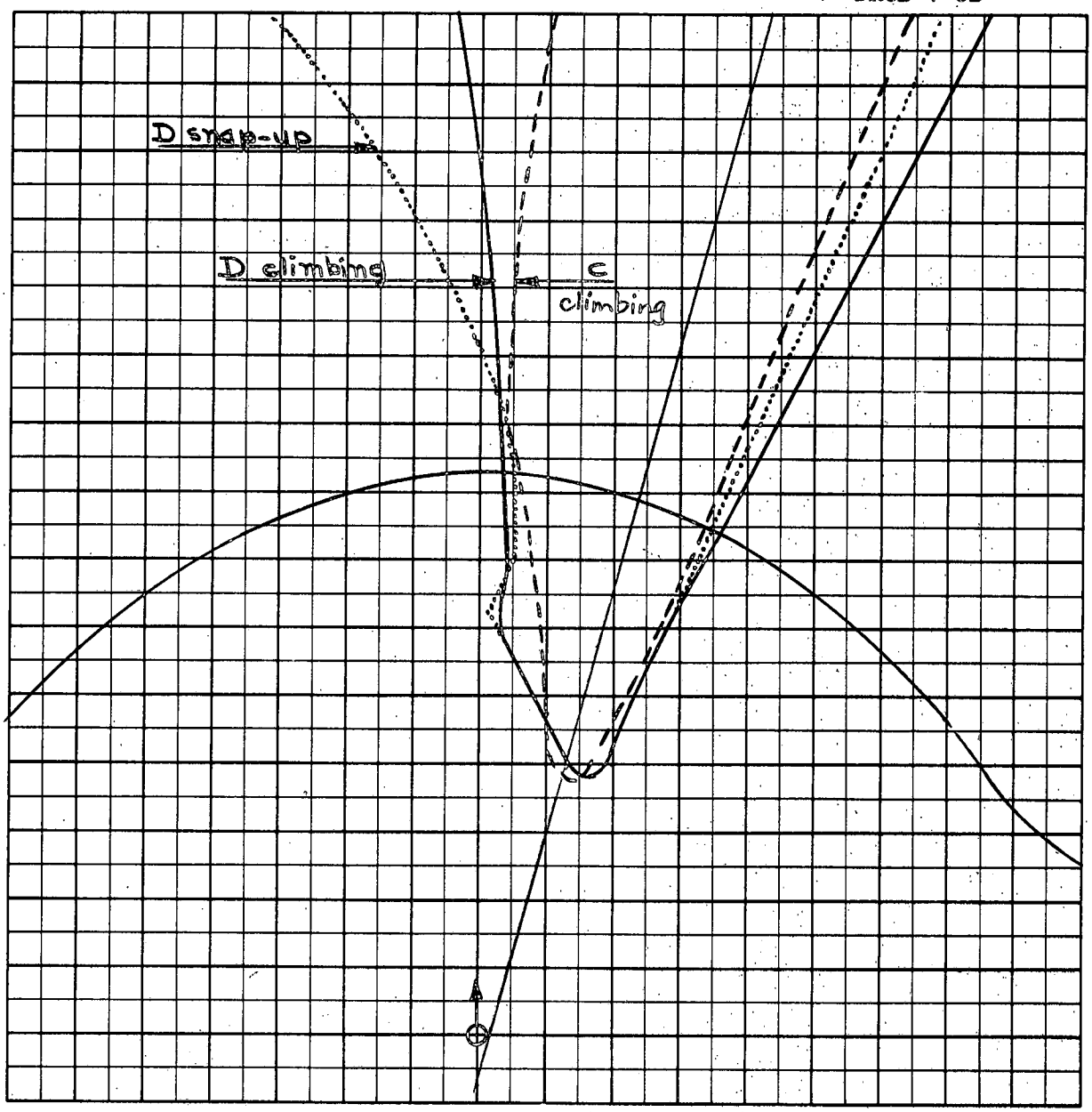

Scale 25,000 ft/cm

M_t = 3.5
h_t = 70 K
M_{fo} = 2.0
h_{fo} C = 60 K
D = 40 K
Γ_o = 135°

A-69

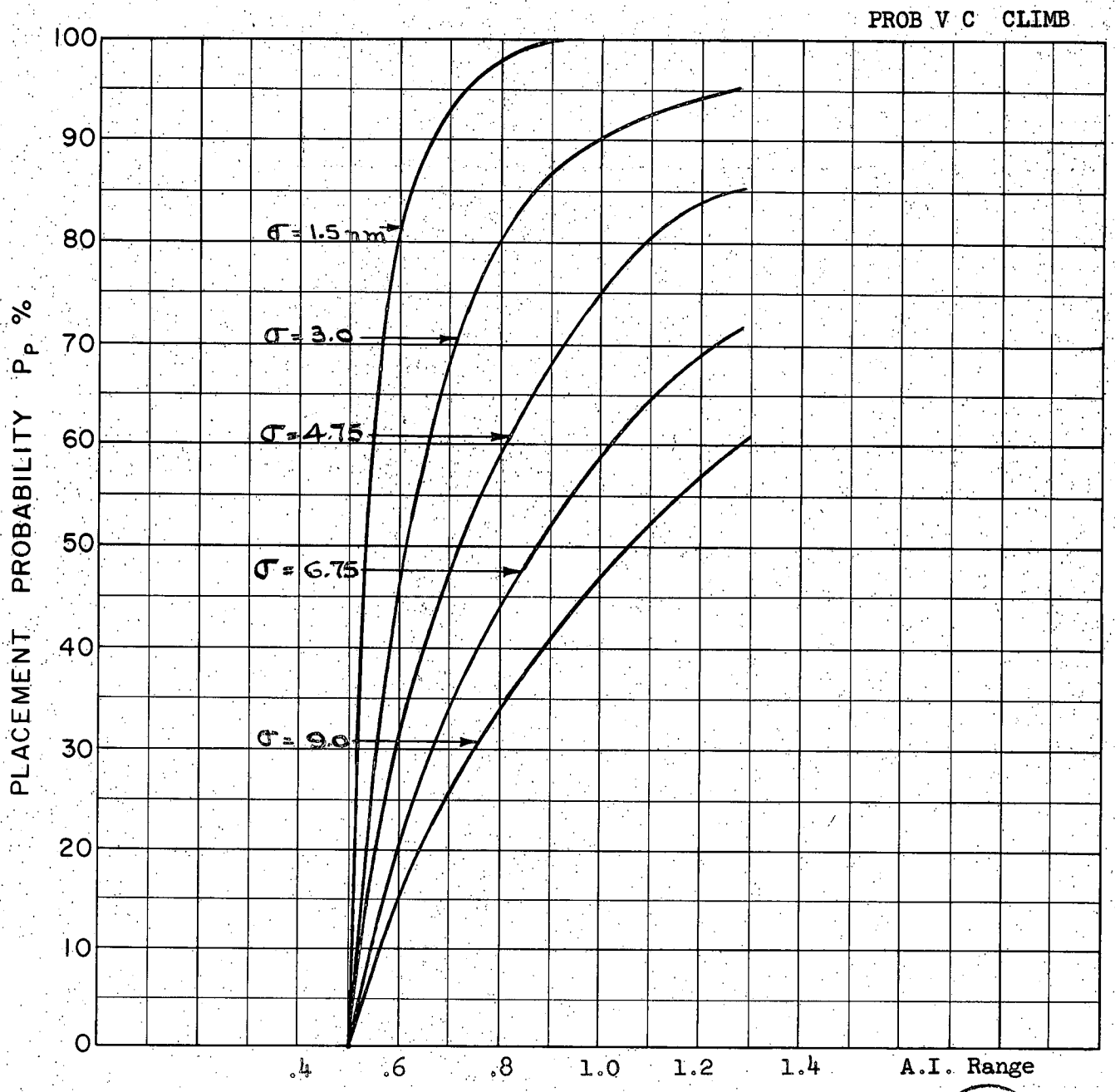

A-70

COURSE DIFFERENCE: 135°
TARGET EVASION: Nil
TARGET MACH NO.: 3.5
INTERCEPTOR LATERAL G's: Avro 3.3
INTERCEPTOR MACH NO.: 2.0
σ OF G.C.I. ACCURACY: 5 Values
A.I. DETECTION RANGE AS FRACTION OF SPECIFICATION RANGE, S: Abscissa
A.I. DETECTION RANGE CONTOUR: Delta
ALTITUDE: H_t = 70 K
H_f = 60 K

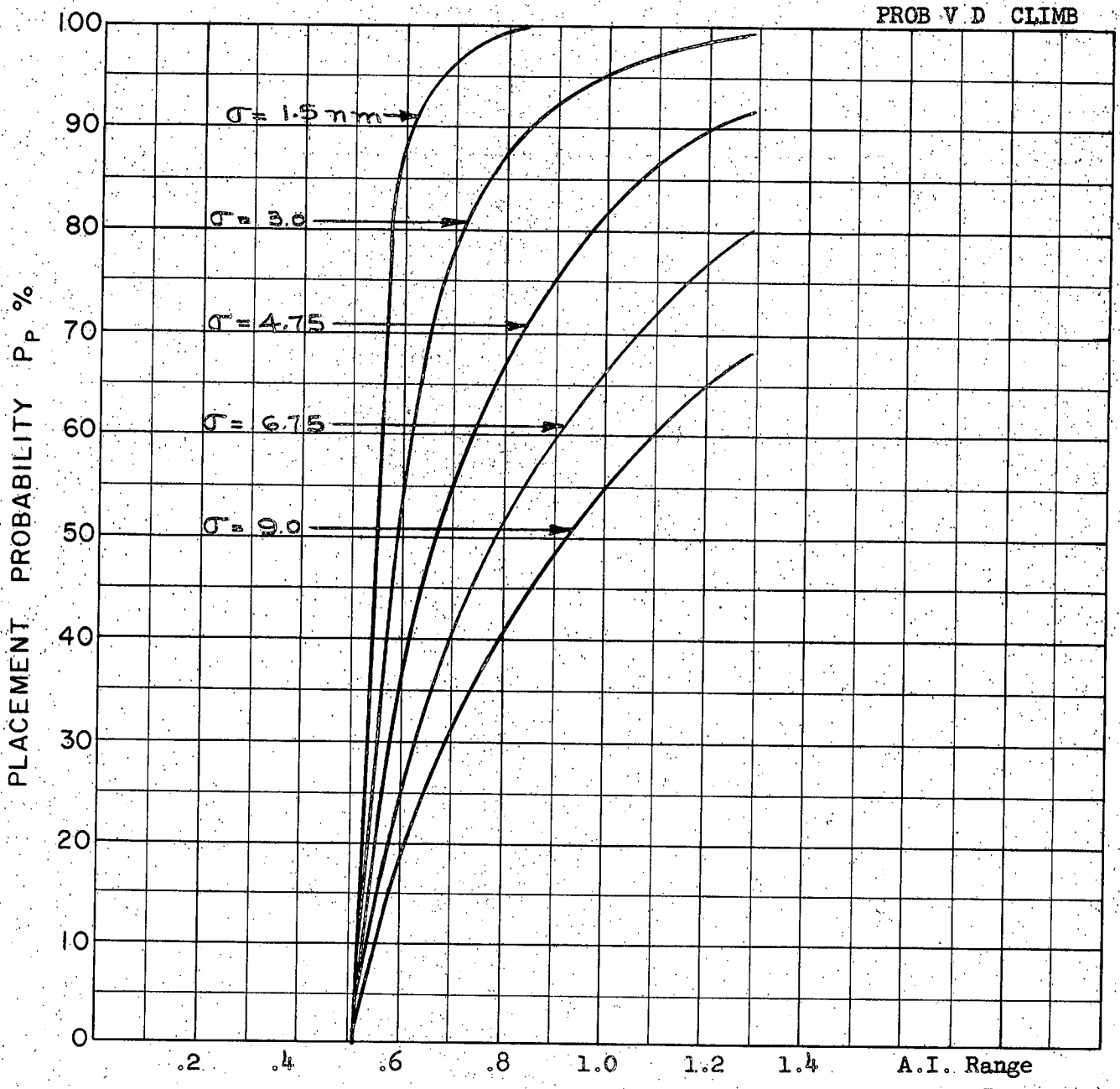

A-71

COURSE DIFFERENCE: 135°
TARGET EVASION: Nil
TARGET MACH NO.: 3.5
INTERCEPTOR LATERAL G's: Avro 3.3
INTERCEPTOR MACH NO.: 2.0
σ OF G.C.I. ACCURACY: 5 Values
A.I. DETECTION RANGE AS FRACTION OF SPECIFICATION RANGE, S: Abscissa
A.I. DETECTION RANGE CONTOUR: Delta
ALTITUDE: H_t = 70 K
H_f = 40 K

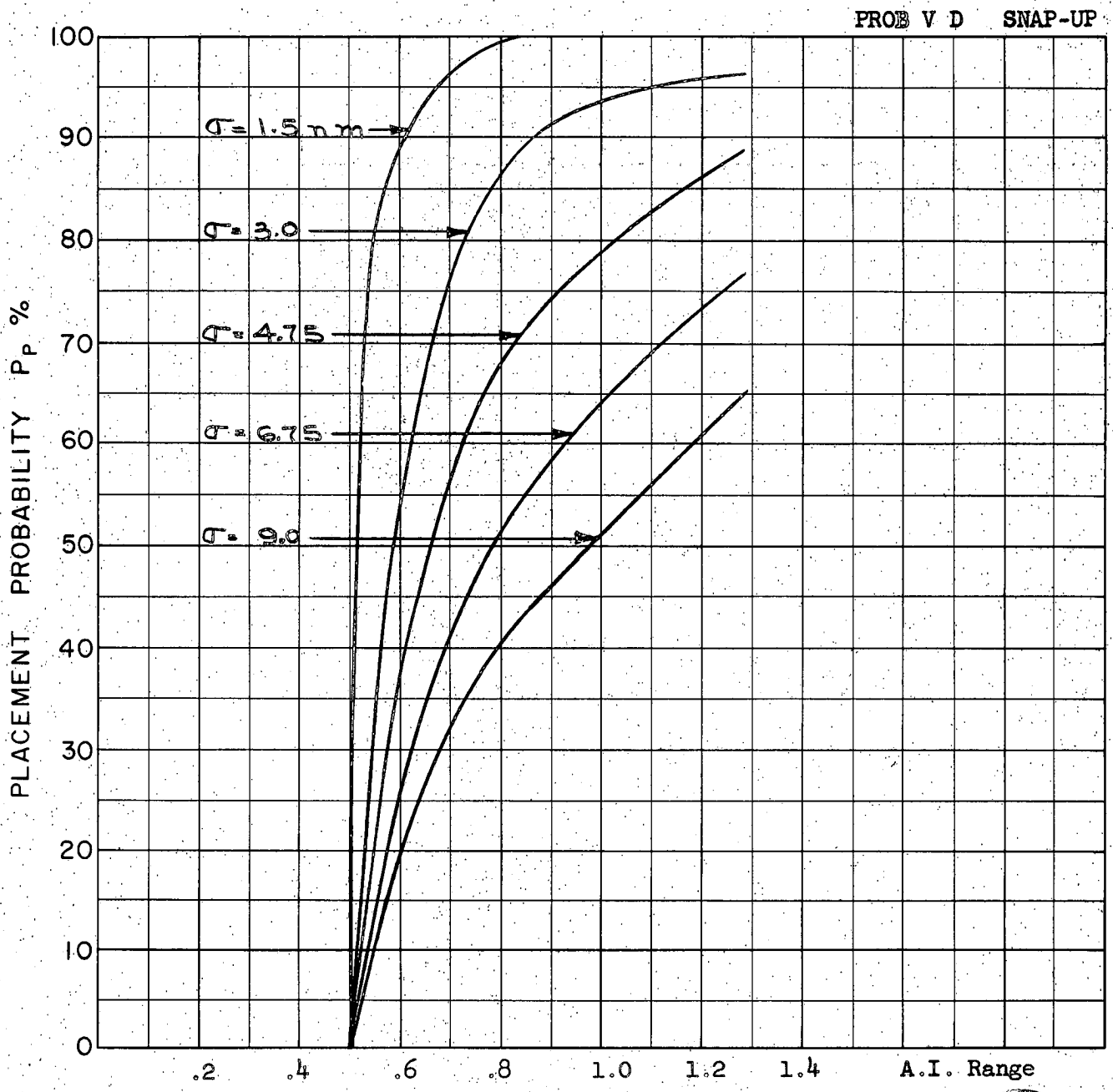

A-72

COURSE DIFFERENCE: 135°
TARGET EVASION: Nil
TARGET MACH NO.: 3.5
INTERCEPTOR LATERAL G's: Avro 3.3
INTERCEPTOR MACH NO.: 2.0
σ OF G.C.I. ACCURACY: 5 Values
A.I. DETECTION RANGE AS FRACTION OF SPECIFICATION RANGE, S: Abscissa
A.I. DETECTION RANGE CONTOUR: Delta
ALTITUDE: H_t = 70 K
H_f = 40 K

PROB VI A

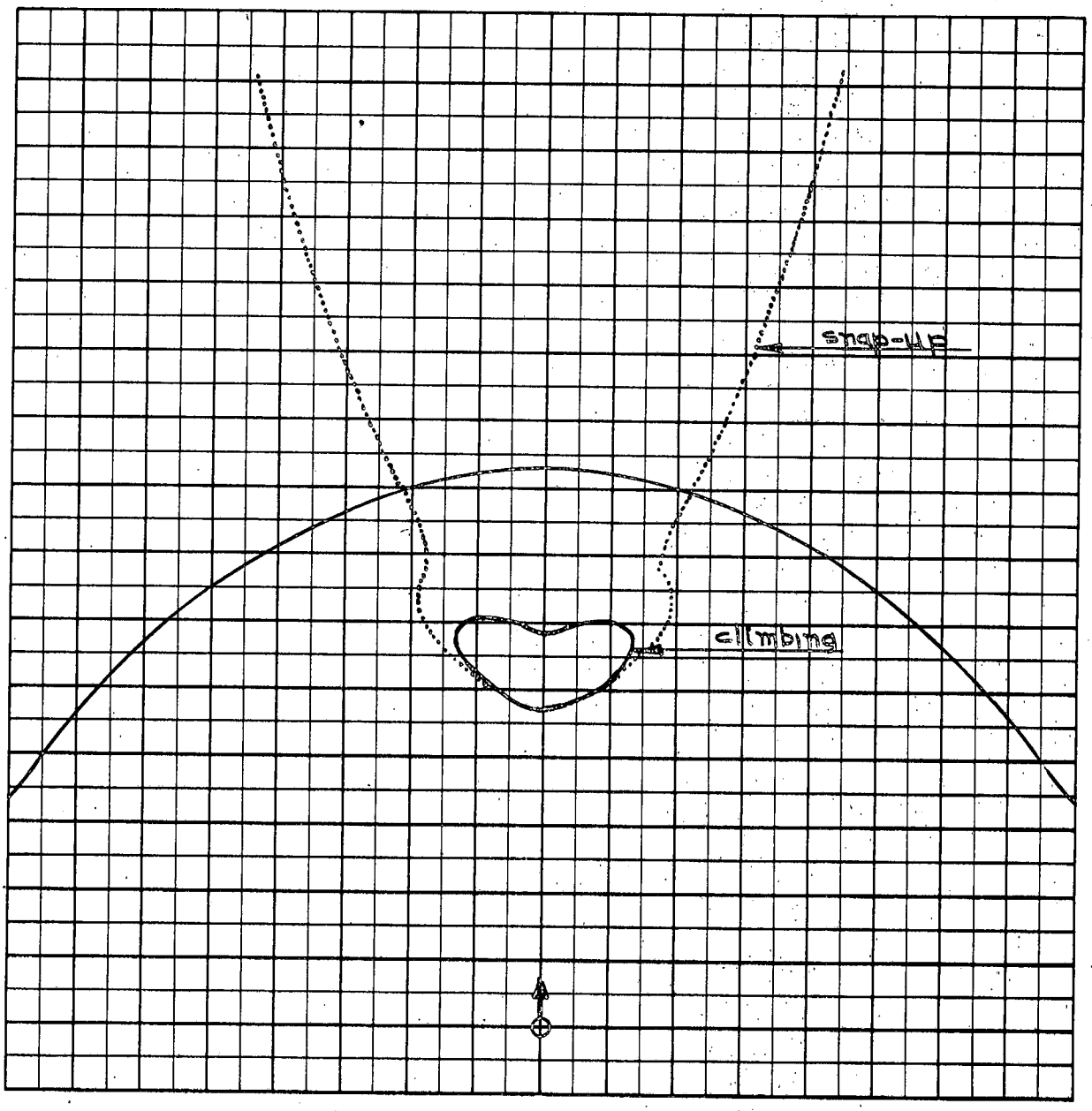

Scale 25,000 ft/cm

M_t = 3.5

h_t = 80 K

M_{fo} = 2.0

$h_{fo\ A}$ = 40 K

Γ_o = 180°

A-73

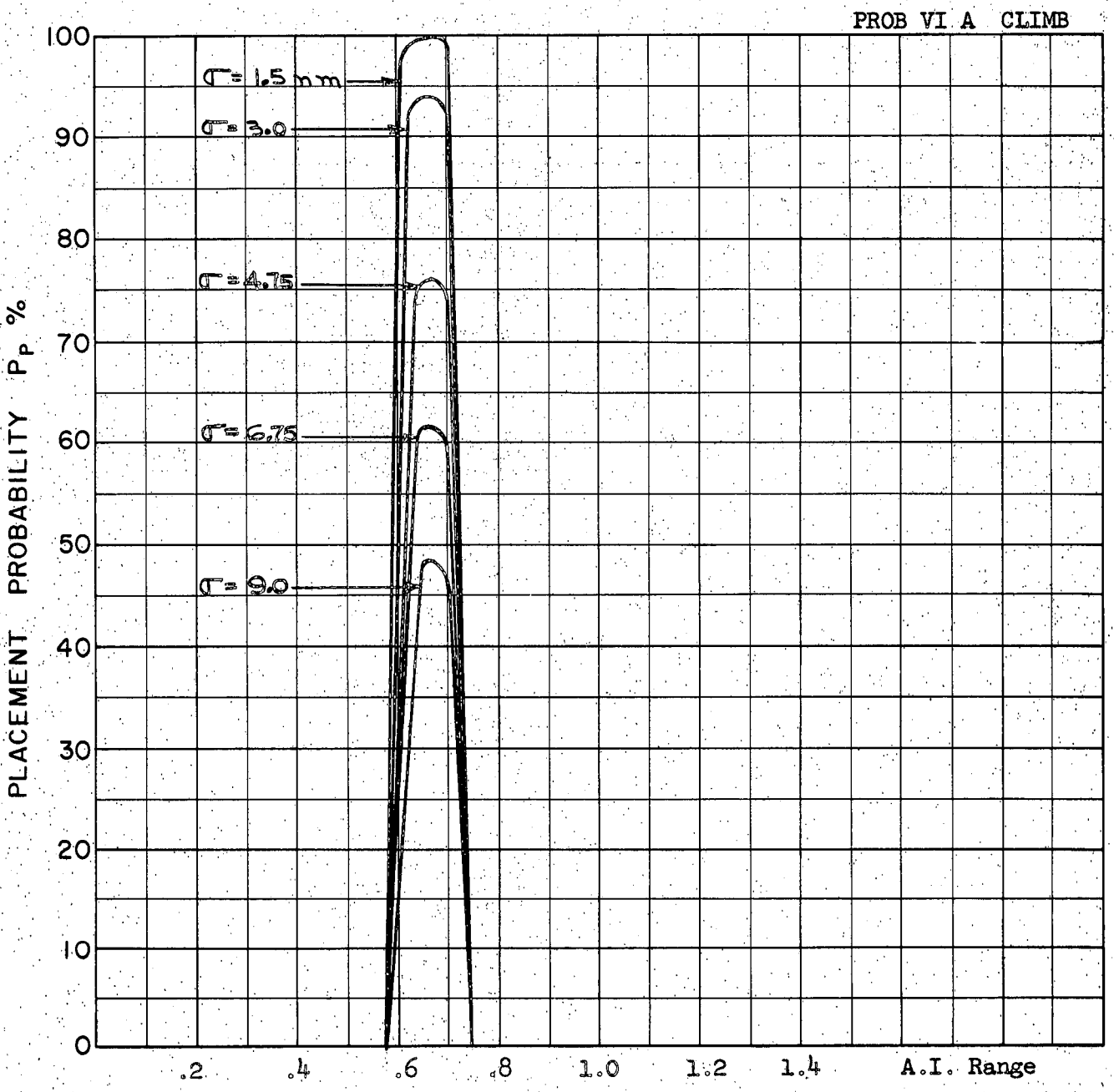

A-74

COURSE DIFFERENCE: 180°
TARGET EVASION: Nil
TARGET MACH NO.: 3.5
INTERCEPTOR LATERAL G's: Avro 3.3
INTERCEPTOR MACH NO.: 2.0
σ OF G.C.I. ACCURACY: 5 Values
A.I. DETECTION RANGE AS FRACTION OF SPECIFICATION RANGE, S: Abscissa
A.I. DETECTION RANGE CONTOUR: Delta
ALTITUDE: H_t = 80 K
H_f = 40 K

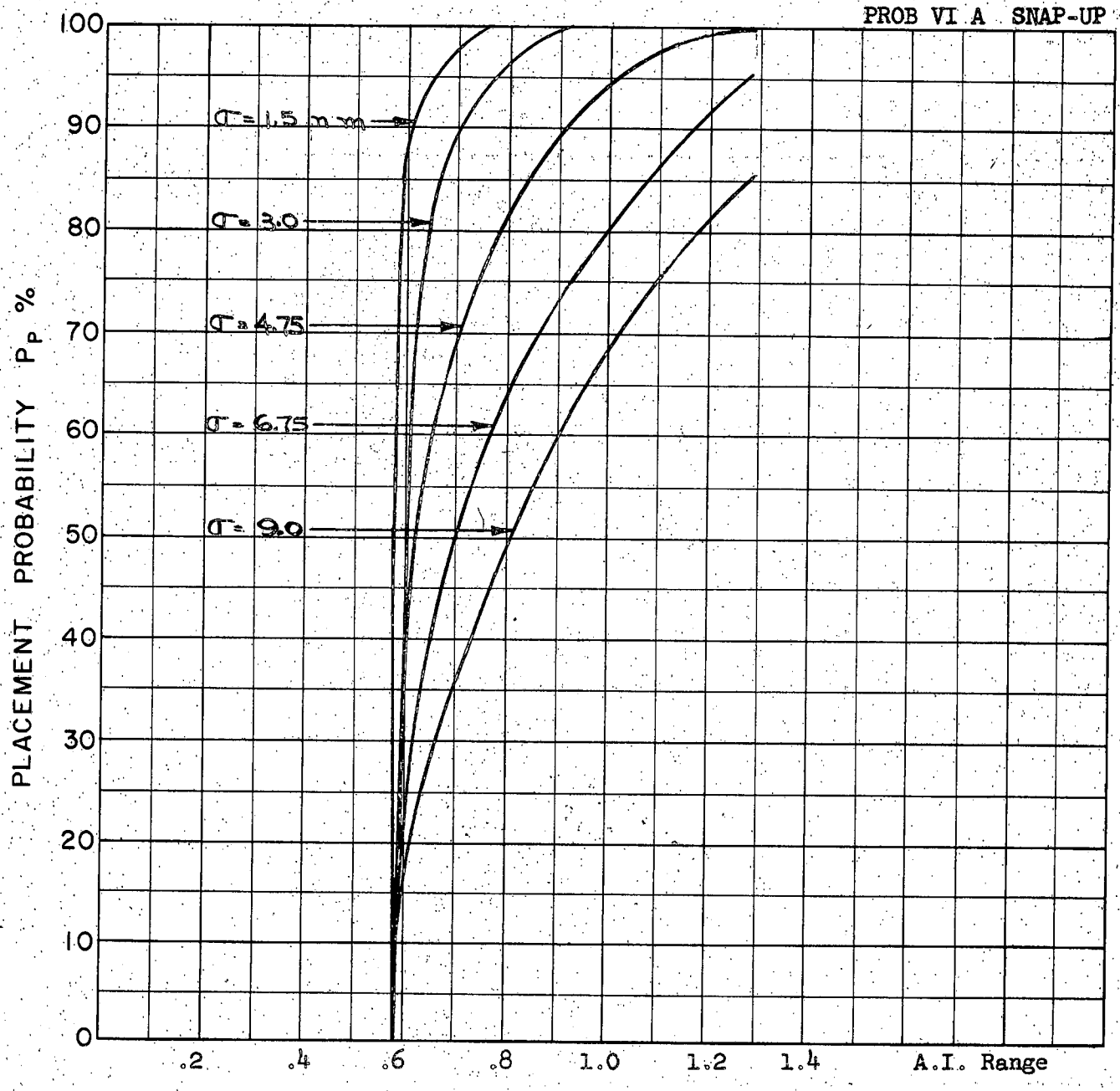

A-75

COURSE DIFFERENCE: 180°
TARGET EVASION: Nil
TARGET MACH NO.: 3.5
INTERCEPTOR LATERAL G's: Avro 3.3
INTERCEPTOR MACH NO.: 2.0
σ OF G.C.I. ACCURACY: 5 Values
A.I. DETECTION RANGE AS FRACTION OF SPECIFICATION RANGE, S: Abscissa
A.I. DETECTION RANGE CONTOUR: Delta
ALTITUDE: H_t = 80 K
H_f = 40 K

PROB VI B

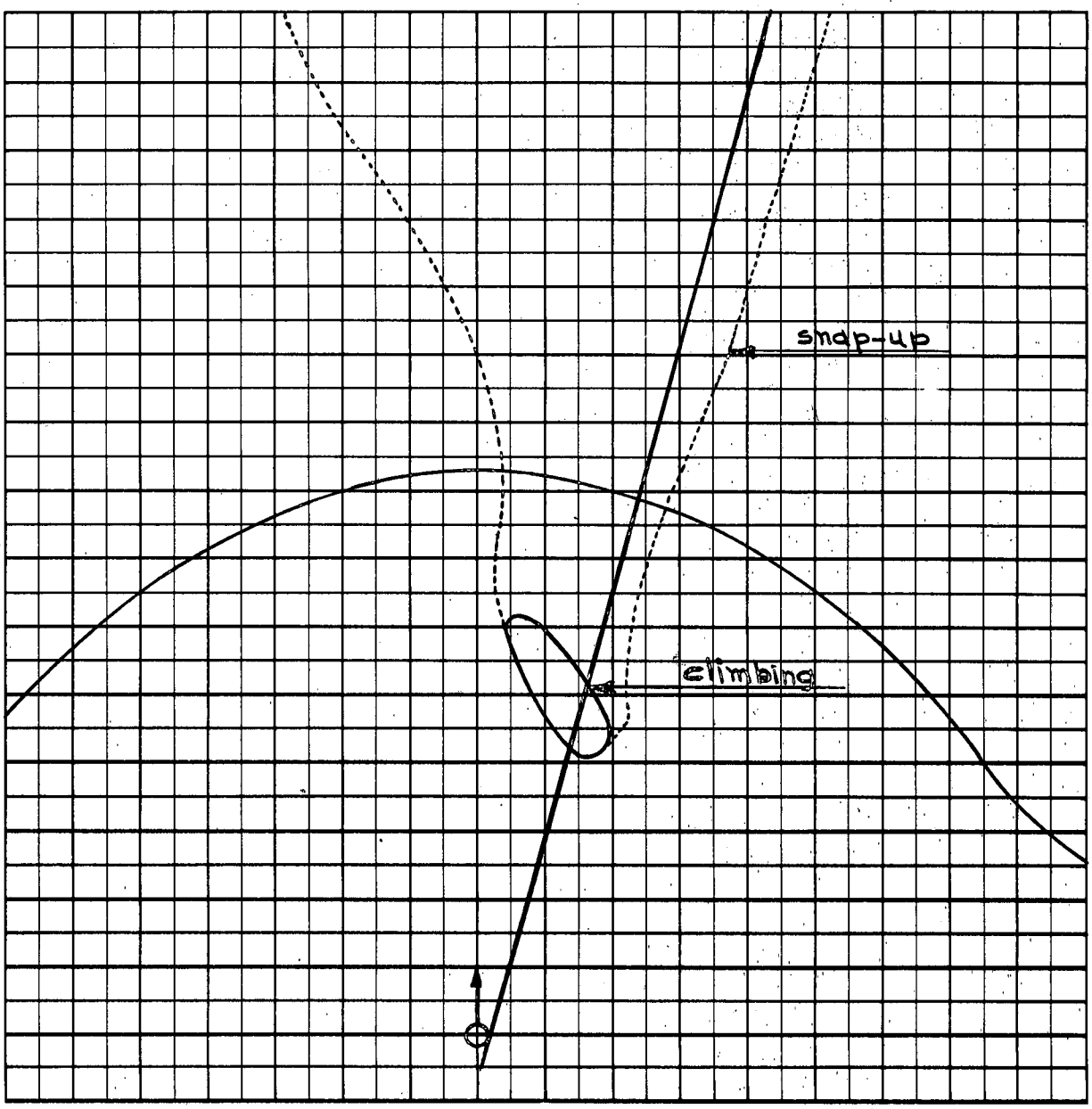

Scale 25,000 ft/cm

M_t = 3.5

h_t = 80 K

M_{fo} = 2.0

$h_{fo\ B}$ = 40 K

Γ_o = 135°

A-76

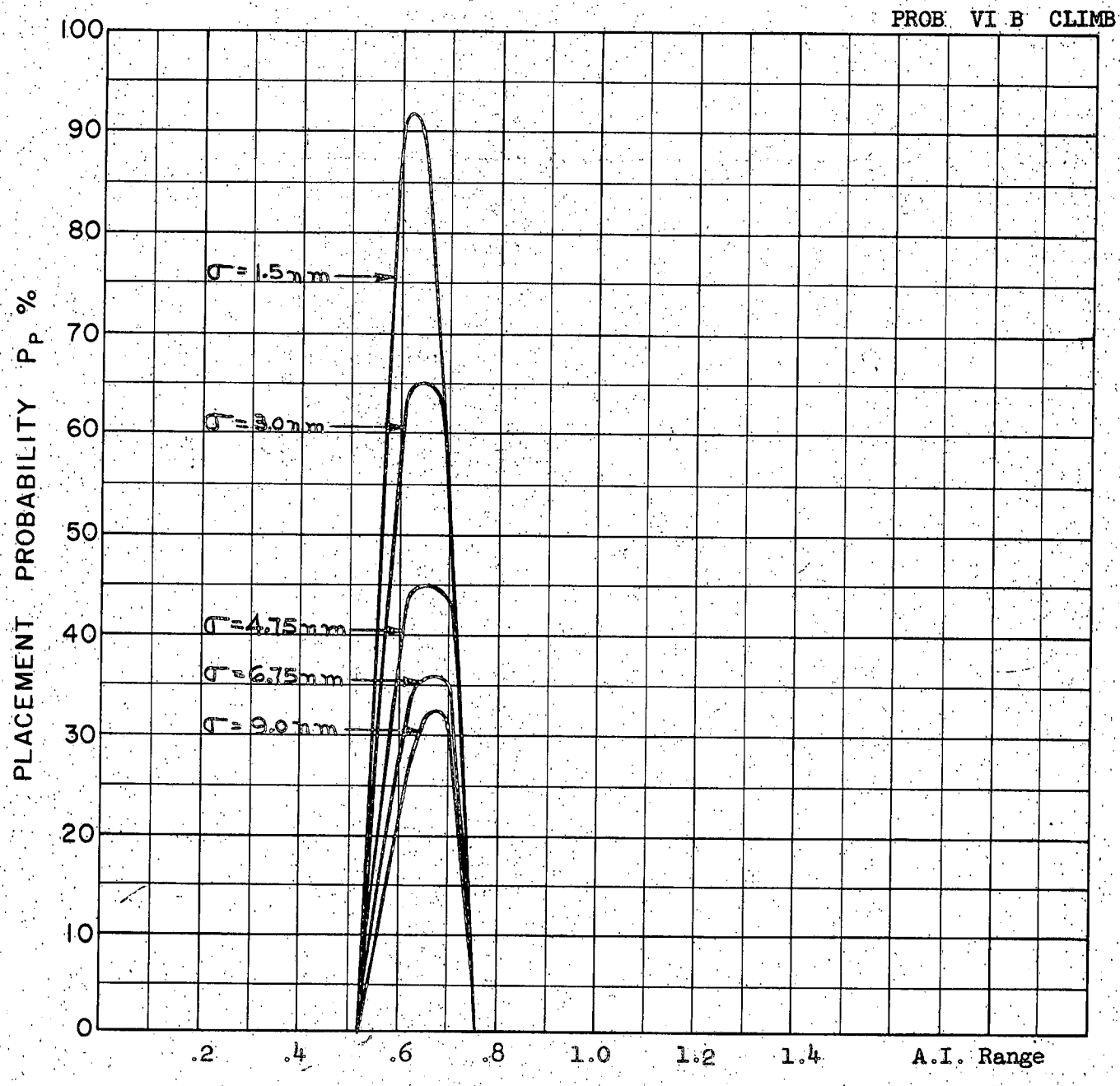

A-77

COURSE DIFFERENCE: 135°
TARGET EVASION: Nil
TARGET MACH NO.: 3.5
INTERCEPTOR LATERAL G's: Avro 3.3
INTERCEPTOR MACH NO.: 2.0
σ OF G.C.I. ACCURACY: 5 Values
A.I. DETECTION RANGE AS FRACTION OF SPECIFICATION RANGE, S: Abscissa
A.I. DETECTION RANGE CONTOUR: Delta
ALTITUDE: H_t = 80 K
H_f = 40 K

PROB VI B SNAP-UP

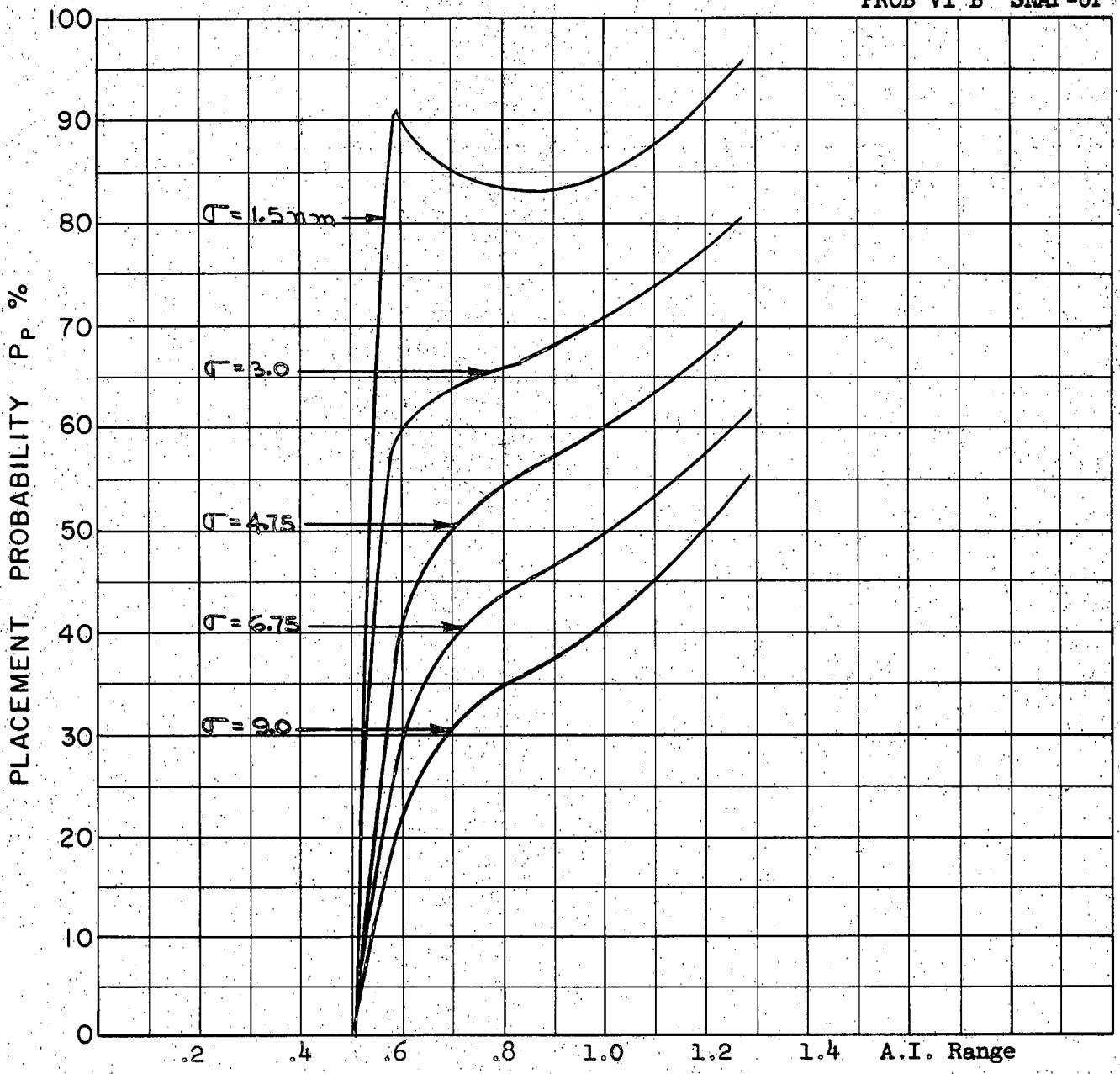

A-78

COURSE DIFFERENCE: 135°
TARGET EVASION: Nil
TARGET MACH NO.: 3.5
INTERCEPTOR LATERAL G's: Avro 3.3
INTERCEPTOR MACH NO.: 2.0
σ OF G.C.I. ACCURACY: 5 Values
A.I. DETECTION RANGE AS FRACTION OF SPECIFICATION RANGE, S: Abscissa
A.I. DETECTION RANGE CONTOUR: Delta
ALTITUDE: H_t = 80 K
H_f = 40 K

PROB VII ABC

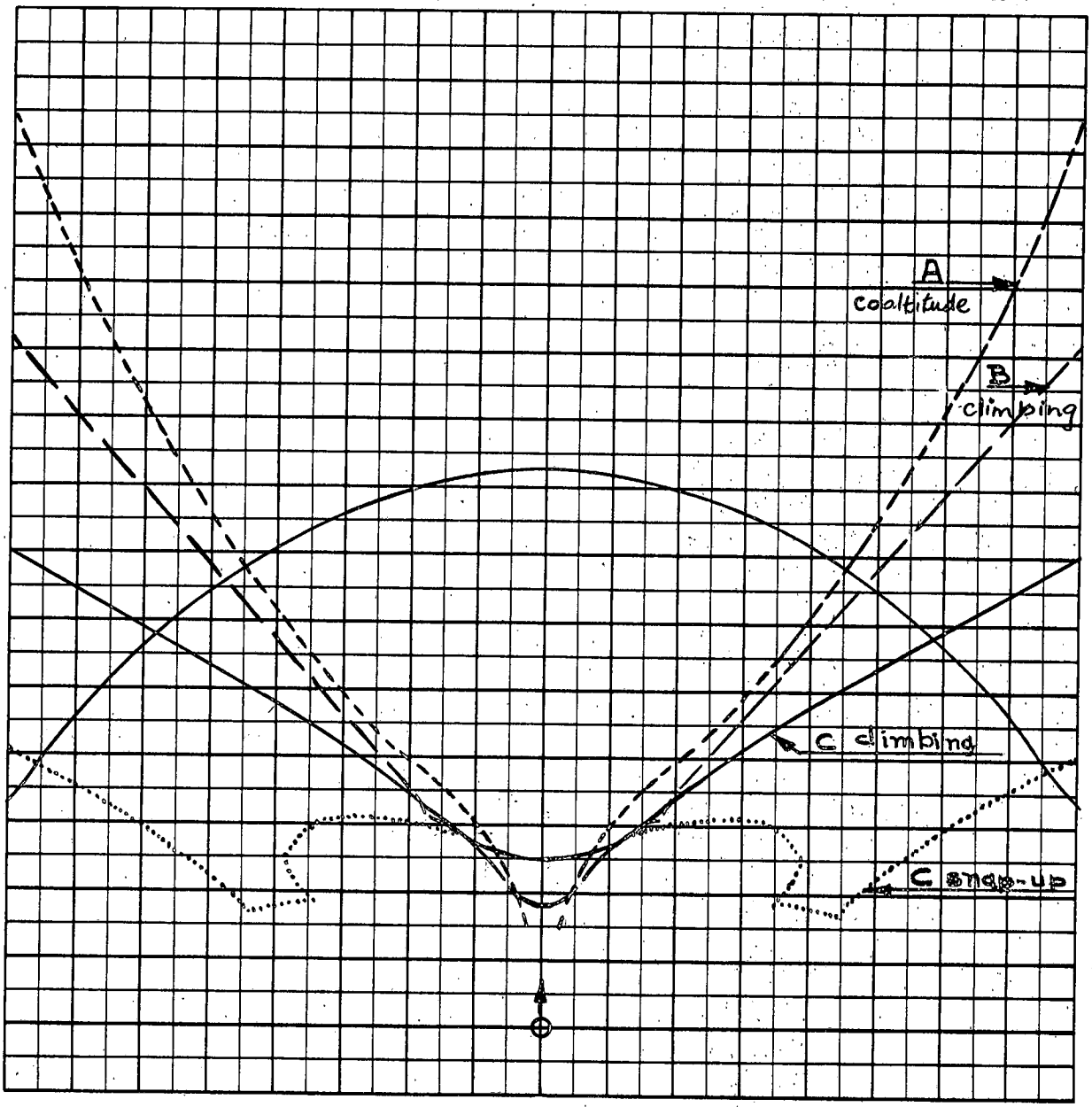

Scale 25,000 ft/cm

M_t = 1.5

h_t = 60 K

M_{fo} = 2.0

h_{fo} A = 60 K

B = 50 K

C = 40 K

Γ_o = 180°

A-79

COALTITUDE

PROB VII A

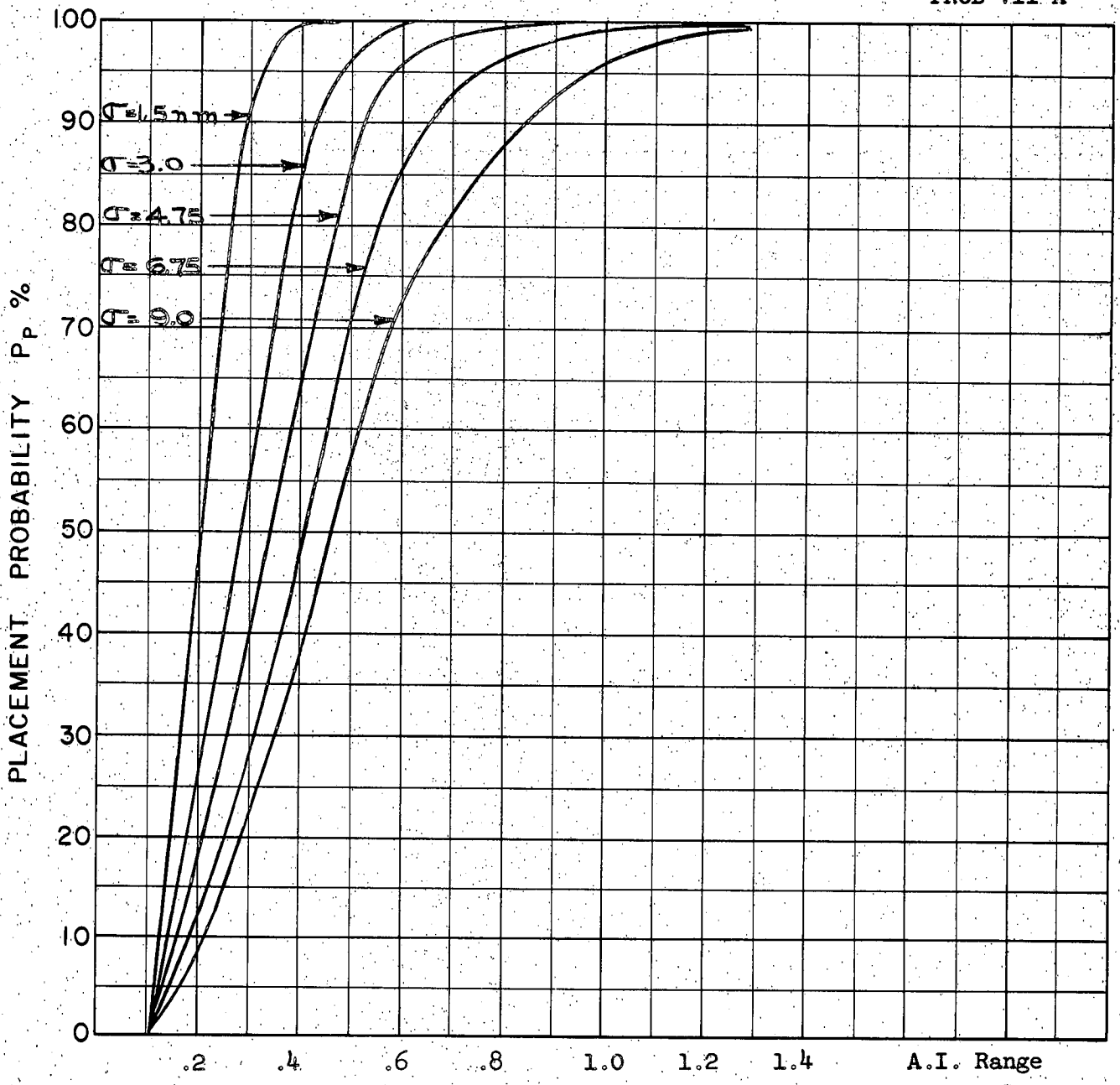

A-80

COURSE DIFFERENCE: 180°
TARGET EVASION: Nil
TARGET MACH NO.: 1.5
INTERCEPTOR LATERAL G's: Avro 3.3
INTERCEPTOR MACH NO.: 2.0
σ OF G.C.I. ACCURACY: 5 Values
A.I. DETECTION RANGE AS FRACTION OF SPECIFICATION RANGE, S: Abscissa
A.I. DETECTION RANGE CONTOUR: Delta
ALTITUDE: H_t = 60 K
H_f = 60 K

CLIMBING

PROB VII B

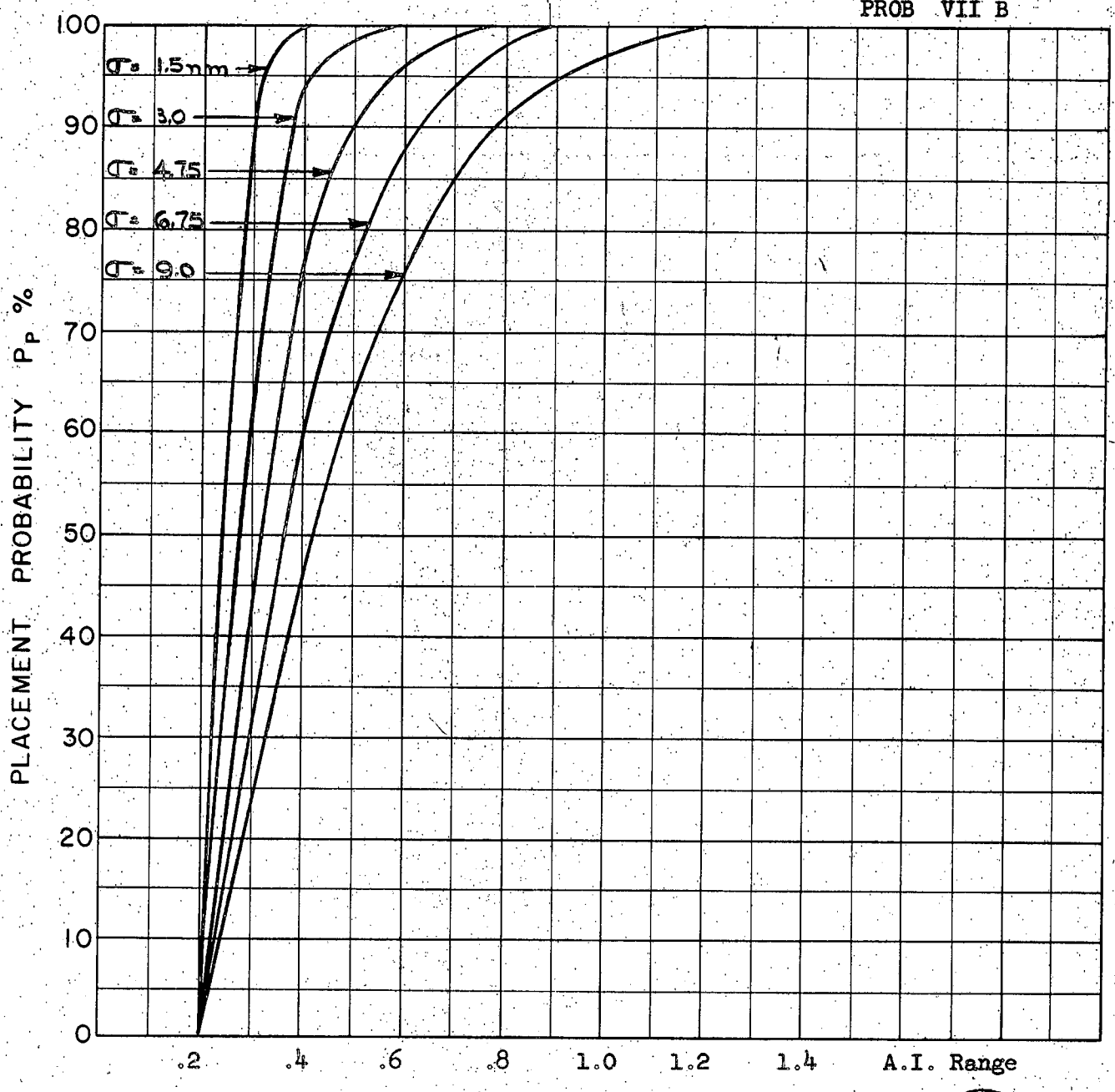

A-81

COURSE DIFFERENCE: 180°
TARGET EVASION: Nil
TARGET MACH NO.: 1.5
INTERCEPTOR LATERAL G's: Avro 3.3
INTERCEPTOR MACH NO.: 2.0
σ OF G.C.I. ACCURACY: 5 Values
A.I. DETECTION RANGE AS FRACTION OF SPECIFICATION RANGE, S: Abscissa
A.I. DETECTION RANGE CONTOUR: Delta
ALTITUDE: H_t = 60 K
H_f = 50 K

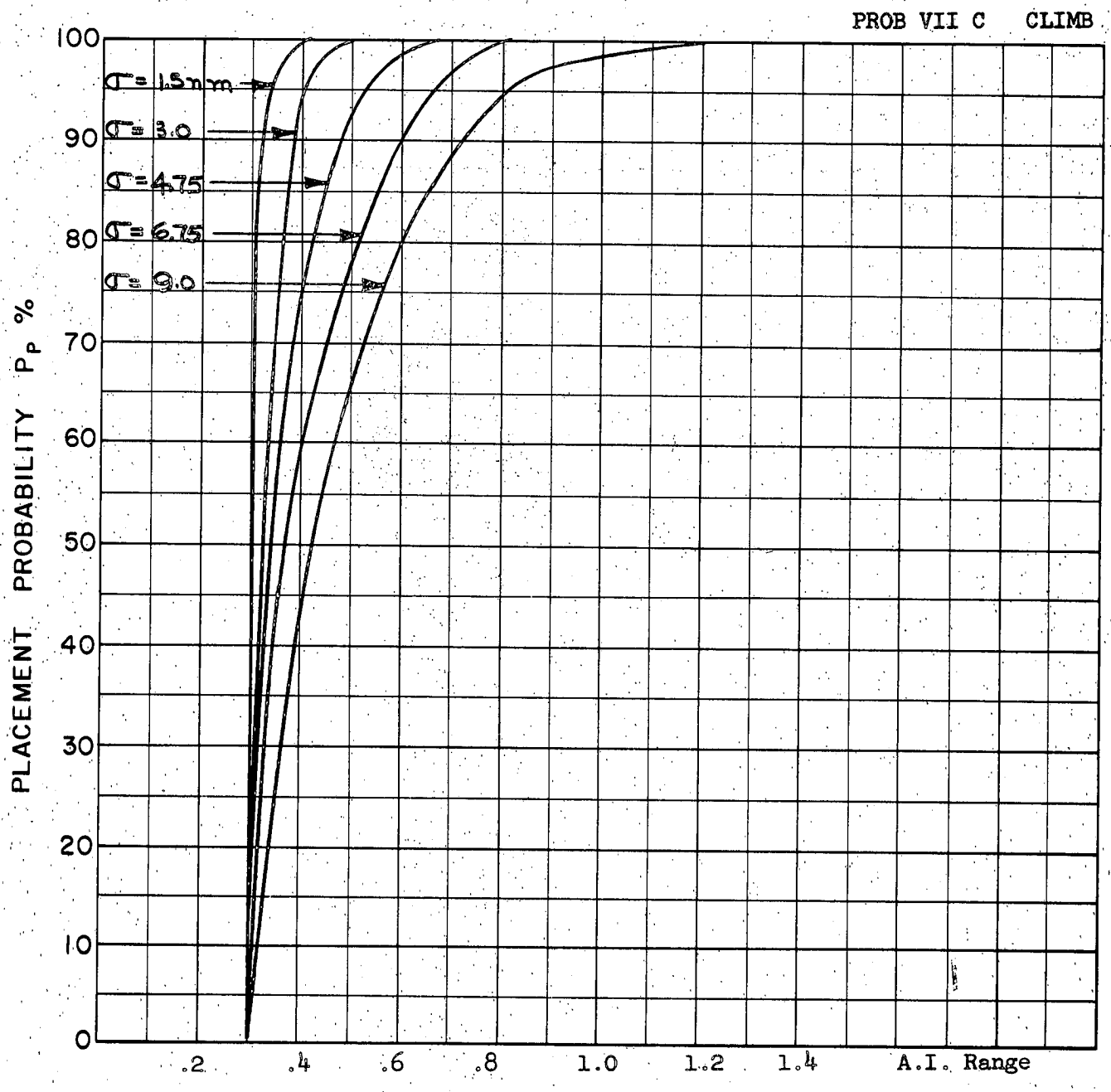

A-82

COURSE DIFFERENCE: 180°
TARGET EVASION: Nil
TARGET MACH NO.: 1.5
INTERCEPTOR LATERAL G's: Avro 3.3
INTERCEPTOR MACH NO.: 2.0
σ OF G.C.I. ACCURACY: 5 Values
A.I. DETECTION RANGE AS FRACTION OF SPECIFICATION RANGE, S: Abscissa
A.I. DETECTION RANGE CONTOUR: Delta
ALTITUDE: H_t = 60 K
H_f = 40 K

PROB VII C SNAP-UP

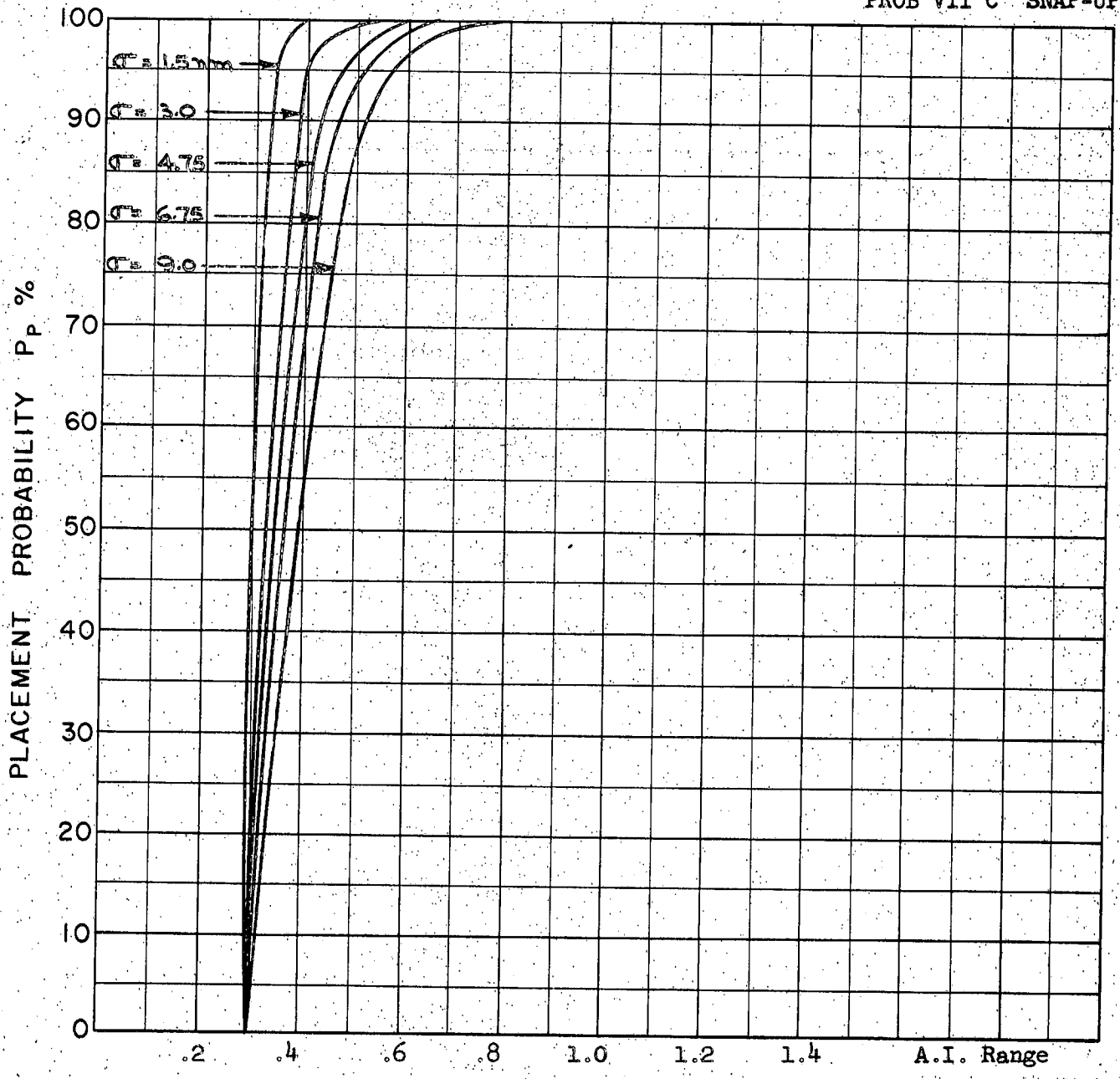

A-83

COURSE DIFFERENCE: 180°
TARGET EVASION: Nil
TARGET MACH NO.: 1.5
INTERCEPTOR LATERAL G's: Avro 3.3
INTERCEPTOR MACH NO.: 2.0
σ OF G.C.I. ACCURACY: 5 Values
A.I. DETECTION RANGE AS FRACTION OF SPECIFICATION RANGE, S: Abscissa
A.I. DETECTION RANGE CONTOUR: Delta
ALTITUDE: H_t = 60 K
H_f = 60 K

PROB VII DEF

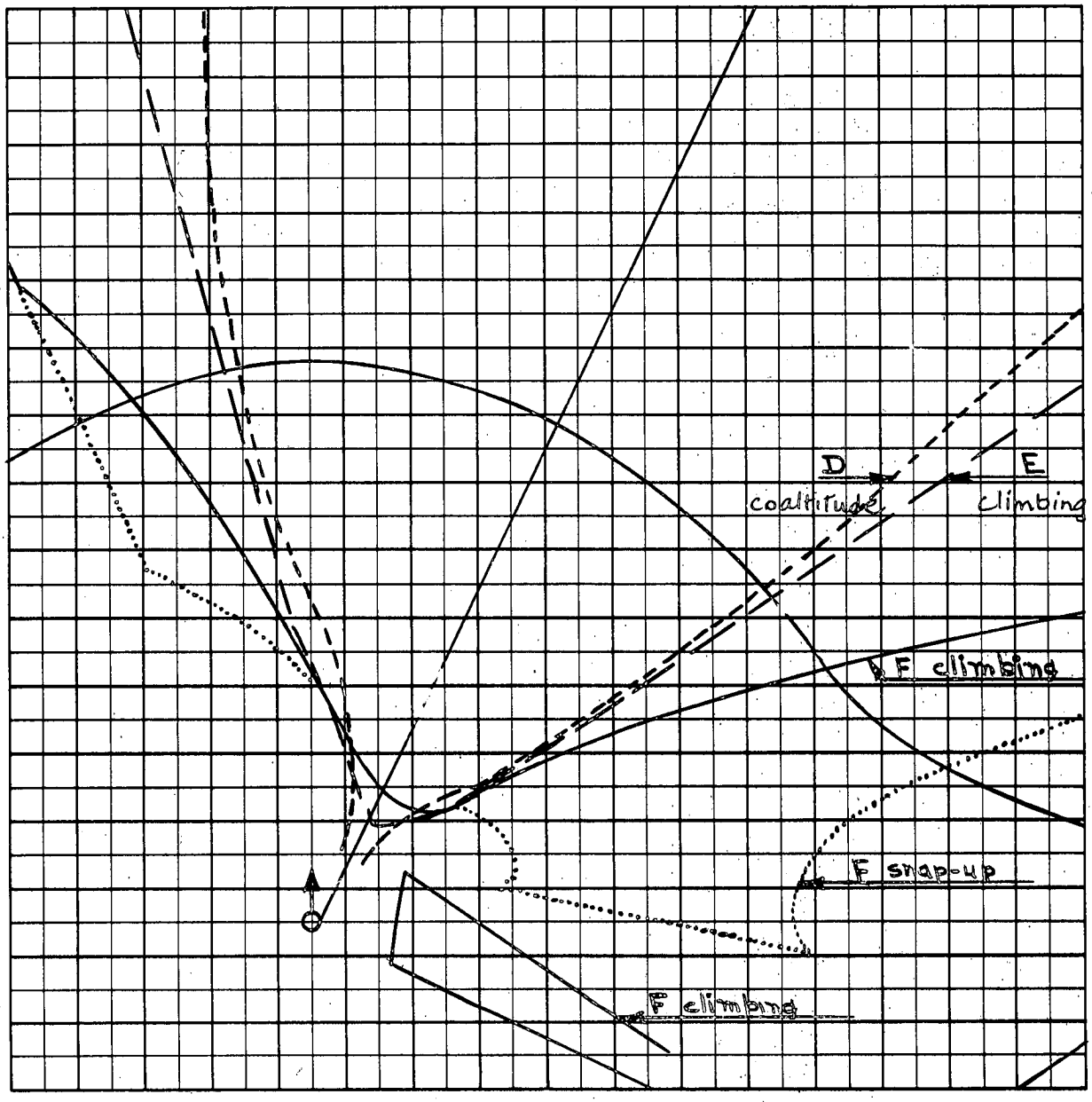

Scale 25,000 ft/cm

A-84

M_t = 1.5

h_t = 60 K

M_{fo} = 2.0

h_{fo} D = 60 K

E = 50 K

F = 40 K

Γ_b = 135°

The separated section of the F climbing placement area is a region from which conversion to tail attacks can be made. This section has been ignored in computing P_p.

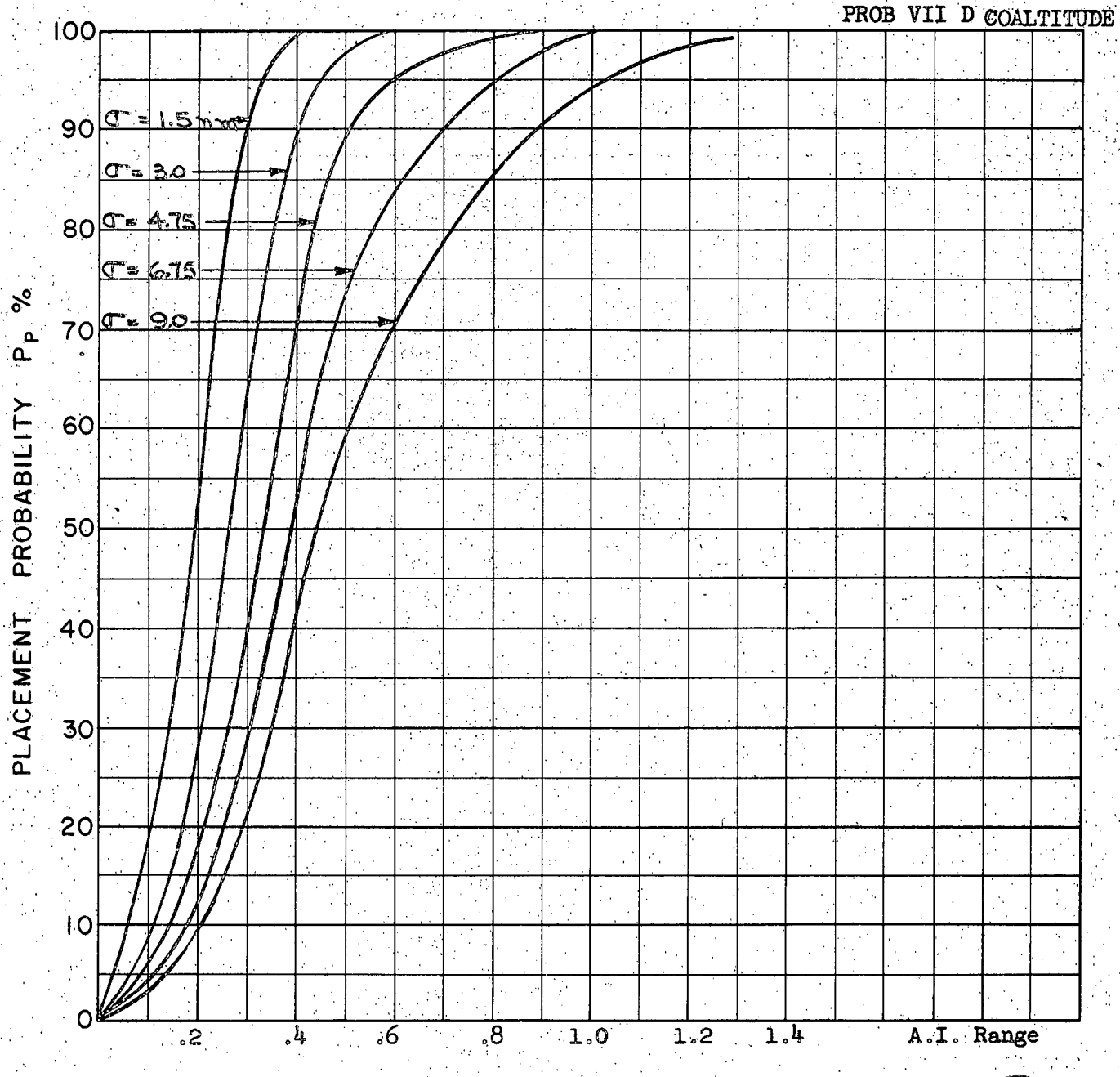

A-85

COURSE DIFFERENCE: 135°
TARGET EVASION: Nil
TARGET MACH NO.: 1.5
INTERCEPTOR LATERAL G's: Avro 3.3
INTERCEPTOR MACH NO.: 2.0
σ OF G.C.I. ACCURACY: 5 Values
A.I. DETECTION RANGE AS FRACTION OF SPECIFICATION RANGE, S: Abscissa
A.I. DETECTION RANGE CONTOUR: Delta
ALTITUDE: H_t = 60 K

H_f = 60 K

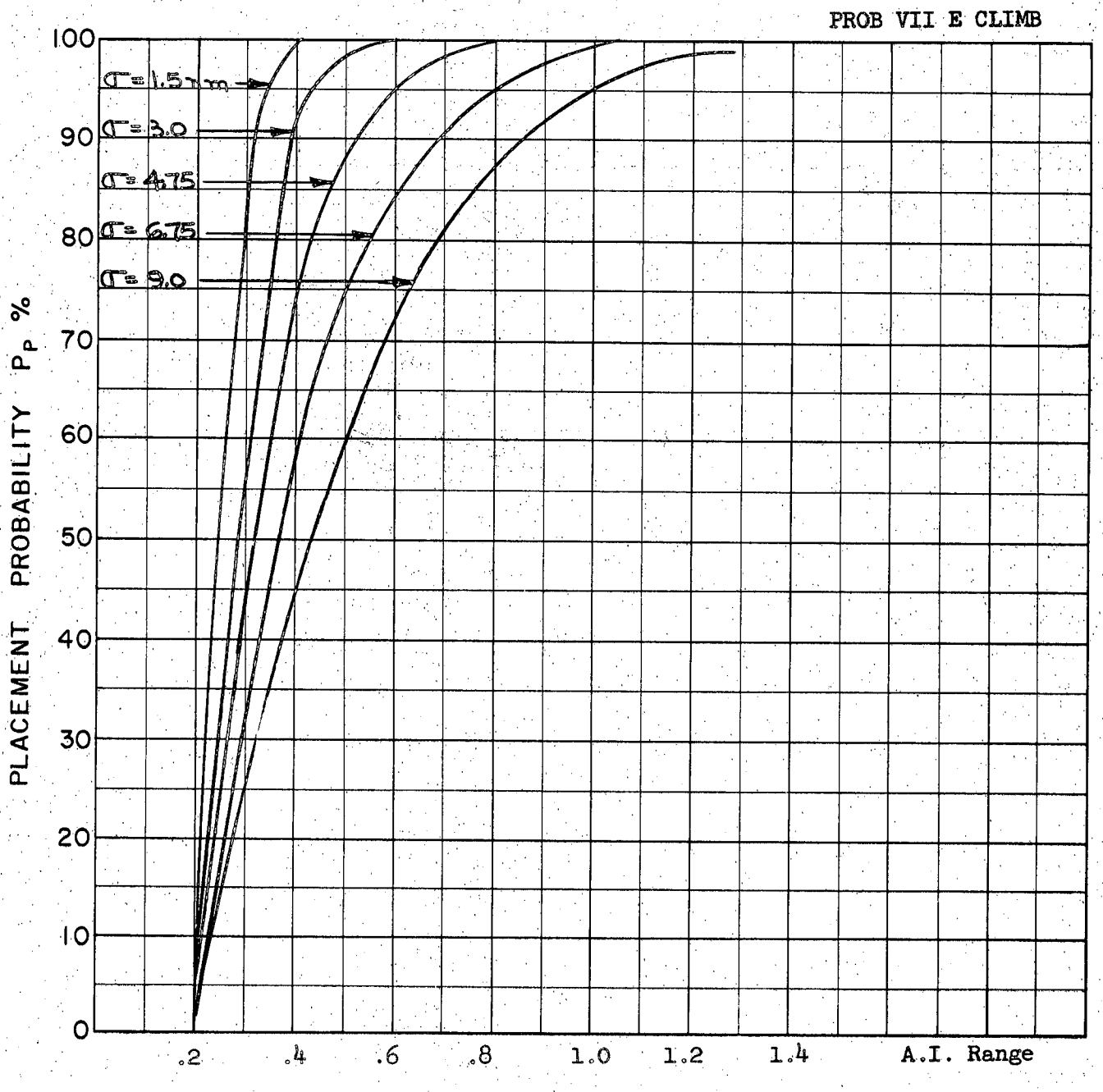

A-86

COURSE DIFFERENCE: 135°
TARGET EVASION: Nil
TARGET MACH NO.: 1.5
INTERCEPTOR LATERAL G's: Avro 3.3
INTERCEPTOR MACH NO.: 2.0
σ OF G.C.I. ACCURACY: 5 Values
A.I. DETECTION RANGE AS FRACTION OF SPECIFICATION RANGE, S: Abscissa
A.I. DETECTION RANGE CONTOUR: Delta
ALTITUDE: H_t = 60 K
H_f = 50 K

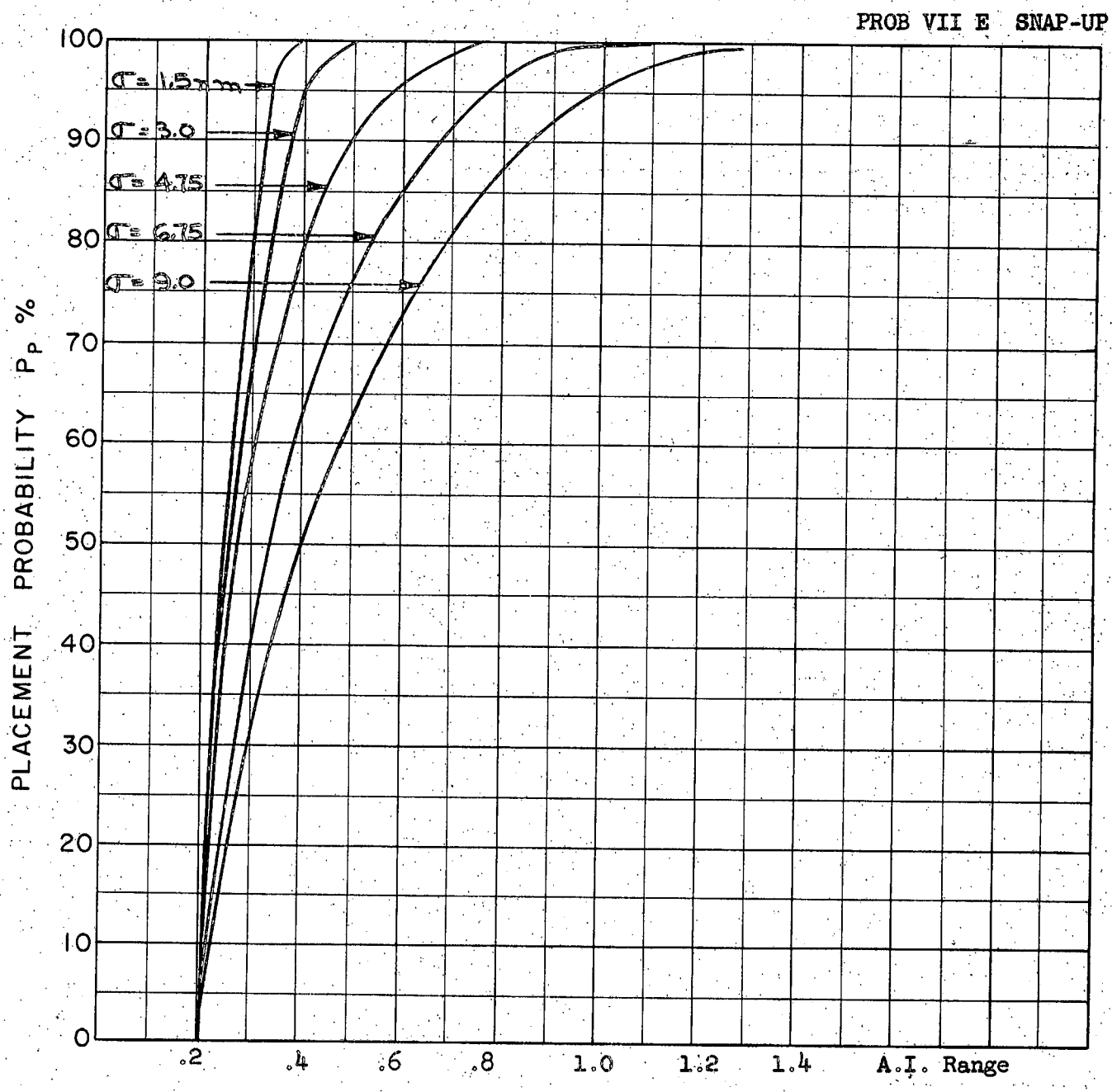

A-87

COURSE DIFFERENCE: 135°
TARGET EVASION: Nil
TARGET MACH NO.: 1.5
INTERCEPTOR LATERAL G's: Avro 3.3
INTERCEPTOR MACH NO.: 2.0
σ OF G.C.I. ACCURACY: 5 Values
A.I. DETECTION RANGE AS FRACTION OF SPECIFICATION RANGE, S: Abscissa
A.I. DETECTION RANGE CONTOUR: Delta
ALTITUDE: H_t = 60 K
H_f = 50 K

PROB VII F CLIMB

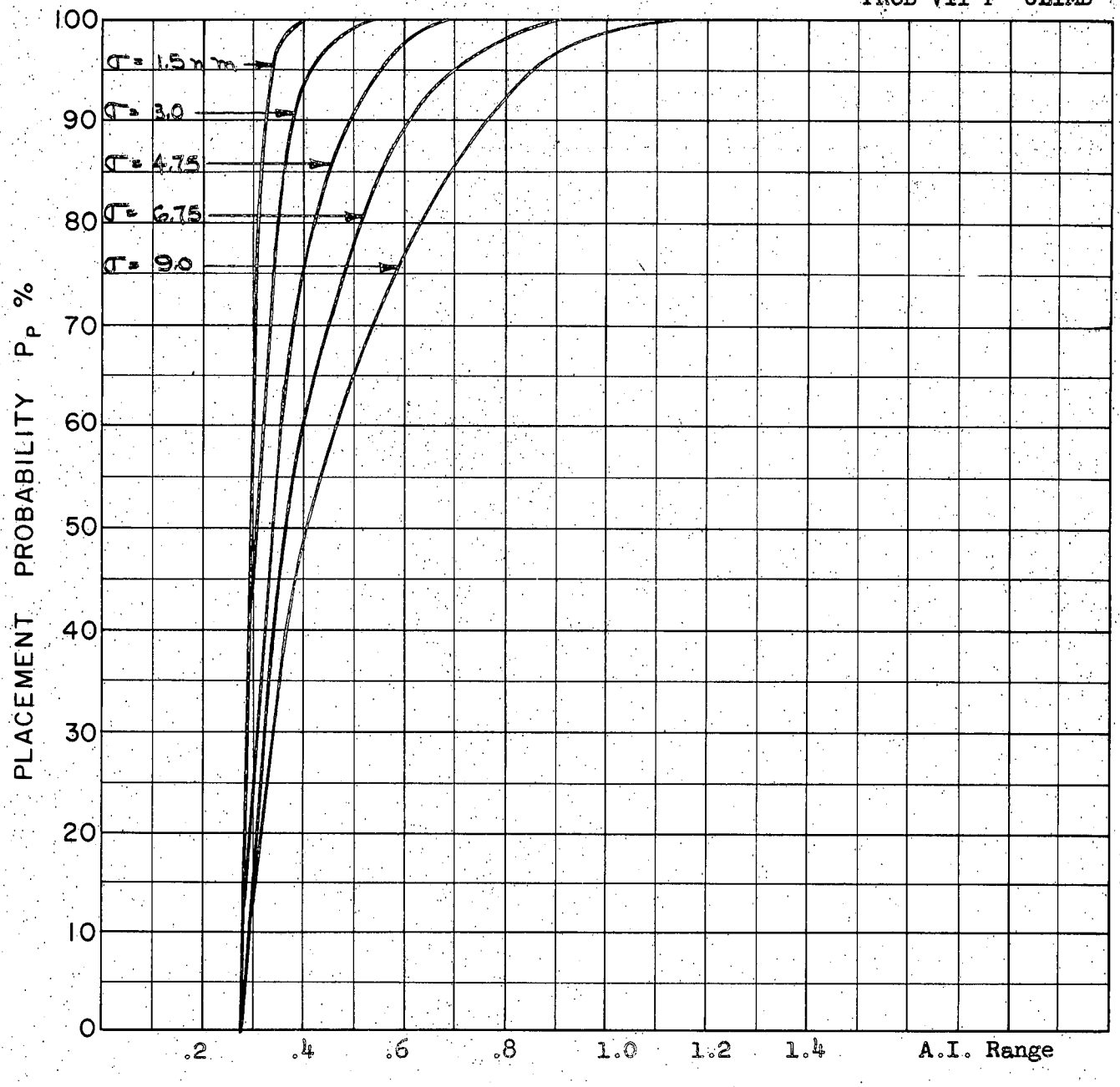

A-88

COURSE DIFFERENCE: 135°
TARGET EVASION: Nil
TARGET MACH NO.: 1.5
INTERCEPTOR LATERAL G's: Avro 3.3
INTERCEPTOR MACH NO.: 2.0
σ OF G.C.I. ACCURACY: 5 Values
A.I. DETECTION RANGE AS FRACTION OF SPECIFICATION RANGE, S: Abscissa
A.I. DETECTION RANGE CONTOUR: Delta
ALTITUDE: H_t = 60 K
H_f = 40 K

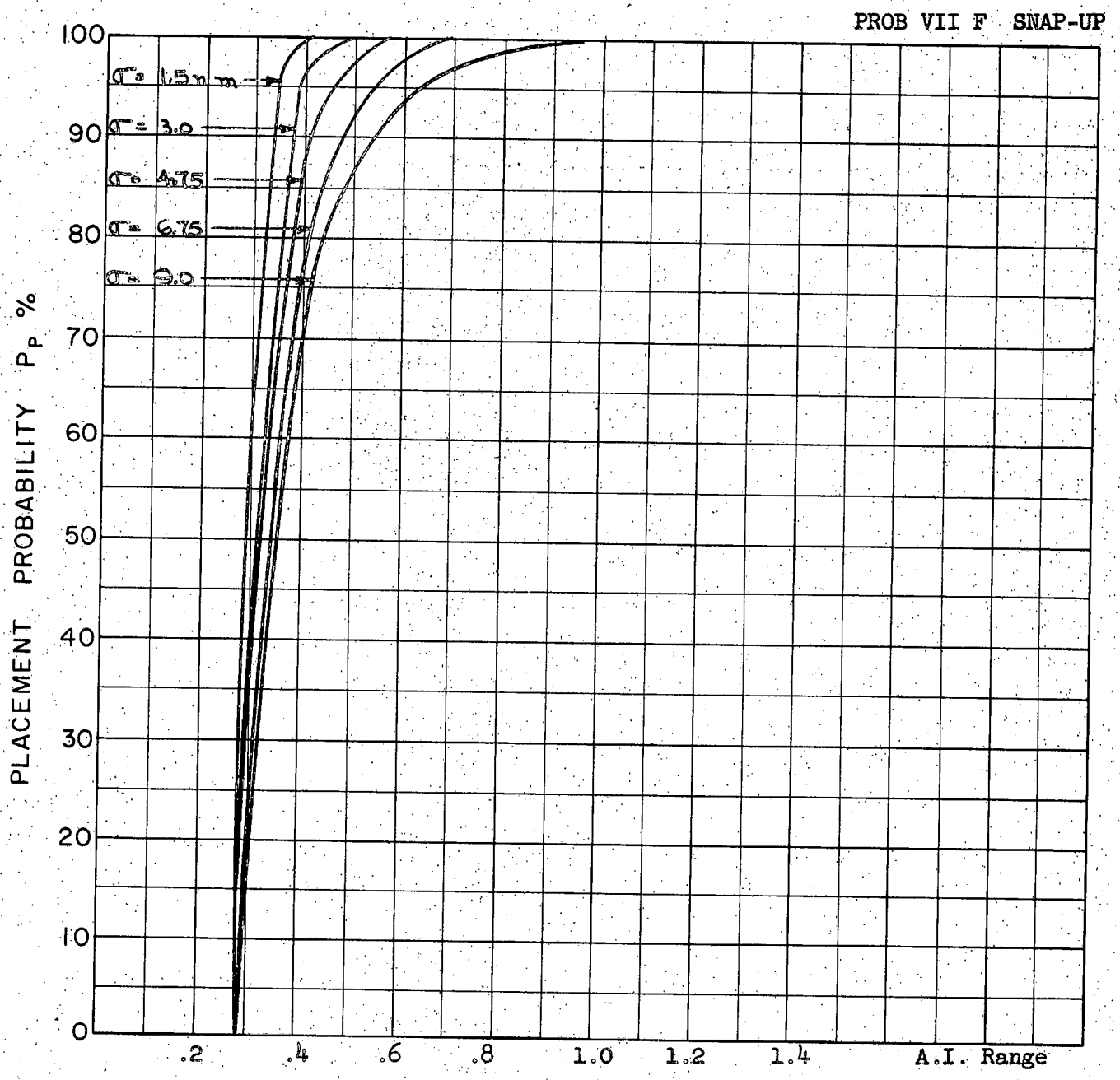

COURSE DIFFERENCE: 135°
TARGET EVASION: Nil
TARGET MACH NO.: 1.5
INTERCEPTOR LATERAL G's: Avro 3.3
INTERCEPTOR MACH NO.: 2.0
σ OF G.C.I. ACCURACY: 5 Values
A.I. DETECTION RANGE AS FRACTION OF SPECIFICATION RANGE, S: Abscissa
A.I. DETECTION RANGE CONTOUR: Delts
ALTITUDE: H_t = 60 K
H_f = 40 K

A-89

PROB VII GHK

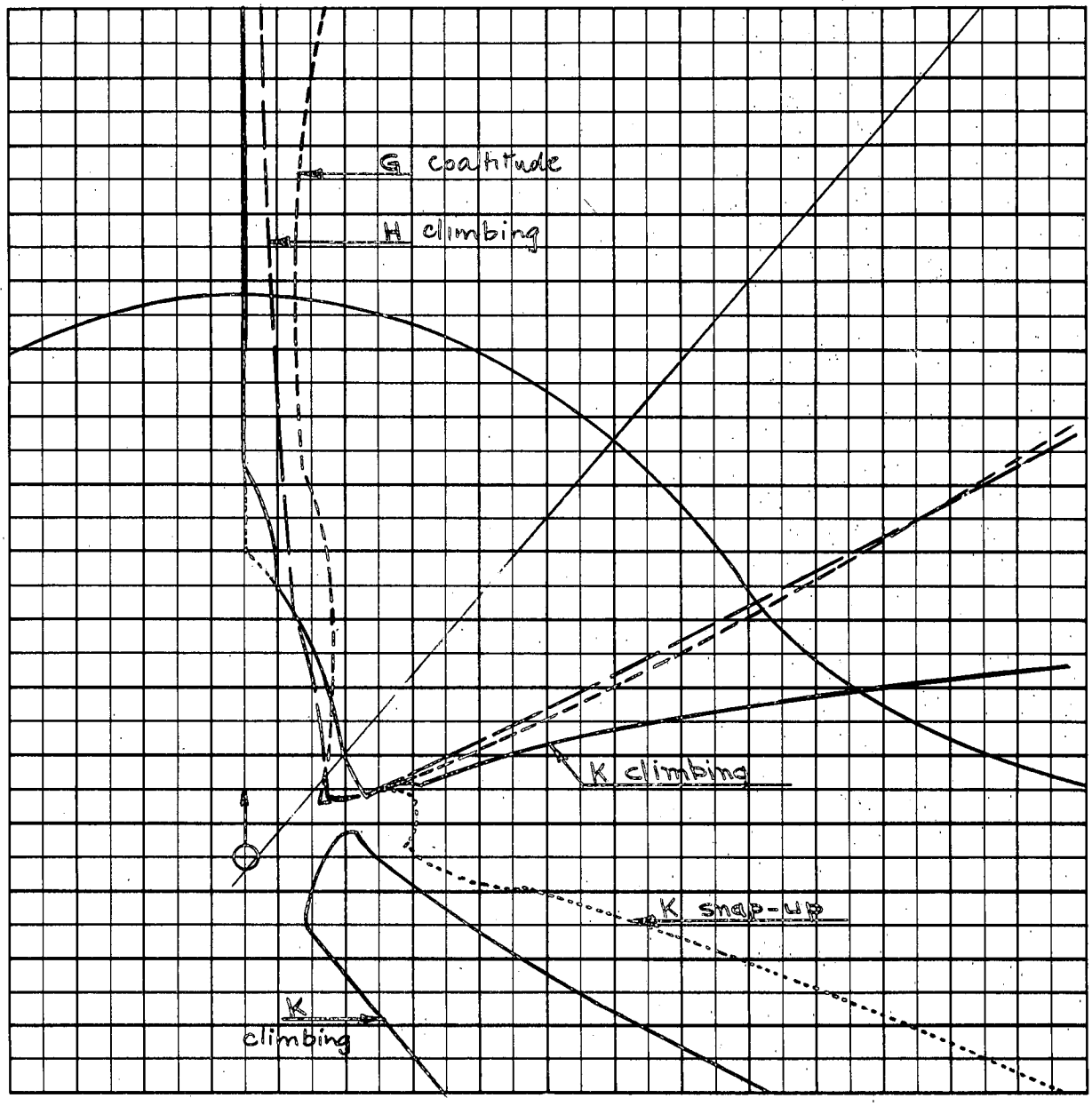

Scale 25,000 ft/cm

M_t = 1.5
h_t = 60 K
M_{fo} = 2.0
h_{fo} G = 60 K
H = 50 K
K = 40 K
Γ_o = 110°

A-90

The separated section of the K climbing placement area is a region from which conversion to tail attacks may be made. This section has been ignored in computing P_p.

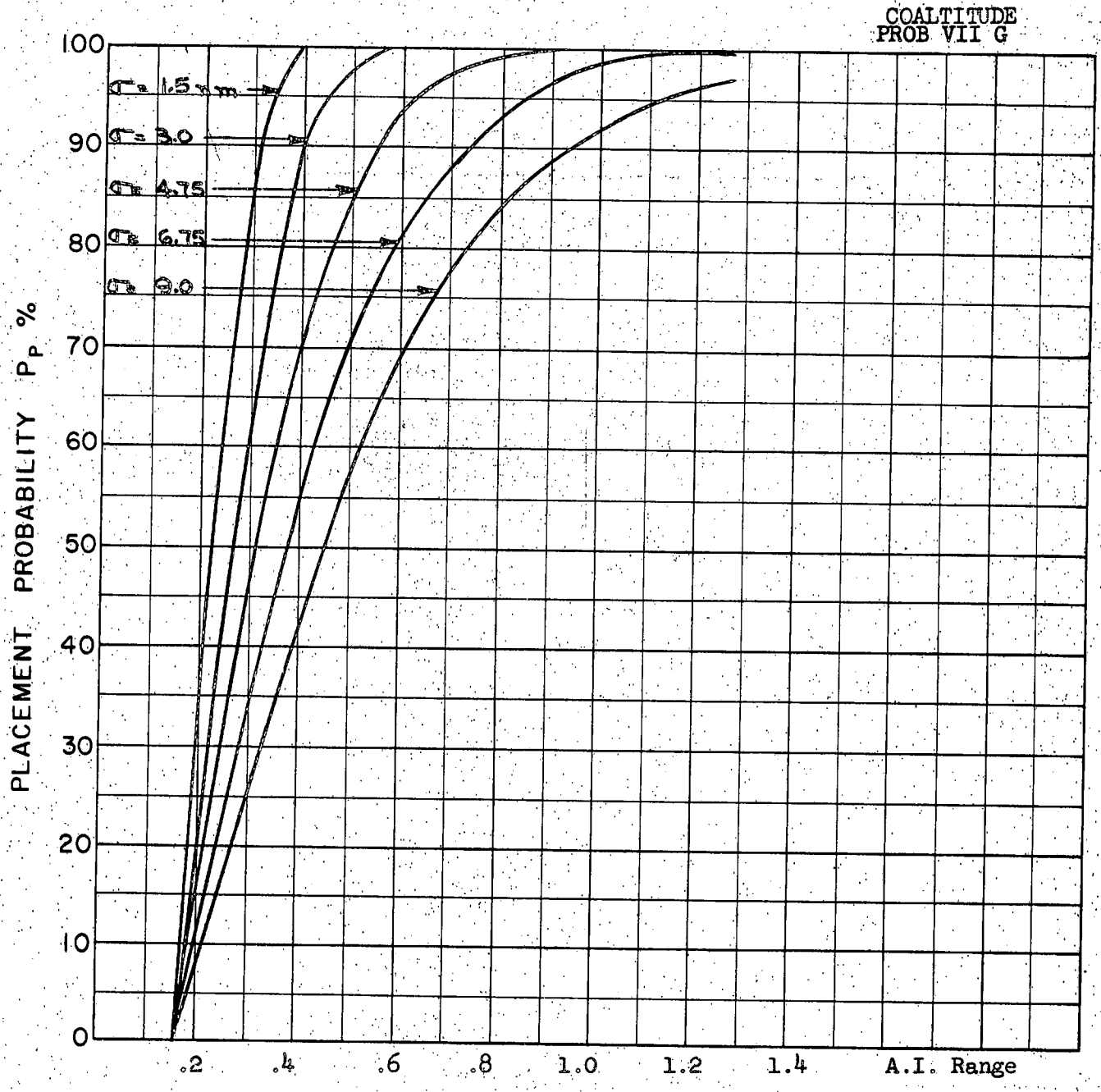

A-91

COURSE DIFFERENCE: 110°
TARGET EVASION: Nil
TARGET MACH NO.: 1.5
INTERCEPTOR LATERAL G's: Avro 3.3
INTERCEPTOR MACH NO.: 2.0
σ OF G.C.I. ACCURACY: 5 Values
A.I. DETECTION RANGE AS FRACTION OF SPECIFICATION RANGE, S: Abscissa
A.I. DETECTION RANGE CONTOUR: Delta
ALTITUDE: H_t = 60 K
H_f = 60 K

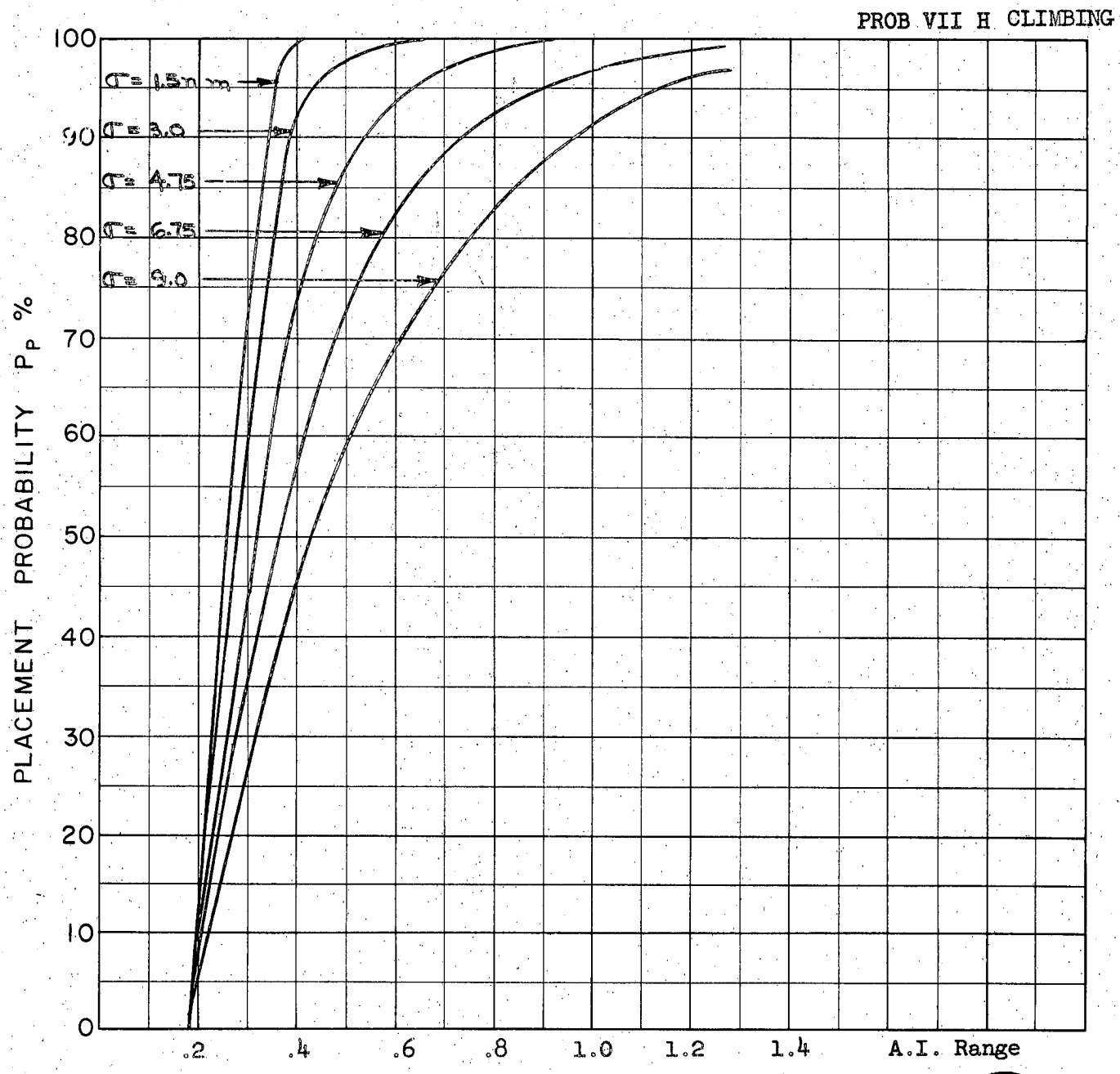

A-92

COURSE DIFFERENCE: 110°
TARGET EVASION: Nil
TARGET MACH NO.: 1.5
INTERCEPTOR LATERAL G's: Avro 3.3
INTERCEPTOR MACH NO.: 2.0
σ OF G.C.I. ACCURACY: 5 Values
A.I. DETECTION RANGE AS FRACTION OF SPECIFICATION RANGE, S: Abscissa
A.I. DETECTION RANGE CONTOUR: Delta
ALTITUDE: H_t = 60 K
H_f = 50 K

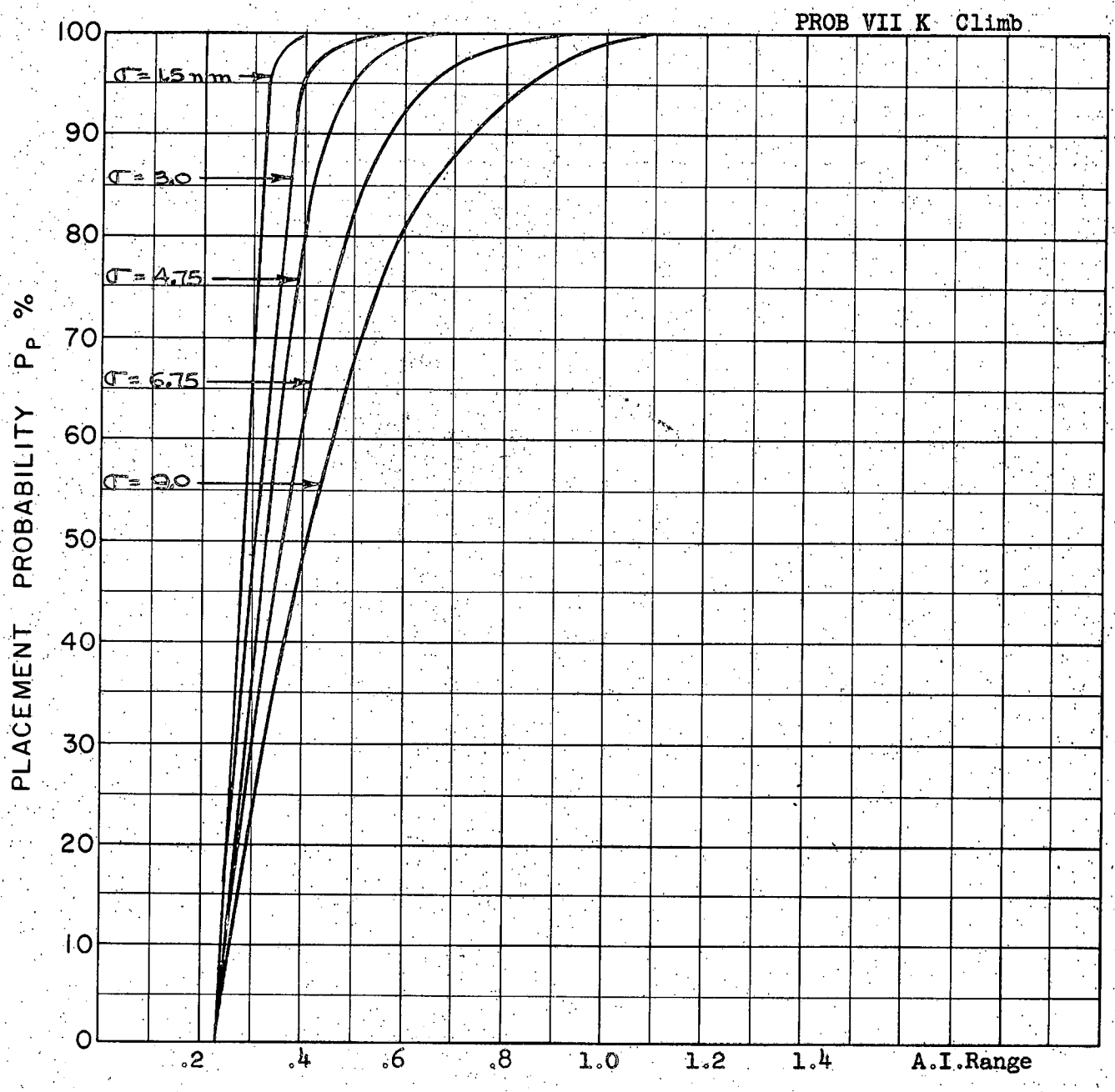

A-93

COURSE DIFFERENCE: 110°
TARGET EVASION: Nil
TARGET MACH NO.: 1.5
INTERCEPTOR LATERAL G's: Avro 3.3
INTERCEPTOR MACH NO.: 2.0
σ OF G.C.I. ACCURACY: 5 Values
A.I. DETECTION RANGE AS FRACTION OF SPECIFICATION RANGE, S: Abscissa
A.I. DETECTION RANGE CONTOUR: Delta
ALTITUDE: H_t = 60 K
H_f = 40 K

Prob. VII K SNAP-UP

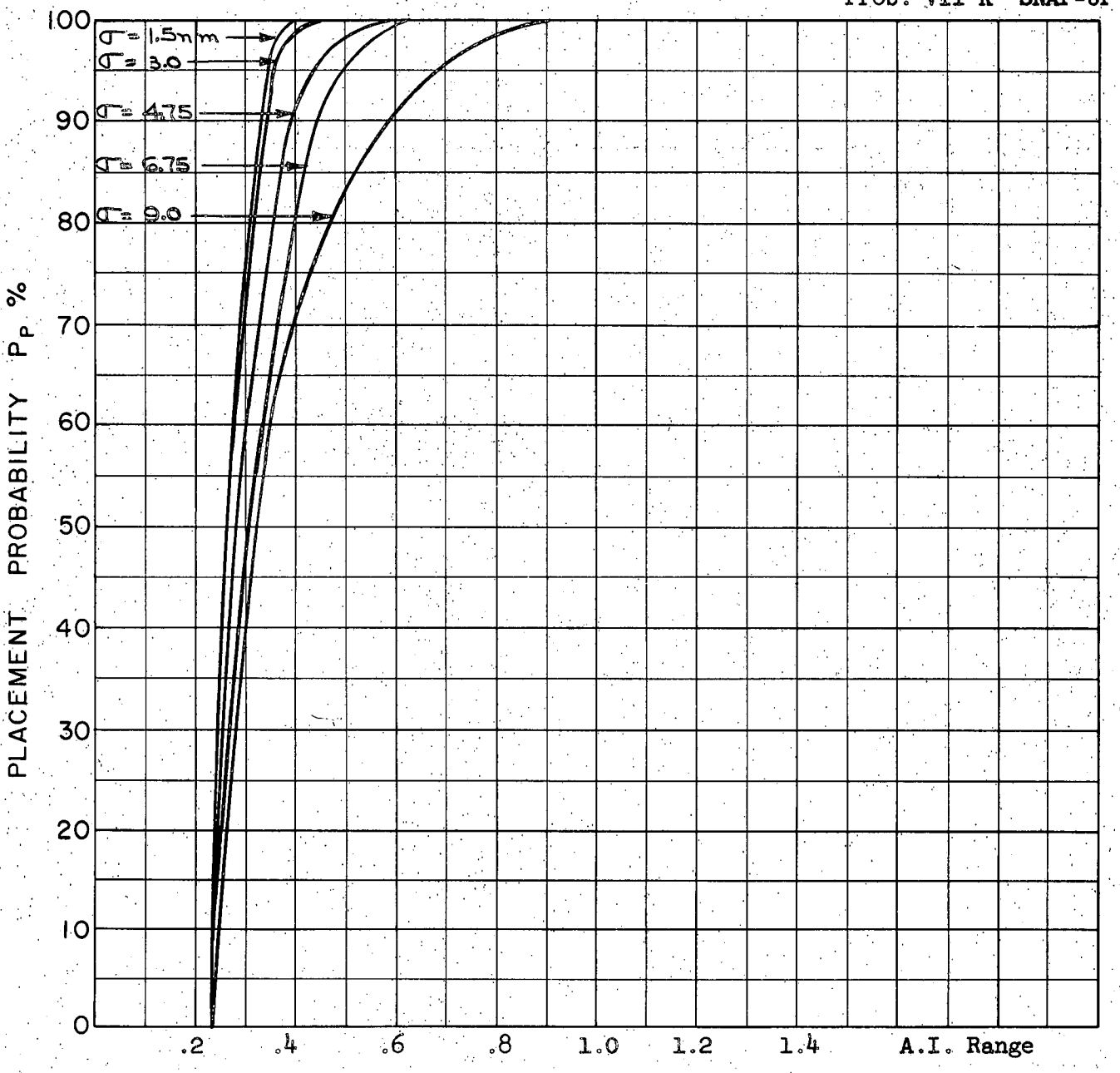

A-94

COURSE DIFFERENCE: 110°
TARGET EVASION: Nil
TARGET MACH NO.: 1.5
INTERCEPTOR LATERAL G's: Avro 3.3
INTERCEPTOR MACH NO.: 2.0
σ OF G.C.I. ACCURACY: 5 Values
A.I. DETECTION RANGE AS FRACTION OF SPECIFICATION RANGE, S: Abscissa
A.I. DETECTION RANGE CONTOUR: Delta
ALTITUDE: H_t = 60 K
H_f = 40 K

PROB VII LMN

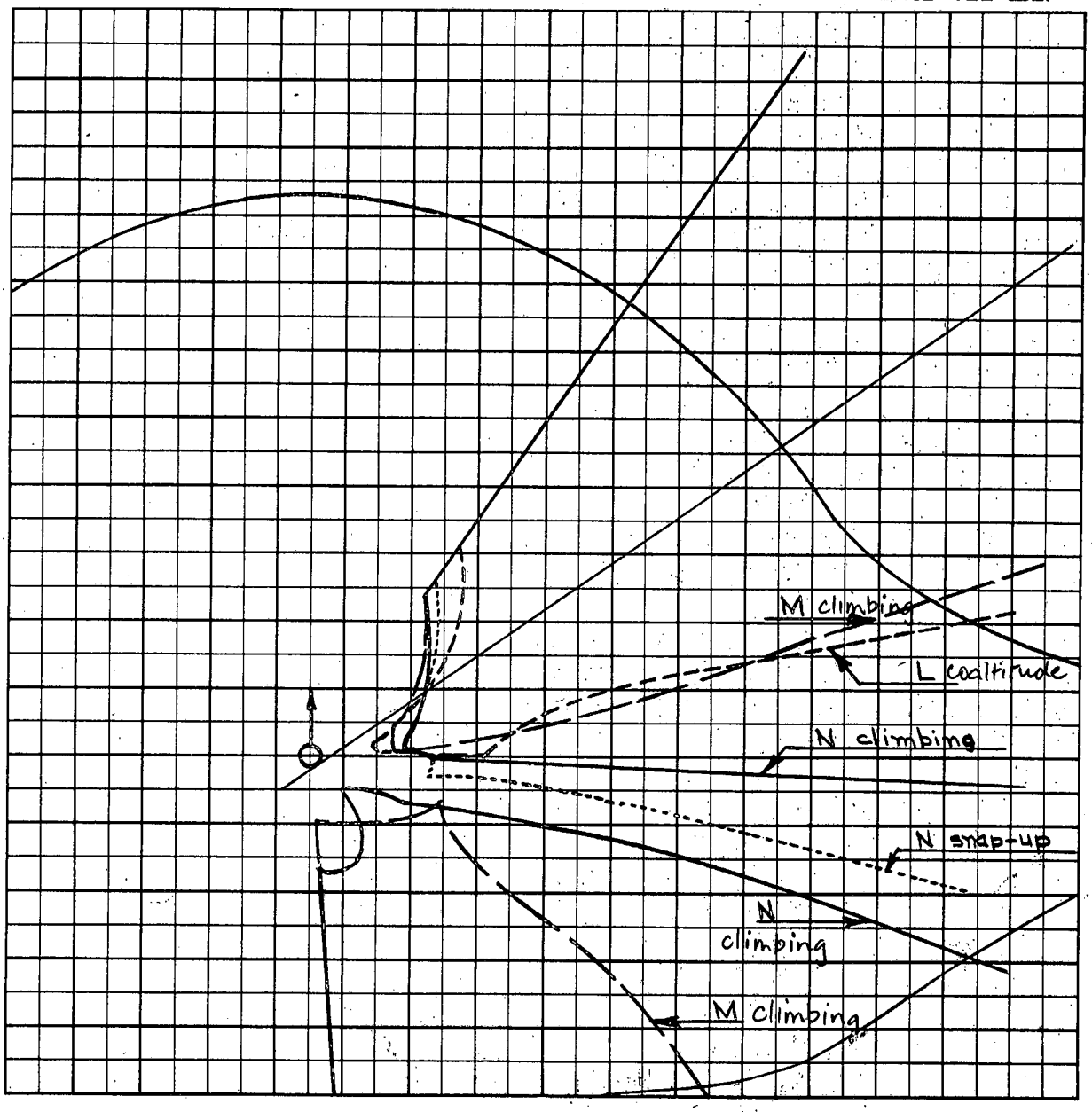

Scale 25,000 ft/cm

M_t = 1.5
h_t = 60 K
M_{fo} = 2.0
h_{fo} L = 60 K
M = 50 K
N = 40 K
Γ_e = 75°

A-95

The separated sections of the M climbing and N climbing placement areas are regions from which conversion to tail attacks can be made. These sections have been ignored in computing P_p.

COALTITUDE

PROB VII L

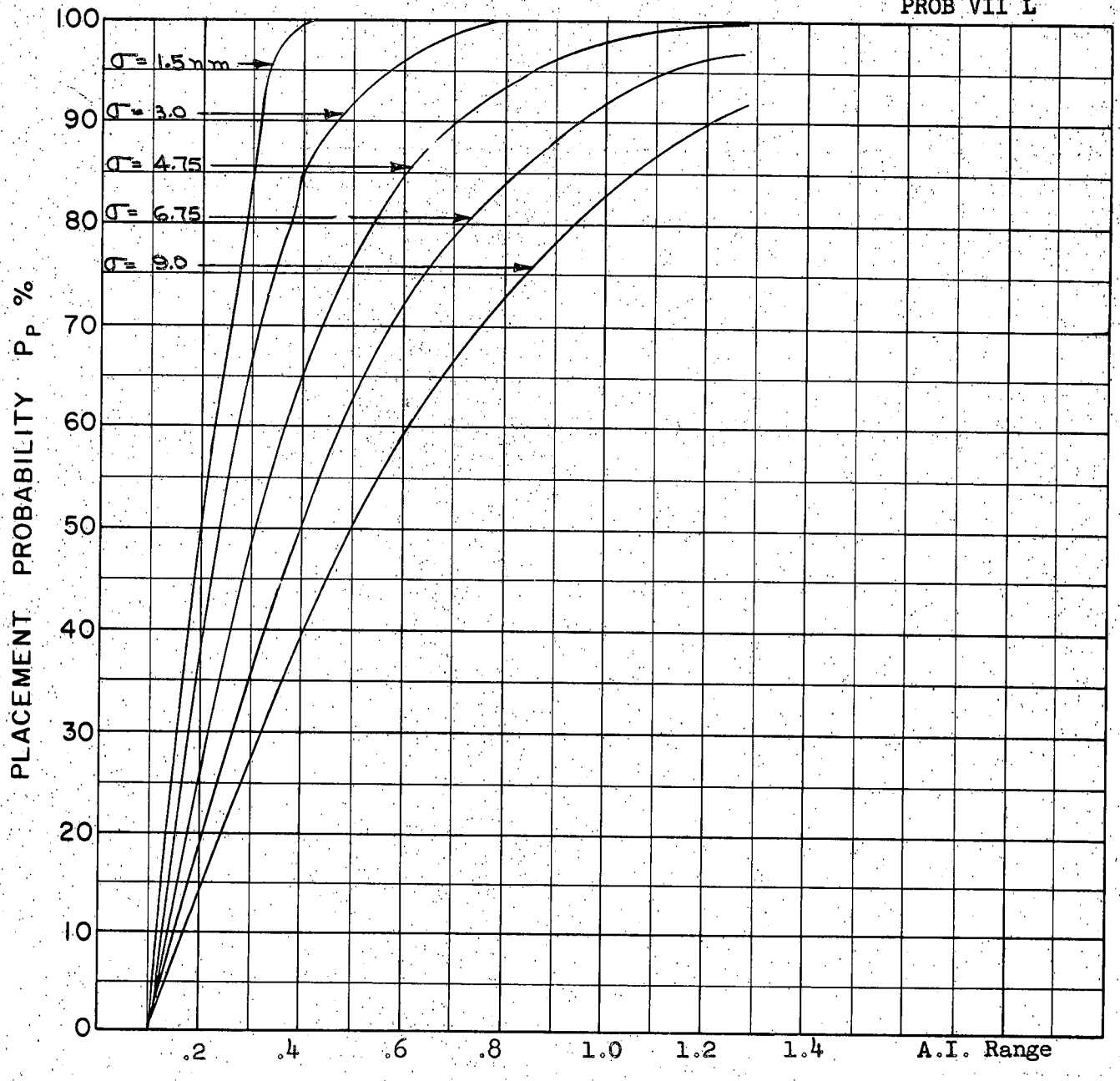

A-96

COURSE DIFFERENCE: 75°
TARGET EVASION: Nil
TARGET MACH NO.: 1.5
INTERCEPTOR LATERAL G's: Avro 3.3
INTERCEPTOR MACH NO.: 2.0
σ OF G.C.I. ACCURACY: 5 Values
A.I. DETECTION RANGE AS FRACTION OF SPECIFICATION RANGE, S: Abscissa
A.I. DETECTION RANGE CONTOUR: Delta
ALTITUDE: H_t = 60 K
H_f = 60 K

CLIMBING
PROB VII M

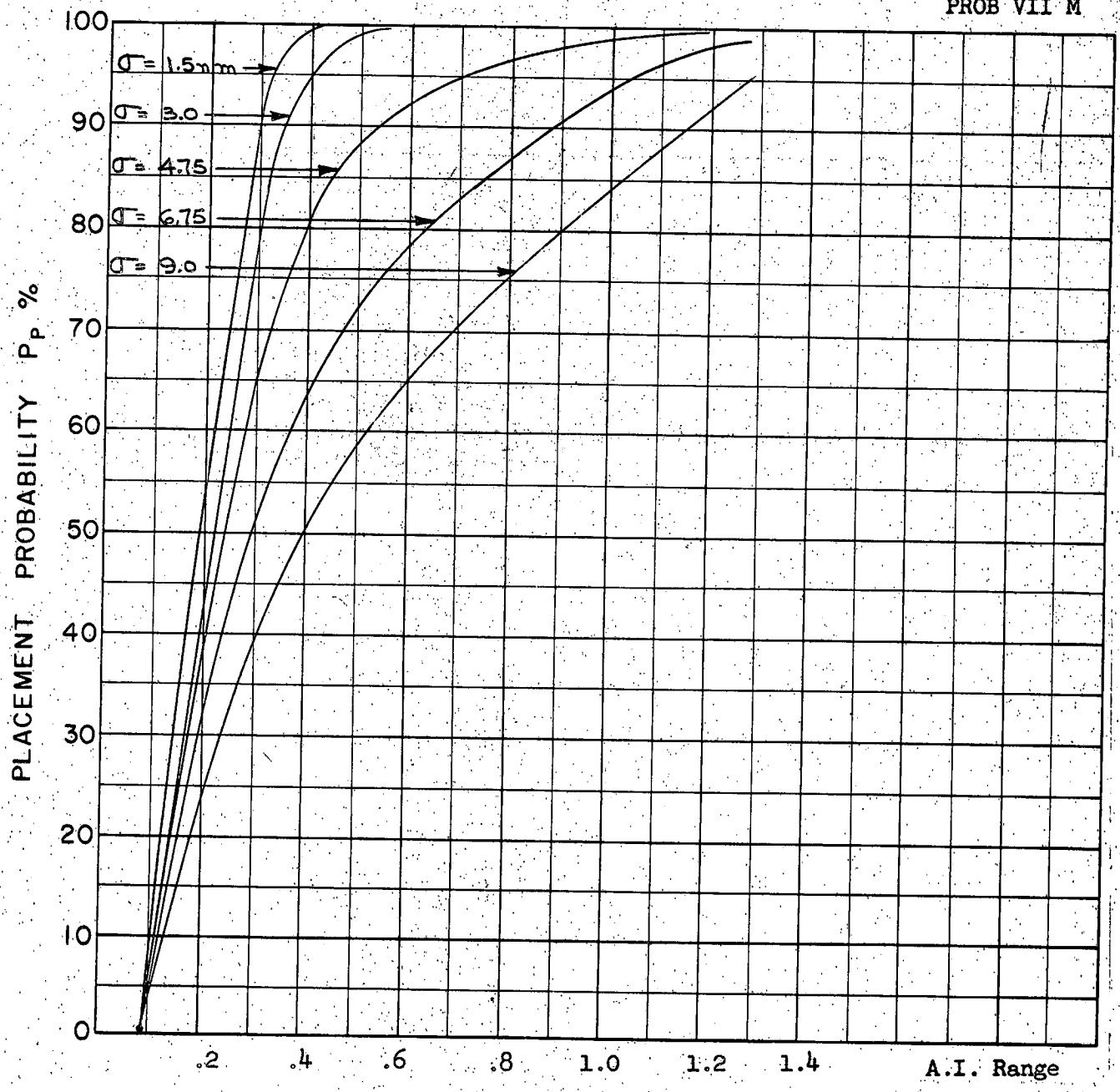

COURSE DIFFERENCE: 75°
TARGET EVASION: Nil
TARGET MACH NO.: 1.5
INTERCEPTOR LATERAL G's: Avro 3.3
INTERCEPTOR MACH NO.: 2.0
σ OF G.C.I. ACCURACY: 5 Values
A.I. DETECTION RANGE AS FRACTION OF SPECIFICATION RANGE, S: Abscissa
A.I. DETECTION RANGE CONTOUR: Delta
ALTITUDE: H_t = 60 K
H_f = 50 K

A-97

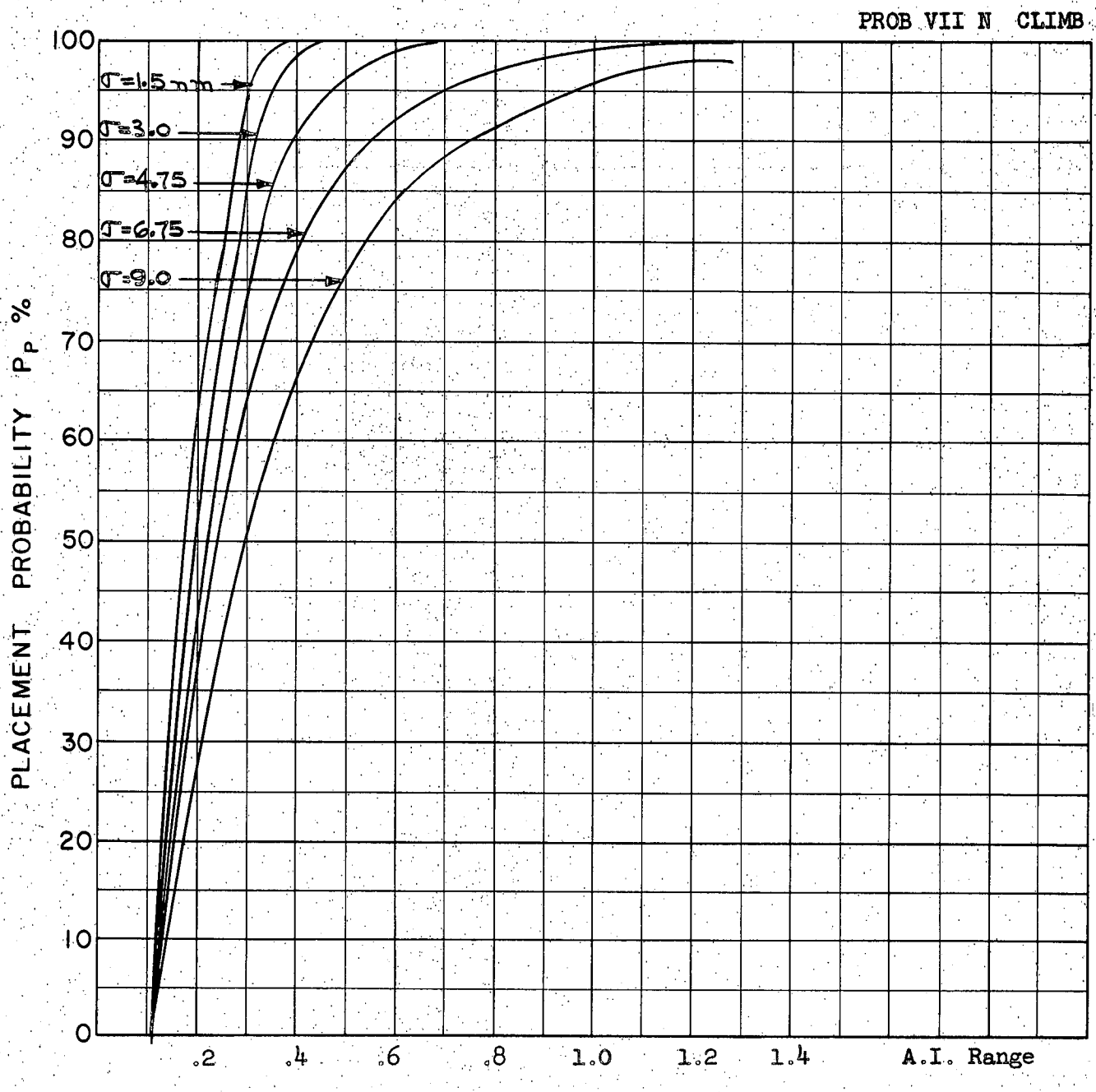

A-98

COURSE DIFFERENCE: 75°
TARGET EVASION: Nil
TARGET MACH NO.: 1.5
INTERCEPTOR LATERAL G's: Avro 3.3
INTERCEPTOR MACH NO.: 2.0
σ OF G.C.I. ACCURACY: 5 Values
A.I. DETECTION RANGE AS FRACTION OF SPECIFICATION RANGE, S: Abscissa
A.I. DETECTION RANGE CONTOUR: Delta
ALTITUDE: H_t = 60 K
H_f = 40 K

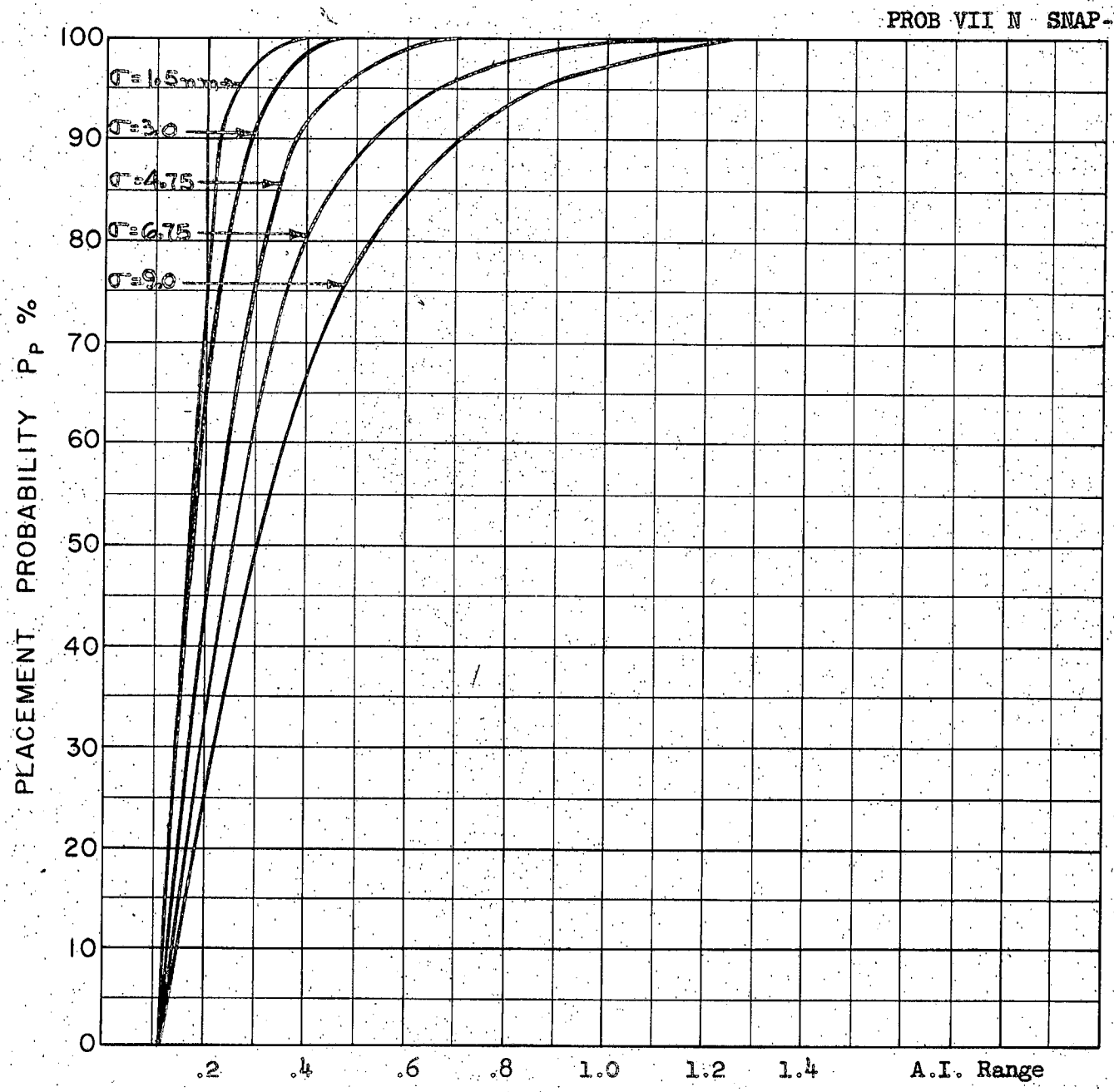

A-99

COURSE DIFFERENCE: 75°
TARGET EVASION: Nil
TARGET MACH NO.: 1.5
INTERCEPTOR LATERAL G's: Avro 3.3
INTERCEPTOR MACH NO.: 2.0
σ OF G.C.I. ACCURACY: 5 Values
A.I. DETECTION RANGE AS FRACTION OF SPECIFICATION RANGE, S: Abscissa
A.I. DETECTION RANGE CONTOUR: Delta
ALTITUDE: H_t = 60 K
H_f = 40 K

PROB VIII AB

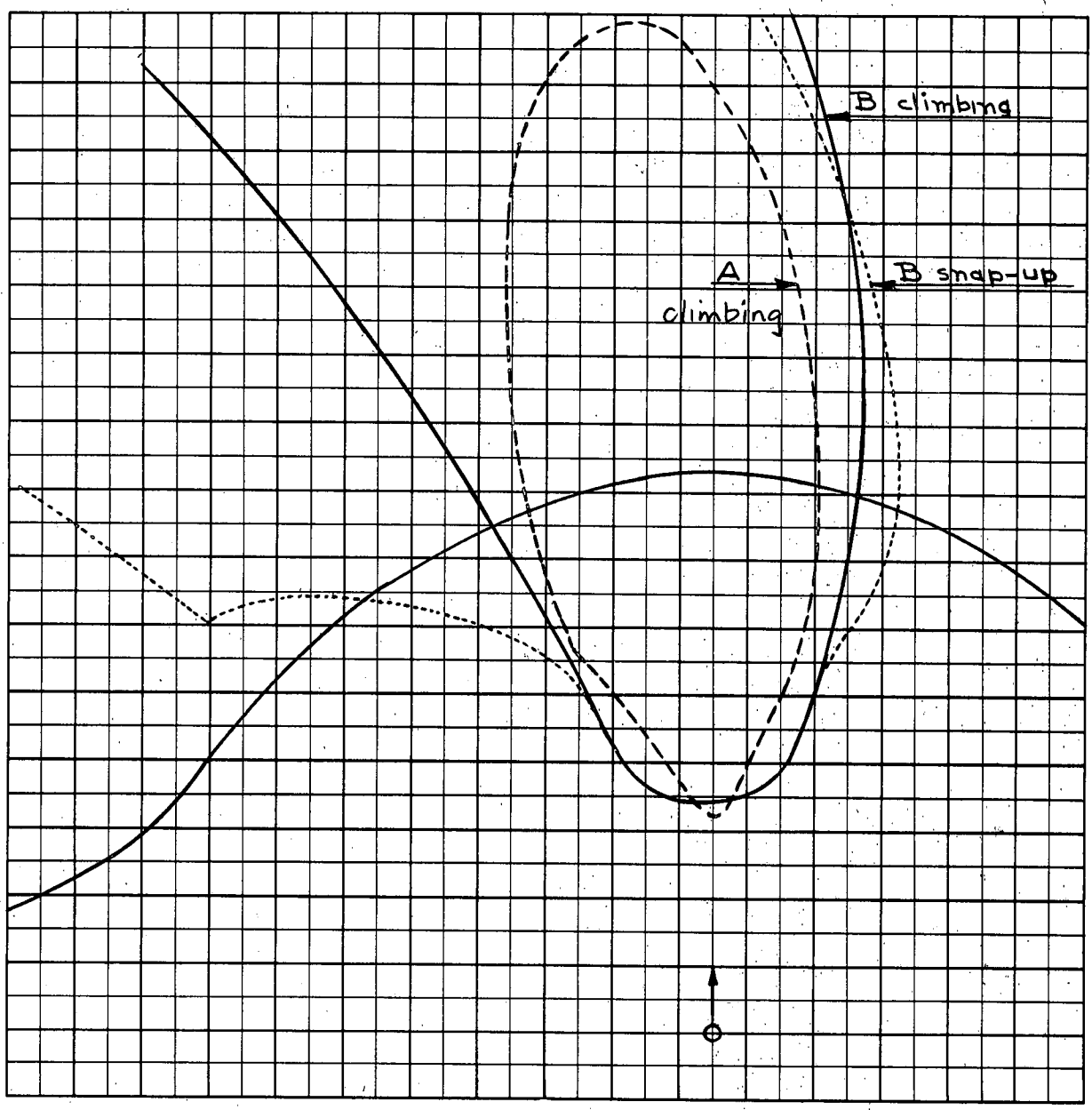

Scale 25,000 ft/cm

M_t = 2.0
h_t = 70 K
M_{fo} = 2.0
h_{fo} A = 60 K
B = 40 K
R_t = .458 g
Γ_o = 180°

A-100

Target turning to the left.

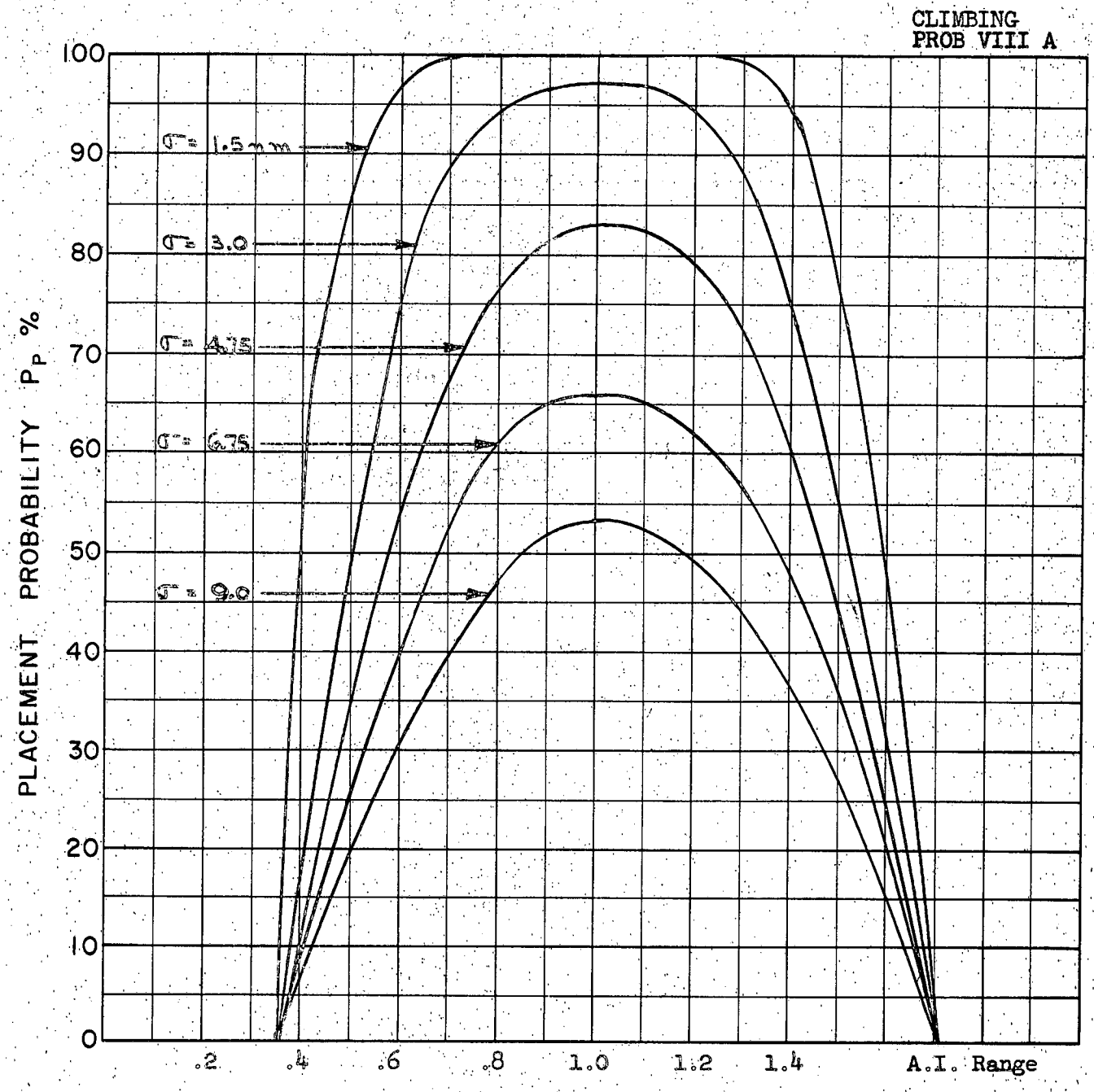

A-101

COURSE DIFFERENCE: 180°
TARGET EVASION: 1.1 g Load Factor
TARGET MACH NO.: 2.0
INTERCEPTOR LATERAL G's: Avro 3.3
INTERCEPTOR MACH NO.: 2.0
σ OF G.C.I. ACCURACY: 5 Values
A.I. DETECTION RANGE AS FRACTION OF SPECIFICATION RANGE, S: Abscissa
A.I. DETECTION RANGE CONTOUR: Delta
ALTITUDE: H_t = 70 K
H_f = 60 K

Probability values calculated from the placement zone common to the positive and negative evasion cases.

PROB VIII B CLIMB

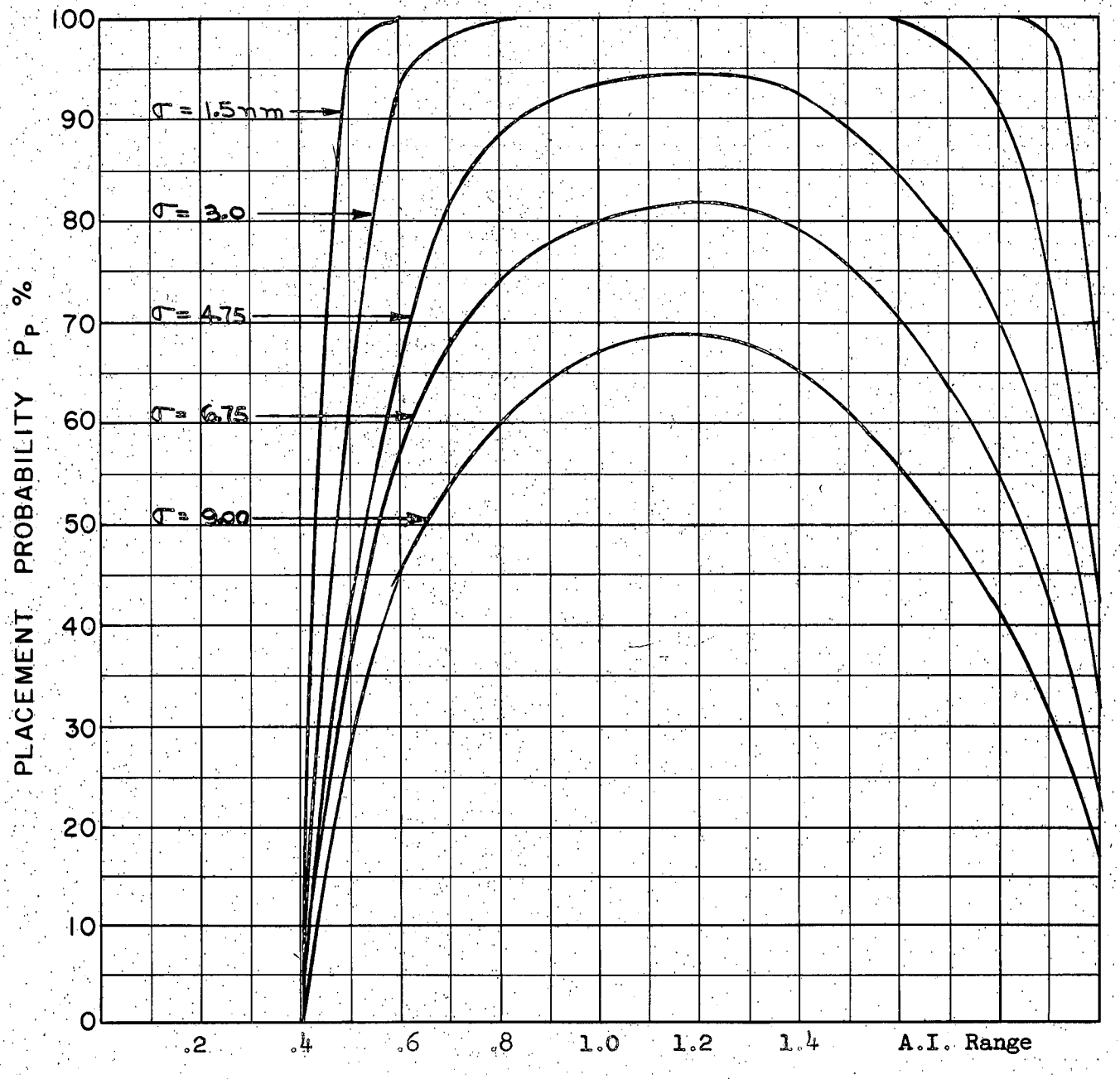

A-102

COURSE DIFFERENCE: 180°
TARGET EVASION: 1.1g Load Factor
TARGET MACH NO.: 2.0
INTERCEPTOR LATERAL G's: Avro 3.3
INTERCEPTOR MACH NO.: 2.0
σ OF G.C.I. ACCURACY: 5 Values
A.I. DETECTION RANGE AS FRACTION OF SPECIFICATION RANGE, S: Abscissa
A.I. DETECTION RANGE CONTOUR: Delta
ALTITUDE: H_t = 70 K
H_f = 40 K

Probability values calculated from the placement zone common to the positive and negative evasion cases.

PROB VIII B SNAP-UP

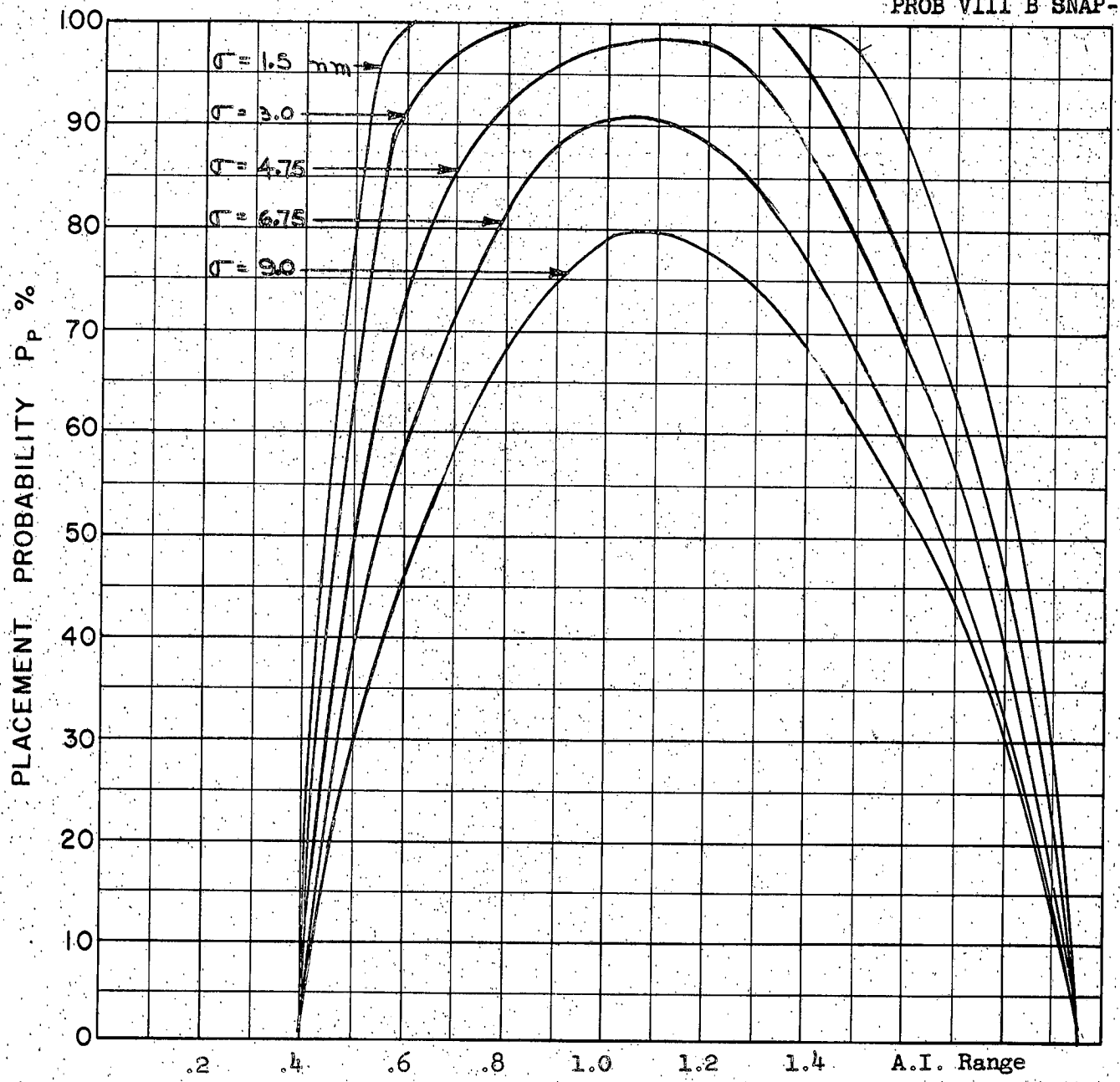

A-103

COURSE DIFFERENCE: 180°
TARGET EVASION: 1.1 g Load Factor
TARGET MACH NO.: 2.0
INTERCEPTOR LATERAL G's: Avro 3.3
INTERCEPTOR MACH NO.: 2.0
σ OF G.C.I. ACCURACY: 5 Values
A.I. DETECTION RANGE AS FRACTION OF SPECIFICATION RANGE, S: Abscissa
A.I. DETECTION RANGE CONTOUR: Delta
ALTITUDE: H_t = 70 K
H_f = 40 K

Probability values calculated from the placement zone common to the positive and negative evasion cases.

PROB VIII CD

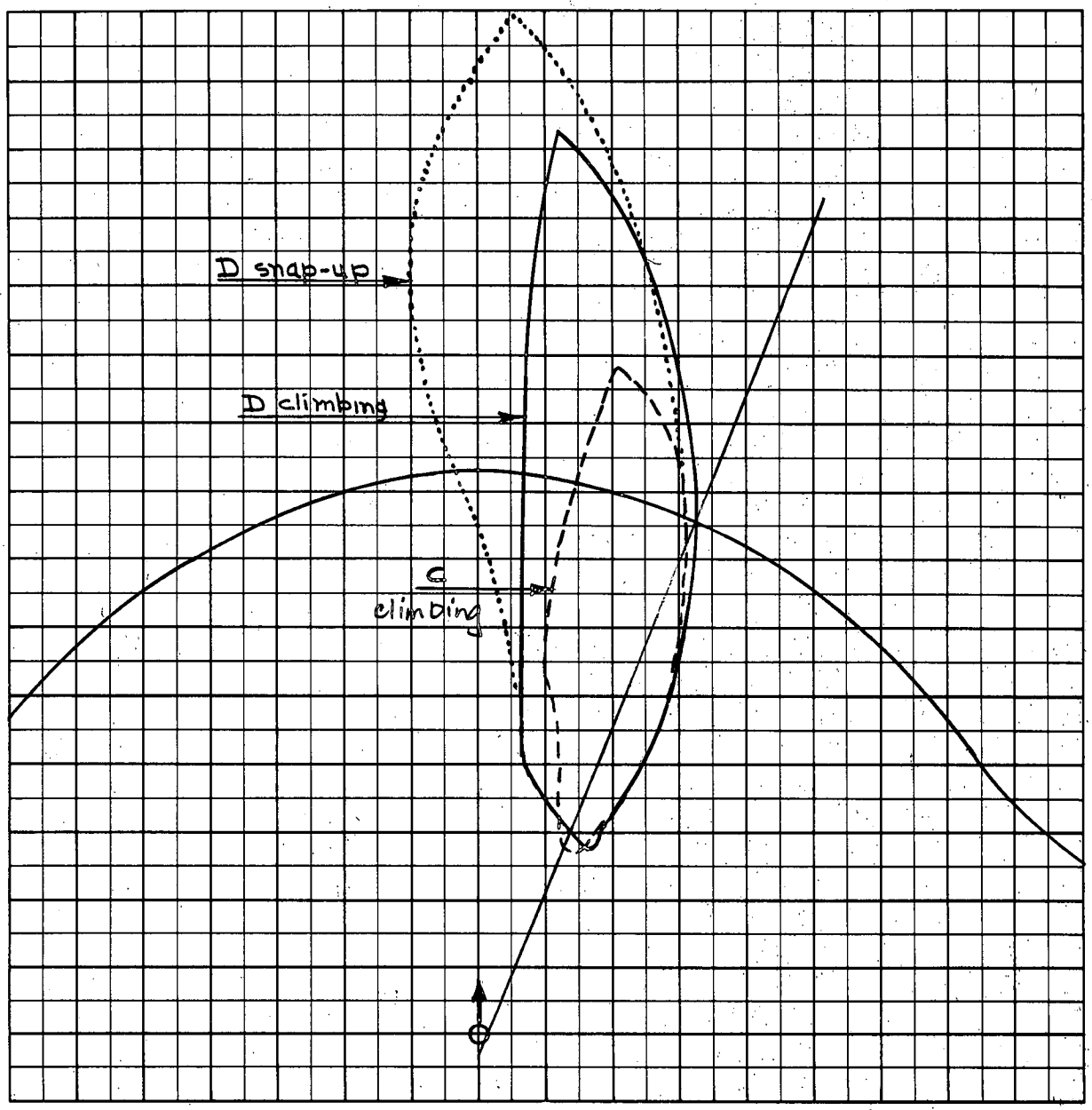

Scale 25,000 ft/cm

M_t = 2.0

h_t = 70 K

M_{fo} = 2.0

h_{fo} C = 60 K

D = 40 K

R_t = .458 g

Γ_o = 135°

Areas between positive and negative evasion placement zones

A-104

CLIMBING
PROB VIII C

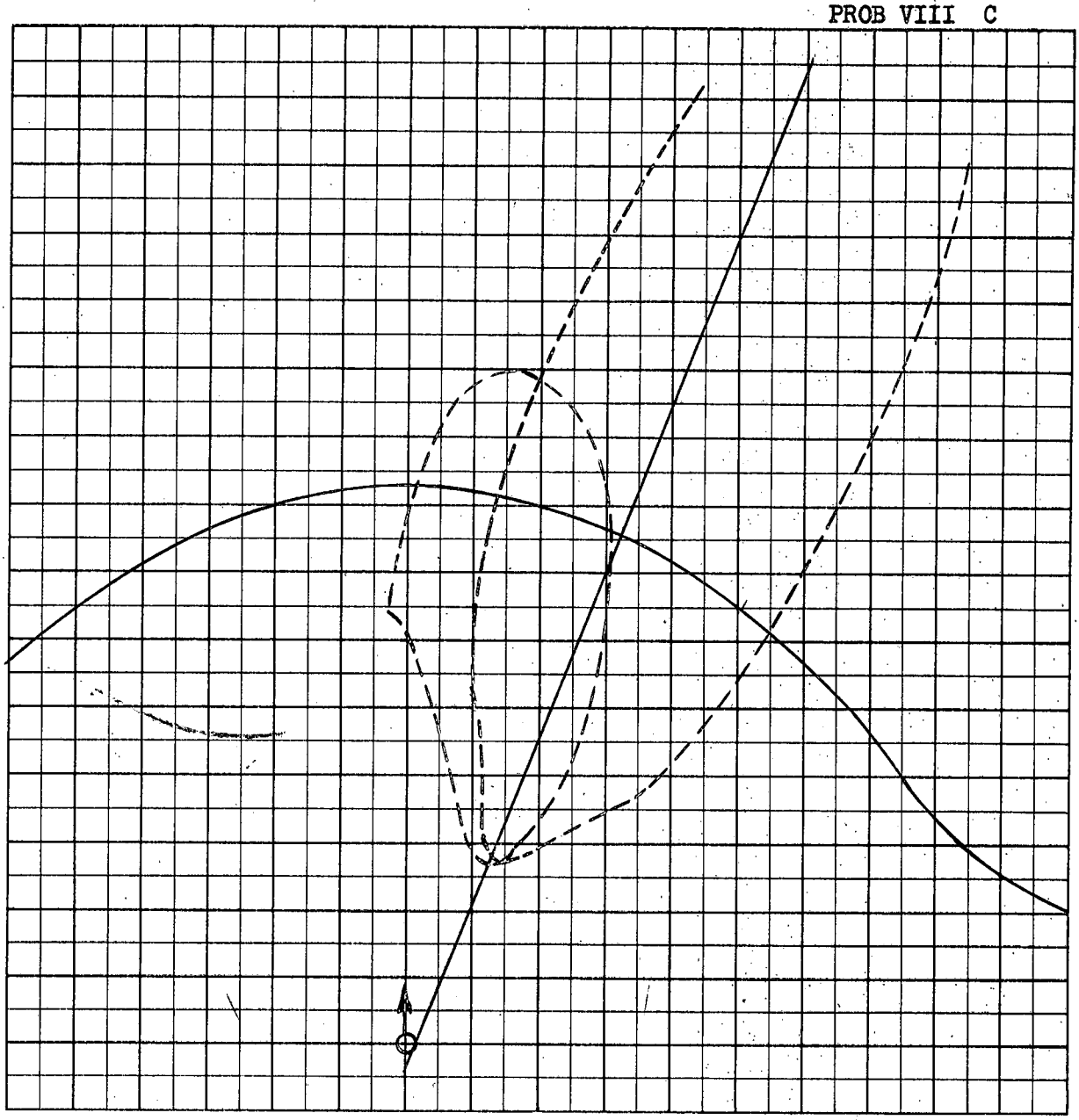

Scale 25,000 ft/cm

M_t = 2.0
h_t = 70 K
M_{fo} = 2.0
$h_{fo\ C}$ = 60 K
R_t = .458 g
Γ_o = 135°

A-105

Zones for target turns to the left and right both shown.

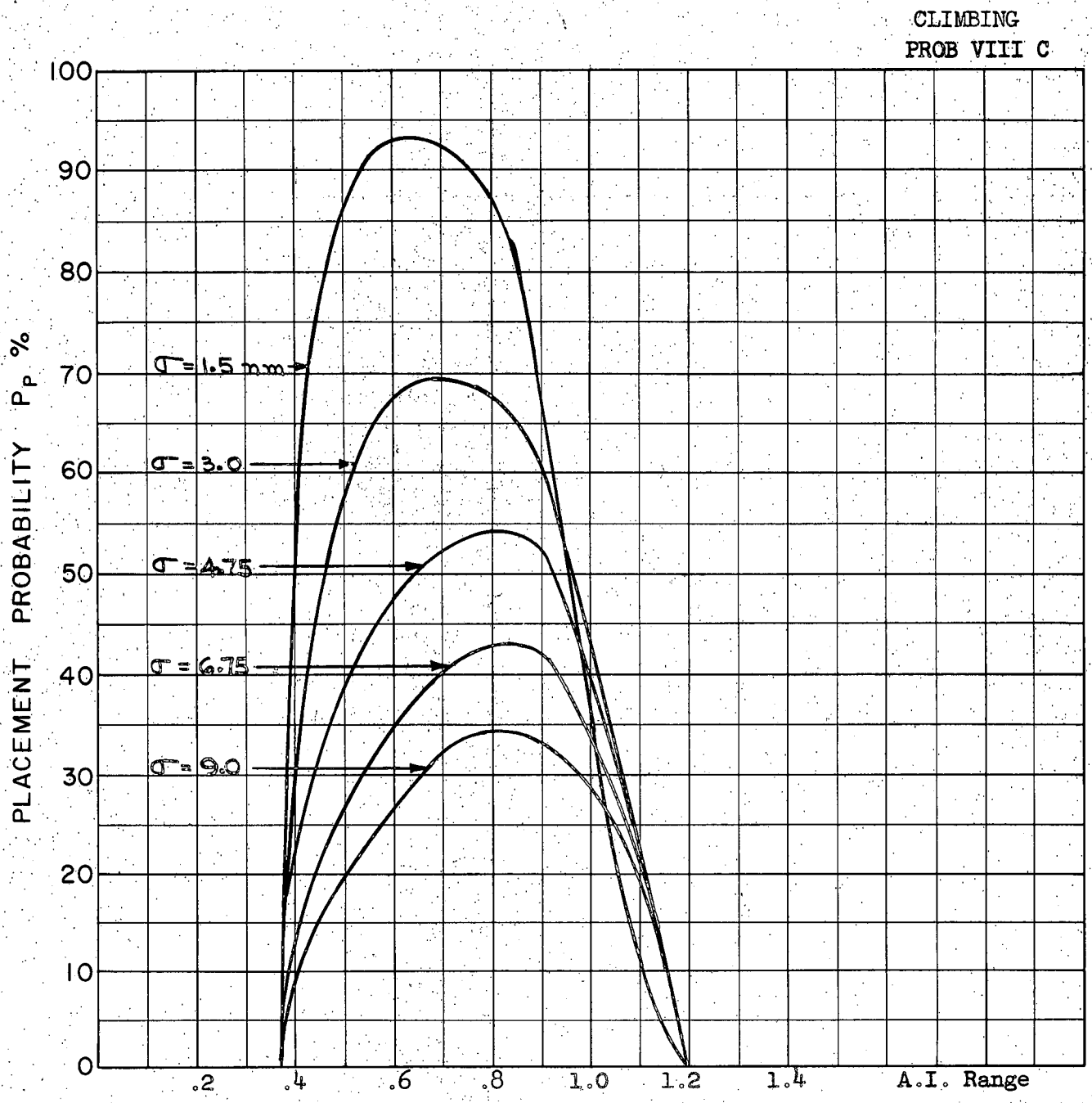

A-106

COURSE DIFFERENCE: 135°
TARGET EVASION: 1.1 g Load Factor
TARGET MACH NO.: 2.0
INTERCEPTOR LATERAL G's: Avro 3.3
INTERCEPTOR MACH NO.: 2.0
σ OF G.C.I. ACCURACY: 5 Values
A.I. DETECTION RANGE AS FRACTION OF SPECIFICATION RANGE, S: Abscissa
A.I. DETECTION RANGE CONTOUR: Delta
ALTITUDE: H_t = 70 K
H_f = 60 K

Probability values calculated from the placement zone common to the positive and negative evasion cases.

PROB VIII D

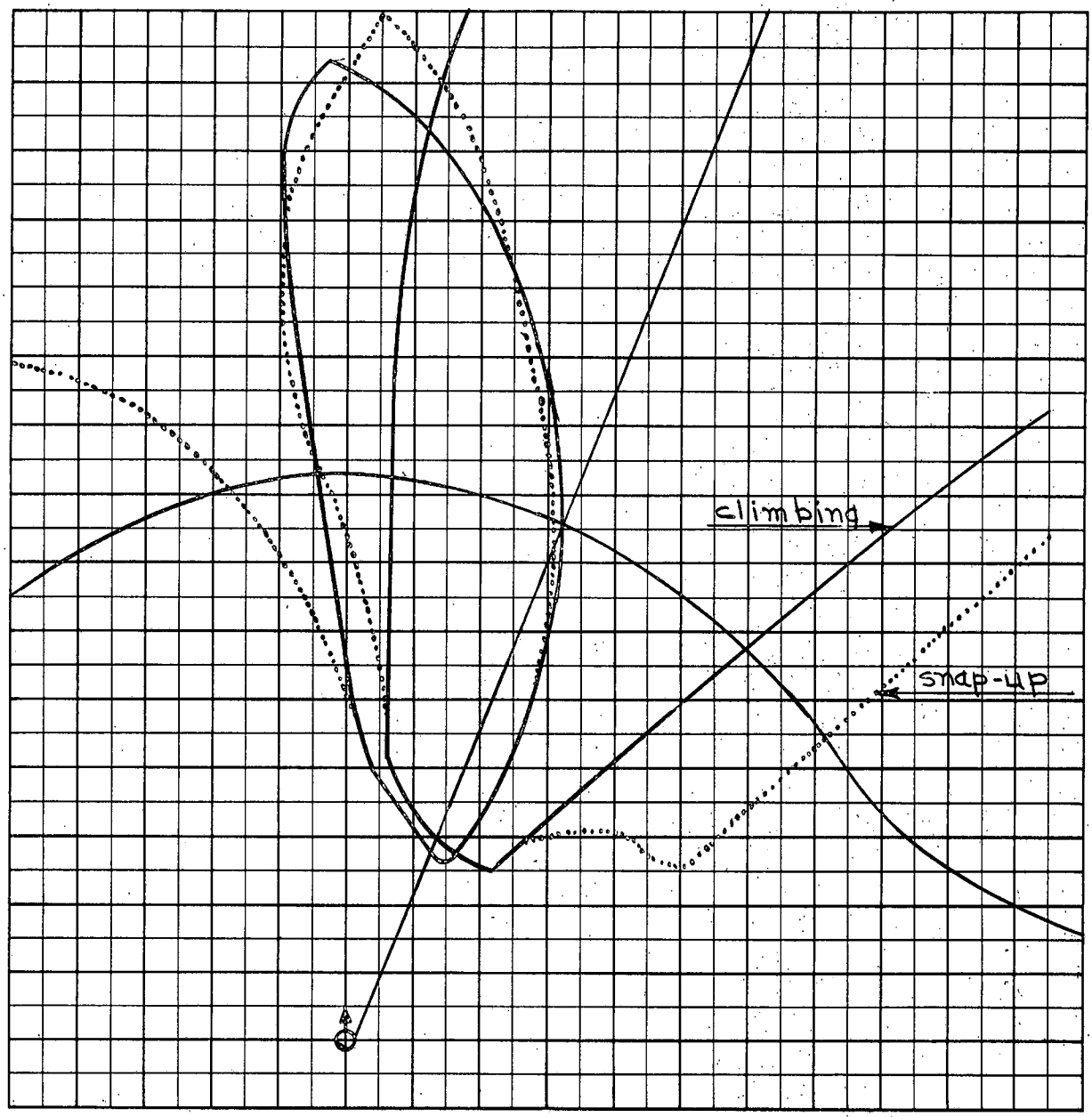

Scale 25,000 ft/cm

M_t = 2.0

h_t = 70 K

M_{fo} = 2.0

$h_{fo\ D}$ = 40 K

R_t = .458 g

Γ_o = 135°

A-107

Zones for target turns to the left and right both shown.

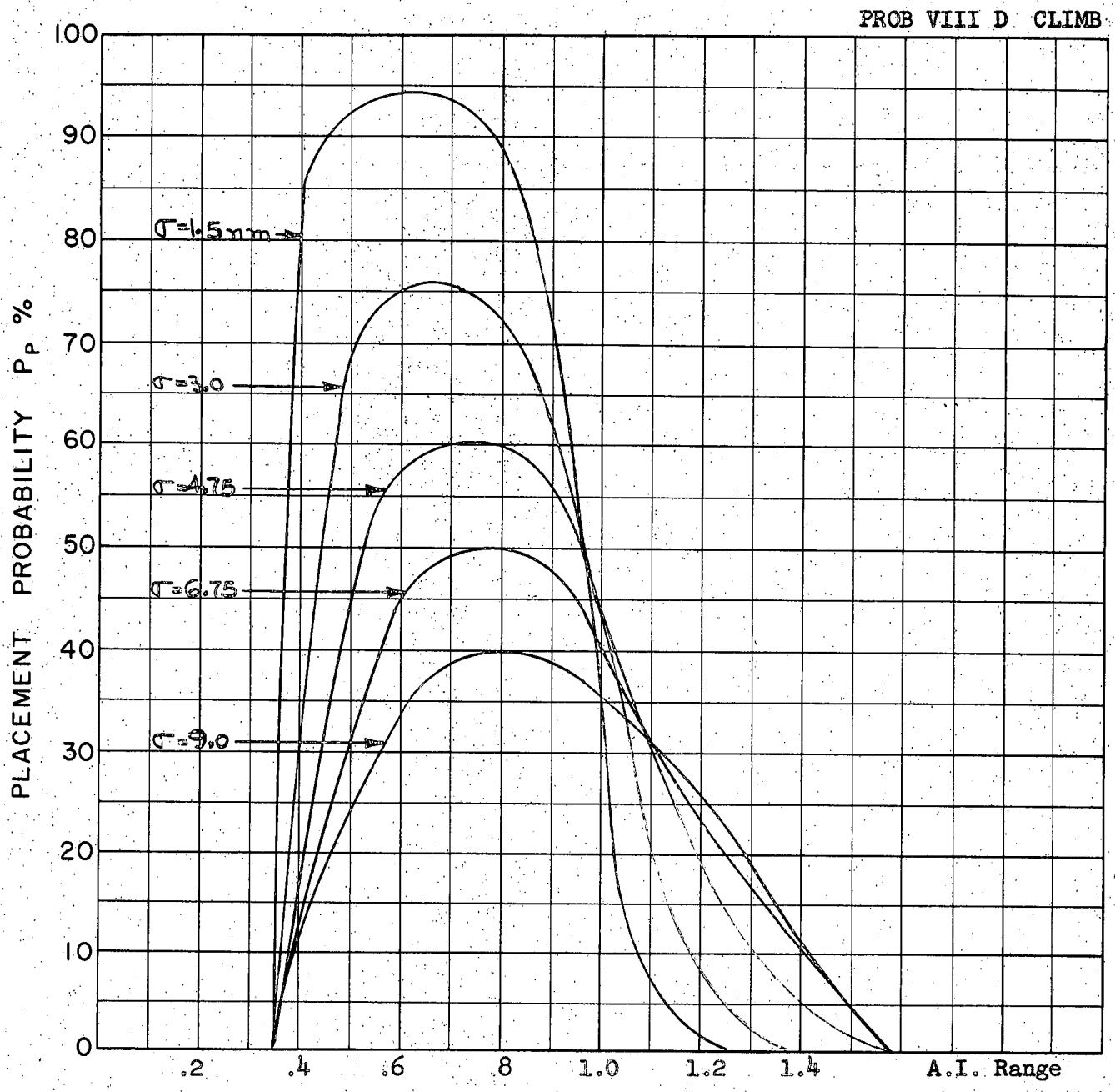

A-108

COURSE DIFFERENCE: 135°
TARGET EVASION: 1.1 g Load Factor
TARGET MACH NO.: 2.0
INTERCEPTOR LATERAL G's: Avro 3.3
INTERCEPTOR MACH NO.: 2.0
σ OF G.C.I. ACCURACY: 5 Values
A.I. DETECTION RANGE AS FRACTION OF SPECIFICATION RANGE, S: Abscissa
A.I. DETECTION RANGE CONTOUR: Delta
ALTITUDE: H_t = 70 K
H_f = 40 K

Probability values calculated from the placement zone common to the positive and negative evasion cases.

PROB VIII D SNAP-UP

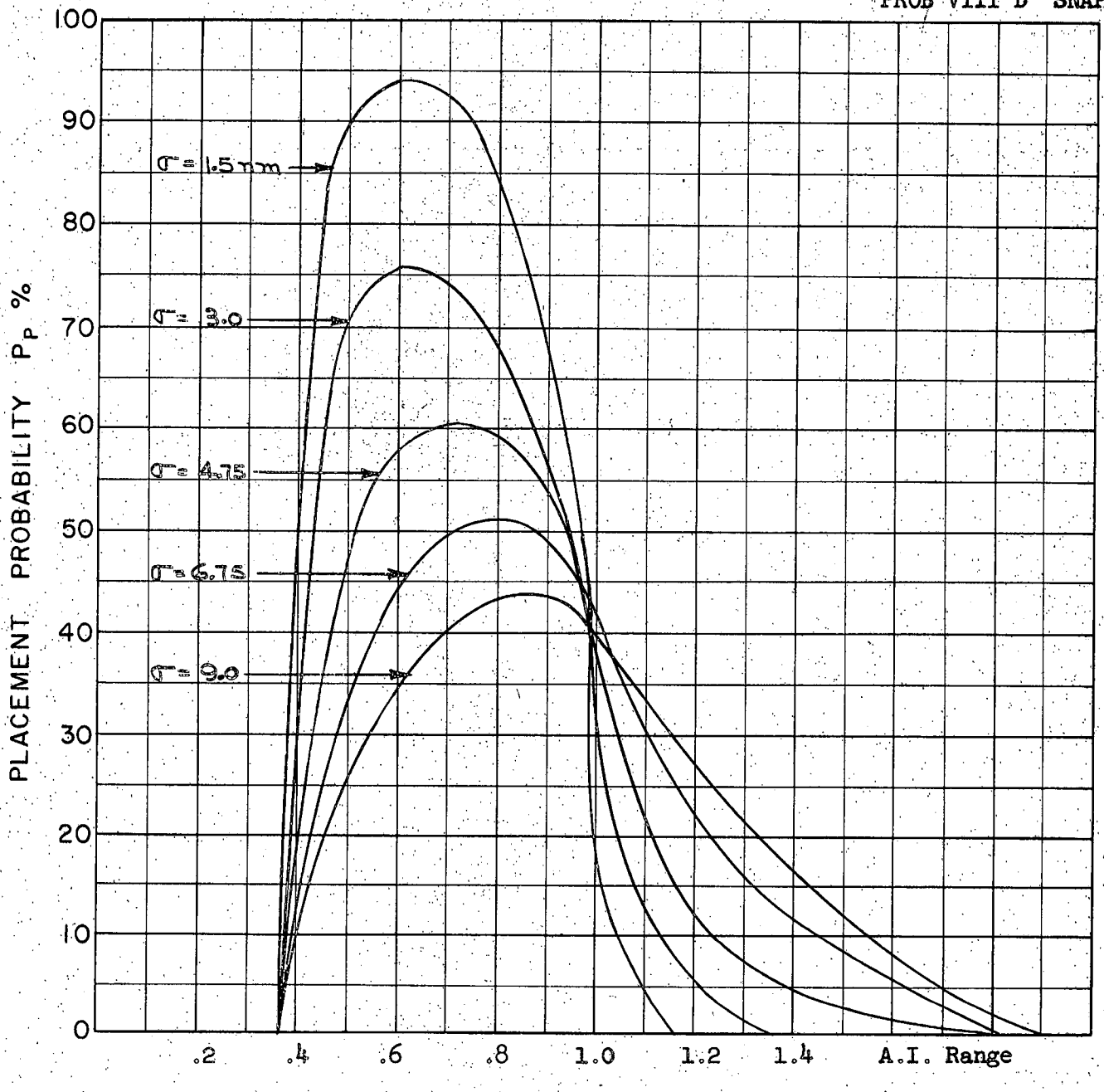

A-109

COURSE DIFFERENCE: 135°
TARGET EVASION: 1.1g Load Factor
TARGET MACH NO.: 2.0
INTERCEPTOR LATERAL G's: Avro 3.3
INTERCEPTOR MACH NO.: 2.0
σ OF G.C.I. ACCURACY: 5 Values
A.I. DETECTION RANGE AS FRACTION OF SPECIFICATION RANGE, S: Abscissa
A.I. DETECTION RANGE CONTOUR: Delta
ALTITUDE: H_t = 70 K
H_f = 40 K

Probability values calculated from the placement zone common to the positive and negative evasion cases.

PROB IX ABC CLIMBING

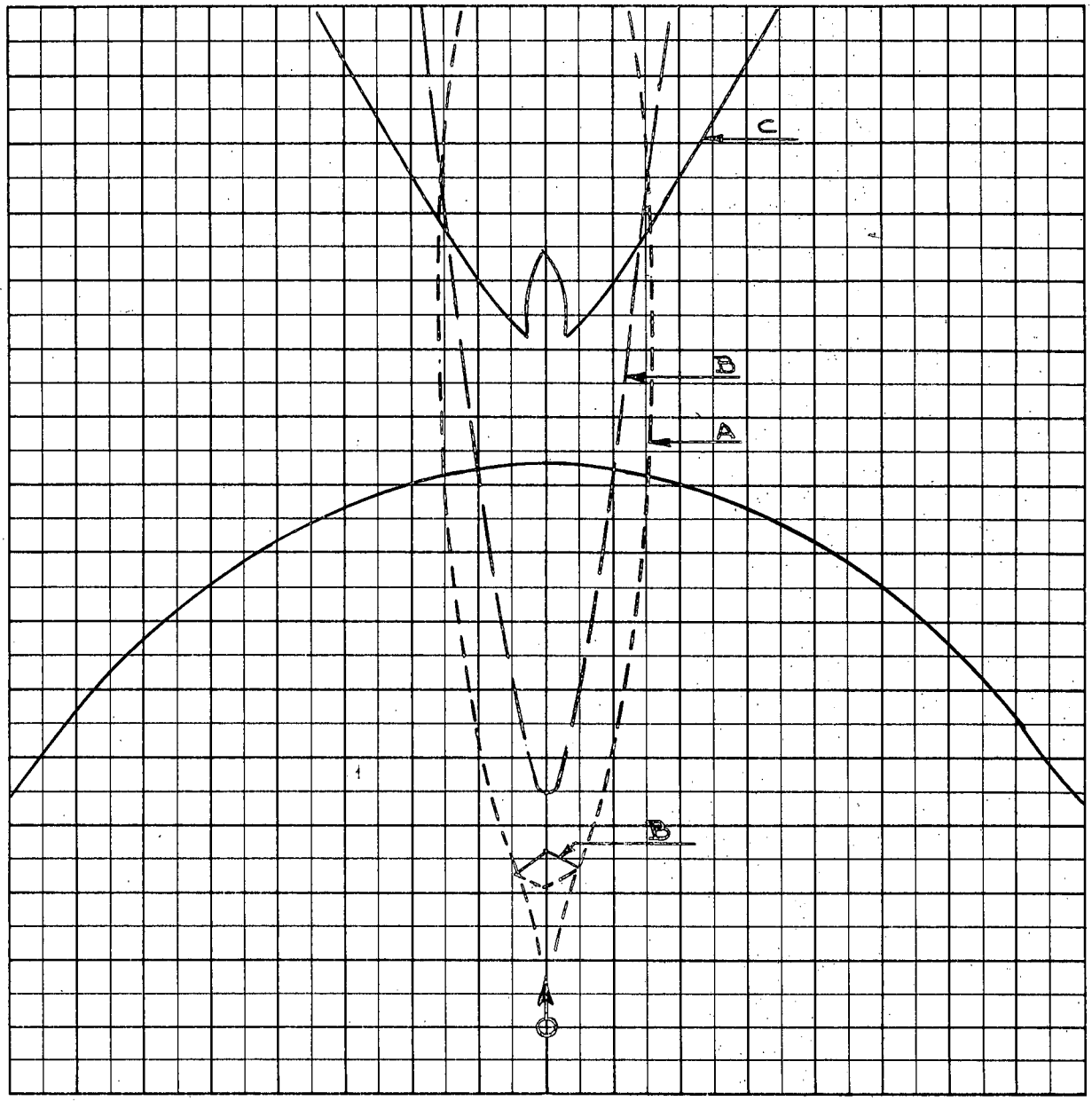

Scale 25,000 ft/cm

M_t = 2.0

h_t = 60 K

M_{fo} = 1.5

h_{fo} A = 60 K

B = 50 K

C = 40 K

Γ_o = 180°

A-110

COALTITUDE
PROB IX A

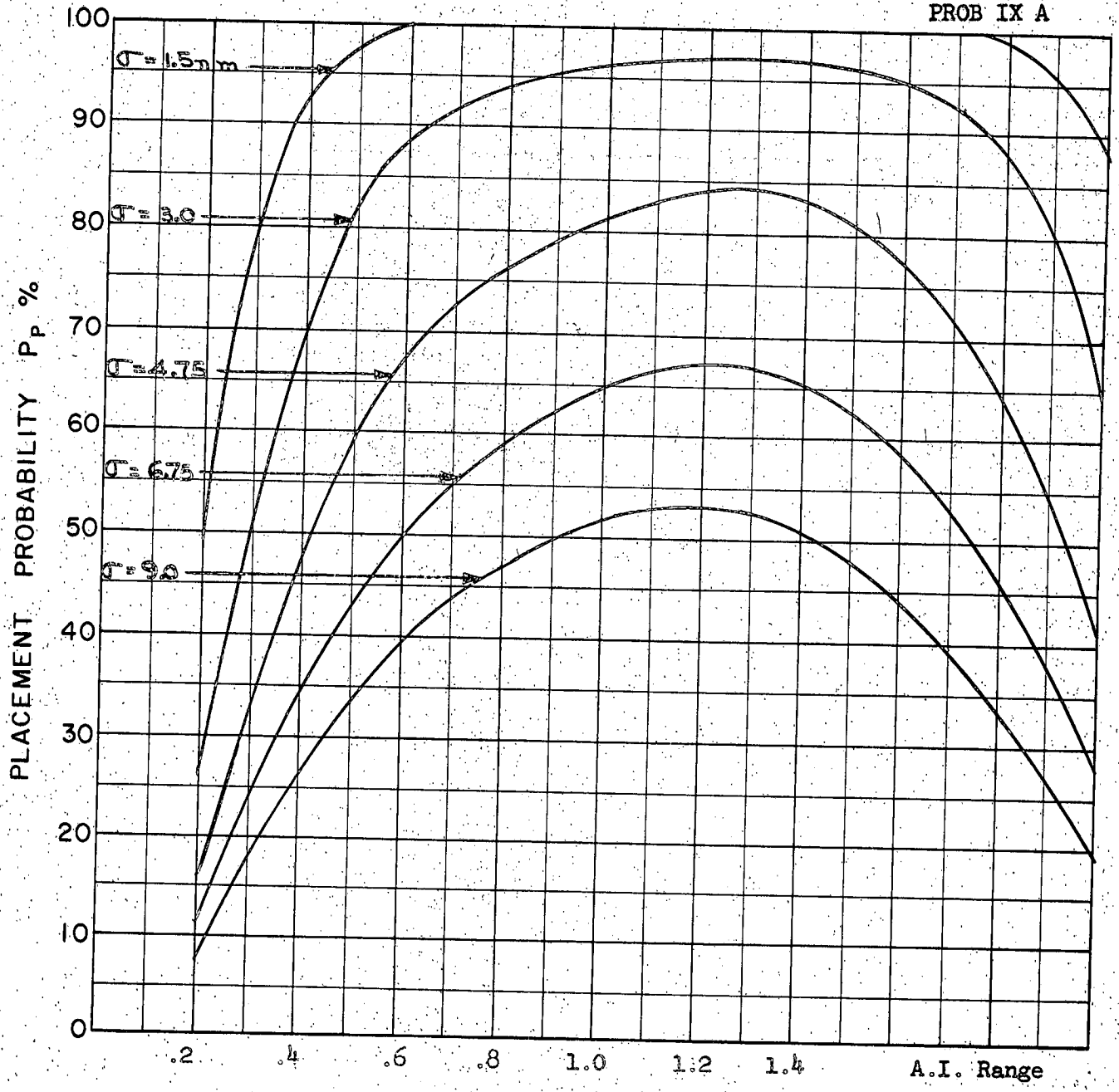

A-111

COURSE DIFFERENCE: 180°
TARGET EVASION: Nil
TARGET MACH NO.: 2.0
INTERCEPTOR LATERAL G's: Avro 3.3
INTERCEPTOR MACH NO.: 1.5
σ OF G.C.I. ACCURACY: 5 Values
A.I. DETECTION RANGE AS FRACTION OF SPECIFICATION RANGE, S: Abscissa
A.I. DETECTION RANGE CONTOUR: Delta
ALTITUDE: H_t = 60 K
H_f = 60 K

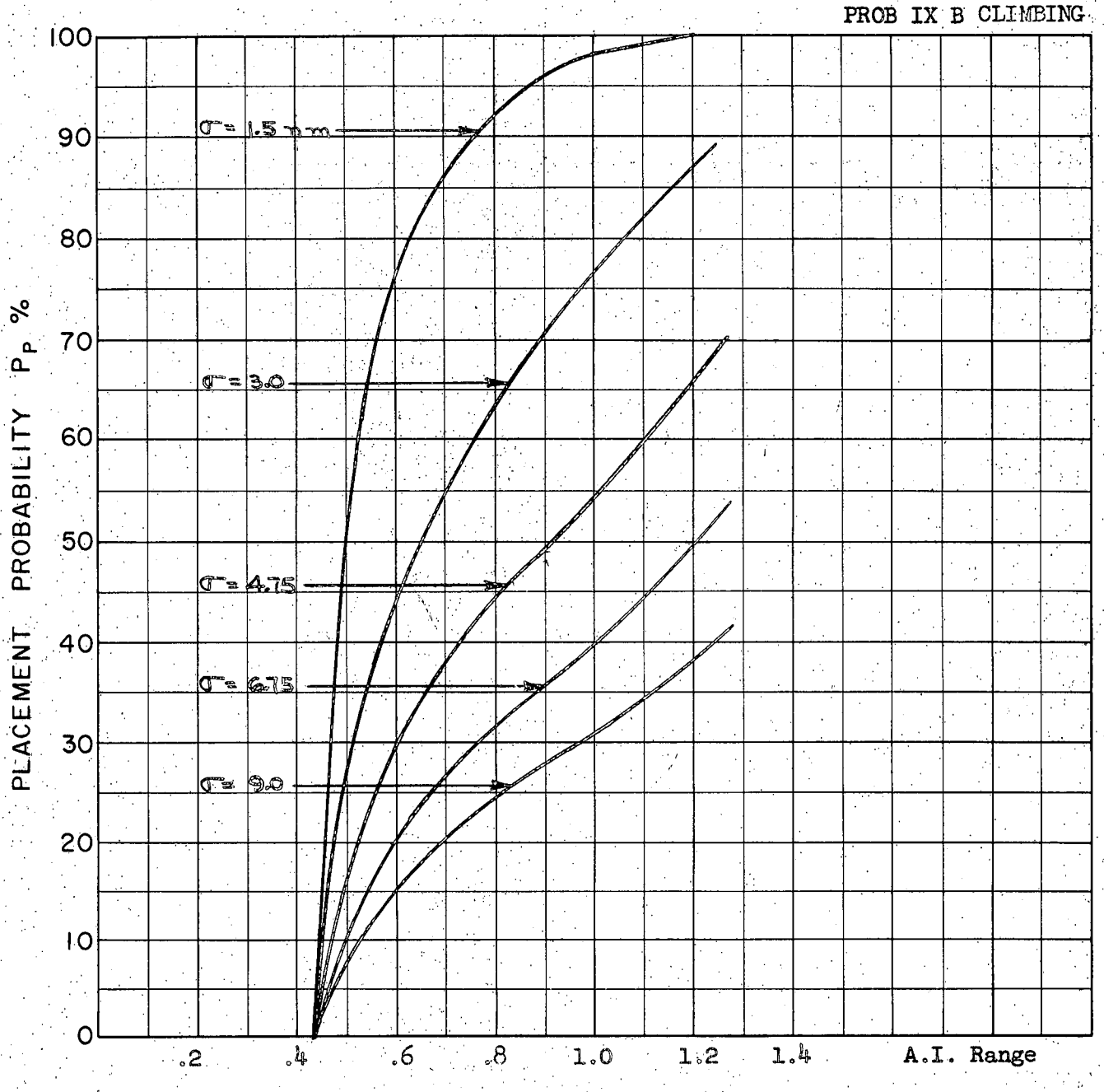

A-112

COURSE DIFFERENCE: 180°
TARGET EVASION: Nil
TARGET MACH NO.: 2.0
INTERCEPTOR LATERAL G's: Avro 3.3
INTERCEPTOR MACH NO.: 1.5
σ OF G.C.I. ACCURACY: 5 Values
A.I. DETECTION RANGE AS FRACTION OF SPECIFICATION RANGE, S: Abscissa
A.I. DETECTION RANGE CONTOUR: Delta
ALTITUDE: H_t = 60 K
H_f = 50 K

CLIMBING
PROB IX C

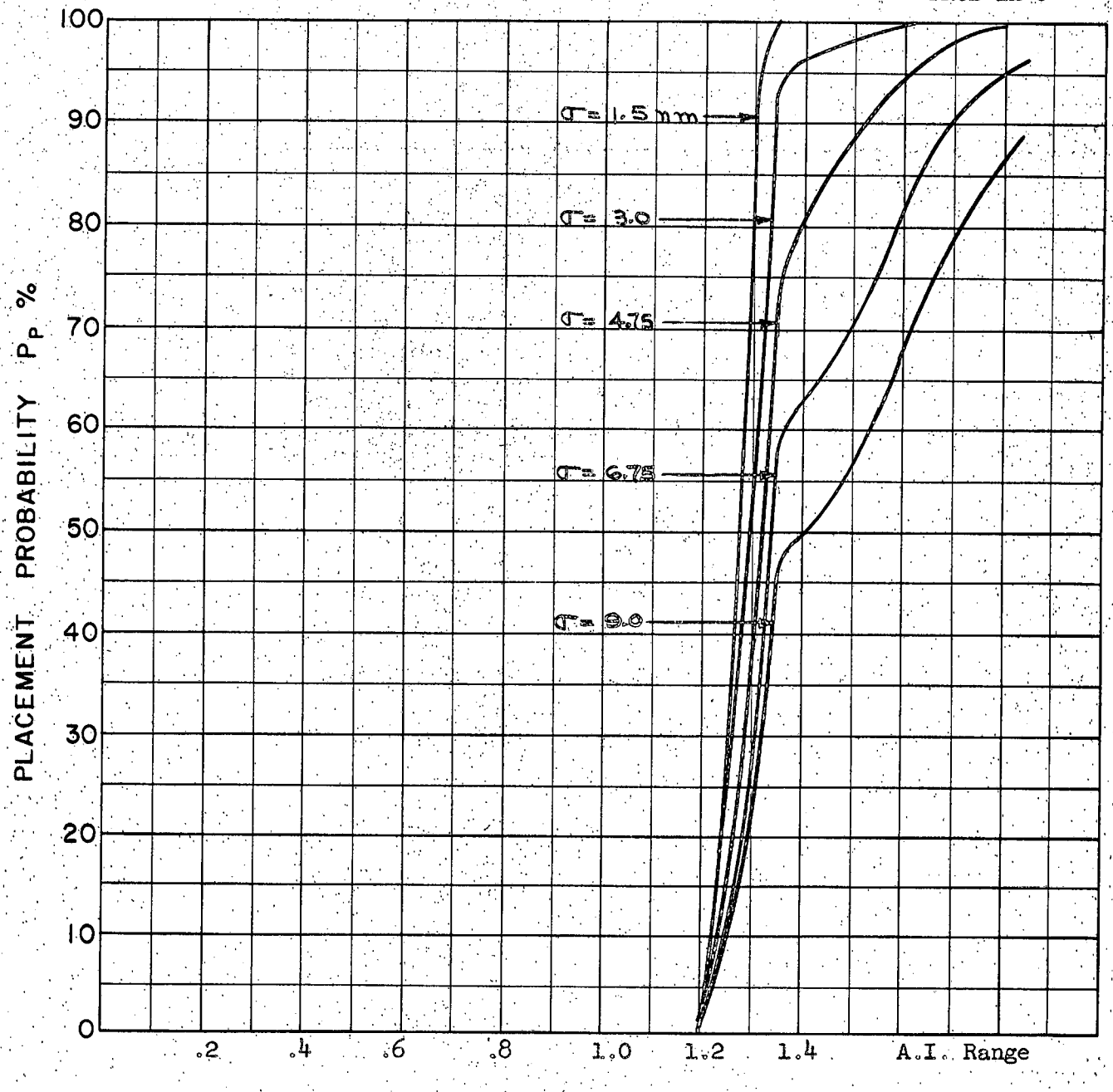

A-113

COURSE DIFFERENCE: 180°
TARGET EVASION: Nil
TARGET MACH NO.: 2.0
INTERCEPTOR LATERAL G's: Avro 3.3
INTERCEPTOR MACH NO.: 1.5
σ OF G.C.I. ACCURACY: 5 Values
A.I. DETECTION RANGE AS FRACTION OF SPECIFICATION RANGE, S: Abscissa
A.I. DETECTION RANGE CONTOUR: Delta
ALTITUDE: H_t - 60 K
H_f = 40 K

PROB IX DEF CLIMBING

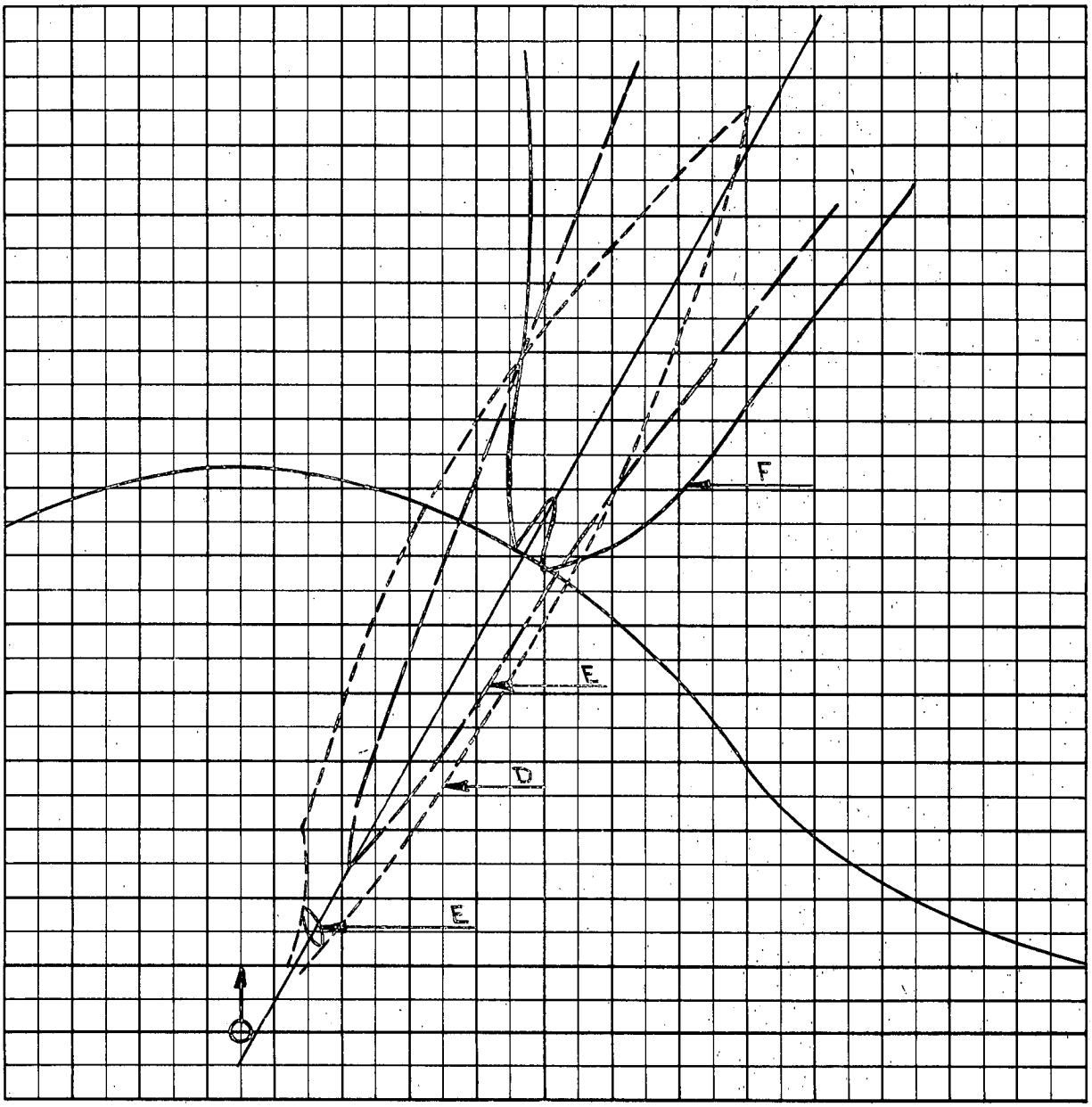

Scale 25,000 ft/cm

M_t = 2.0
h_t = 60 K
M_{fo} = 1.5
h_{fo} D = 60 K
E = 50 K
F = 40 K
Γ_o = 110°

A-114

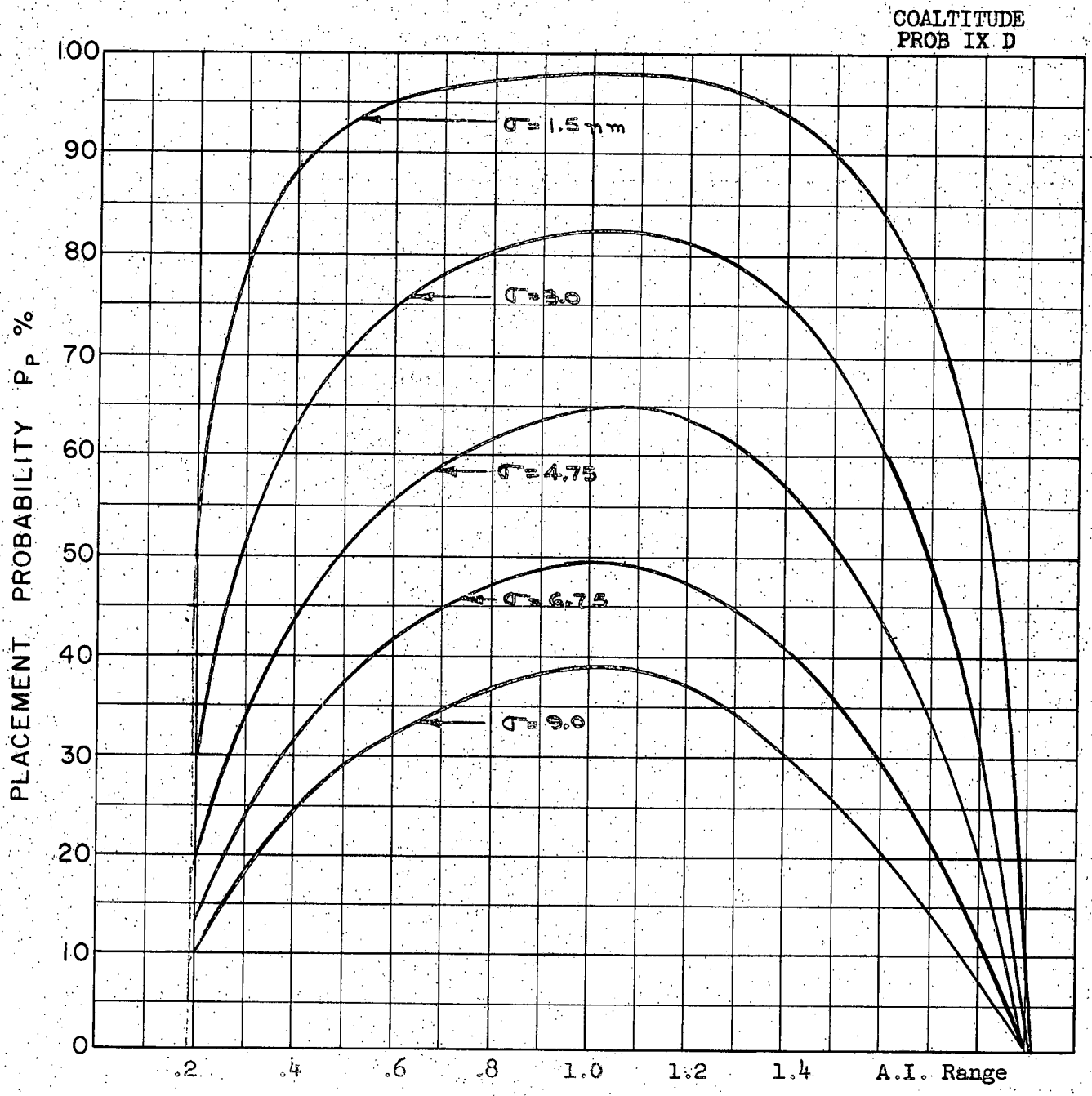

A-115

COURSE DIFFERENCE: 110°
TARGET EVASION: Nil
TARGET MACH NO.: 2.0
INTERCEPTOR LATERAL G's: Avro 3.3
INTERCEPTOR MACH NO.: 2.0
σ OF G.C.I. ACCURACY: 5 Values
A.I. DETECTION RANGE AS FRACTION OF SPECIFICATION RANGE, S: Abscissa
A.I. DETECTION RANGE CONTOUR: Delta
ALTITUDE: H_t = 60 K
H_f = 60 K

CLIMBING

PROB IX E

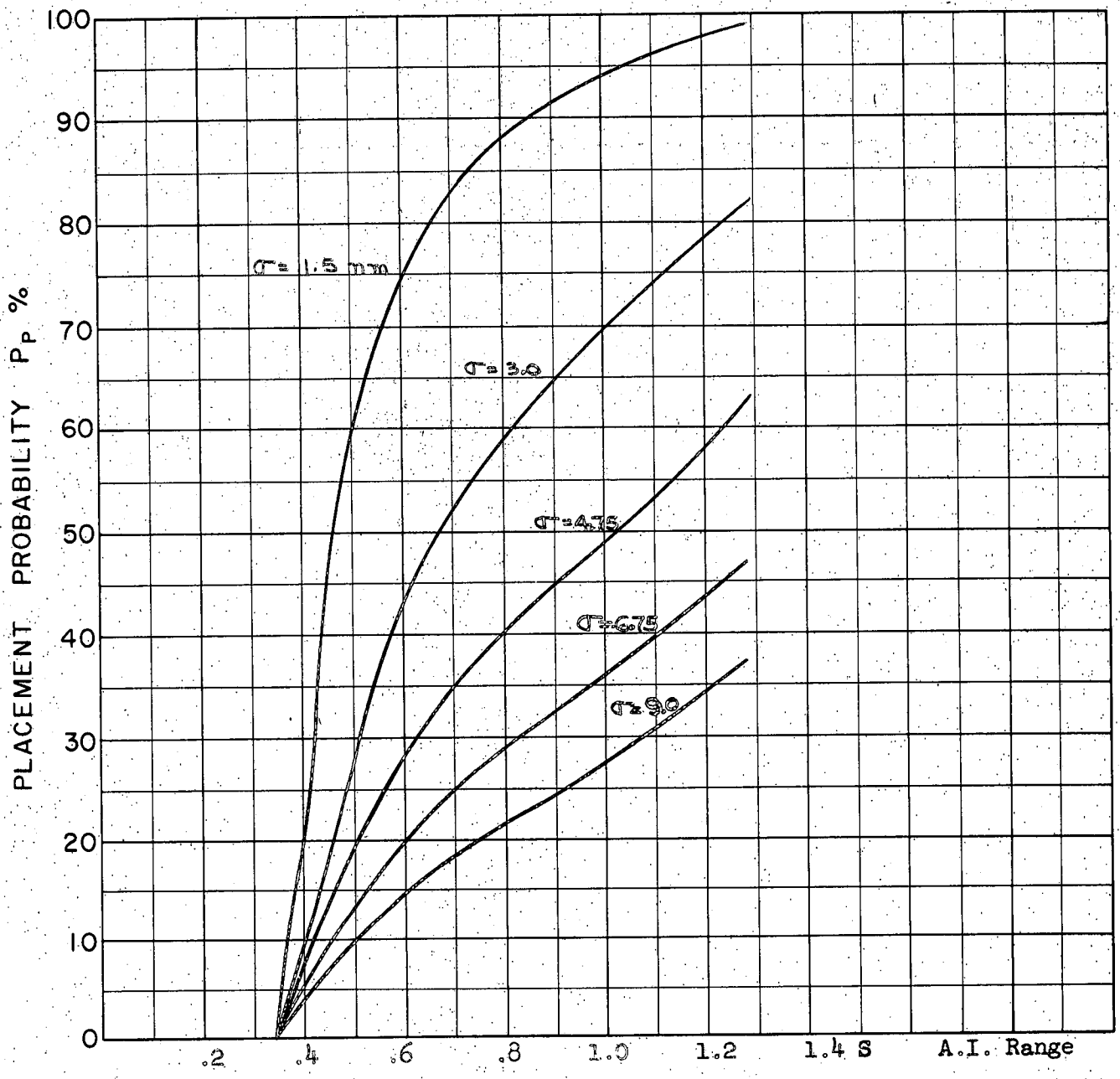

A-116

COURSE DIFFERENCE: 110°
TARGET EVASION: 0
TARGET MACH NO.: 2.0
INTERCEPTOR LATERAL G's: Avro 3.3
INTERCEPTOR MACH NO.: 1.5
σ OF G.C.I. ACCURACY: 5 Values
A.I. DETECTION RANGE AS FRACTION OF SPECIFICATION RANGE, S: Abscissa
A.I. DETECTION RANGE CONTOUR: Delta
ALTITUDE: H_t = 60 K
H_f = 50 K

CLIMBING

PROB IX F

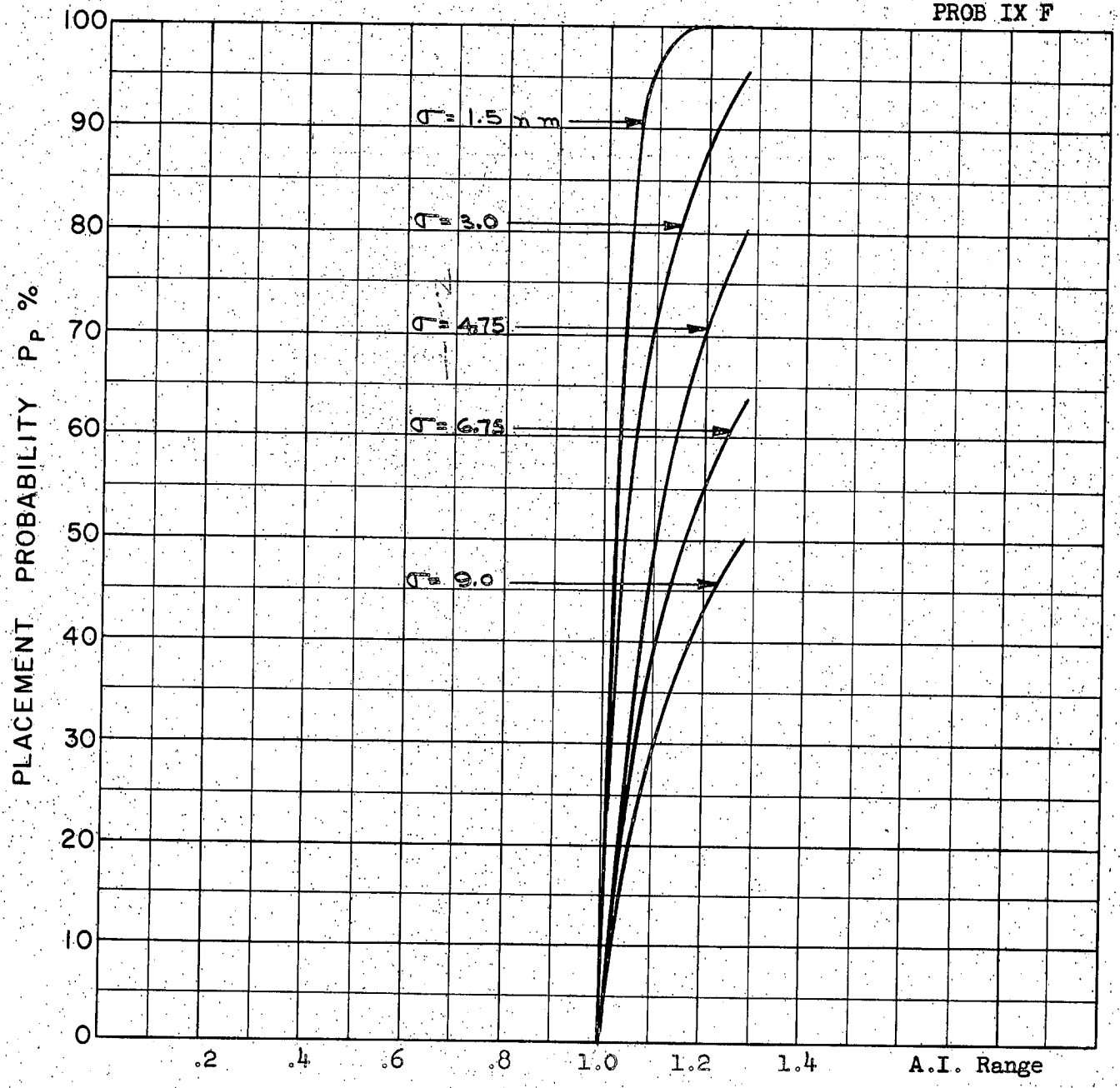

A-117

COURSE DIFFERENCE: 110°
TARGET EVASION: Nil
TARGET MACH NO.: 2.0
INTERCEPTOR LATERAL G's: Avro 3.3
INTERCEPTOR MACH NO.: 1.5
σ OF G.C.I. ACCURACY: 5 Values
A.I. DETECTION RANGE AS FRACTION OF SPECIFICATION RANGE, S: Abscissa
A.I. DETECTION RANGE CONTOUR: Delta
ALTITUDE: H_t = 60 K
H_f = 40 K

APPENDIX 'B'

MINIMUM INFORMATION STUDY

by

A. Bell, G.P. Coverley & F. Van Humbeck

1.0 INTRODUCTION

The work to be described concerns ways in which a range-jammed AI may home to a successful, known, launch position. Five methods of homing are being investigated currently and some results on the overall probability of success from a specified AI range contour are available. The effect of target evasion, the evasion consisting of 1/2 g turns, was examined in some cases. These methods are merely listed here, they will be described in detail in sections 4 and 5.

(1) Fixed R & T course
(2) Fixed lead course
(3) Zero lead course (pure pursuit)
(4) Fixed line of sight rate course
(5) True collision course

The determination of correct launch range has been based on $R/\dot{R}$ measurements (ref. 1), derived from power and power rate of the received jammer signal. Other methods have been suggested such as I.R. range finding, GCI command, visual range estimation, $\omega/\dot{\omega}$ measurements, fighter lateral acceleration, and oscillating fighter manoeuvres. Fighter lateral acceleration came into the scope of this study and was investigated, but rejected as unsuitable.

The homing studies were restricted to co-altitude manoeuvres and were carried out on the REAC or by hand computation.

2.0 PRELIMINARY WORK

2.1 General Description

Common to all the five methods considered is the need for launch zone data, $R/\dot{R}$ contours and 'g' contours.

2.2 Launch Zone and Residual Launch Zones

A missile launch zone was derived from Douglas data (ref. 2). Some interpolation was necessary from the data available in order to produce a zone that was applicable to a common fighter and target speed of M 1.5

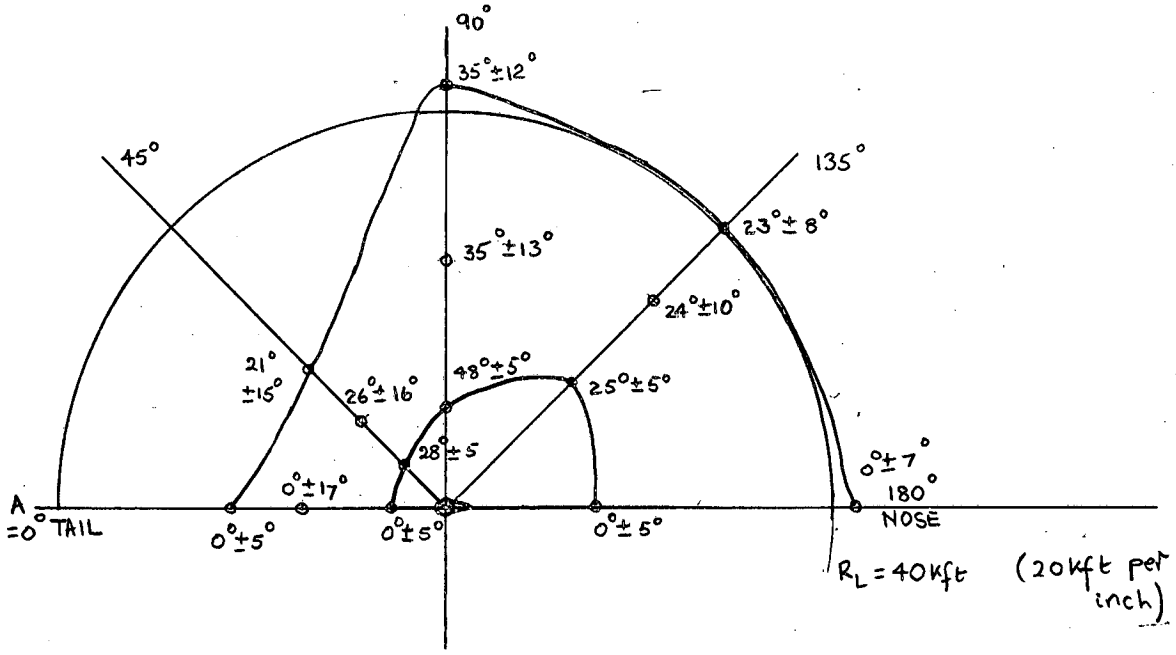

LAUNCH ZONE (Derived from Douglas data)

$V_T = V_F$ = M1·5 , H = 50 Kft.

MIN. RANGE DEFINED AT LEAD ANGLE ALLOWANCE OF ±5° *

MAX. " " " " " " " "

OR 22 SECONDS TIME OF FLIGHT, WHICHEVER GIVES SMALLER RANGE.

MISSILE SEEKER RANGE ALLOWED FOR.

IDEAL LEAD ANGLE AND ALLOWANCE SHOWN THUS:- 35° ± 13°.

* INCREASED BY 2000 FT, DUE TO NOISE PROBLEMS, OVER THAT GIVEN IN REF 2,

FIGURE 1B

at a height of 50,000 ft. The launch zone so produced (Fig.1B) has its minimum range based on a 5^{o} error in fighter heading and maximum range based on 22 seconds of missile flight time and missile radar seeker range on a delta-winged target aircraft.

Residual launch zones are, in general, different for each course studied, and are used in this preliminary work to influence the selection of an $R/\dot{R}$ contour to initiate missile firing. They are derived from Fig. 1B by considering the lead angles produced by each course. The fighter and target speeds and height for this derivation are the same as stated above.

2.3 $R/\dot{R}$ Contours

For each course these contours were obtained and plotted on the residual launch zone. Constant fighter and target speeds of M 1.5 at 50,000 ft. altitude were used in all cases. A visual inspection of the $R/\dot{R}$ contours led to a suitable choice of $R/\dot{R}$ value to initiate missile firing. The choice of $R/\dot{R}$ for each course is stated in sections 4 and 5.

2.4 Isogee Contours (Fighter Lateral Acceleration)

For each course, using the same conditions stated above, isogee contours were constructed in the hope that these contours could be used successfully to initiate missile firing. It was found that these contours, in general, tended to lie along command trajectories and would therefore make accurate positioning of the launch point uncertain. This possibility of fire control was therefore abandoned.

3.0 PROBABILITIES

3.1 Definitions

Probabilities used in the text are defined as follows:-

P_{Li} = prob. of successful launch associated with attack from centre of the ith section on any specified AI range contour.

P_{Pi} = prob. of placement by GCI in ith section

P_{i} = contribution to overall success from specified AI range contour by ith section on that contour

P = overall probability of success from the specified AI range contour.

The determination of overall probability P includes a probability due to GCI, and a probability due to $R/\dot{R}$ measurement. The $R/\dot{R}$ sensing equipments are assumed to have a Gaussian distribution of error about the chosen $R/\dot{R}$ value. The standard deviation of the $R/\dot{R}$ error curve is given two values of 20% and 60% of the chosen value.

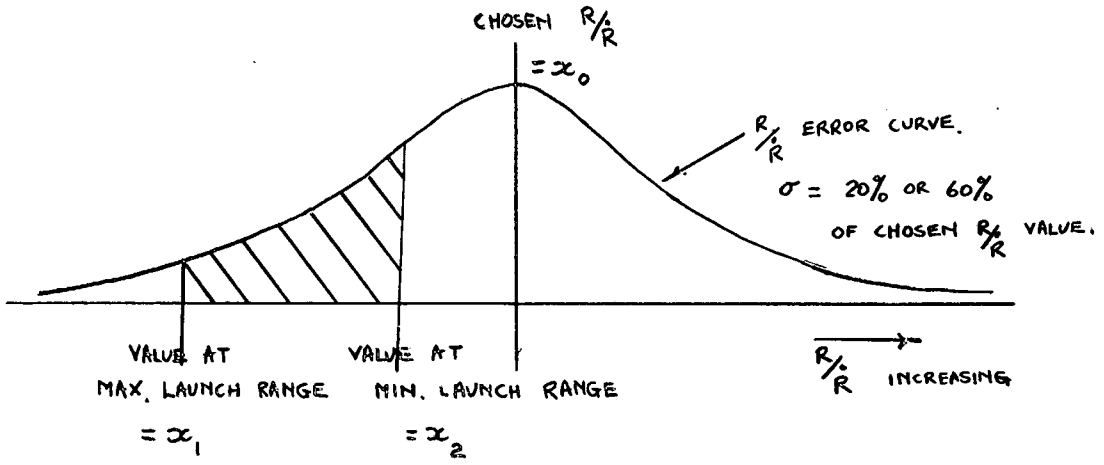

P_{L_i} = AREA OF SHADED PORTION

$$= \frac{1}{\sqrt{2\pi}} \int_{\frac{(x_1 - x_0)}{\sigma}}^{\frac{(x_2 - x_0)}{\sigma}} e^{-\frac{1}{2}t^2} \, dt$$

FIG. 2B.

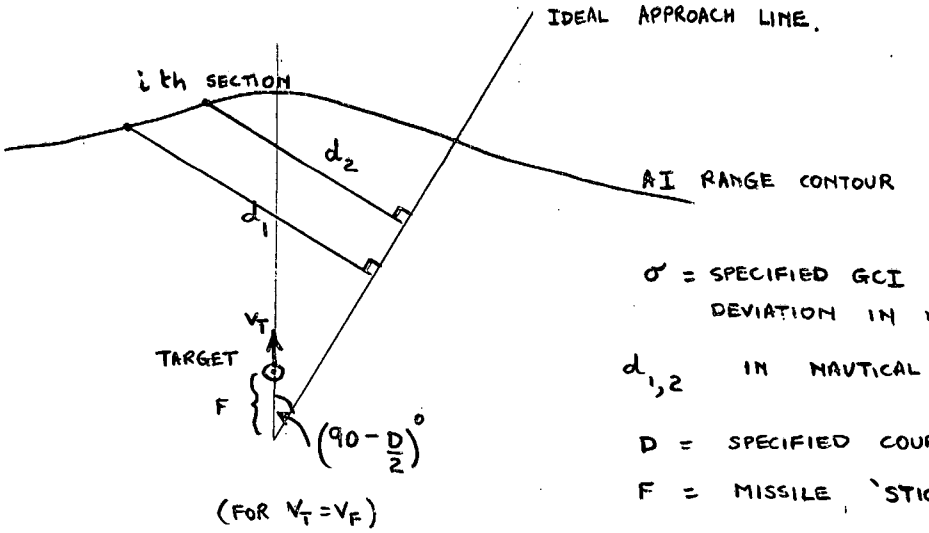

σ = SPECIFIED GCI STANDARD DEVIATION IN NAUTICAL MILES

$d_{1,2}$ IN NAUTICAL MILES.

D = SPECIFIED COURSE DIFFERENCE

F = MISSILE 'STICK' LENGTH.

$$P_{P_i} = \frac{1}{\sqrt{2\pi}} \int_{\frac{d_2}{\sigma}}^{\frac{d_1}{\sigma}} e^{-\frac{1}{2}t^2} \, dt.$$

FIG 3 B

In general the probability P is obtained by dividing the specified AI range contour into a number, n, of small sections, of which the ith section is the general one, and using the following relationship:

$$P_i = P_{Li} \times P_{Pi}$$

and

$$P = \sum P_i$$

over specified AI range contour

$$= \sum_{i=1}^{n} P_{Li} \times P_{Pi}$$

P_{Li} is obtained by considering the range of $\dot{R}/R$ values encountered in the residual launch zone for an attack initiated at the centre of the ith section. The probability that the chosen $\dot{R}/R$ is measured by the equipment while the interceptor is in the launch zone* is then calculated (Fig. 2B).

P_{Pi} is obtained from the specified GCI standard deviation and a knowledge of the perpendicular distances of the ends of the ith section from the ideal approach line (Fig. 3B).

4.0 REAC STUDY

4.1 General

The REAC study divides naturally into two parts. First, preliminary work as suggested in 2.1 was done for a constant speed fighter and target at Mach 1.5, for modes 1, 4 and 5 as described in section 1. Secondly, further work to determine overall probability of successful launch for a variable fighter** has been scheduled for all modes. Fighter initial speed and target speed were Mach 1.5, maximum fighter speed was M 2.0, minimum fighter speed Mach 1.0. This program is partially completed.

* In REAC solutions the residual launch zone used here differs from that discussed in section 2.2. This is because a variable speed fighter is simulated. It is derived from the heading errors produced by these REAC solutions and from the Douglas zone shown in Fig. 1B. Using paper and pencil method, no such complication arises since V_F is assumed constant at M 1.5.

** Avro 3.3 Aerodynamics as described by D.W. Pounder in a memorandum on file SN-47-3 dated Feb. 22, 1957. They correspond to an ability to manoeuvre at 1.63 g's power limited at Mach 1.5 at 50,000 ft.

4.2 Fixed R & T Course

This course depends on fixing constant values of R and T into the lead collision equation such that the correct heading is approximated in the front half of the Douglas launch zone. (Fig. 1B)

From the lead collision equations

$$\left(V_F + \frac{F}{T}\right) \sin L_a = V_T \sin A \qquad (1)$$

and $$R\omega = V_F \sin L_a - V_T \sin A \qquad (2)$$

we get $$\sin L_a = -\frac{RT}{F}\omega , \qquad (3)$$

Considering the launch point $R = R_L$ and $T = T_L$

then $$\sin L_a = -K\omega, \text{ where } K = \frac{R_L T_L}{F} ; \qquad (4)$$

$K = 30$ seconds for $\Delta V = 970$ ft/sec and $R_L = 29{,}000$ ft. for a launch range centrally located in the launch zone.

For the constant speed study we get from (2) and (4)

$$\sin L_a = \frac{V_T \sin A}{(R/K + V_f)}$$

and differentiating, $$\dot{L}_a = \frac{\dot{A}\,(\dot{R} + V_T \cos A)}{(R/K + V_F)\cos L_a}$$

because $\dot{A} = \omega$ if the target does not manoeuvre.

For g_h contours (lateral g contours)

$$g_h = \frac{(V_F\,(\dot{A} - \dot{L}_a)}{32.2}$$

For heading error contours

$$\delta^* = L_a^* - L_a$$

where

$$L_a^* = \sin^{-1}\left[\frac{V_T \sin A}{V_F + \Delta V}\right]$$

The $\dot{R}/R$ contours were also recorded, and these together with the Douglas launch zone data for Mach 1.5 fighter and target formed the basis for choosing launch criteria. An $\dot{R}/R$ contour of 12 seconds was chosen as giving the best coincidence with the residual launch in this case. The circuits of Figs. 48and 58were used in this solution.

For the variable-speed study, the previous steering system for lead collision was

$$\omega_a = K_1'/K_1 \cdot K_1 \left[\frac{R\omega + F/T \sin L_a}{V_F + \Delta V} \right]$$

with $K_1 = 4$ per second.*

The modified steering system is

$$\omega_a = K_2'/K_2 \cdot K_2 \left[\omega + \frac{\sin L_a}{K} \right]$$

where

$$K_2 = \frac{K_1 R_L}{V_F + \Delta V} = 48$$

for $R_L = 29{,}000$ ft, $V_F =$ M 1.5, $\Delta V = 970$ ft/sec. at the launch point.

This gain was instrumented for the steering system. The results of this for 180°, 135° and 110° initial course differences for standard deviations of 1.5, 4.75, and 9 nautical miles in GCI accuracy are given in Table 1. An additional launch condition, that the missile flight time should always exceed 4 seconds, was used in this work. The results are shown for cases with no evasion, and with evasion at 1.118 load factor.

4.3 Fixed Lead

A constant $\dot{R}/R$ contour of 12 seconds was chosen as criterion from the hand-computation approach to the constant speed study dealt with in section 5.3.

The equation for a fixed lead course

$$\omega_a = \frac{K_3'}{K_3} \cdot K_3 \left[K_4 - L_a \right]$$

can be related to the equation for a fixed R and T course

* $\frac{K'}{K} = 1$ when demanded lift is less than maximum available lift; when demanded lift is greater than available lift $\frac{K'}{K}$ is automatically adjusted to some value less than 1 so that achieved lift is equal to maximum available lift.

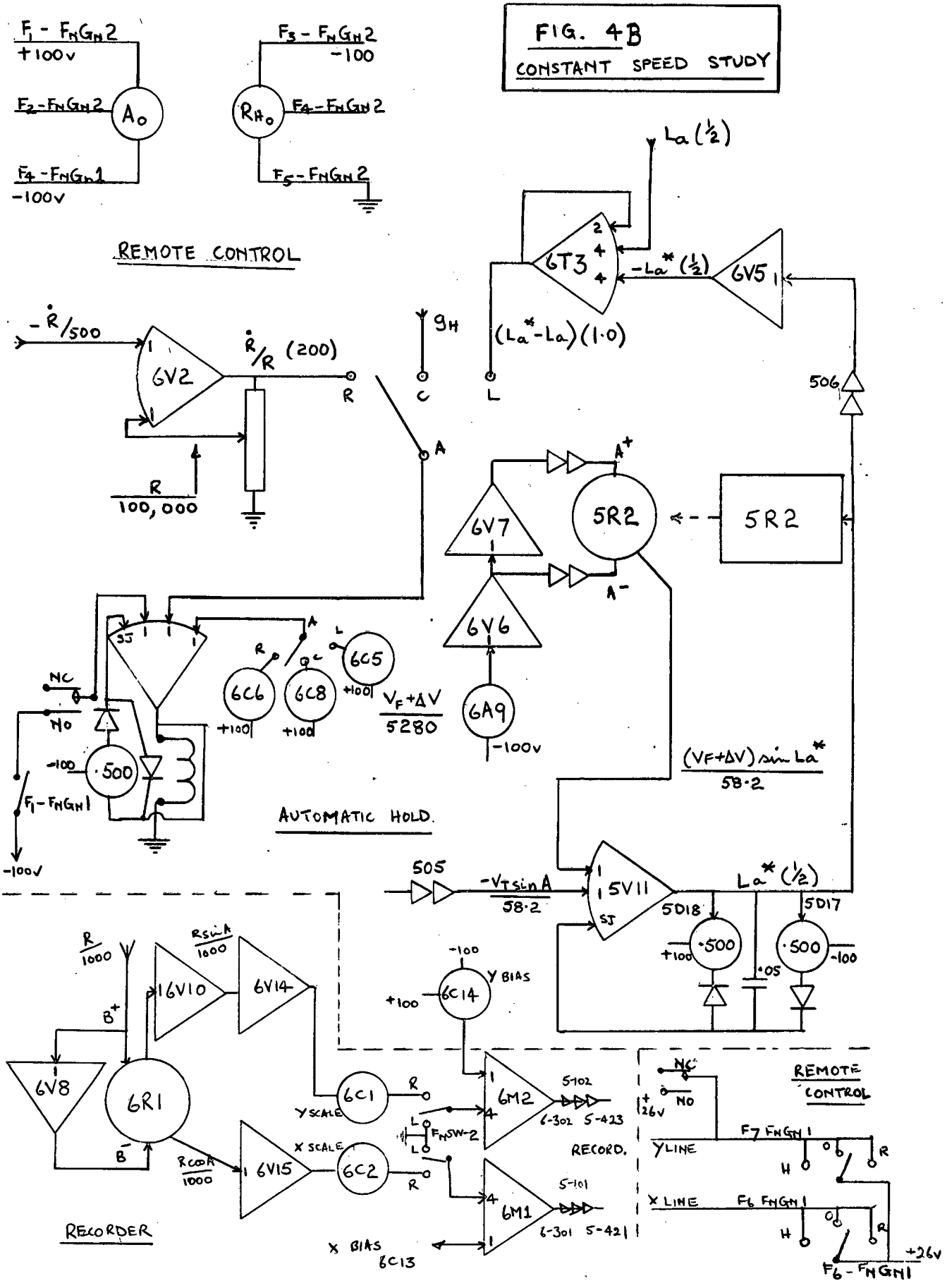
FIG. 4B
CONSTANT SPEED STUDY
F1 - FNGN2
+100v
F2 - FNGN2
A0
F4 - FNGN1
-100v
F3 - FNGN2
-100
RH0
F4 - FNGN2
F5 - FNGN2
REMOTE CONTROL
La (1/2)
6T3
-La* (1/2)
6V5
(La*-La)(1·0)
gH
C
L
506
-Ṙ/500
6V2
Ṙ/R (200)
R
R
100,000
A
6V7
5R2
5R2
A+
A-
6V6
6A9
-100v
6C5
6C6
6C8
+100
VF+ΔV
5280
NC
NO
-100
·500
F1 - FNGN1
-100v
AUTOMATIC HOLD.
(VF+ΔV) sin La*
58·2
505
-VT sin A
58·2
5V11
SJ
La* (1/2)
5D18
5D17
·500
·05
·500
+100
-100
6C14
Y BIAS
+100
R/1000
RSinA/1000
16V10
6V14
B+
6V8
6R1
B-
RCosA/1000
6V15
6C1
6C2
YSCALE
XSCALE
R
R
L
L
FNSW-2
6M2
6M1
5-102
6-302
5-423
5-101
6-301
5-421
RECORD.
X BIAS
6C13
RECORDER
NC
NO
+26v
REMOTE CONTROL
YLINE
F7 FNGN1
H
R
XLINE
F6 FNGN1
H
R
+26v
F6 - FNGN1

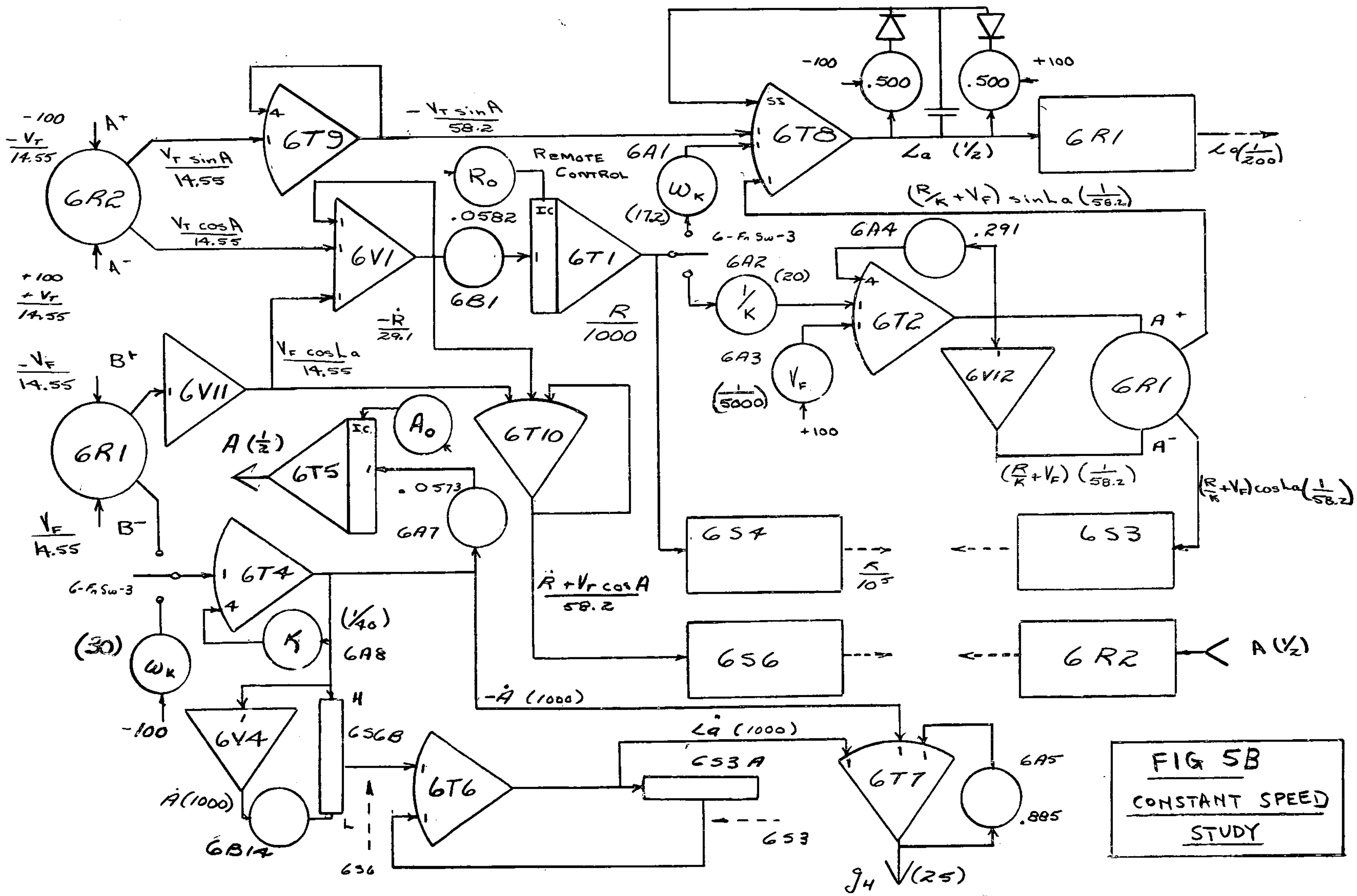

FIG 5B
CONSTANT SPEED
STUDY

TABLE I - OVERALL SUCCESS PROBABILITIES (%)

FOR PROBLEM 4.2

FIXED R AND T COURSE

	$R/\dot{R}(\sigma)$ 20%				$R/\dot{R}(\sigma)$ 60%				
	1.28S	S	0.85S	0.6S	1.28S	S	0.85	0.6S	
σ_1 1.5 nm	53.29		59.24		37.9		38.19		D 180° no evasion
σ_2 4.75	50.39		60.61		35.17		38.11		
σ_3 9 nm	54.89		61.43		36.21		36.31		
σ_1	82.08		71.51		37.92		39.15		D 135° no evasion
σ_2	81.11		79.86		41.94		42.40		
σ_3	69.42		69.65		42.25		37.57		
σ_1	78.20		86.09		37.14		43.40		D 110° no evasion
σ_2	62.62		83.17		41.93		43.16		
σ_3	62.84		65.89		35.79		36.52		
σ_1	16.0	60.8	88.3	84.6	27.3	33.7	44.3	45.5	D 180° 1/2 g evasion
σ_2	5.6	30.0	55.4	65.5	12.3	22.7	34.5	35.3	
σ_3	3.1	16.2	32.6	41.4	6.8	13.5	22.4	22.7	
σ_1	13.0	13.0	34.5	56.8	6.0	7.5	28.1	37.0	D 135° 1/2 g evasion
σ_2	26.3	29.4	36.7	34.3	12.7	15.0	23.1	26.3	
σ_3	20.4	24.3	28.4	29.5	10.8	13.4	16.6	18.2	
σ_1		8.4	9.4	12.9		9.5	7.2	9.2	D 110° 1/2 g evasion
σ_2		25.0	23.3	22.1		15.0	13.0	12.6	
σ_3		26.5	24.6	19.0		15.1	13.0	10.4	

$$\omega_a = \frac{K_2'}{K_2} \cdot K_2 \left[\omega + \frac{\sin L_a}{K} \right]$$

If the approximation $\sin L_a \doteq L_a$ is made and $K_3 = -K_2/K = -1.6$ per second

REAC Data has been recorded for the fixed lead mode and is presently being reduced.

4.4 Zero Lead Course (Pure Pursuit)

Preliminary work was done for this mode from a paper and pencil standpoint and is treated in section 5.4.

4.5 Fixed Line of Sight Rate

The steering equation for a fixed line of sight rate course

$$\omega_a = K_5'/K_5 \cdot K_5 \left[\omega - \omega_K \right]$$

can be related to the equation for a fixed R and T course

$$\omega_a = K_2'/K_2 \cdot K_2 \left[\omega + \frac{\sin L_a}{K} \right]$$

if $K_5 = K_2 = 48$

The constant speed study where

$$L_a = \sin^{-1} \left[\frac{R\omega_K + V_T \sin A}{V_F} \right]$$

$$\dot{L}_a = \frac{\dot{A} \ (\dot{R} + V_T \cos A)}{V_F \cos L_a}$$

also instrumented in Figs. 4 and 5 resulted in the choice of an $\dot{R}/R$ contour of 12 seconds as a best fit for the residual launch zone. It was used as the launch criterion. Data recorded from REAC runs for the "fixed line of sight rate" mode is presently being reduced.

4.6 Pure Collision

By setting $\omega_K = 0$ in the preceding section, a pure collision mode is produced. Data for this mode has been recorded and is awaiting reduction.

5.0 PAPER AND PENCIL METHOD FOR DETERMINING PROBABILITY

5.1 General

A paper and pencil method for determining probability will be described for the fixed lead angle, $L_a = 20^o$ navigation mode. The same method can be applied to other modes where the applicable equations are soluble. For the $L_a = 20^o$ mode, results are to be obtained on the REAC as well (see section 4.3) to compare the results obtained by the two methods. The paper and pencil work could only be conveniently carried out for no target evasion whereas the REAC work also includes the case of target evasion.

In the paper and pencil method, power-limited performance was assumed, i.e. fighter lateral g's were limited so that there was no fighter deceleration due to manoeuvring. At M 1.5 at 50,000 ft. the appropriate lateral g limit is 1.3 g. It was also assumed that for a successful launch, the fighter must get on a command trajectory before it entered the launch zone. This, of course, is not necessarily true but results obtained for command trajectories approximate those for actual successful trajectories within the launch zone quite closely. (See section 5.3).

5.2 Fixed R and T Course

The applicable equations are not readily solved so this mode was left for the REAC. (see section 4.2)

5.3 Fixed Lead Angle Course

The lead angle L_a was set to 20^o where L_a is defined to be positive when the fighter's radar looks to the left. The residual launch zone was determined and is shown in figure 6. There is no residual launch zone to the left of the target since as L_a is defined, the fighter is directed behind the target and a "hit" is impossible from this region.

Constant $R/\dot{R}$ contours for command trajectories were plotted. The equation for these contours is (see annex I):-

$$R = \frac{R}{\dot{R}} \times 1.46 \times 10^3 (\cos A - 0.940)$$

The $\frac{R}{\dot{R}} = 12$ sec. contour seemed to best fit the residual launch zone so it was chosen as the "firing" contour. It is shown in figure 6.

Next, a family of 2-dimensional command trajectories initiated at a range of 40 n.m. was constructed. The equation for these curves is (see annex II):-

$$R = 240 \times 10^3 \left(\frac{\cos^2 \left[\frac{20 + A_o}{2} \right]}{\cos^2 \left[\frac{20 + A}{2} \right]} \right)$$

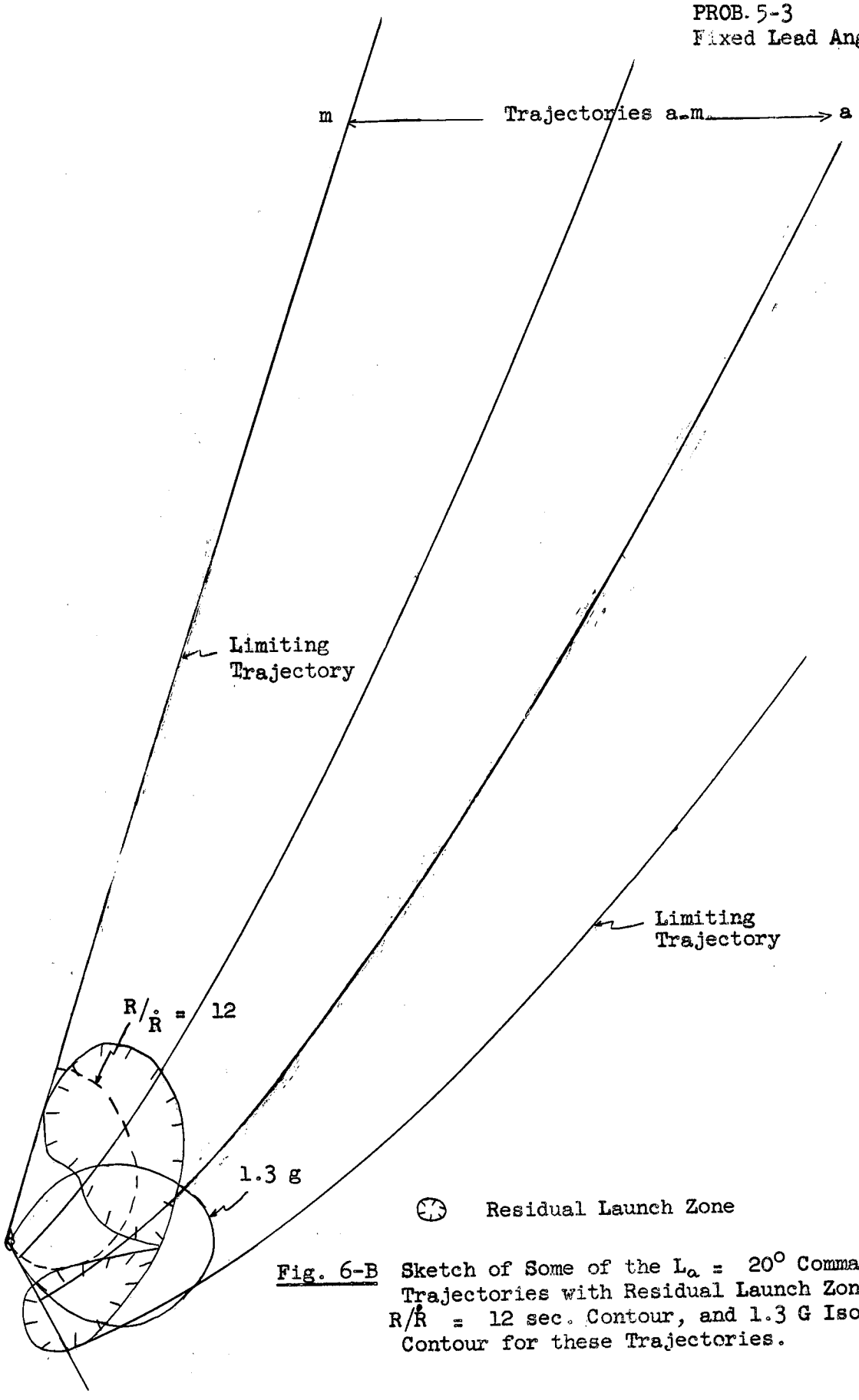

Fig. 6-B Sketch of Some of the $L_a = 20^\circ$ Command Trajectories with Residual Launch Zone, $R/\dot{R}$ = 12 sec. Contour, and 1.3 G Isogee Contour for these Trajectories.

Where A_o is the value of A at R = 240×10^3 ft. Some trajectories are shown in figure 6B.

Limiting trajectories were then determined, as limited by fighter g's, A.I. look angle and residual launch zone. The last limit implies that only trajectories entering the residual launch zone are of interest. All trajectories approaching from the left default on this count.

To examine the effects of fighter g limitations, set at 1.3 g for power limited flight, isogee contours were drawn from the equation (see annex III):-

$$R = \frac{6.62 \times 10^4}{g_H} \quad (0.342 - \sin A)$$

Where g_H is the number of horizontal g's. The 1.3 g contour is shown in figure 6B. It is seen that a number of the trajectories exceed this limit. As it turns out, however, most of these trajectories lie in a region which contributes very little to the overall probability. For the region that does make an accountable contribution, the 1.3 g limit occurs within the residual launch zone and deceleration effects occur for only very short lengths of time. On the basis of these facts, any deceleration due to exceeding the 1.3 g limits was ignored. Also, for a few of the trajectories, the fighter is called upon to exceed the "elevator" manoeuvre limit which is about 3.15 g for a Mach 1.5 fighter at 50,000 ft. Again, it turns out that the trajectories affected make very little contribution to the probability. Furthermore, the 3.15 g limit is exceeded for only short periods of time near the end of the trajectories. Consequently no account was taken of the 3.15 g limit.

The fighter attempts to make its look angle 20^o. Hence, if its initial look angle is within the look angle limit there are no subsequent look angle barriers. Banking and pitching of the aircraft, etc., could not be taken into account but these are unlikely to introduce A.I. look angle barriers.

The limiting trajectories are shown in figure 6B. Only those command trajectories in the region between the limiting trajectories meet the missile launch range and heading requirements somewhere in the residual launch zone. For each of these trajectories, a probability, P_t, can be defined. This is the probability that a fighter on this trajectory will measure $R/\dot{R}$ accurately enough to fire inside the residual launch zone. It depends on the values of $\frac{R}{\dot{R}}$ along this trajectory that lie within the residual launch zone. The calculated values for 13 trajectories, designated a to m, are listed in table 2. The validity of remarks made above about the negligible contribution to overall probability by trajectories which exceed the g limits becomes apparent from these results.

It is proposed, then, that commencing with some initial course difference and lead angle, the fighter turns continuously with 1.3 g until it gets on to some command trajectory upon which it completes its interception. In relative target coordinates, the equation of the fighter path during the constant 1.3 g manoeuvre is (see annex IV):-

TABLE 2 - CALCULATED VALUES OF P_t FOR R.M.S.

ERRORS IN $R/_{\dot{R}}$ OF 20% AND 60%

PROBLEM 5.3

FIXED LEAD ANGLE COURSE

R.M.S. ERROR	20%	60%
Traj.		
a	0	0
b	.0119	.0224
c	.1550	.1010
d	.6138	.2666
e	.8107	.3565
f	.9124	.4309
g	.9325	.4590
h	.9337	.4670
i	.9144	.4480
j	.8809	.4203
k	.8091	.3981
l	.5226	.2844
m	0	0

PROB. 5-3
Fixed Lead Angle Course

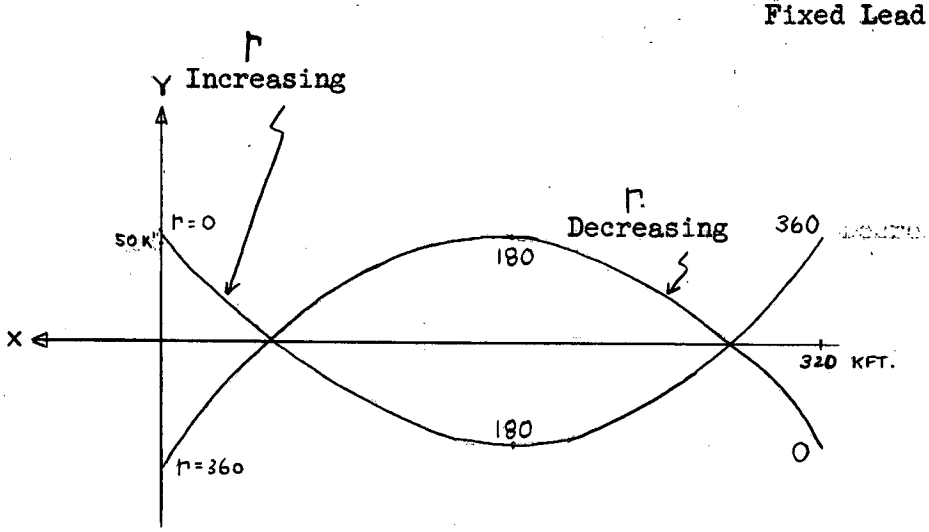

Fig. 7-B Trochoidal Path of Fighter on Constant 1.3 G. Turn.

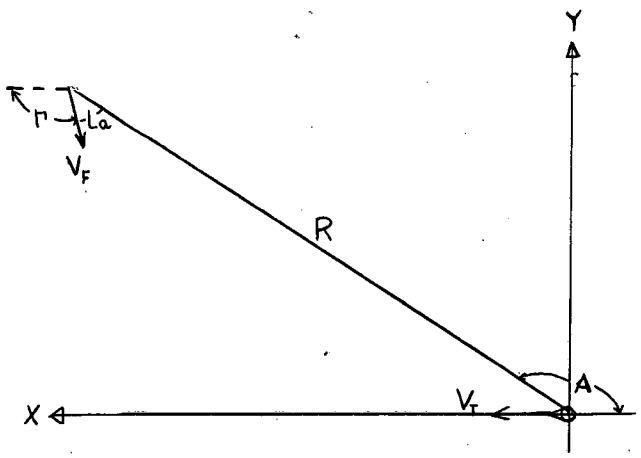

Fig. 10-B Diagram Showing Fighter Relative to Target.

$$-x = V_T t - \frac{V_F}{k} \cdot \sin(\Gamma_o + kt)$$

$$y = \frac{V_F}{k} \cdot \cos(\Gamma_o + kt)$$

Where k is the rate of turn of the fighter in space. These are the parametric equations of a trochoid, which is shown in figure 7B with course differences marked.

For any command trajectory, the point in space may be found from which a fighter with some initial course difference and turning with continuous 1.3 g will manoeuvre onto this trajectory. This is done by placing the trochoid with its axes properly orientated and with the course difference on the curve coinciding with the course difference on the command trajectory. (On a command trajectory, the course difference may easily be calculated from Γ = A-20). Then, by moving along the trochoid to the initial course difference desired, the point in space is found. For each command trajectory, a series of such points can be found and a curve drawn. This curve intersects the A.I. range contours to give the initial points of runs eventually manoeuvring on to this command trajectory from these A.I. range contours. For these points, there is a particular value of P_t, namely the P_t of the command trajectory to which the fighter manoeuvres.

By repeating this procedure for several trajectories, the variation of P_t along each A.I. range contour was determined and a curve of P_t vs. distance from G.C.I. "ideal" approach line was drawn for each contour. Two A.I. ranges, namely .85 S and 1.28S, were considered for various initial course differences. The "ideal" approach line was fixed assuming that G.C.I. placement is for a stick length of 7,000 feet. 7,000 feet was used to coincide with the value used in the 3D study with non-jamming conditions. It is actually quite arbitrary since in its determination, and in the determination of the corresponding "ideal" approach line, it is assumed that V_m is constant and that the missile flies in a straight line. In practice, this is not true. Also, small changes in stick length and "ideal" approach line have very little effect on probability. Therefore 7,000 feet was used although this figure was derived in the 3D study for t_f = 8 seconds and ΔV_m = 875 feet/second, and not ΔV_m = 970 feet/second as in our case.

From the curve of P_t against distance from G.C.I. "ideal" approach line, values of P_{L_i} can be determined. Values of P_{P_i} can be determined by integrating sections of G.C.I. placement probability curve. Hence the overall success probability, P, can be found by the rule given in sect. 3.1, above. A summary of the results for G.C.I. σ's of 1.5, 4.75 and 9 n.m. are given in table 3, and the accompanying graphs are shown in figure 8B and 9B.

TABLE 3 - OVERALL PROBABILITIES IN %

PROBLEM 5.3

FIXED LEAD ANGLE COURSE

$R/\dot{R}$ rms. Errors		20%			60%		
Γ_o	R	1.5 nm	4.75 nm	9 nm	1.5 nm	4.75 nm	9 nm
90	.85 S	9	28	25	5	13	12
	1.28 S	0.08	10	19	0.05	5	10
110	.85 S	84	56	34	38	26	16
	1.28 S	70	54	37	29	24	18
120	.85 S	91	60	36	45	29	17
	1.28 S	89	66	42	45	34	21
135	.85 S	73	52	34	32	23	15
	1.28 S	86	58	40	34	26	19
160	.85 S	0.09	14	19	.03	7	9
	1.28 S	0	5	16	0	2	8

PROB. 5-3
Fixed Lead Angle Course

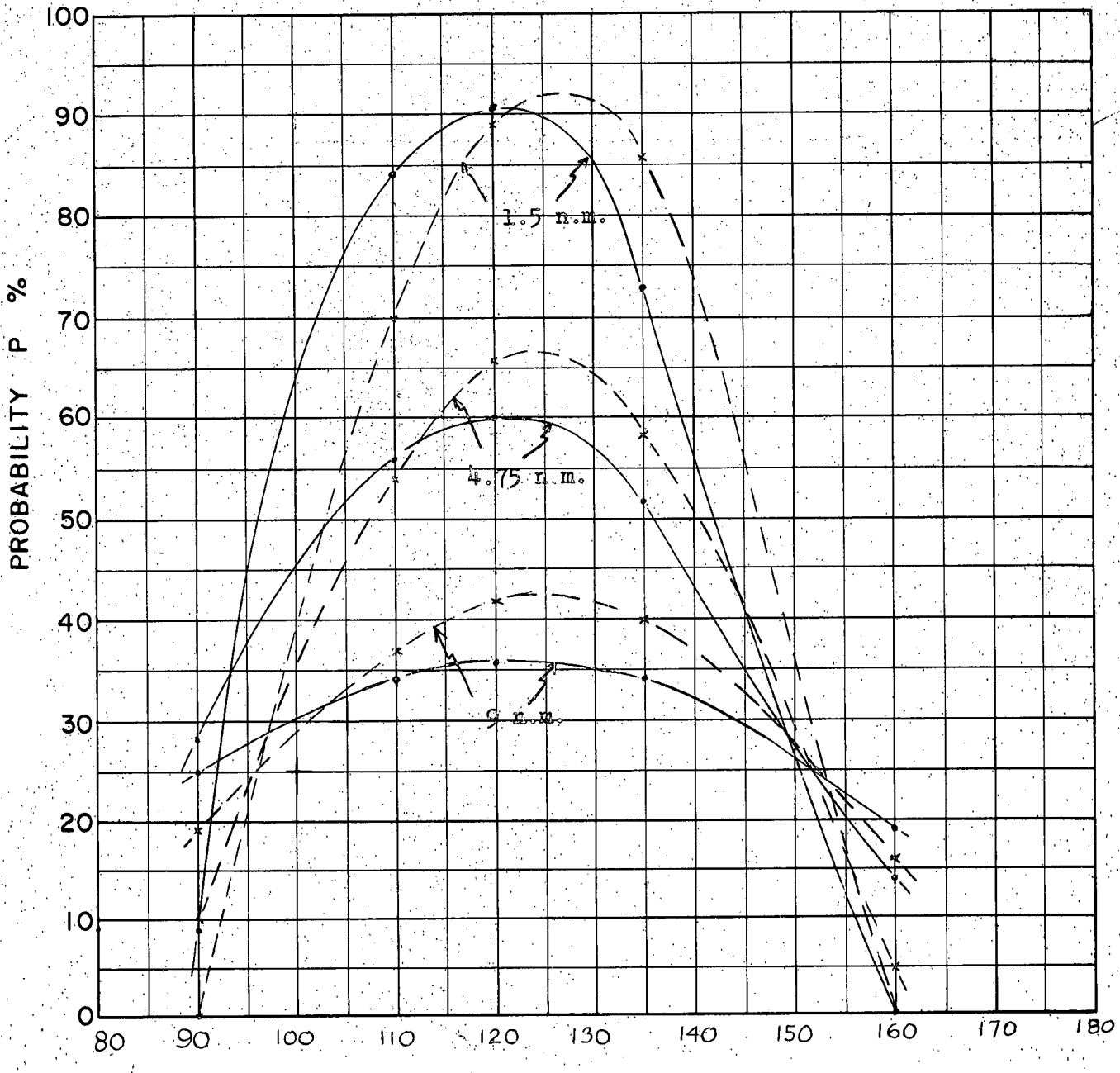

COURSE DIFFERENCE: Abscissa
TARGET EVASION: 0
TARGET MACH NO.: 1.5
INTERCEPTOR LATERAL G's: 1.3 G
INTERCEPTOR MACH NO.: 1.5
σ OF G.C.I. ACCURACY: 1.5, 4.75, 9 n.m.
A.I. DETECTION RANGE AS FRACTION OF SPECIFICATION RANGE, S: .85, 1.28
A.I. DETECTION RANGE CONTOUR: Delta
ALTITUDE: 50,000 feet

Fig. 8B Curves of Probability vs Initial Course Difference for R.M.S. Error in $(R/\dot{R})$ = 20%

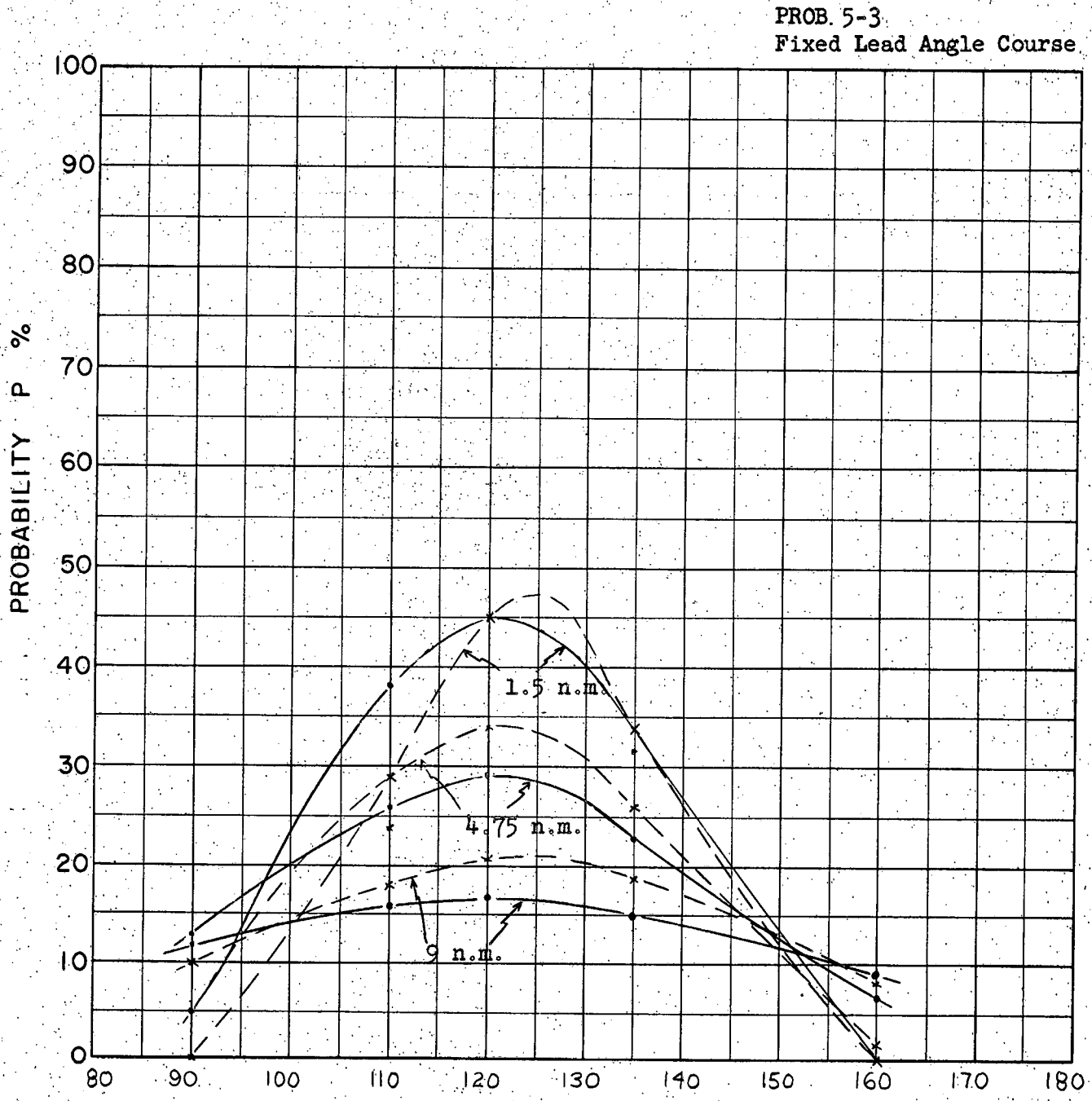

COURSE DIFFERENCE: Abscissa
TARGET EVASION: 0
TARGET MACH NO.: 1.5
INTERCEPTOR LATERAL G's: 1.3 G
INTERCEPTOR MACH NO.: 1.5
σ OF G.C.I. ACCURACY: 1.5, 4.75, 9 n.m.
A.I. DETECTION RANGE AS FRACTION OF SPECIFICATION RANGE, S: 8.5, 1.28
A.I. DETECTION RANGE CONTOUR: Delta
ALTITUDE: 50,000 feet

Fig. 9B Curves of Probability vs Initial Course Difference for R.M.S. Error in $(R/\dot{R})$ = 60%

From these results, the following conclusions can be drawn:

(1) With no target evasion, there seems to be a reasonable probability of success, especially for an rms. error in $\frac{R}{\dot{R}}$ of 20%. Increasing the error to 60% reduces the probabilities $\frac{R}{\dot{R}}$ by about a factor of two. Probabilities up to 92% were obtained where the error is 20%, and only up to about 46% where the error is 60%.

(2) Increasing R_o from .85 S to 1.28 S seems to shift the probability curves to greater Γ_o's, giving slightly greater peaks. From an R_o of .85 S to 1.28 S, the peak shifts from about 120° to 125°.

(3) Increasing σ reduces probability in general, but broadens the probability curves so that at higher and lower Γ_o's, the probability is increased. This is not an important effect since by this time the probabilities are already quite low.

5.4 Zero Lead Course (Pure Pursuit)

This mode is presently being investigated by paper and pencil methods but no results are available. $\frac{R}{\dot{R}}$ = 10 was chosen for firing.

5.5 Fixed Line of Sight Rate Course

Because of the difficulty in solving the applicable equations, this work was done on the REAC. (see section 4.5).

5.6 True Collision Course

Because this involved very little modification to the REAC circuit of section 4.5, the work was done on the REAC. (see section 4.6).

6.0 REFERENCES

1. CARDE Technical Letter 1012/57 "Other Range-Finding Methods" F.W. Slingerland, p. 85.

2. CARDE Technical Letter N-47-16, pp. 123-153.

ANNEX I

Derivation of Equation For Constant $\frac{R}{\dot{R}}$ Contours. $L_a = 20^\circ$ Mode.
From figure 10B:

$$\dot{R} = V_T \cos A - V_F \cos L_a$$

$$\frac{R}{\dot{R}} = \frac{R}{V_T \cos A - V_F \cos L_a}$$

Whence $$R = \frac{R}{\dot{R}} \times 1.46 \times 10^3 \quad (\cos A - 0.940)$$

This is the equation of a cardioid.

ANNEX II

Derivation of Equation for $L_a = 20^\circ$ Command Trajectories
From figure 10B:

$$\dot{R} = V_T \cos A - V_F \cos L_a \qquad (1)$$

$$R\dot{A} = -V_T \sin A + V_F \sin L_a \qquad (2)$$

(1) and (2) must be solved simultaneously with

$$L_a = \text{a constant} \qquad (3)$$

Divide (1) by (2)

$$\frac{\dot{R}}{R} = \dot{A} \cdot \left[\frac{V_T \cos A - V_F \cos L_a}{-V_T \sin A + V_F \sin L_a} \right]$$

$$V_T \sin A \neq V_F \sin L_a$$

Let $$\frac{V_T}{V_F} = C, \quad \cos L_a = D, \quad \sin L_a = B$$

Then $$\frac{\dot{R}}{R} = \dot{A} \left[\frac{C \cos A - D}{-C \sin A + B} \right]$$

Integrating between $R_o \leq R \leq R, \qquad A_o \leq A \leq A$

Where A_o, R_o are initial aspect and range respectively.

Then $$\int_{R_o}^{R} \frac{dR}{R} = \int_{A_o}^{A} \left[\frac{C \cos A - D}{-C \sin A + B} \right] dA$$

This finally works out to be

$$R = R_o \left[\frac{\cos^2 \left[\frac{L_a + A_o}{2} \right]}{\cos^2 \left[\frac{L_a + A}{2} \right]} \right]$$

Setting $R_o = 240 \times 10^3$ ft. and $L_a = 20^o$

$$R = 240 \times 10^3 \left[\frac{\cos^2 \left[\frac{20 + A_o}{2} \right]}{\cos^2 \left[\frac{20 + A}{2} \right]} \right]$$

The line $A = 20^o$ is a line of "stability", all trajectories ending on this line.

ANNEX III

Derivation of Equation for Isogee Contours. $L_a = 20^o$ Mode.

With no target evasion, g_H the number of lateral g's pulled by the fighter, is

$$g_H = \frac{V_F \ (\dot{A} - \dot{L}_a)}{32.2}$$

But $\dot{L}_a = 0$ $\quad \therefore \ g_H = \frac{V_F \ \dot{A}}{32.2}$

From equation (2) in Annex II,

$$\dot{A} = \frac{V_F \sin L_a - V_T \sin A}{R}$$

$$\therefore \ g_H = V_F \left[\frac{V_F \sin L_a - V_T \sin A}{32.2 \quad R} \right]$$

or $$R = V_F \left[\frac{V_F \sin L_a - V_T \sin A}{32.2 \ g_H} \right]$$

Simplifying $R = \frac{6.62 \times 10^4}{\ddot{g}_H} (0.342 - \sin A)$

ANNEX IV

Derivation of Equation for Fighter Path during Constant 1.3 g Manoeuvre. From figure 10B:

$$-\dot{x} = V_T - V_F \cos \Gamma \quad (1)$$

$$\dot{y} = V_F \sin \Gamma \quad (2)$$

Where $\Gamma = \Gamma_o + kt$

and $k = \dot{\Gamma}$, the fighter rate of turn in space.

Integrating (1) and (2), the following result is obtained

$$-x = V_T t - \frac{V_F}{k} \sin (\Gamma_o + kt)$$

$$y = \frac{V_F}{k} \cos (\Gamma_o + kt)$$

These are the parametric equations of a trochoid.

Appendix "C"

"Homing with Jammed-AI"

by

D. P. Flemming

1 In the "Minimum Information Study" of method of using the residual information from a range-jammed AI to home to a successful launch position the following courses were suggested:

(i) Fixed R and T course

(ii) Fixed lead course

(iii) Zero lead course (Pure pursuit)

(iv) True collision

(v) Fixed line of sight rate.

2 Specific tasks dealing with launch ranging were the following:

(a) For each of the above courses (where applicable) choose a fixed range contour, an isogee contour and a $R/\dot{R}$ contour which best fit within the launch zones so that the missile's launch range and heading requirements can be met.

(b) For each course, estimate accuracy with which these values of $R/\dot{R}$ and g's can be determined by power and W measurements and by accelerometer measurements, respectively. For the g measurements consideration should be given to the noise on the command trajectory, since this will result in g noise. Construct error probability contours about R, isogee and $R/\dot{R}$ contour of (a). (For True Collision Course substitute Manoeuvre Ranging for Isogee Ranging).

(c) For Fixed R and T course and Fixed Lead course repeat (b) for clockwise and counterclockwise horizontal evasion by the target at .5g lateral.

(d) By superposition of these error contours on the residual launch zone determine the probability of launching at a range suitable to the missile.

3 This Appendix presents an outline of the work concerned with two of the study aspects outlined above. These problems are as follows:

(1) Accuracy of $R/\dot{R}$ measurements as stated in (b) and (c) above, using $W/\dot{W}$ method as in CARDE Technical Letter No. 1012/57 Appendix "G".

(2) $R/\dot{R}$ contours, as outlined in (a) using a fixed R and T course.

The parameters used are seen in Figure 0-C, where

V_T = target speed = 1500 ft/sec.

V_F = fighter speed = 1500 ft/sec.

R = instantaneous range (feet)

ψ = aspect angle measured from nose of target.

θ = fighter lead angle (neglecting angle of attack)

ω = anticlockwise angular velocity of line of sight

A_T = target normal acceleration - positive when target evading away from fighter.

When the target evades, A_T will always be either $+\frac{1}{2}g$. or $-\frac{1}{2}g$.

4 ACCURACY OF $\dot{R}/R$ MEASUREMENTS

These measurements are limited by noise and by the possibility of target evasion. Only target evasion is considered here. From kinematics:

$$-\dot{R} = V_F \cos\theta + V_T \cos\psi \qquad (1)$$

$$W = \frac{V_F \sin\theta - V_T \sin\psi}{R} \qquad (2)$$

For uniform target and fighter* motion,

$$\frac{2\dot{W}}{W} + \frac{\dot{R}}{R} = 0 \qquad (3)$$

and one can attempt to measure $-\frac{R}{\dot{R}}$ by the equation

$$-\frac{R}{\dot{R}} = \frac{2W}{\dot{W}} \qquad (4)$$

* It is assumed that the fighter flies uniformly while the measurement is being made.

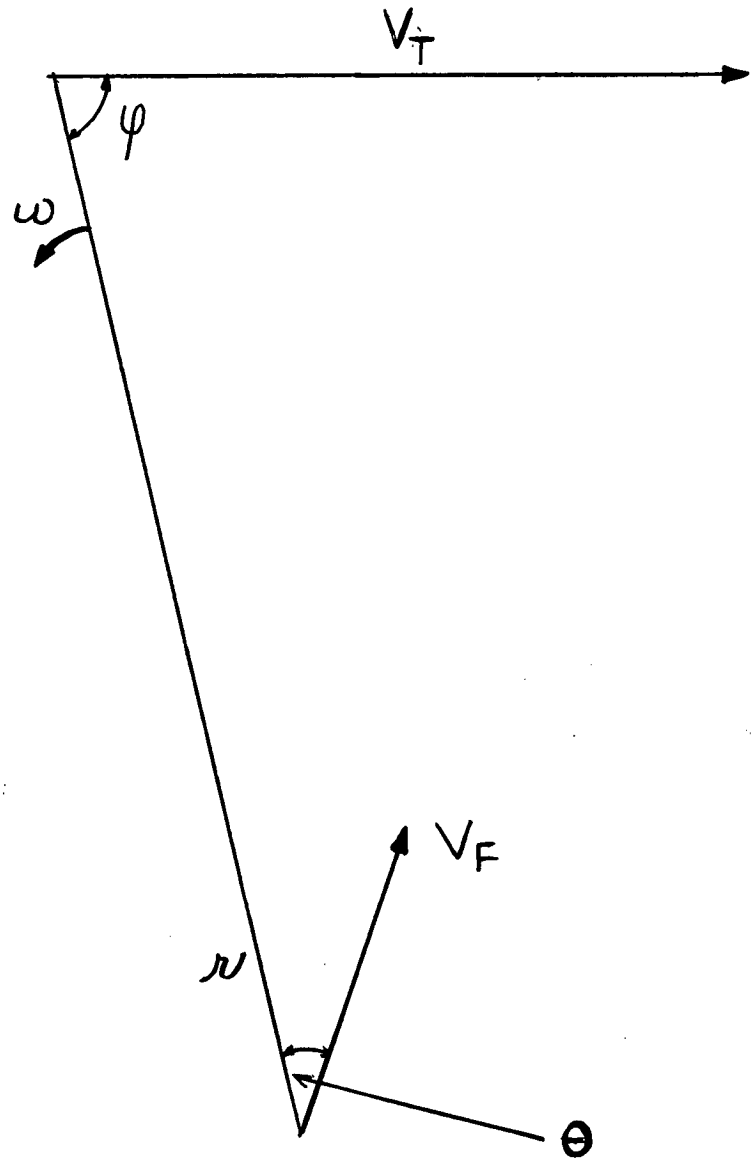

Figure O-C

With target evasion, however, (3) becomes

$$\frac{2W}{W} + \frac{R}{R} = \frac{-A_T \cos\psi}{R W} \qquad (5)$$

Thus the relative error obtained, in using (4) is equal to

$$\text{"P"} = \frac{\frac{2W}{W} - \left(-\frac{R}{R}\right)}{\left(-\frac{R}{R}\right)} \qquad \frac{-\left(\frac{2W}{W} + \frac{R}{R}\right)}{\frac{R}{R}} \qquad (6)$$

From (5) and (6),

$$P = \frac{A_T \cos\psi}{R W} \qquad (7)$$

Differentiating (2), using the fact that $\dot{\theta} = W$, since the fighter is not turning,

$$\dot{W} = \frac{R\left\{V_F \cos\theta\,(W) - V_T \cos\psi\left(\frac{A_T}{W_T} - W\right)\right\}}{R^2} - \frac{\dot{R}\left\{V_F \sin\theta - V_T \sin\psi\right\}}{R^2}$$

and making use of (1) and (2) this equation can be written

$$R\dot{W} = -2\dot{R}W - A_T \cos\psi \qquad (8)$$

Thus (7) becomes

$$P = -\frac{A_T \cos\psi}{A_T \cos\psi + 2\dot{R}W} \qquad (9)$$

Therefore given ψ, θ and R, P can be calculated from (9), using (1) and (2) to evaluate $\dot{R}$ and W.

For the parameters chosen we obtain

$$P = \frac{-A_T \cos \psi}{A_T \cos \psi - \frac{2(1500)^2}{R} (\cos \theta + \cos \psi)(\sin \theta - \sin \psi)} \quad (10)$$

where

$$A_T = \pm \quad 16.1 \text{ ft/(sec)}^2$$

Equation (10) can also be written in the form

$$P = \frac{-A_T \cos \psi}{A_T \cos \psi - \frac{2(1500)^2}{R} \left[1 + \cos(\theta + \psi)\right] \sin(\theta - \psi)} \quad (11)$$

"P" (in percent) is plotted against θ in Figures 1C to 6C for $\psi = 0^\circ$, 30°, 60°, 120°, 150°, and 180° respectively. On each graph three values of R, and both positive and negative evasion, are incorporated. P was not plotted for $\psi = 90^\circ$ because P vanishes identically at this aspect.

The graphs are not extremely accurate because P was only computed for 10° increments in θ, and as may be seen from the graphs, the function is badly behaved at some points.

While the error P gets very large under some conditions, as may be seen from the graphs, nevertheless for ψ between 30° and 120°, the pure pursuit heading ($\theta = 0$) is perhaps tolerable, since the errors shown are all 50% or less.

5 R/$\dot{R}$ CONTOURS

The fighter navigation equation is assumed to be

$$\sin \theta = -KW \quad (12)$$

as was outlined in the original work statement, and K is assumed to be 35 sec.

From (2) and (12)

$$-\frac{R \sin \theta}{K} - V_F \sin \theta = -V_T \sin \psi \quad (13)$$

so that

$$\sin \theta = \frac{V_T \sin \psi}{V_F + \frac{R}{K}} \quad (14)$$

In order to compute $R/\dot{R}$, as a function of R and Ψ, we first compute Θ from (14) (Θ is always acute) and then use the formula

$$-\frac{R}{\dot{R}} = \frac{R}{V_F \cos \Theta + V_T \cos \chi} \qquad (15)$$

One can then plot equation (15) and then graphically find the values of R and φ for which $(-R/\dot{R})$ is equal to a particular value, and draw $R/\dot{R}$ contours in the (R, φ) plane. Four such contours are shown in Figure 7C.

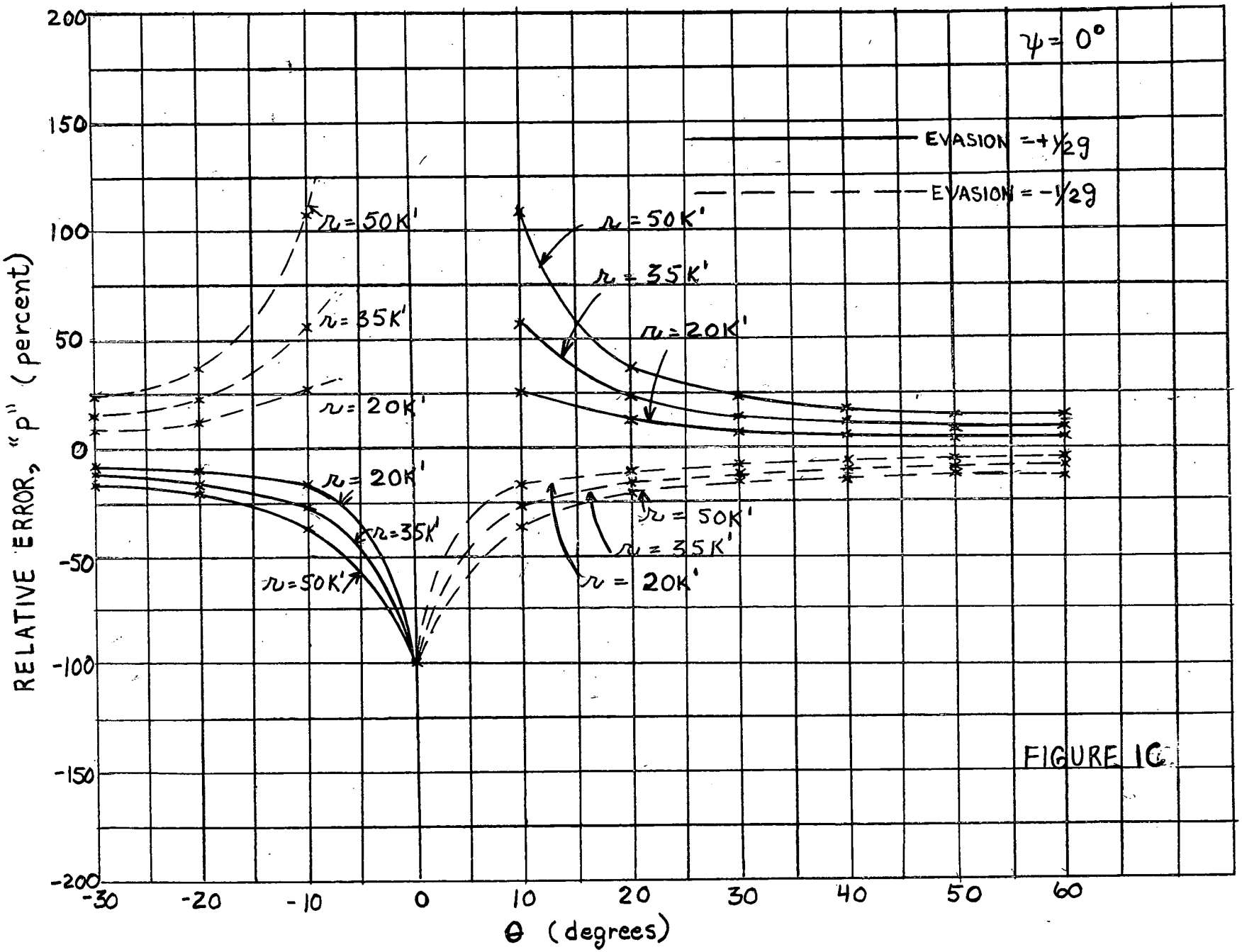
ψ = 0°
EVASION = +½g
EVASION = -½g
r = 50K'
r = 35K'
r = 20K'
r = 50K'
r = 35K'
r = 20K'
r = 20K'
r = 35K'
r = 50K'
r = 50K'
r = 35K'
r = 20K'
RELATIVE ERROR, "p" (percent)
θ (degrees)
200
150
100
50
0
-50
-100
-150
-200
-30
-20
-10
0
10
20
30
40
50
60

FIGURE 10

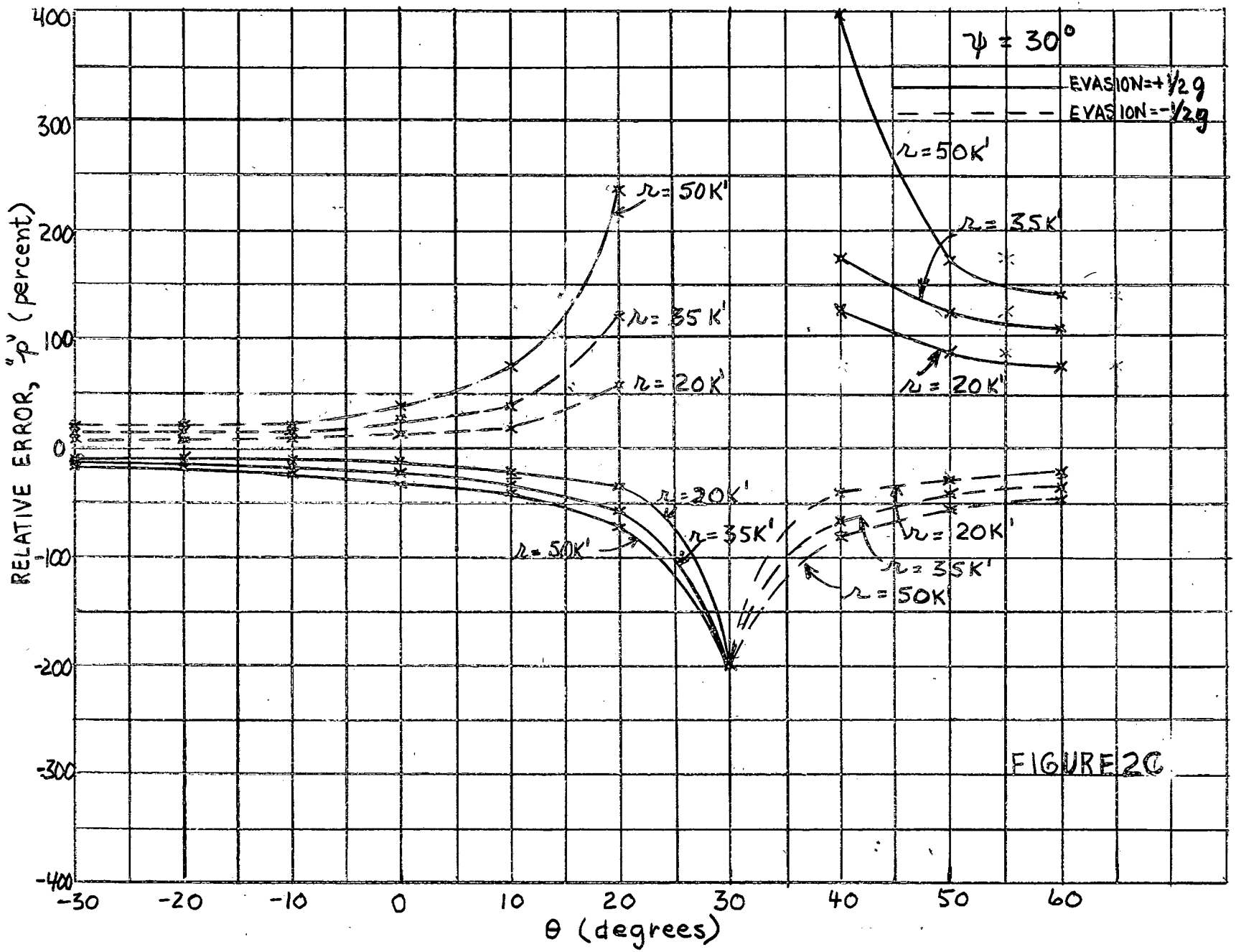
ψ = 30°
EVASION=+½g
EVASION=-½g
r=50K'
r=35K'
r=20K'
r=20K'
r=35K'
r=50K'
r=20K'
r=35K'
r=20K'
r=35K'
r=50K'
r=50K'
RELATIVE ERROR, "p" (percent)
θ (degrees)
400
300
200
100
0
-100
-200
-300
-400
-30
-20
-10
0
10
20
30
40
50
60

FIGURE 20

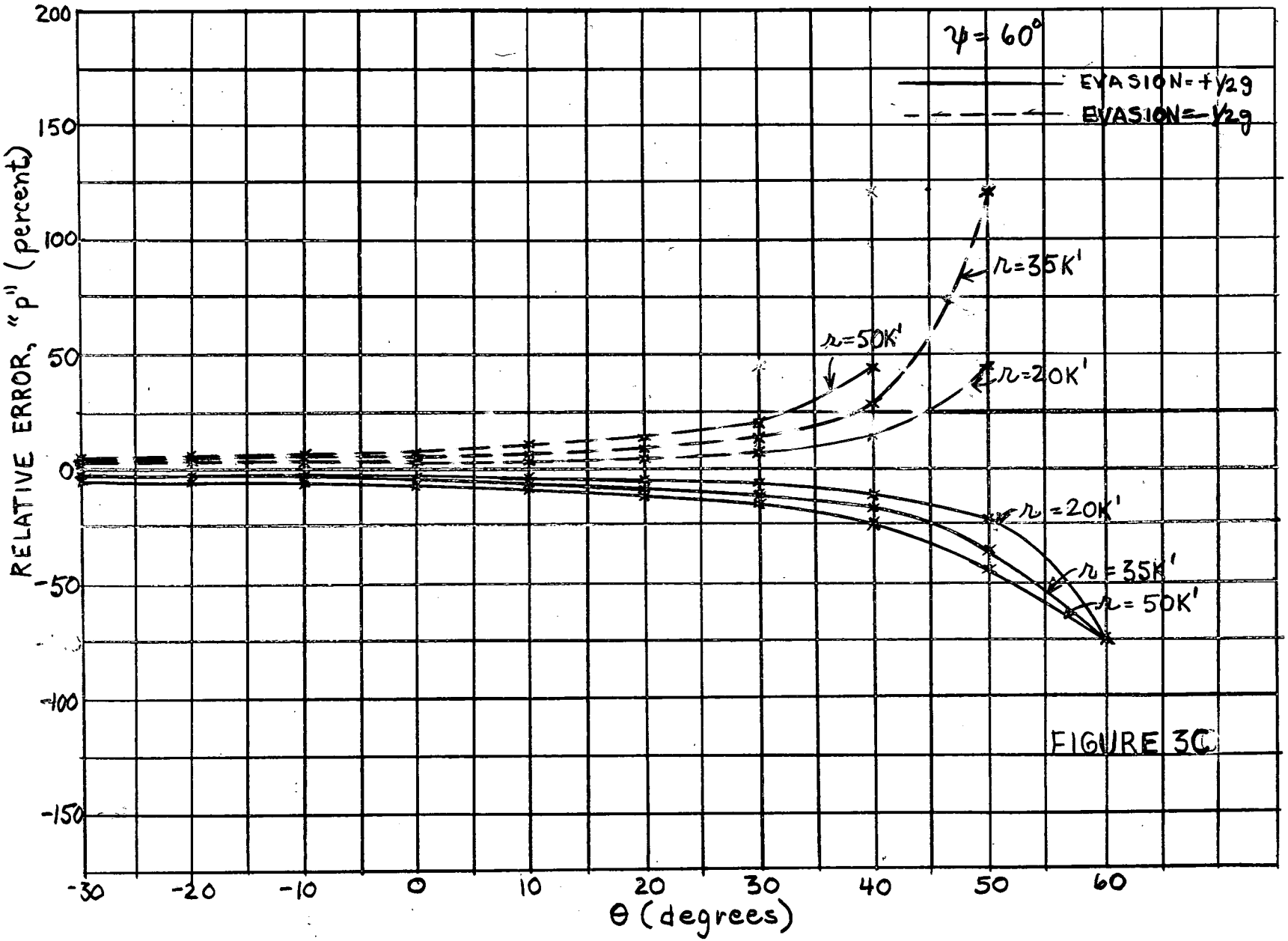
ψ = 60°
EVASION = +½g
EVASION = -½g
r = 35K'
r = 50K'
r = 20K'
r = 20K'
r = 35K'
r = 50K'
RELATIVE ERROR, "p" (percent)
200
150
100
50
0
-50
-100
-150
-30
-20
-10
0
10
20
30
40
50
60
θ (degrees)

FIGURE 3C

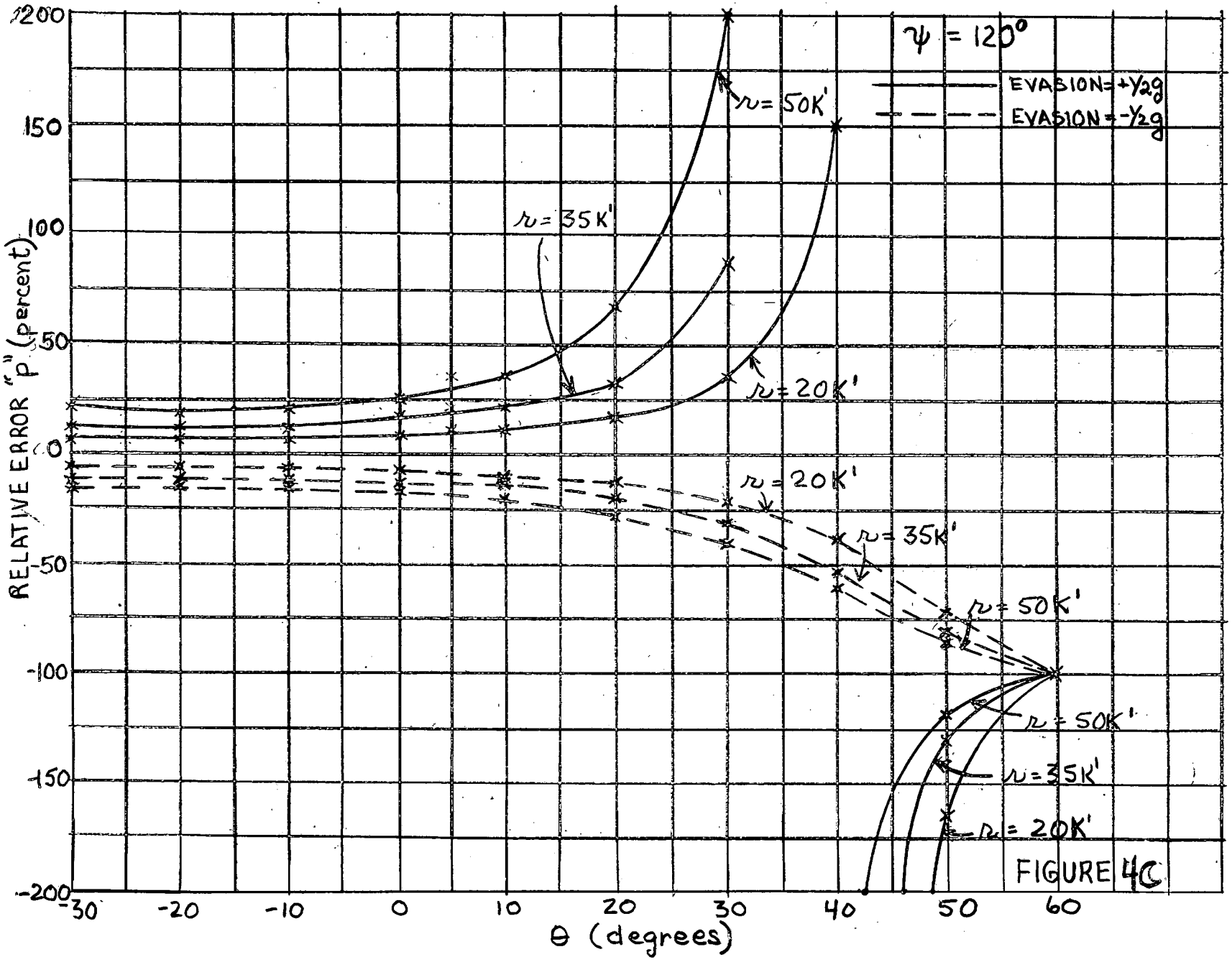
ψ = 120°
EVASION = +½g
EVASION = -½g
r = 50K'
r = 35K'
r = 20K'
r = 20K'
r = 35K'
r = 50K'
r = 50K'
r = 35K'
r = 20K'
RELATIVE ERROR "p" (percent)
θ (degrees)
200
150
100
50
0
-50
-100
-150
-200
-30
-20
-10
0
10
20
30
40
50
60

FIGURE 4C

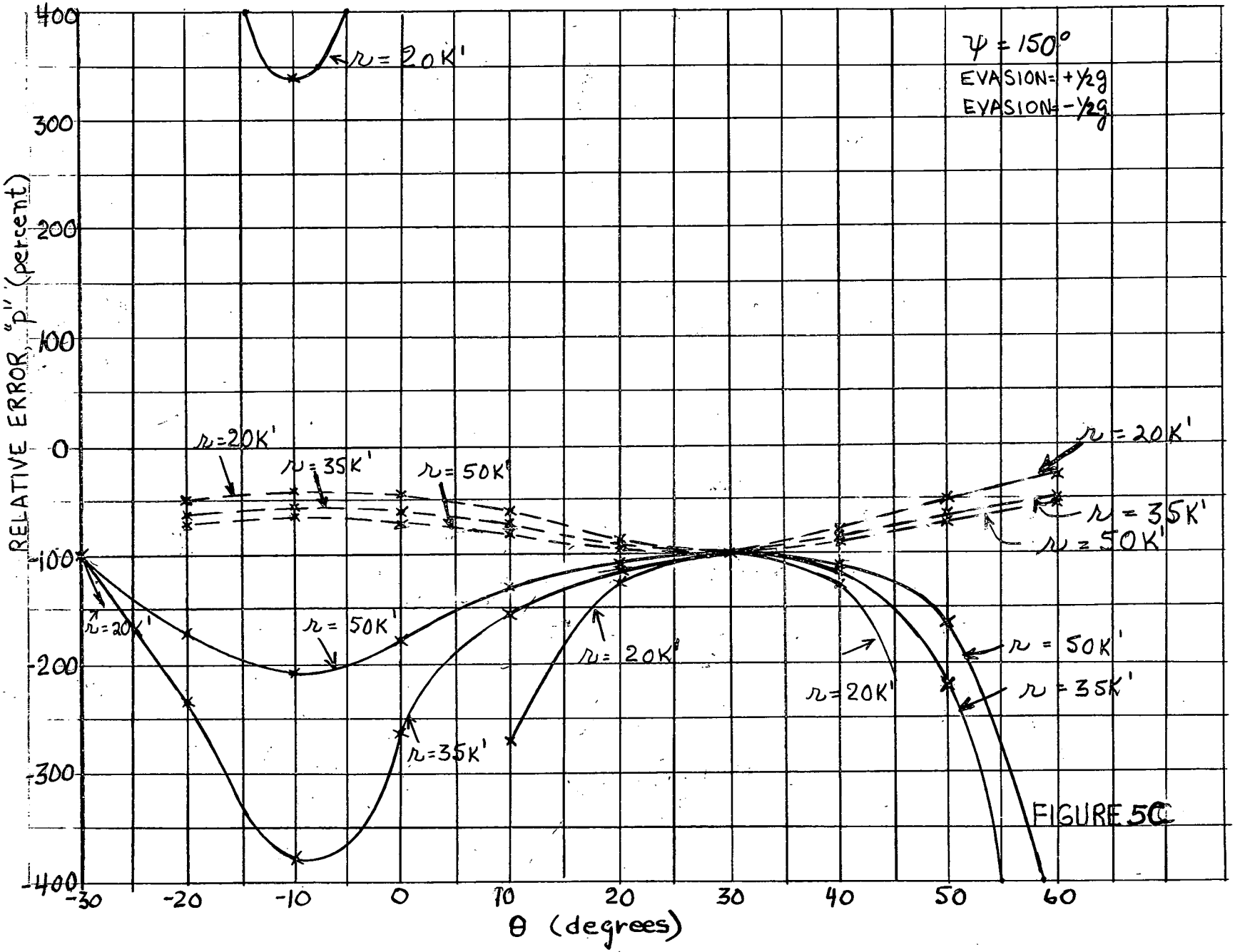
ψ = 150°
EVASION = +½g
EVASION = -½g
r = 20K'
r = 35K'
r = 50K'
RELATIVE ERROR, "p" (percent)
θ (degrees)
400
300
200
100
0
-100
-200
-300
-400
-30
-20
-10
0
10
20
30
40
50
60

FIGURE 5C

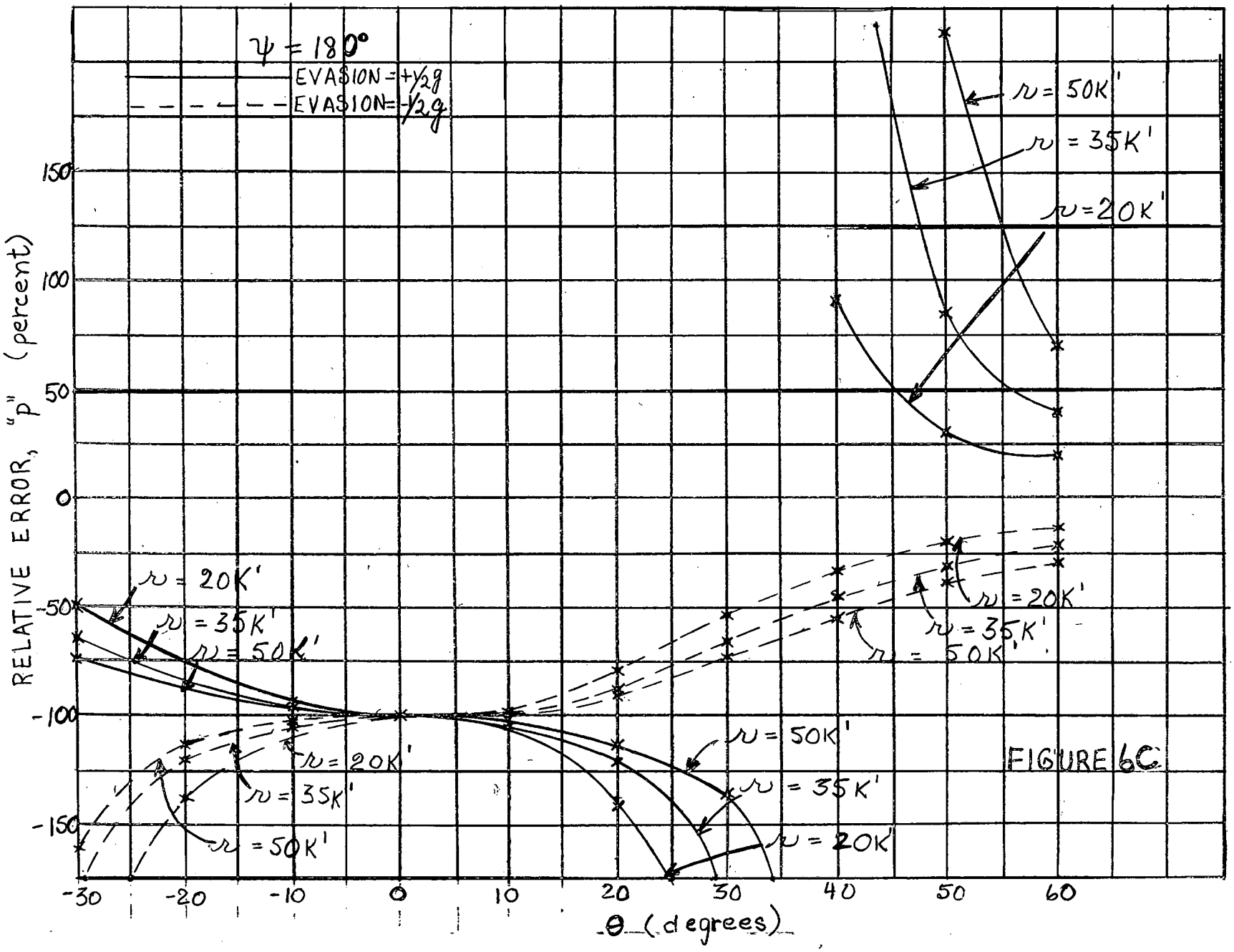
ψ = 180°
EVASION = +½g
EVASION = -½g
r = 50K'
r = 35K'
r = 20K'
r = 20K'
r = 35K'
r = 50K'
r = 20K'
r = 35K'
r = 50K'
r = 50K'
r = 35K'
r = 20K'
RELATIVE ERROR, "p" (percent)
150
100
50
0
-50
-100
-150
-30
-20
-10
0
10
20
30
40
50
60
θ (degrees)

FIGURE 6C

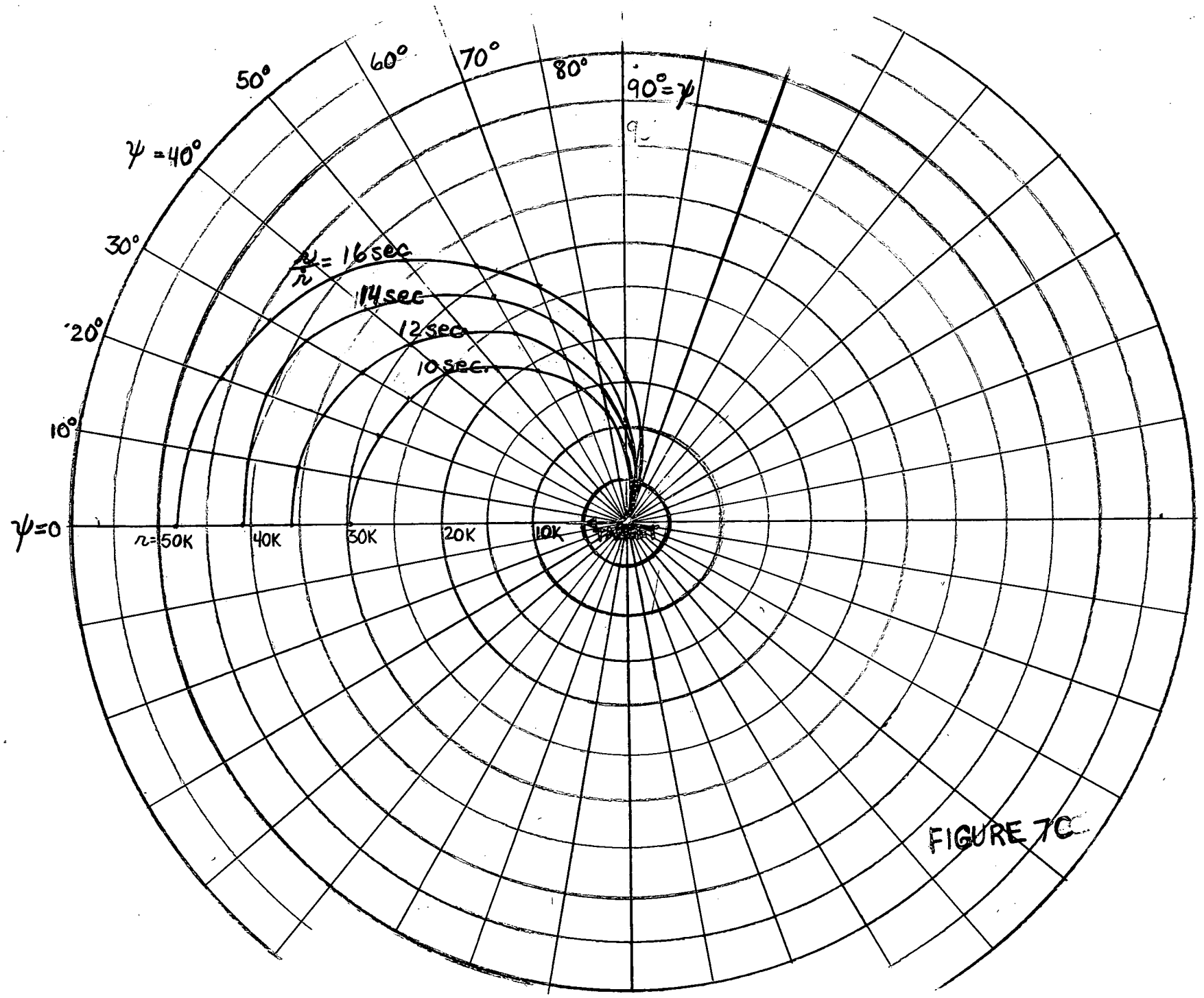
50°
60°
70°
80°
90°=ψ
ψ=40°
30°
20°
10°
ψ=0
r=50K
40K
30K
20K
10K
16sec
14sec
12sec
10sec

FIGURE 7C

Appendix "D"

Visit to The Douglas Aircraft Company

Missile Miss Distance Distributions

by C.J. Wilson

1 INTRODUCTION

CARDE asked the Douglas Aircraft Company, Santa Monica, if they could supply information from their Sparrow II simulation work which would assist in prediction of missile miss distance distributions. As a result of this request a CARDE representative was invited to make a visit and examine the available data.

C.J. Wilson visited Douglas for two weeks during September and also made one-day visits to Bendix Pacific Division, North Hollywood, and Bendix Research Laboratories, Detroit, during the same journey to the U.S. A complete report on these visits is being prepared and will be published separately as a CARDE Technical Letter.

2 DOUGLAS SIMULATOR STUDIES ON SPARROW II

A two-dimensional analogue computer simulation of the latest Sparrow II missile has been used; it is described in Douglas report SM-27331, "1242D Missile Simulation". Much of the work with this model has been carried out without introducing noise into the control system*; work with noise in the system is more recent and designed to indicate where adjustments should be made to the launch zones obtained from noise-free simulation. These adjustments take two forms

(i) adjustments to the missile's maximum range capability, based on oil consumption by the oscillating wings,

(ii) adjustments to the minimum range and to the launch heading tolerances at intermediate ranges due to unacceptable miss distributions.

* The launch zones published in CARDE Technical Letter N-47-16, pages 126-153, were obtained without noise, not, as stated on page 123 of that report, "by the usual Douglas statistical method with noise introduced in the simulation".

Douglas use the criterion that 10 out of 10 simulated runs must terminate with a separation of less than 15 feet between missile and target centres of gravity for the launch conditions to be acceptable. This corresponds to a centre of gravity to centre of gravity root mean square miss of about five feet and would, of course, produce very high kill probabilities indeed if it could be achieved in practice. It is felt that the two-dimensional simulation gives an optimistic picture of miss distances to be expected, in part because cross talk and aerodynamic cross-coupling effects are necessarily neglected. Furthermore, Douglas are not convinced that the noise characteristics used in their simulation are correct, they have been experimenting in an attempt to match flight test results more closely. However, the simulator can be used to define the launch zone boundaries, although kill from launches inside the boundary is not necessarily a certainty.

Douglas have used their simulator, with appropriate modifications to the circuit where necessary, to investigate snap-up attacks and the possibilities of Sparrow II in attacks against high altitude targets with a tracking seeker and proportional navigation. Launch zones are increased in size very significantly with this type of navigation.

3 MISSILE FLIGHT TESTS

It was concluded that the simulator results could not provide an accurate figure for miss distance distributions and kill probability, so attention was turned to the flight test results. Douglas report No. SM-27303 "Flight Test Report for the Sparrow II Missile through January 18th, 1957" summarizes results for almost all 1242-B and 1242-C missiles.

Analysis of the results of the tests gives a root mean square miss distance, centre of gravity to centre of gravity, of about 15 feet for attacks against an F6F target. Reliable missiles only have been considered in obtaining this figure. The F6F is a small aircraft (wing span 45 feet, length 33 feet) and root mean square miss distance will probably increase in proportion to target size; the U.S.S.R. "Bear" has a wing span of about 190 feet.

4 DOUGLAS' ESTIMATES OF HIT PROBABILITIES

The probability of a Sparrow II continuous rod warhead intersecting some part of the target's airframe has been determined from a digital computer programme. Some results of this work appear in Douglas Report SM-27182 "Sixth Quarterly Report", figures 22 and 23.

It has been assumed that a root mean square miss distance of 15 feet will be obtained and that the warhead effective radius will be 27 feet. Hit probabilities of the order of 0.8 are predicted for beam and tail attacks on a B47 with a guidance actuated fuse and of 0.85 in tail attacks and 0.95 in beam attacks with a V.T. fuse. There is no data for head-on attacks.

A 45 foot root mean square miss against the 116 foot wing span B47 seems more probable to the author. Unfortunately values of R.M.S. miss other than 15 feet have not been considered and it is difficult to predict how the above figures would be changed by increased miss distances, but probabilities appear to fall steeply for R.M.S. miss values above 15 feet. It is suggested that hit probabilities against a B47 with 27 foot lethal radius and 45 foot R.M.S. miss distance would be not greater than 0.5 from the tail or the beam, even with the V.T. fuse.

5 VISITS TO BENDIX

The two visits to Bendix were made to discuss noise in the Sparrow II system and the simulation of noise effects. Bendix make a more complete simulation of the missile seeker but the noise data used by both Douglas and Bendix is derived from two flight tests, numbered M181 and M195, during which wide-band telemetry was used to transmit discriminator outputs. It has not proved possible to separate the guidance signals from the noise at low frequencies and the assumption that the noise level down to zero frequency is the same as at higher frequencies is not completely backed up by observations.

APPENDIX "E"

FIRE CONTROL STUDIES - A.I. PHASE NAVIGATION

by

J.A. Ockenden

1. INTRODUCTION

It is proposed that the A.I. radar in the Astra I System be operated in two navigational modes, lead collision for rockets and missiles, and lead pursuit for missiles only. Both modes have been investigated at R.C.A., and lead collision has been recommended as superior to lead pursuit in all the cases studied. It is felt at CARDE that some aspects of the problem have not been considered by R.C.A., and that there may exist a significant number of cases where lead collision steering is not satisfactory.

As a result of the R.C.A. comparison study, it is claimed that (1) interception times are longer in lead pursuit, (2) lead pursuit is more likely to put the interceptor into the target tail zone, where it will fall back if it has a speed disadvantage, and (3) the lateral acceleration demand is usually higher in lead pursuit. In addition, (4) the claim that lead collision, which prescribes a particular firing instant, is inefficient for missiles is refuted, since the missile may be fired at times other than the ideal firing instant, because of its heading tolerance. CARDE is in general agreement with these claims, but it appears that cases of computer instability in the lead collision mode have not received attention at R.C.A.

Lead collision instability has been considered in some detail, and a REAC study is proposed to investigate alternate forms of navigation which do not suffer from the same disadvantages. It is regretted that the REAC program has not yet permitted the study of this problem, so that quantitative results cannot be included in this Appendix.

2. WEAKNESSES OF LEAD COLLISION

It is recognized that the lead collision steering computer will fail if the range rate becomes positive (i.e. interceptor to target range increasing). Positive range rate leads to a negative time-to-go value, and only positive values are computed, so that the steering signals become incorrect and instability may result. In most cases, this situation represents an unsuccessful attack, although the interceptor may be capable of accelerating to regain a negative range rate. However, in general, where a positive range rate occurs, other limits are exceeded first, so that the problem may be approached from a different point of view.

If the interceptor is slower than the target, there exist speed ratio barriers, which are lead collision courses (in target coordinates) behind which there is no solution to the lead collision equations. In the vicinity of and behind these lines, steering instability will cause excessive look angles and a positive range rate.

The steering computer (considering the two-dimensional case) evaluates $\Delta\theta$, the angle to turn through to get onto course, from

$$\Delta\theta = \frac{M}{F + V_F T}$$

where $M = R\,\omega T + F \sin\theta$, the miss distance perpendicular to the present line of sight. A more accurate expression is:

$$\Delta\theta' = \frac{-\dot{R}}{V_F - V_T \cos\Gamma} \times \frac{M}{F + V_F T}$$

where Γ is the course difference*. The omission of the first term is not normally serious. However, at the speed ratio barrier, the denominator will become negative while $-\dot{R}$ remains positive, so that the simpler equation tells the interceptor to turn the wrong way. Since $V_F = V_T \cos\Gamma$ when the interceptor is heading perpendicular to the speed ratio barrier (on course on the speed ratio barrier), the first term of $\Delta\theta'$ is large when near this condition, so that the magnitude of $\Delta\theta$ is much smaller than that of $\Delta\theta'$.

Computation of $\Delta\theta'$ in the steering computer instead of $\Delta\theta$ would not be beneficial except in a few cases. With the excepted interceptor-target speed combinations, whenever the speed ratio barrier is passed, the antenna look angle limit also is exceeded. Hence a better approach to the situation would be to switch to another form of navigation whenever the antenna look angle exceeds some arbitrary value near its limit.

3. PROPOSED REAC STUDY

A brief two-dimensional study program is suggested, to investigate the effect on placement probability of various forms of navigation in specific cases. Of particular interest is the effect on the fall-back and look angle barriers behind the ideal approach line.

The following navigational modes are suggested for consideration:

(1) Lead collision.
(2) Lead pursuit.
(3) Lead collision, switching to lead pursuit when the antenna look angle is within 5° of its limit.
** (4) Lead collision, switching to fixed lead steering when the antenna look angle is within 5° of its limit, and back to lead collision when the look angle tends to reduce again. (See footnote)
(5) Lead collision, with the interceptor flying power limited, instead of maximum rate turns.

* See derivation at end of memo

** Cases 4 and 5 were studied and discussed in Appendix K in Technical Letter N-47-18.

If the target speed is equal to or greater than the maximum interceptor speed, a significant difference between the various forms of navigation is unlikely, since the interceptor cannot catch the target once the speed ratio barrier has been crossed. Thus an interesting case to study would be target speed Mach 1.5 and initial interceptor speed Mach 2.0. If the initial vectoring error is large, the corrective turn will decelerate the interceptor to a speed slower than the target, so that kinematic instability is likely, but the interceptor can regain its speed advantage by flying straight. Another important case would be initial interceptor speed Mach 1.5, with capability to Mach 2.0.

Beam attacks constitute the main interest, so that initial course differences of 135° and 110° are suggested. Only rear barriers need be determined, in which case the placement probability figures obtained will represent the rear contribution to the total probability. One altitude, 50,000 feet, should be sufficient. Since the engagement times are likely to be very long in some cases, a time limit of five minutes should be imposed. Attacks taking longer than this time should be considered failures.

If time permits, the study could be repeated with target evasion, for instance, a constant rate turn of 1.25g load factor.

It should be noted that the cases to be studied are chosen as being most likely to demonstrate the weaknesses of lead collision steering and the advantages of other systems. Hence the trends cannot be considered representative of the entire situation. For this reason, the improvement in placement probability would have to be very significant to justify any modifications to the existing steering mode.

Derivation of Two-Dimensional Lead Collision Steering Equation

Consider the interceptor, speed V_F, at a position relative to the target, speed V_T, defined by range, R , and aspect A. Let the lead angle, θ, differ from the correct lead angle for lead collision, by the small angle $\Delta\theta$, so that there is a miss distance, M.

Time to go until the component of miss along the direction of the present line of sight is zero is computed from:

$$T = \frac{R - F \cos \theta}{-\dot{R}}$$

at which time, the miss distance, perpendicular to the present line of sight, will be:

$$M = R \quad T + F \sin \theta$$

where $R\omega = V_F \sin \theta - V_T \sin A$

and $\dot{R} = V_T \cos A - V_F \cos \theta$

Differentiating the time equation with respect to θ:

$$\frac{dT}{d\theta} = \frac{-\dot{R} F \sin \theta + (R - F \cos \theta) \; V_F \sin \theta}{\dot{R}^2}$$

$$= \frac{(F + V_F \; T) \sin \theta}{-\dot{R}}$$

and differentiating the miss equation with respect to θ:

$$\frac{dM}{d\theta} = R \omega \frac{dT}{d\theta} + V_F \; T \cos \theta + F \cos \theta$$

$$= \frac{F + V_F \; T}{-\dot{R}} (V_F \sin^2 \theta - V_T \sin A \sin \theta - V_T \cos A \cos \theta + V_F \cos^2 \theta)$$

$$= \frac{F + V_F \; T}{-\dot{R}} (V_F - V_T \cos \Gamma)$$

since $\Gamma = A - \theta$ (the course difference).

The angle to turn through, $\Delta\theta$, to reduce M to zero, is given by:

$$\Delta\theta = \frac{d\theta}{dM} \times M$$

$$= \frac{-\dot{R}}{V_F - V_T \cos\Gamma} \cdot \frac{R\omega T + F \sin\theta}{F + V_F T}$$

APPENDIX "F"

Dispersions of Sparrow II Missile Launched from CF-105

by

H. R. Warren.

Description based on discussions with S.F.Kwiatkowski and Geo. Haynes at Avro, Oct. 10, 1957. Information should not be regarded as final, but subject to change.

1 METHODS

Because of various technical difficulties, it was impossible for Avro to use wind-tunnel results directly in the calculation of the dispersion to be expected during the launching of the Sparrow II missile from the CF-105. In their place, a semi-theoretical method is currently in use based on the following assumptions.

a) Flow Field is based on two dimensional incompressible potential flow representation of cross flow around a rectangular fuselage.
b) Resultant angles of attack on the missile produce forces acting on the missile CG based on current non-linear lift data for Sparrow II.
c) No flow curvature or aircraft yaw are assumed.
d) Dispersions only in the pitch plane have been calculated.
e) Launcher rails are assumed to be rigid.
f) Acceleration during boost is 18g.
g) Gravity effects are included.

The actual calculation of missile position and heading as a function of time is carried out using a digital computer. Where comparison was possible between results so obtained and those from wind-tunnel tests, good agreement was obtained.

2 GEOMETRY

Missile numbering

1 Forward Inboard
2 Forward Outboard
3 Aft Inboard
4 Aft Outboard

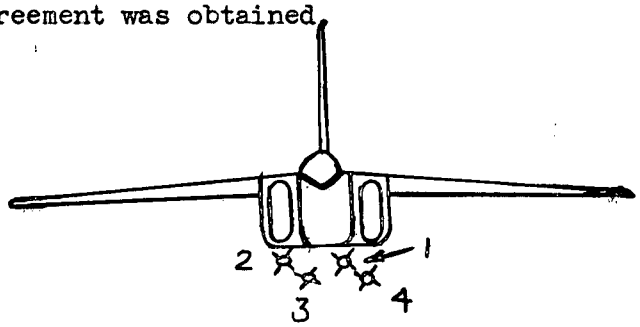

Launch rails are positioned at zero yaw, with an incidence

3° down relative to the wing and allow 5 feet of travel from "pin shear" to "both feet off".

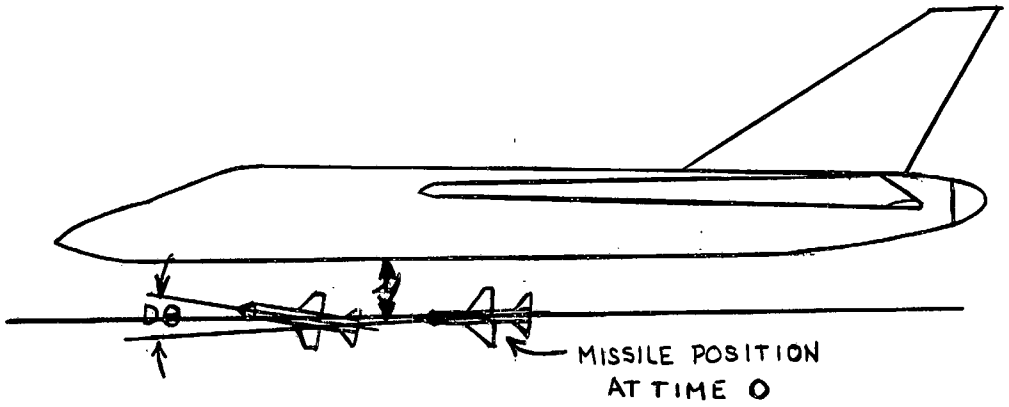

DΘ is the angle between the missile axis during the flight and its direction when still on the launch rails, positive for missile nose up. Y is the distance of missile CG below the lower surface of the fuselage.

3 RESULTS

The study includes the calculation of DΘ and Y during the first 0.25 seconds of free flight for all four missiles, over the following range of conditions:

30,000 ft. altitude, Mach Nos. from 0.5 to 1.6, each at load factors = -1, +1, +2, and +4.

40,000 ft. altitude, Mach Nos. from 0.5 to 2.0, each at load factors = -1, +1, +2, and +4.

The following table gives a selection of values taken from the Avro results, all at a load factor of n = +1, i.e., for straight and level flight. The effect of load factor is indicated in Figure 1F. Note that in the table, time t = 0 is taken just as both hooks disengage from the launcher rails. It takes about 0.13 seconds for the missile to reach this point after pin shear, and it is at about 0.20 or 0.25 seconds after time 0 that the arming delay is finished, and the controls are engaged. Missiles 1 and 4 in most cases cover the widest variation of DΘ for each set of conditions.

n = +1 at 30,000 ft.

t sec.	M = 0.9 Dθ deg.	M = 0.9 Y ft.	M = 1.2 Dθ deg.	M = 1.2 Y ft.	M = 1.6 Dθ deg.	M = 1.6 Y ft.	
.05	-.026	2.204			.008	2.235	
.10	-.098	2.679			.037	2.801	
.15	-.210	3.335			.093	3.602	Missile
.20	-.354	4.174	-.385	4.384	.181	4.626	No. 1
.25	-.524	5.196	-.564	5.523	.301	5.864	
.05	-.015	3.196			.008	3.231	
.10	-.057	3.653			.035	3.789	
.15	-.120	4.279			.088	4.570	Missile
.20	-.196	5.074	-.309	5.296	.171	5.589	No. 4
.25	-.282	6.036	-.452	6.386	.285	6.809	

n = +1 at 40,000 ft.

t sec.	M = 0.9 Dθ deg.	M = 0.9 Y ft.	M = 1.2 Dθ deg.	M = 1.2 Y ft.	M = 1.6 Dθ deg.	M = 1.6 Y ft.	M = 2.0 Dθ deg.	M = 2.0 Y ft.	
.05	-.021	2.201			.007	2.232			
.10	-.079	2.668			.034	2.787			
.15	-.167	3.310			.083	3.568			Missile
.20	-.276	4.125	-.335	4.324	.160	4.565	1.636	4.731	No. 1
.25	-.398	5.112	-.486	5.422	.262	5.765	2.311	5.907	
.05	-.005	3.190			.006	3.224			
.10	-.016	3.629			.028	3.761			
.15	-.027	4.224			.071	4.515			Missile
.20	-.032	4.971	-.209	5.180	.136	5.475	1.613	4.718	No. 4
.25	-.023	5.886	-.299	6.196	.223	6.632	2.280	6.830	

4 FUTURE WORK

A program is presently in hand at Avro which is intended to

give dispersion in both pitch and yaw under the following assumptions.

a) Elastic launcher rails (will cause a negative increment in Dθ compared to figures above).
b) Effect of wing on flow field included.
c) Missile thrust misalignments included.
d) Flow curvature effects included.
e) Effect of ambient temperature on rocket thrust included.

It was estimated that results from this study, which will also be completed on the digital computer, would not be available within the next 3 months.

ANNEX I

The following figures 2F, 3F and 4F show the effect of missile lowering on the aircraft.

In figure 2F a steady state change of elevator trim is shown as a function of Mach No. and altitude. The average correction required is one degree of elevator up.

Figure 3F shows the resulting steady state normal acceleration for clean airframe which at design altitude are of the order of 0.1 g (negative).

The augmented airframe will experience a transient with amplitudes not exceeding approx. 20% of values shown on figure 3F since the disturbance has a form of ramp input of approximately one second duration.

Above data were obtained from wind tunnel tests of a somewhat different configuration and appropriate estimated corrections were introduced.

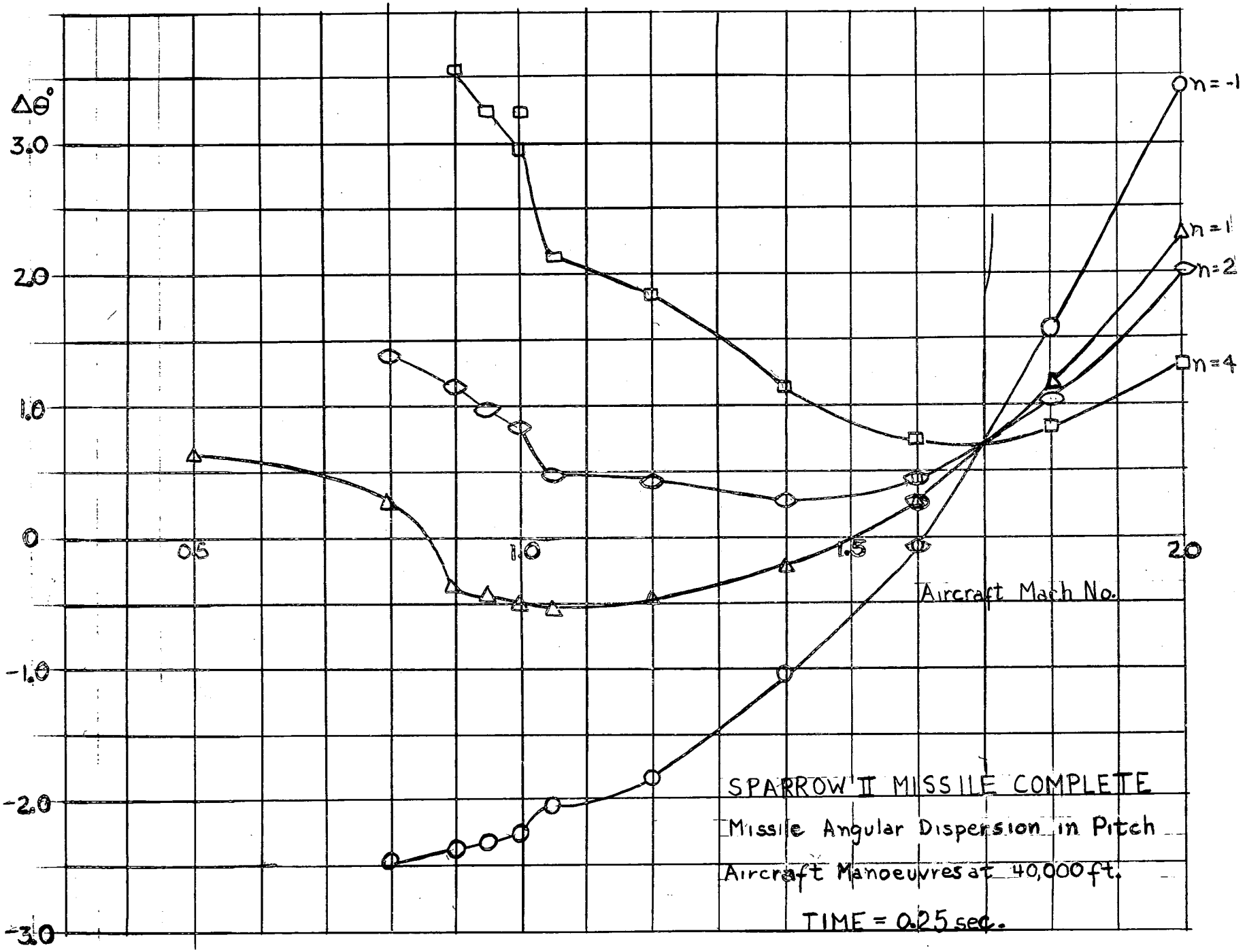
Δθ°
3.0
2.0
1.0
0
-1.0
-2.0
-3.0
0.5
1.0
1.5
2.0
Aircraft Mach No.
n = -1
n = 1
n = 2
n = 4
SPARROW II MISSILE COMPLETE
Missile Angular Dispersion in Pitch
Aircraft Manoeuvres at 40,000 ft.
TIME = 0.25 sec.

Figure 1F

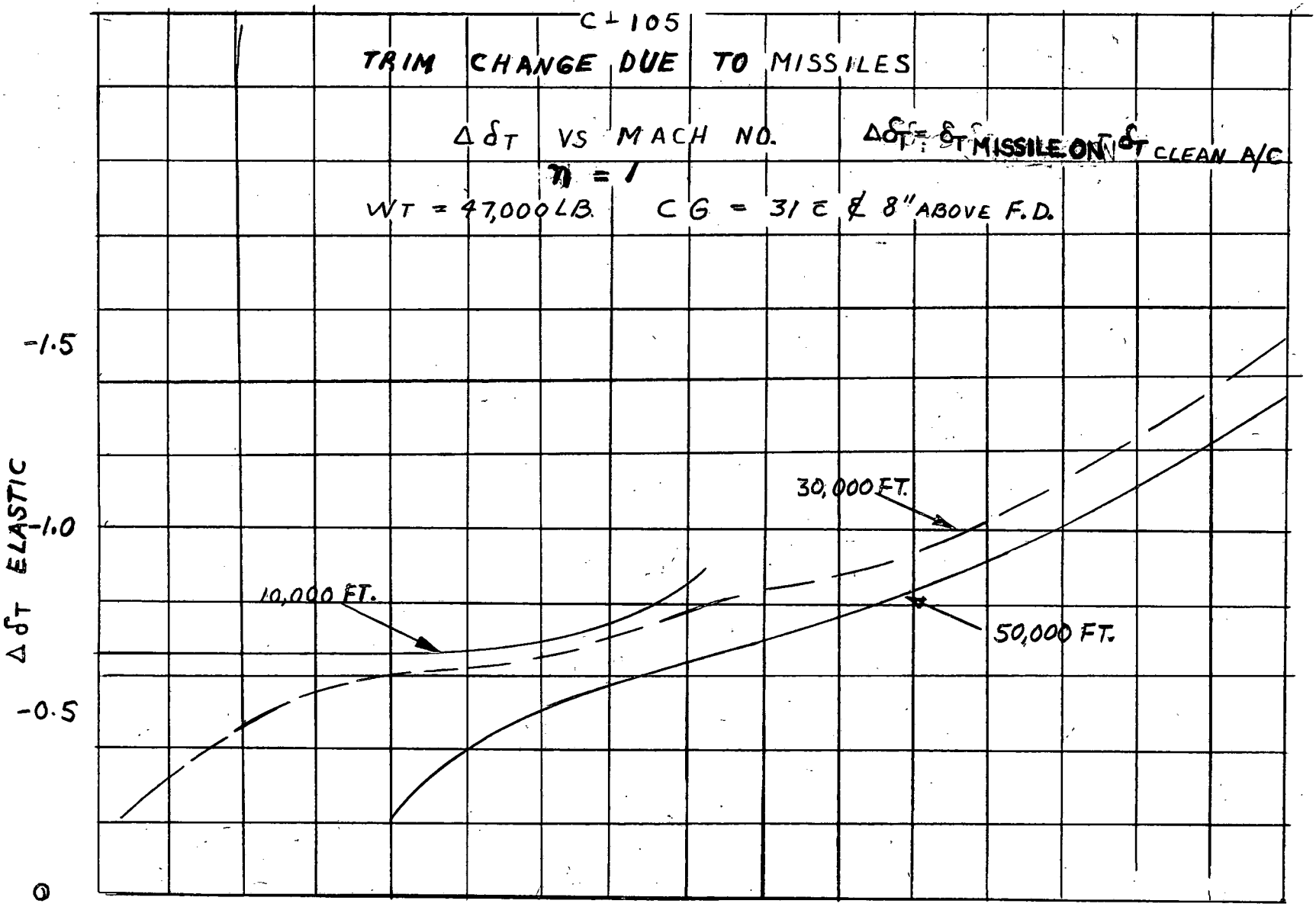
C-105
TRIM CHANGE DUE TO MISSILES
Δδ_T VS MACH NO.
Δδ_T = δ_T MISSILE ON − δ_T CLEAN A/C
n = 1
WT = 47,000 LB. CG = 31 C & 8" ABOVE F.D.
-1.5
-1.0
-0.5
0
Δδ_T ELASTIC
30,000 FT.
10,000 FT.
50,000 FT.

Figure 2F

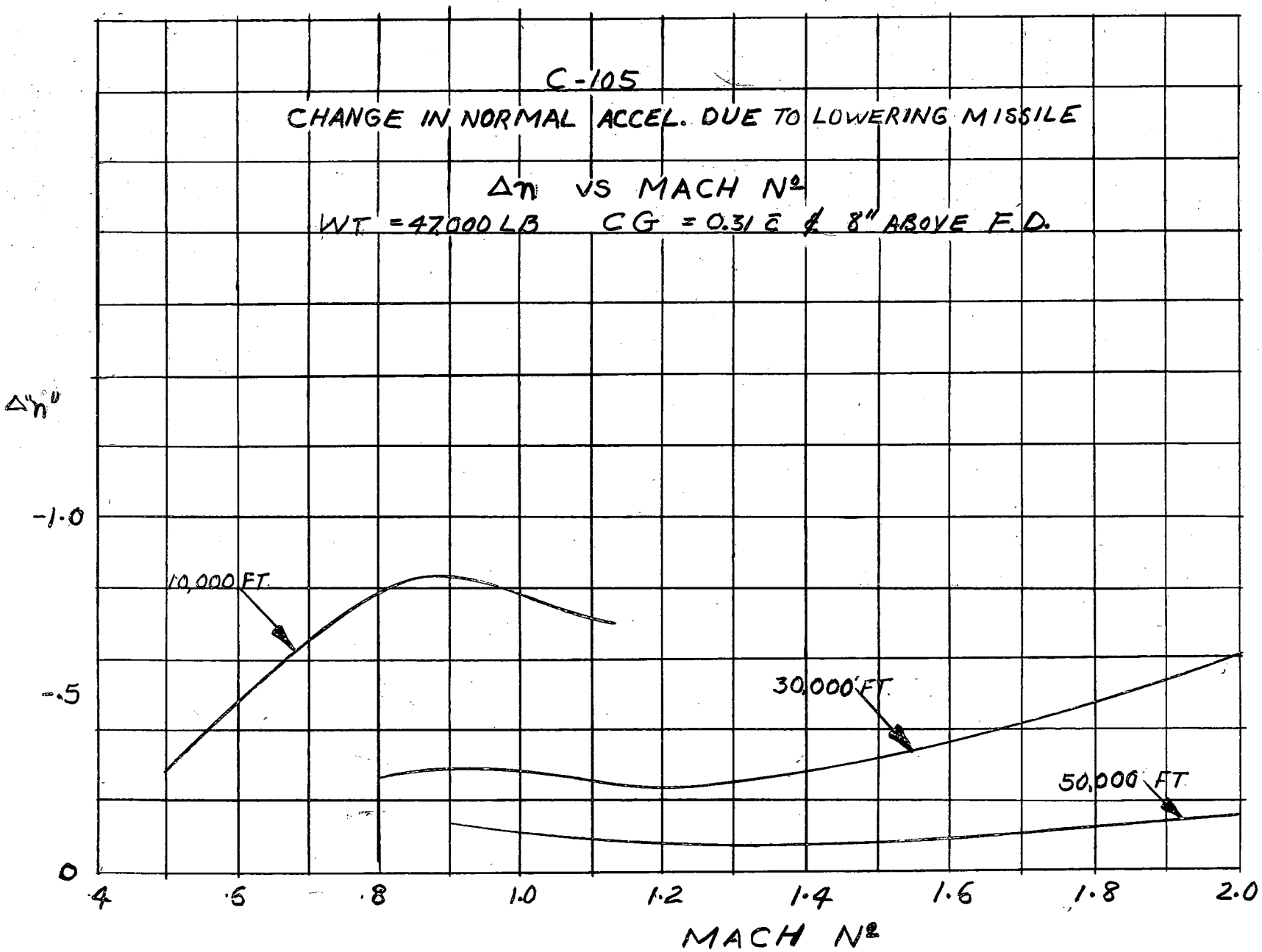
C-105
CHANGE IN NORMAL ACCEL. DUE TO LOWERING MISSILE
Δn VS MACH Nº
WT = 47,000 LB CG = 0.31 c̄ @ 8" ABOVE F.D.
Δ"n"
-1.0
-.5
0
10,000 FT.
30,000 FT.
50,000 FT.
.4
.5
.8
1.0
1.2
1.4
1.6
1.8
2.0
MACH Nº

Figure 3F

Appendix "G"

Detection Probabilities

by

R. S. Mitchell

1 Work in this assessment study to date has not taken into account the cumulative probability of detection in computing placement chance. The median value of acquisition range was considered equivalent to the range for 85% cumulative probability of detection. This concept was used in constructing detection contours, (see Technical Letter N-47-12).

2 It was thought desirable to make a comparison, even though rough, between the above procedure and one which considers cumulative probability. Information on the probability of detection of single scan versus range was obtained from an RCA Astra I progress report. Data given therein was for a $1M^2$ target. By using the values of reflection area given in Technical Letter N-47-12, the appropriate scaled curve was obtained by using the formula $r = K\sqrt[4]{\sigma}$. A complementary probability $q = 1-P_{ds}$ was obtained, where P_{ds} is the single scan detection probability. Signifying a particular point on this curve as q_i, a cumulative detection probability versus range was derived by using the formula $P_c = 1 - \prod q_i$. This summation was accomplished by a histogram approximation to the q curve. The 85% point on this P_c graph determined a range which corresponded to the specification detection range in former work. Having thus established a scale, a set of contours similar to the detection contours in Technical Letter N-47-12 were drawn which represented values of probability of not detecting the target on a single scan. Overlays with these contours were drawn and used on sample placement charts.

3 The specific cases investigated were:

(1) $M_t = 2.0$, $M_f = 2.0$, h = 60K, $\angle = 110^\circ$

(2) $M_t = 2.0$, $M_i = 1.5$, h = 40K, $\angle = 160^\circ$

The situation employing variable speed fighter with AVRO 2.2 aerodynamics was studied. On these charts a series of fighter approaches parallel to the ideal approach line were considered. On a given line, by using the formula $P_d = 1 - \prod q_i$, the cumulative probability of

detection was determined along the line up to the point where a placement barrier was reached. The values of P_d obtained with the various approach lines were weighted according to the normal distribution, and summed to obtain the total probability of successful placement. In using the normal distribution, a histogram approximation was again employed. This procedure would give a value of probability of placement for one specification range. To obtain results for a degraded AI set, or a set above specification, the contours on the overlay were scaled appropriately. For example, a .5 specification range would use 1/2 the range given on the cumulative probability curve for the 85% value. Whenever the approach line was near the ideal line, probability of placement was essentially 100%. As the line of approach departed from the ideal, this probability was gradually decreased to zero. A comparison of previous work is shown in Figure 16 . It will be seen that generally the results are somewhat better than were obtained using the median value. However, because of the various approximations made, no great significance should be attached to this point. The main object of the work was to establish that the two procedures would give approximately the same results.

Figure 1G

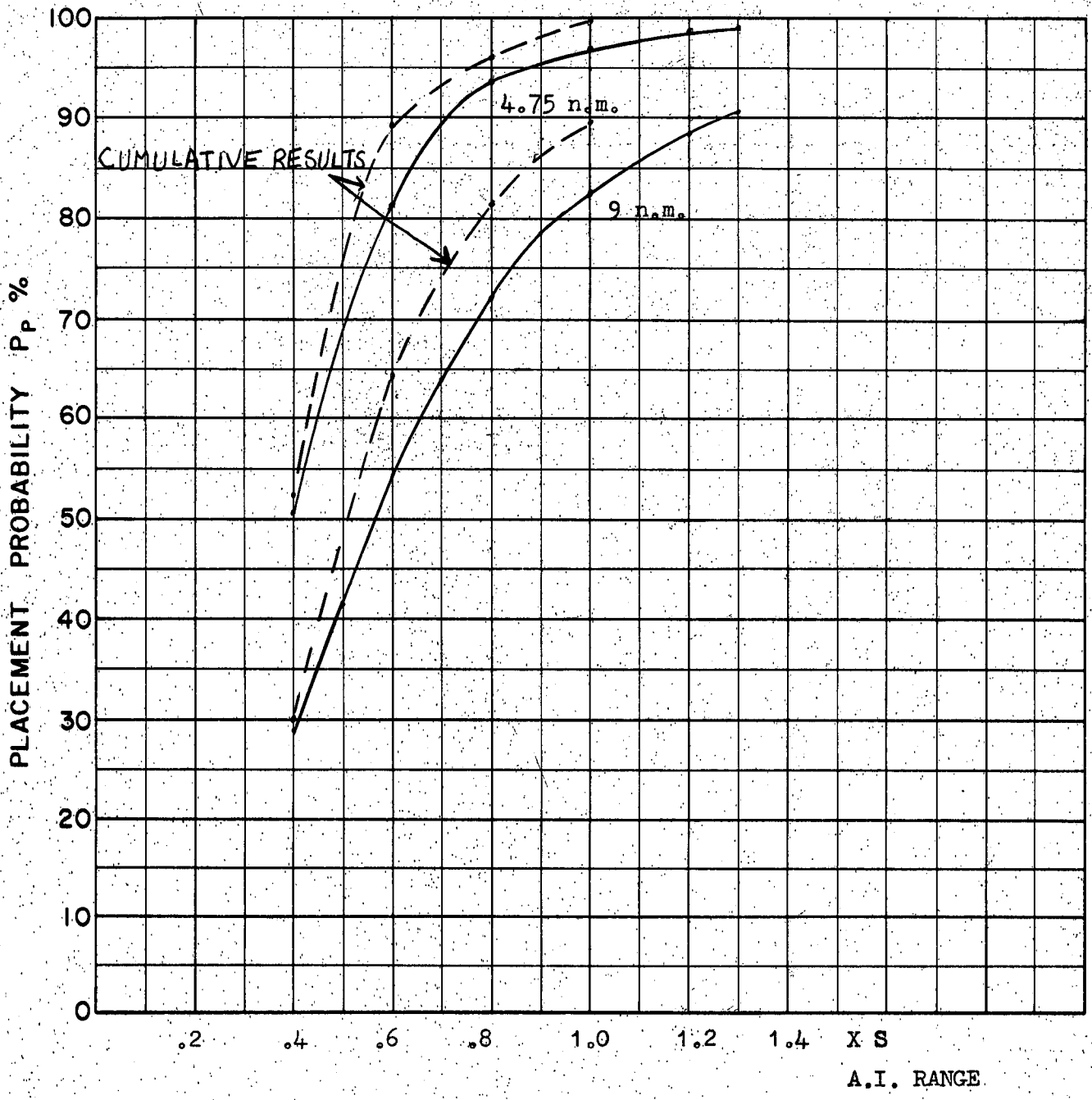

COURSE DIFFERENCE: 110°
TARGET EVASION: $2^{\circ}.0$
TARGET MACH NO.:
INTERCEPTOR LATERAL G's: Avro 2.2. Aerodynamics
INTERCEPTOR MACH NO.: 2.0 Initial
σ OF G.C.I. ACCURACY: 3 Values
A.I. DETECTION RANGE AS FRACTION OF SPECIFICATION RANGE, S: ABSCISSA
A.I. DETECTION RANGE CONTOUR: Delta
ALTITUDE: 60K

Appendix "H"

Investigation of CF-105 Interception to Determine Engagement Time and Aspect from Target at Missile Launch

by

F. Van Humbeck

1 Interest was expressed by DSE in the distribution of missile launching aspects with respect to the target and the time of interception for a typical case. To this end co-attitude attacks on a Mach 2.0 target at 50,000 feet were simulated on the REAC. The aerodynamic characteristics of the CF-105 interceptor (drag and lift as functions of Mach numbers) were simulated.* Attacks were started at Mach 2.0 and subject to a Mach number upper limit of 2.0.

2 Attacks from an initial course difference of 135° were studied, placement zone being drawn for a non-manoeuvring target (Fig. I-H) and also for target making conversion maneouvres to the right and to the left with 1.25 g load factors. (Figs. 2-H and 3-H respectively).

3 Contours of constant elapsed time between initiation of attack and missile launch and contours of constant aspect angle from the tail of the target at launch were then superimposed on the placement zones.

4 Lead-collision attacks were made with an F-pole of 7,000 feet. Missile time of flight was assumed to be 8 secs. Launch lead angle errors of up to 10° from optimum were allowed. For simplicity these characteristics were kept independent of aspect at launch and of actual interceptor velocity at the moment of launch.

5 It is planned to reduce these time and launch contours to a probability distribution.

* AVRO 3.3 characteristics were used; described by D.W. Pounder in a memorandum on File SN-47-3 dated Feb. 22, 1957; they correspond to an ability to manoeuvre at 1.63 g's, power limited, at Mach 1.5 at 50,000 feet.

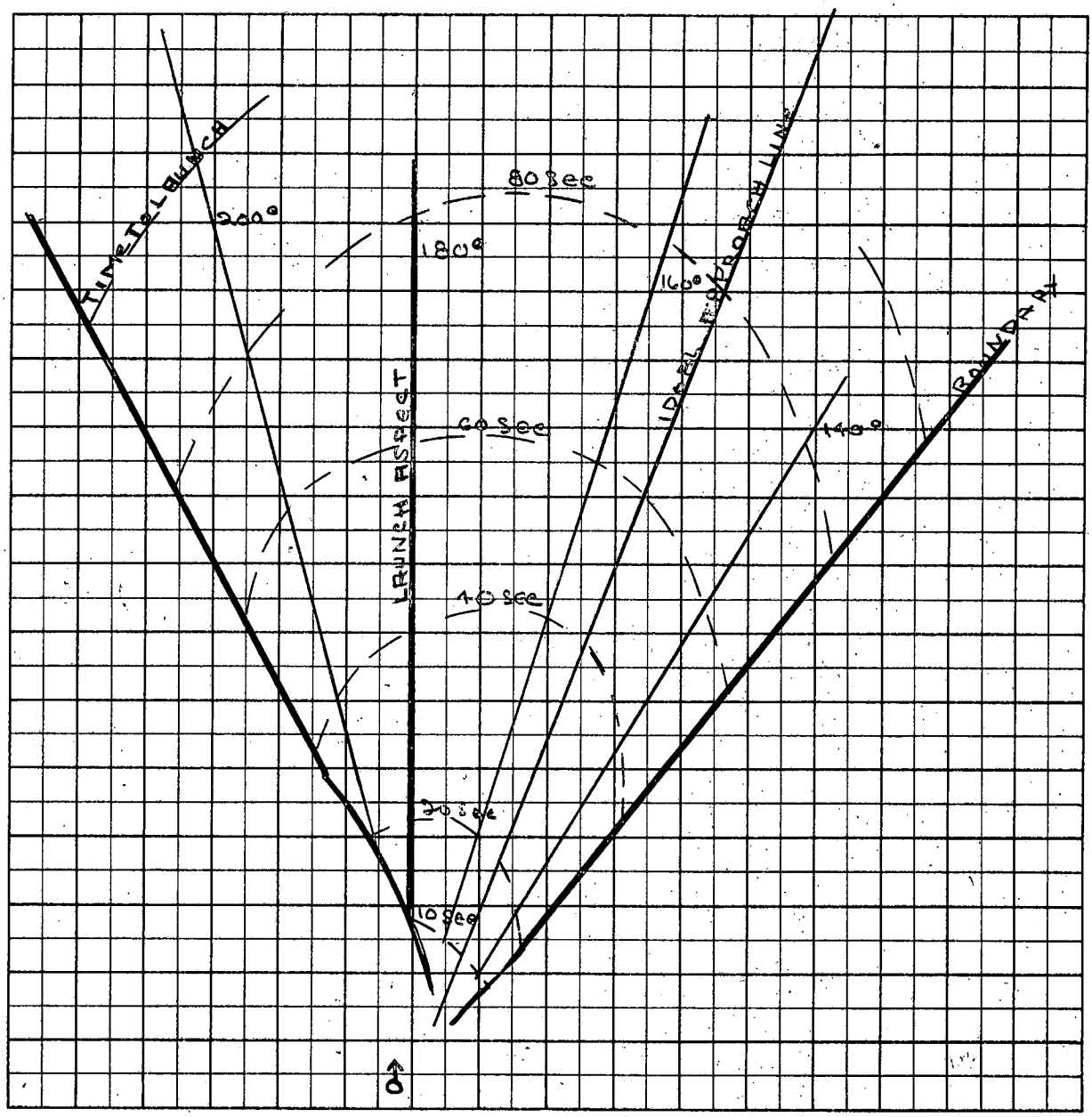

Figure I-H

Height of Target + Fighter	=	50,000'
Maximum Initial Fighter Velocity	=	2 M
Initial Course Difference	=	135°
Evasion	=	0
F	=	7,000 ft
T_f	=	8 sec
1 cm	=	25,000 ft.

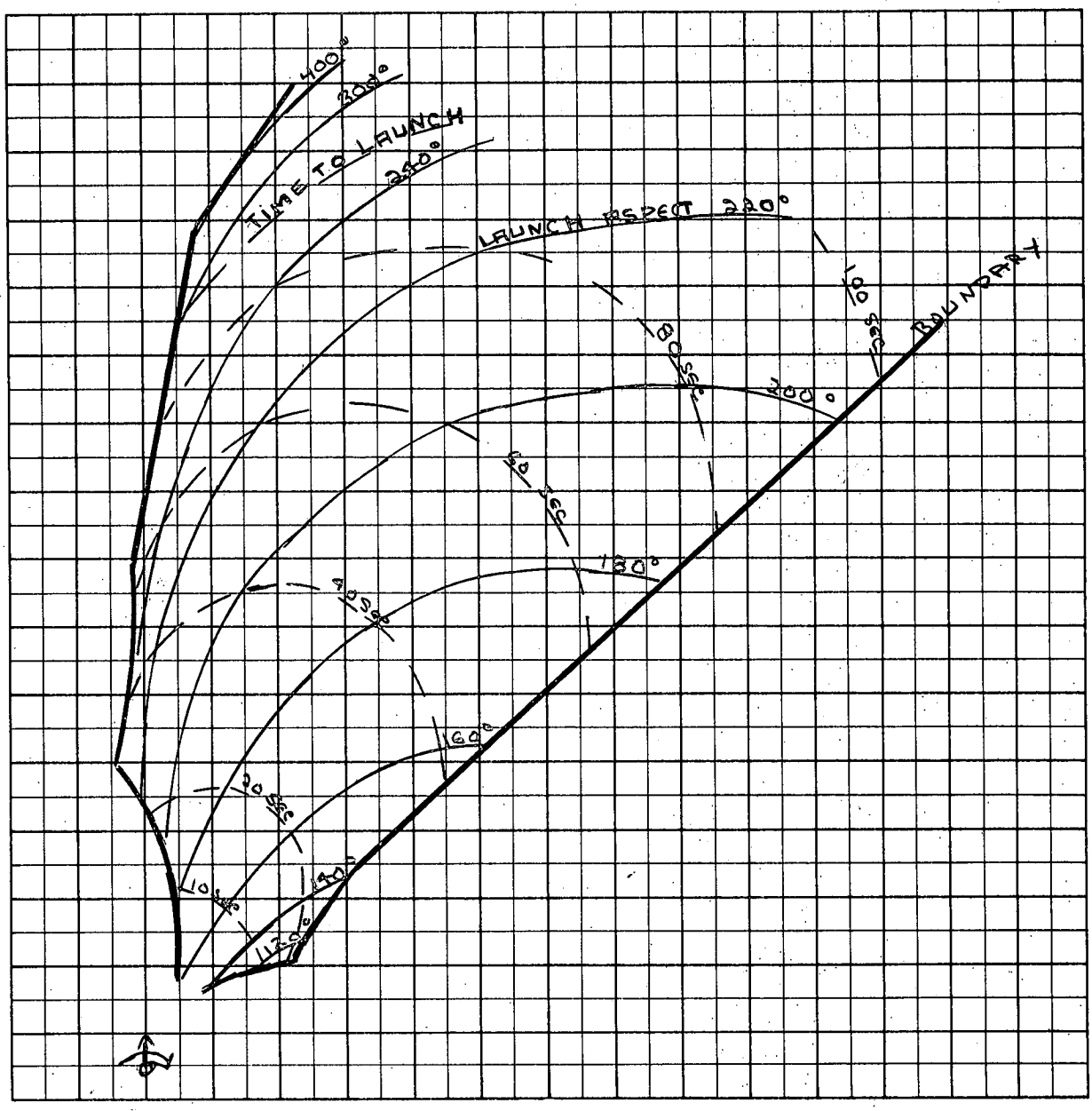

Figure 2-H

Height of Target + Fighter = 50,000'

Velocity of Target = 2 M

Maximum + Initial Fighter Velocity = 2 M

Clockwise Evasion at 3/4 g

Γ_3 = 135°

F = 7,000 ft

T_f = 8 sec

1 cm = 25,000 ft.

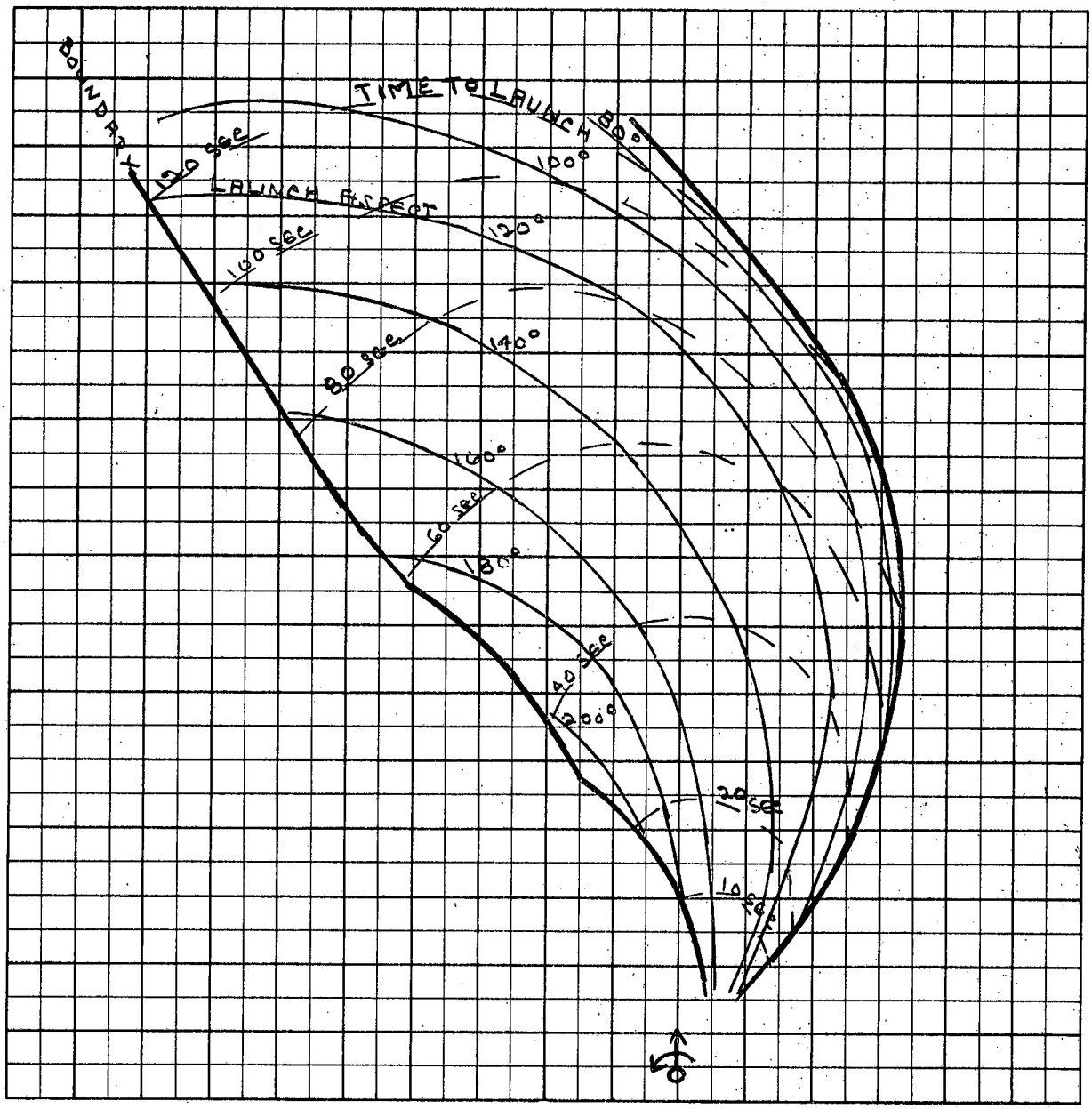

Figure 3-H

Height of Target + Fighter = 50,000'

Velocity of Target = 2 M

Initial + Maximum Fighter Velocity = 2 M

Counter Clockwise Evasion at 3/4 g
- Initial Course Difference = 135°

F = 7,000 ft

T_f = 8 secs

1 cm = 25,000 ft

APPENDIX "J"

EXAMINATION OF PROPOSED RCA METHOD OF INSTRUMENTING THE FIRE CONTROL COMPUTER IN THE CF105 WEAPONS SYSTEM

by

P.L. Roney

1. GENERAL

RCA have not as yet published the equations they intend to use in computing launch zones. However Mr. Wellinger of RCA has listed the following equations for the launch zone parameters:-

Average Relative Missile Velocity $V_M = 615 + \frac{82}{(P/P_{sl})}$ ft/sec (1)

Firing point at time-to-go $T = 7$ secs.

Hence F-pole given by $F = 7V_M$ ft. (2)

Maximum permissible aiming error

$$\delta_{max} = \left[\frac{2\,V_M}{V_I+V_M}\right]\left(\frac{158\,(P/P_{sl}) - 137\,(P/P_{sl})^2}{1 + 4.8\left(\frac{P}{P_{sl}}\right) - 5\left(\frac{P}{P_{sl}}\right)^2}\right) \quad (3)$$

Maximum and Minimum Range

$$R_{max} = -\frac{K_2\,\dot{R}}{1000} + K_3 \quad (4)$$

$$R_{min} = -9\,\dot{R}_1 + K_1 \quad (5)$$

Where: R_{max} always $< 36{,}000$

$\dot{R}_L = \dot{R}$ for $-\dot{R} < 1100$ ft/sec., $= -1{,}100$ otherwise

$K_1 = 11{,}500 - 27{,}400\,\frac{P}{P_{sl}}$ for $\frac{P}{P_{sl}} < 0.345$, $= 2{,}000$ otherwise

$$K_2 = 18,700 - 5,800 \frac{P}{P_{sl}}$$

$$K_3 = 22,400 - 18,400 \frac{P}{P_{sl}}$$

The form of the computed launch zone is shown on the next page and is similar to the mechanisation of the launch zone used by Douglas. See Reference 1.

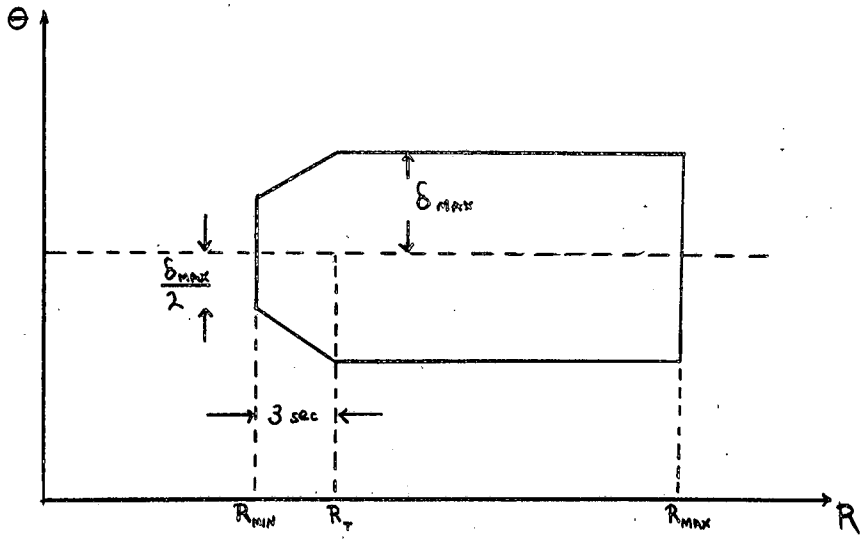

It would seem that RCA intend to use the same formulae as Douglas with the exception of equation (3) for δ_{max} the maximum permissible Aiming error. In this equation RCA have inserted the term $2V_M/(V_M + V_I)$.

The reasons for the inclusion of this term are not yet known. In order to give some idea of the effect of the new term some magnitudes are given in the table below. Note that the CF105 is to have optimum velocities of 1.2 and 2 Mach, an optimum altitude of 40,000 feet but good performance at 60,000 feet.

	V_I	V_M	$\frac{2V_M}{(V_M + V_I)}$
H = 40,000'	1.2M	1.06	0.94
	2.0M	1.06	0.69
H = 60,000'	1.2M	1.82	1.2
	2.0M	1.82	0.95

2. FIGHTER "ON-COURSE"

An examination was carried out to determine the correlation between equation (1) - (5) in the formulation of launch zones for Lead Collision navigation. This study was in two dimensions only as it was felt that this would give sufficient indication of the behaviour of the equations. The effect of variation of altitude was considered and emphasis was placed on supersonic velocities of both fighter and target. Thus three values of fighter-target velocity ratio were covered: equal velocities, fighter velocity advantage and target velocity advantage. One case of subsonic fighter and target velocities was also considered. The cases considered are listed below.

Case (1) Altitude H = 40K	Case (2) H = 50K	Case (3) H = 60K
(a) $V_I = V_T = 1.5m$	(a)	(a)
(b) $V_I = 2m$, $V_T = 1.5m$	(b)	(b)
(c) $V_I = V_T = 2m$	(c)	(c)
(d) $V_I = 1.5$, $V_T = 2m$	(d)	(d)
(e) $V_I = 0.92$, $V_T = 0.85m$	(e)	(e)

First of all it was necessary to obtain the Lead Collision equations in a form such that they could be combined with equations (1) to (5) for the computed launch zone, i.e. in terms of parameters which would be used in the Fire Control computer, R, $\dot{R}$, θ, A, V_T, V_I.

The Lead Collision equations are:-

$$R\omega = V_I \sin\theta - V_T \sin A$$

$$-\dot{R}T = R - F\cos\theta$$

$$R\omega T + F\sin\theta = \theta$$

$$\dot{R} = V_T \cos A - V_I \cos\theta \qquad (6)$$

Eliminating T and ω from the first three equations yields

$$\ddot{R} - F\sin\theta = (R - F\cos\theta)(V_I \sin\theta - V_T \sin A) \qquad (7)$$

The range parameter R in equations (6) and (7) was given its maximum or minimum value (R_{max} or R_{min}) and these equations were solved with equations (4) and (5) to give R_{max} or R_{min} in terms of lead angle θ. The analytical solution led to quartic equations, and the REAC was used to give solutions. The results were obtained as R_{max} and R_{min} plotted against A and A plotted against θ. From these R_{max} and R_{min} were plotted

against θ on a launch zone diagram for particular values of aspect angle A. The ideal lead angle θ_i was determined together with δ_{max} (from equation (3)) and a launch zone constructed.

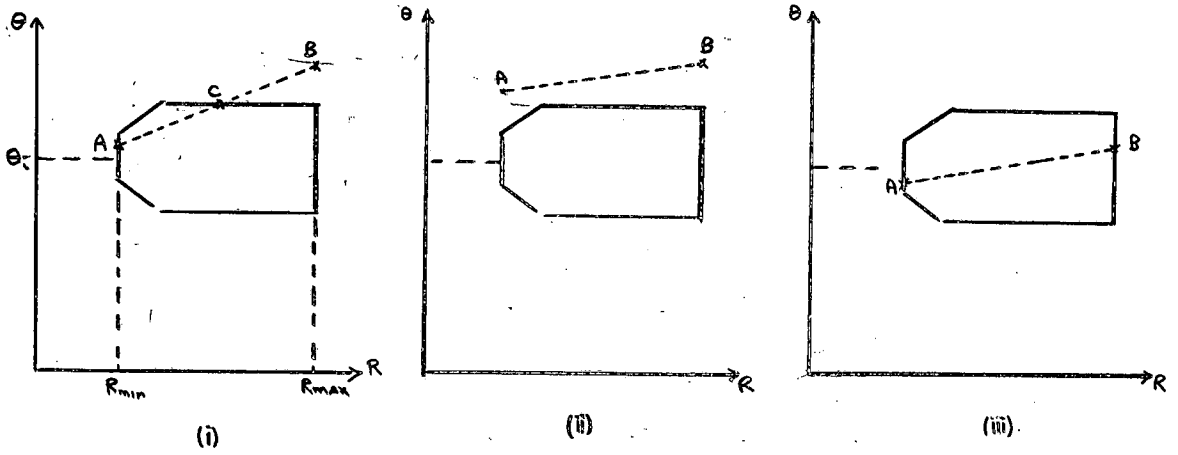

Some of the results are illustrated above. The points A and B represent R_{max} and R_{min} at the angles θ given by the solution of equations (4) and (5) with (6) and (7). In diagram (i) successful firing would be possible along AC. No successful firing could be achieved at the aspect angle of diagram (ii). Diagram (iii) shows the type of result required. Here A and B lie within the launch zone angular width given by δ_{max}; θ for points A and B lies within $\theta_i \pm \delta_{max}$. Most of the results obtained were of the types shown in (i) and (iii). The former types are acceptable providing that the "restricted" range width AC of the launch zone is large enough from a practical point of view.

The results are given in figures (1), (2) and (3). Note the number of the figure refers to the altitude and the letter refers to a particular case of fighter-target velocity ratio given by the table listing the cases. Thus (1) (a) refers to Case (1) of altitude 40,000 ft with $V_I = V_T = 1.5$ Mach. For convenience the launch zones for a particular aspect angle A and its complement have been drawn on the same figure where they both existed.

3. RESULTS

Cases (a) and (c): Equal Fighter and Target Velocities

With equal fighter and target velocities there is a fall-back line at right angles to the line of flight of the target. This necessarily restricts the aspect angle A to angles greater than around 60°. For aspects slightly greater than this the launch zone is rather narrow and the lead angle θ at R_{max} falls outside the permissible aiming error limit $\theta_i \pm \delta_{max}$.

As A becomes larger the situation improves and θ at R_{max} becomes less than $\theta_i + \delta_{max}$. Also R_{min} approaches the value set by the limit on $-\dot{R} < 1100$ ft/sec.

There is a slight improvement with increasing altitude.

Cases (b) and (e): Fighter Advantage

(b) Supersonic Velocities

With fighter velocity advantage the computed values of R_{max} and R_{min} give quite good results. θ lies, for the most part, within $\theta_i \pm \delta_{max}$. With small aspect angles, however, rather low values of R_{min} result. R_{max} is lowered also, compared with cases (a) and (c), so that the launch zone width is not in general increased. As aspect angle A decreases, θ at R_{min} tends towards θ_i, and as A increases θ, for R_{max}, tends towards θ_i. For aspects in the region of 90°, the values of θ at R_{max} exceed the desired maximum of $\theta_i + \delta_{max}$.

(e) Subsonic Velocities

The fighter advantage in velocity here was much less than that in case (b), and thus the results are rather similar to those of cases (a) and (c). In the latter the fighter-target velocity ratio was 4:3, whereas in the subsonic case the ratio was 1.1 to 1.

Case (d): Target Advantage

The restriction on aspect angle A due to the fall-back line is quite large in this case, being about 110° (depending on altitude) as a minimum value for A. The $R_{max} = R_{min}$ line straddled the ideal lead angle line fairly symmetrically throughout, though for A near 120° θ at R_{max} was larger than $(\theta_i + \delta_{max})$. The discrepancies were not as bad as in some cases in case (a). The results improved slightly with increasing altitude and increasing aspect angle.

4. GENERAL OBSERVATIONS

The launch zone range-width given by the computed parameters would seem to be rather large in many cases, attacks at and near head-on.

The equations give relatively good results for both fighter and target velocity advantage, but poorer results for equal velocities.

The case of fighter advantage seems to have an unusual feature in the relatively poor results given in the region of A = 90°. This would no doubt be less noticeable as the ratio of fighter to target velocity increased.

Over the altitude range 40K to 50K feet considered there was a slight improvement of results with increasing altitude.

5. EFFECT OF OFF-COURSE STEERING

The question arises when the aircraft is off-course whether this will cause an incorrect launch zone to be computed, which would in turn lead to an error in aim when the missile is fired. Information from the radar is transmitted to the computer to steer the air using lead collision or lead pursuit. The radar also produces information (e.g. θ, $\dot{R}$) to be used by the Fire Control computer to mechanise launch zones. This means that the launch zone so computed is independent of any off-course steering errors because the latter are not introduced into the launch zone computation.

6. VARIATION OF δ_{MAX} WITH ASPECT ANGLE A

The equation (3) used by RCA to compute δ_{max}, the maximum permissible aiming error, allows for no variation of δ_{max} with aspect angle. In order to obtain some idea as to how realistic this assumption is a comparison was made with launch zones simulated by Douglas for a D-configuration missile. The data used was obtained from ref. 2 in which launch zones were simulated for both subsonic and supersonic velocities for altitudes of 0K, 5K, 30K and 50K. Of these, launch zones simulated at 30K and 50K were used. The maximum possible aiming error, denoted by δ'_{max} in this case, was measured directly and plotted against aspect angle A for the simulated launch zones. The results are shown in figure (4).

It will be seen that there can in some cases be a relatively large variation of δ_{max} with A. The important point is that the computed launch zone should lie within and be more or less symmetrically enclosed by the true launch zone. Hence δ'_{max}, of the true launch zone, should always be greater than δ_{max} computed. Figure (5) shows how a launch zone computed by means of equation (3) for δ_{max} compares with a Douglas simulated zone at different aspect angles. Provided the computed zones compared with true launch zones as well as they do with the Douglas simulated zones in Figure (5) then the variation of δ'_{max} with A would remain relatively unimportant.

7. REFERENCES

1. Douglas-Bendix Quarterly Report SM 19564

2. CARDE Technical Letter N-47-16.

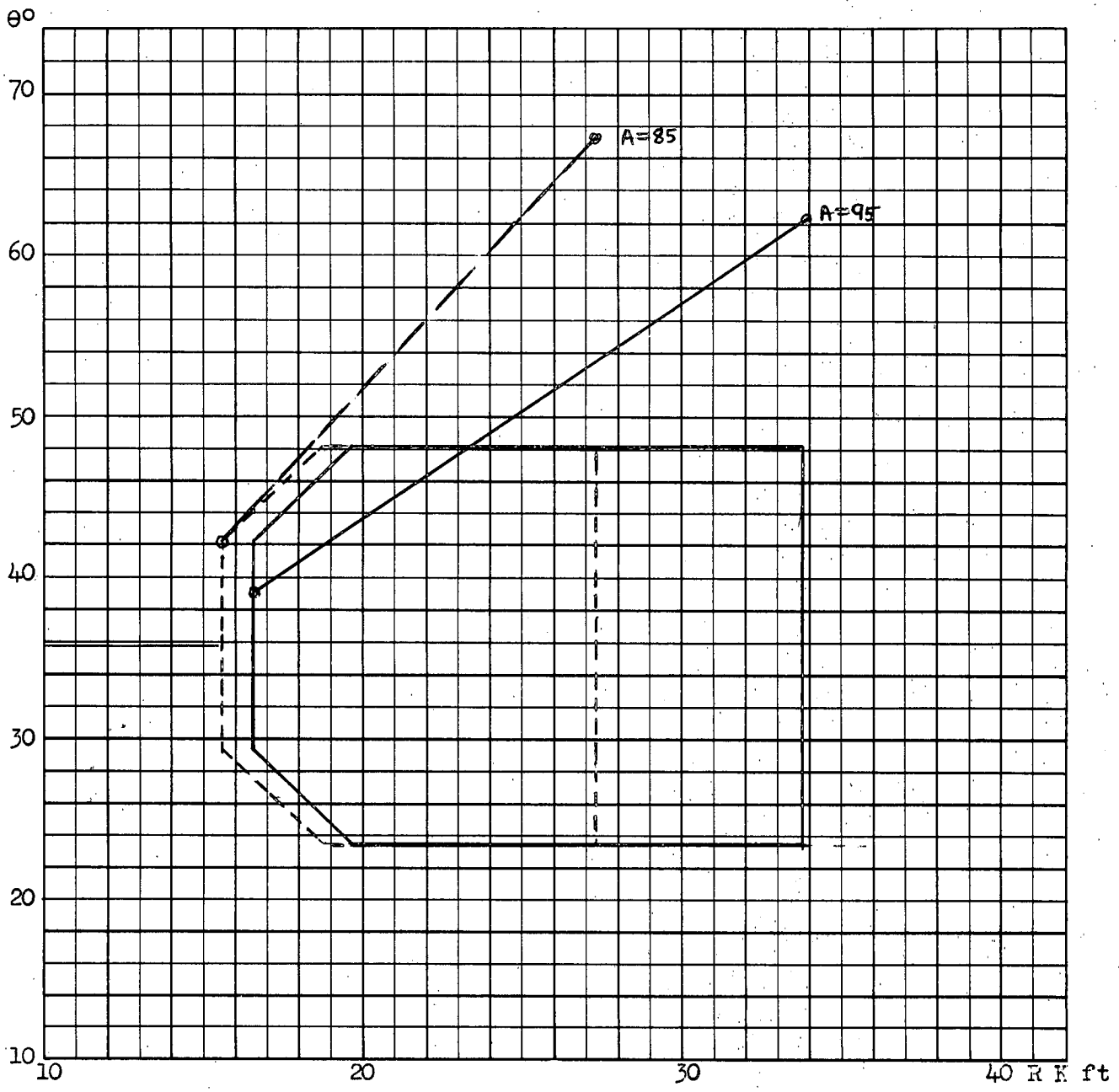

1 (a) H=40K (i) A= 85°, 95° $V_T = 1456.5 = V_F$

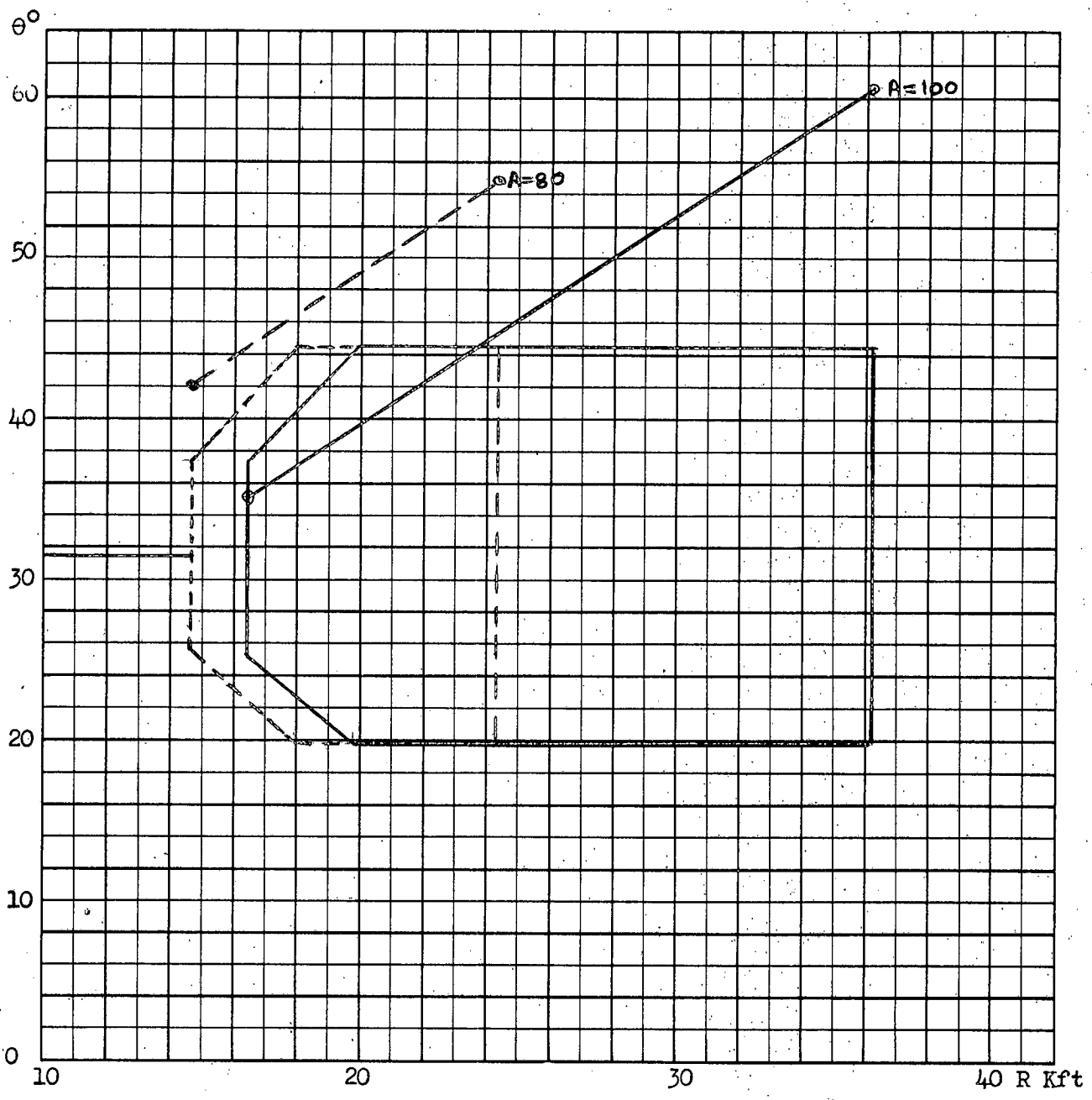

1(a) (ii) A = 80°, 100°

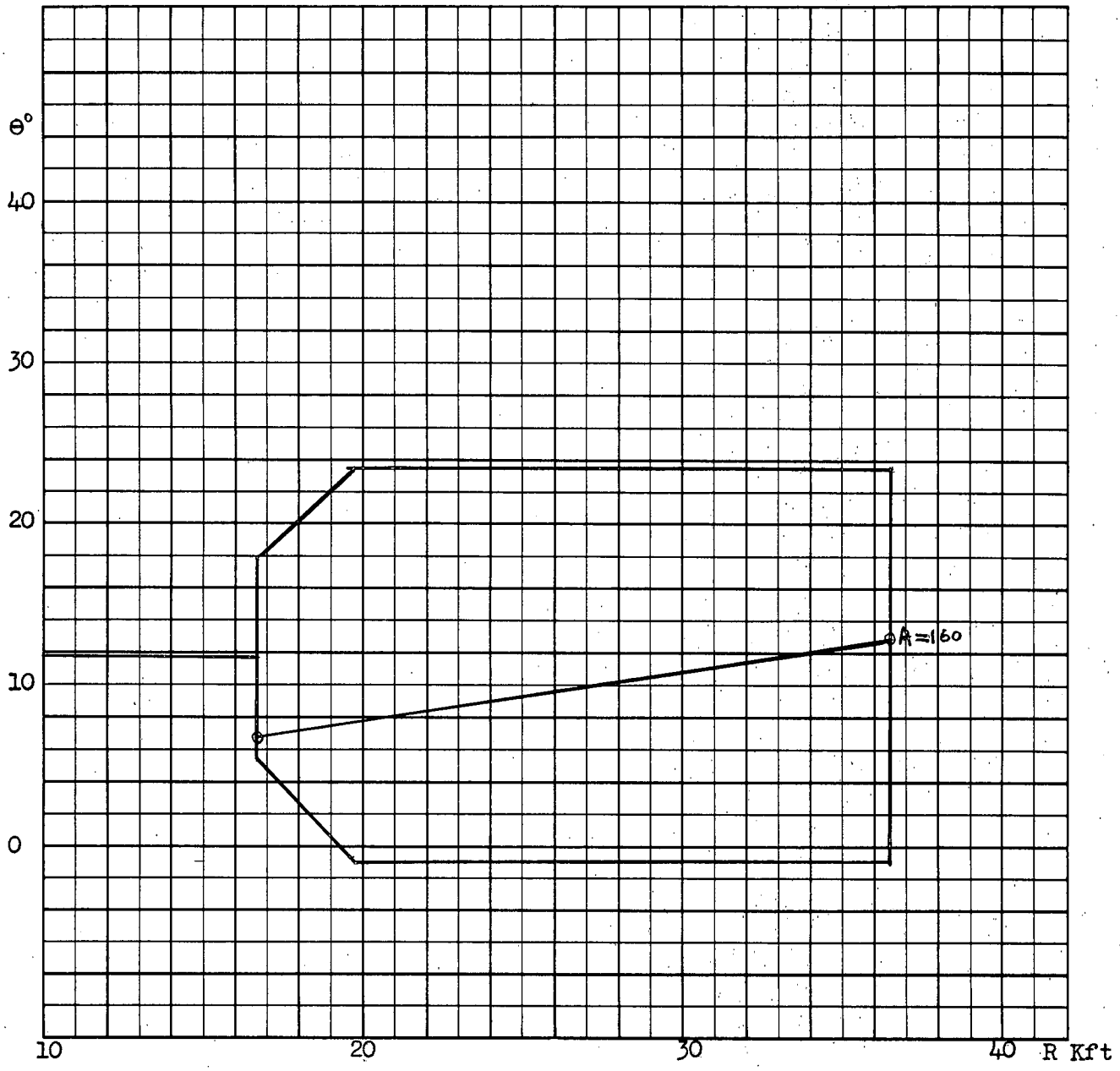

1(a) (iii) A=160

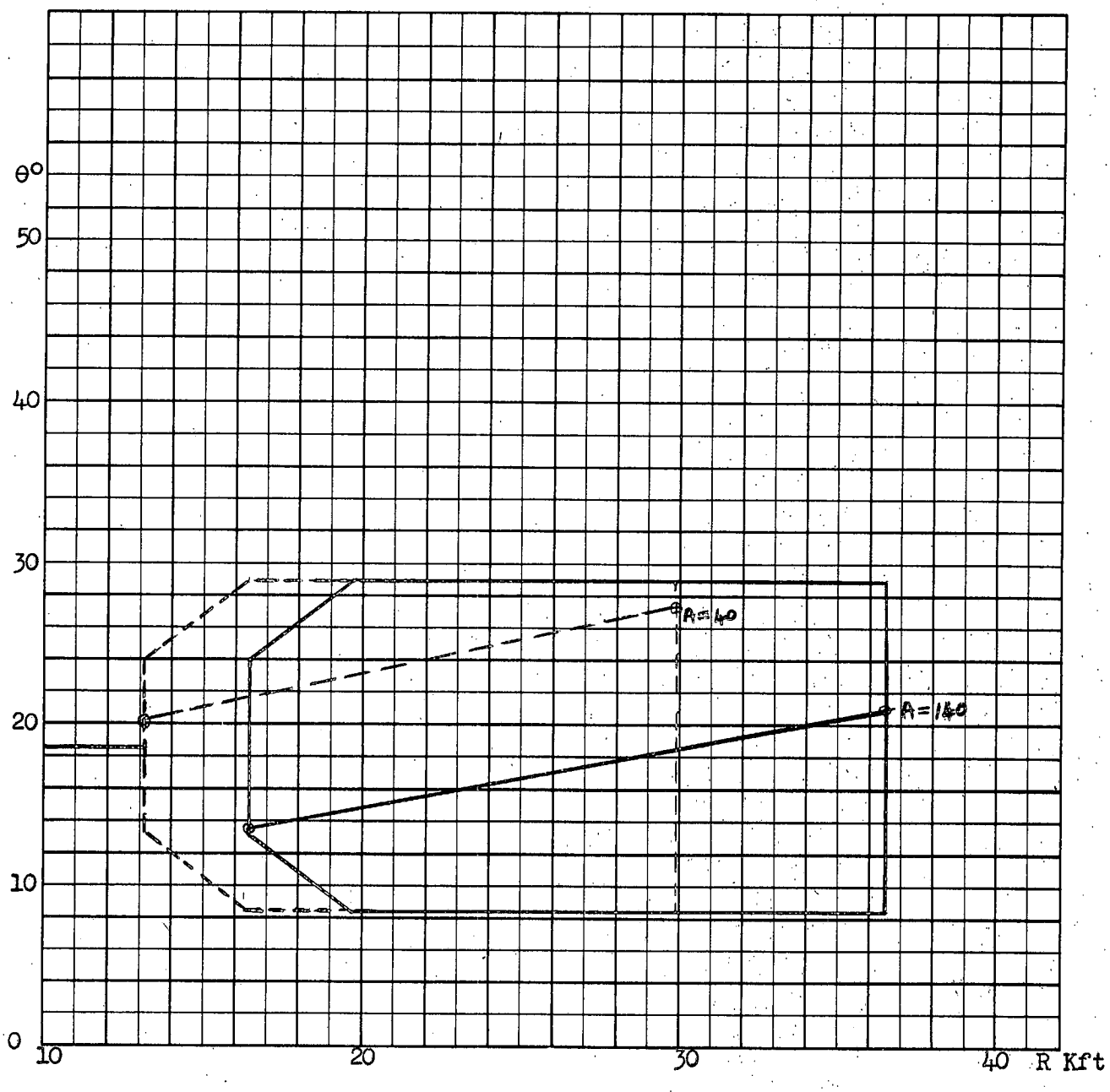

1(b) H=40K (i) A=40, 140 V_T= 1456.5 V_F= 1942

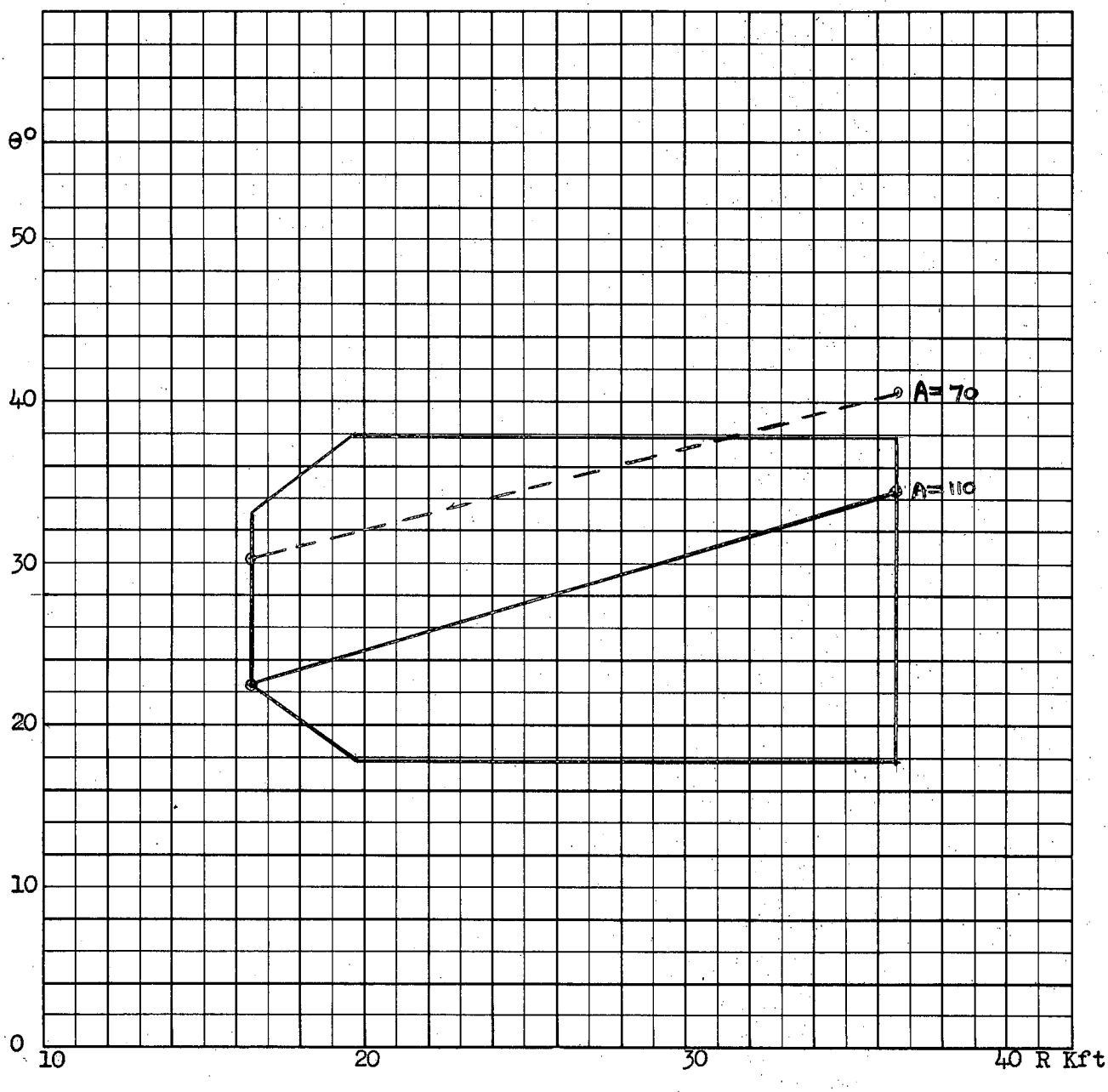

1(b) (ii) A=70, 110

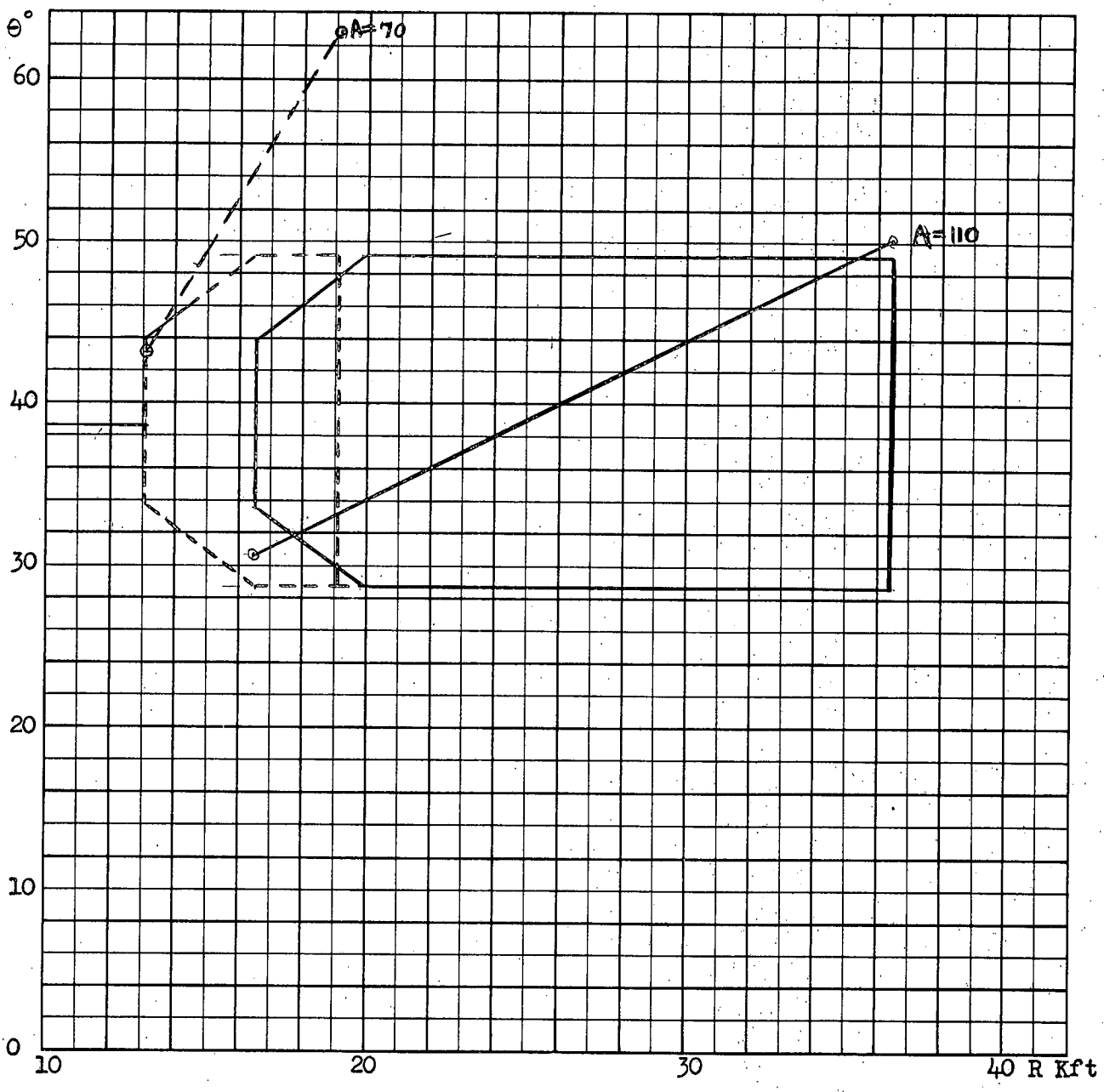

1(c) H=40K (i) A=70, 110 V_T= 1942 = V_F

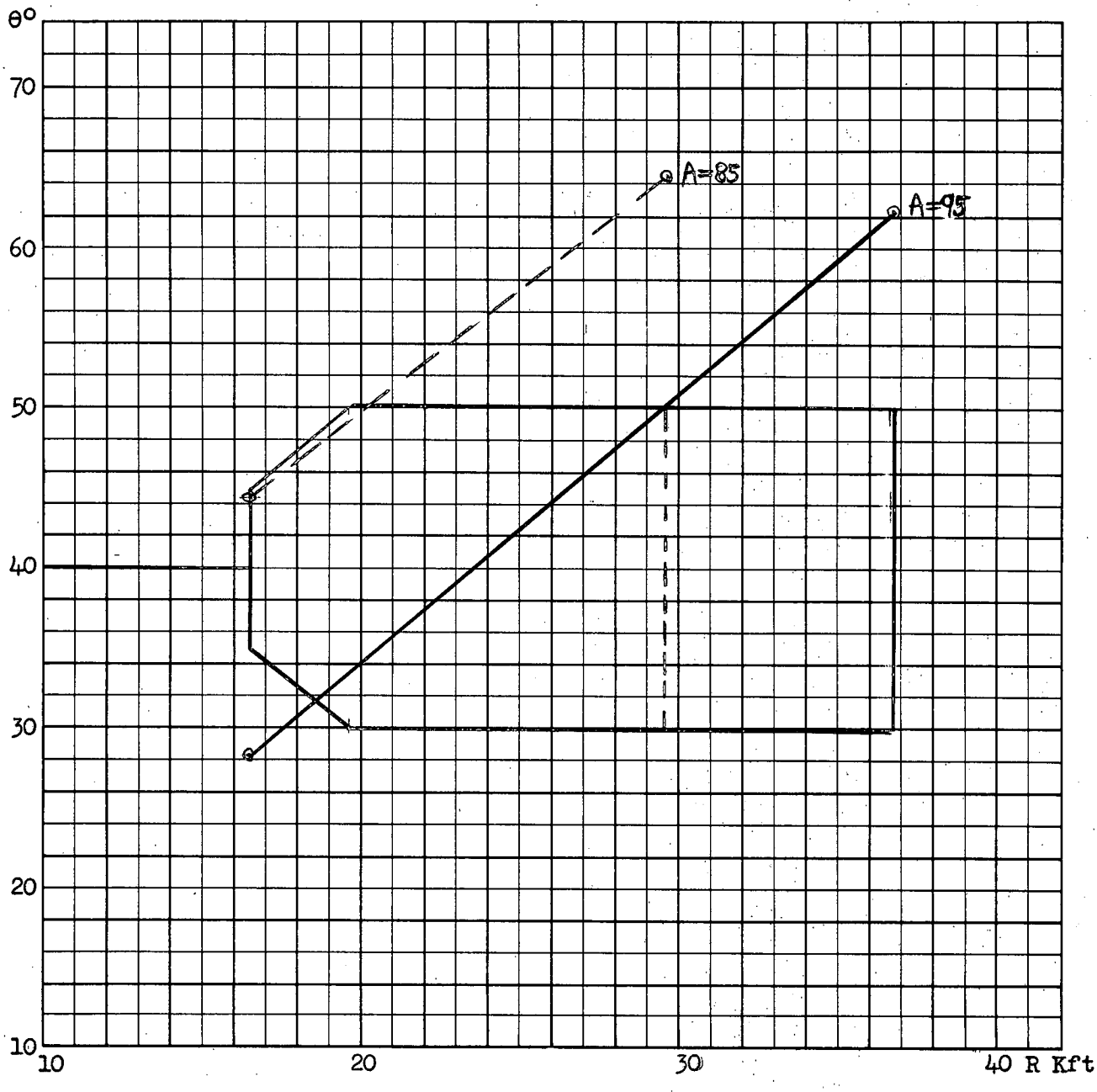

1(c) (ii) A=85, 95

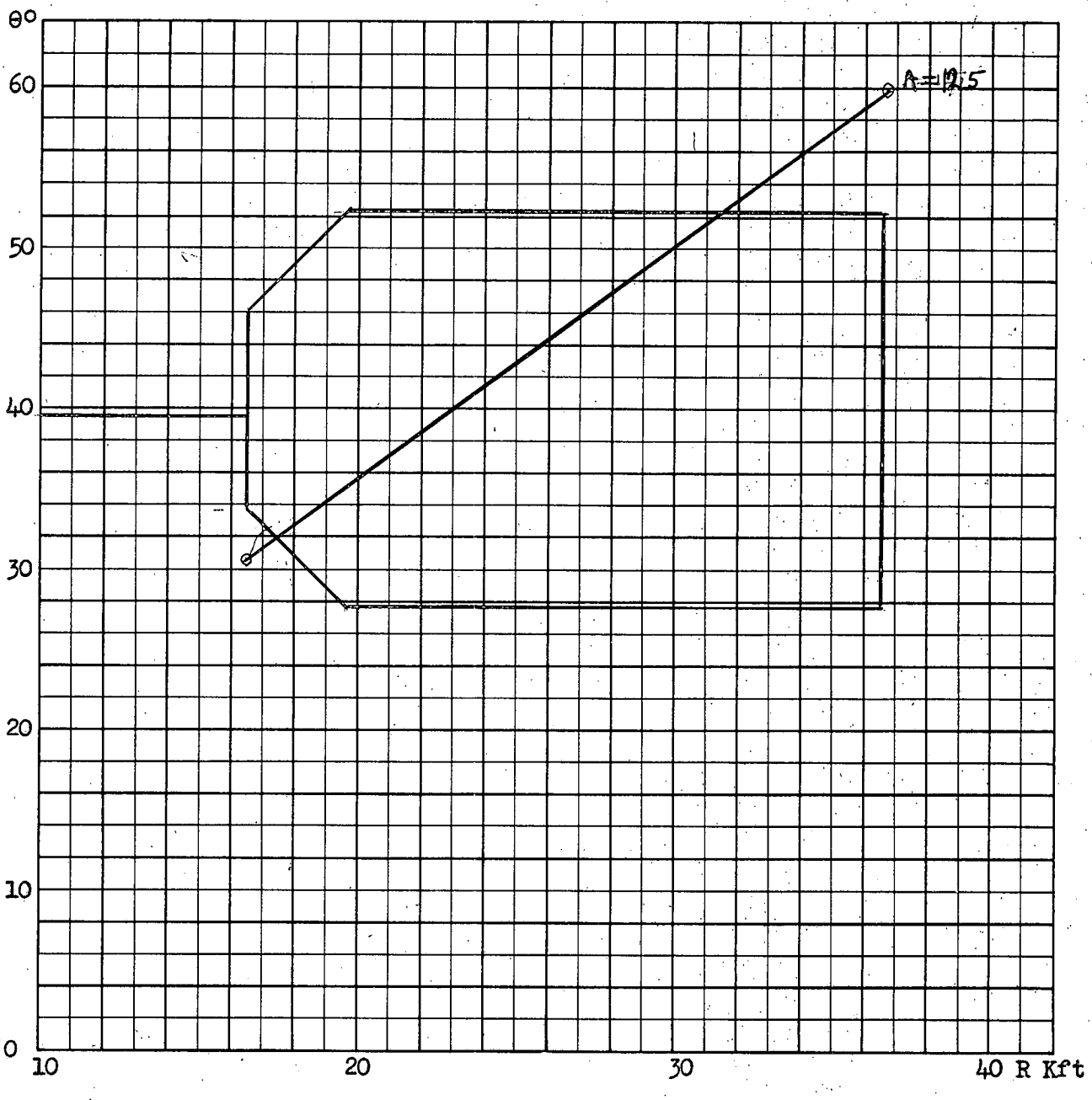

1(d) H=40K (i) A=125 V_T= 1942 V_F= 1456.5

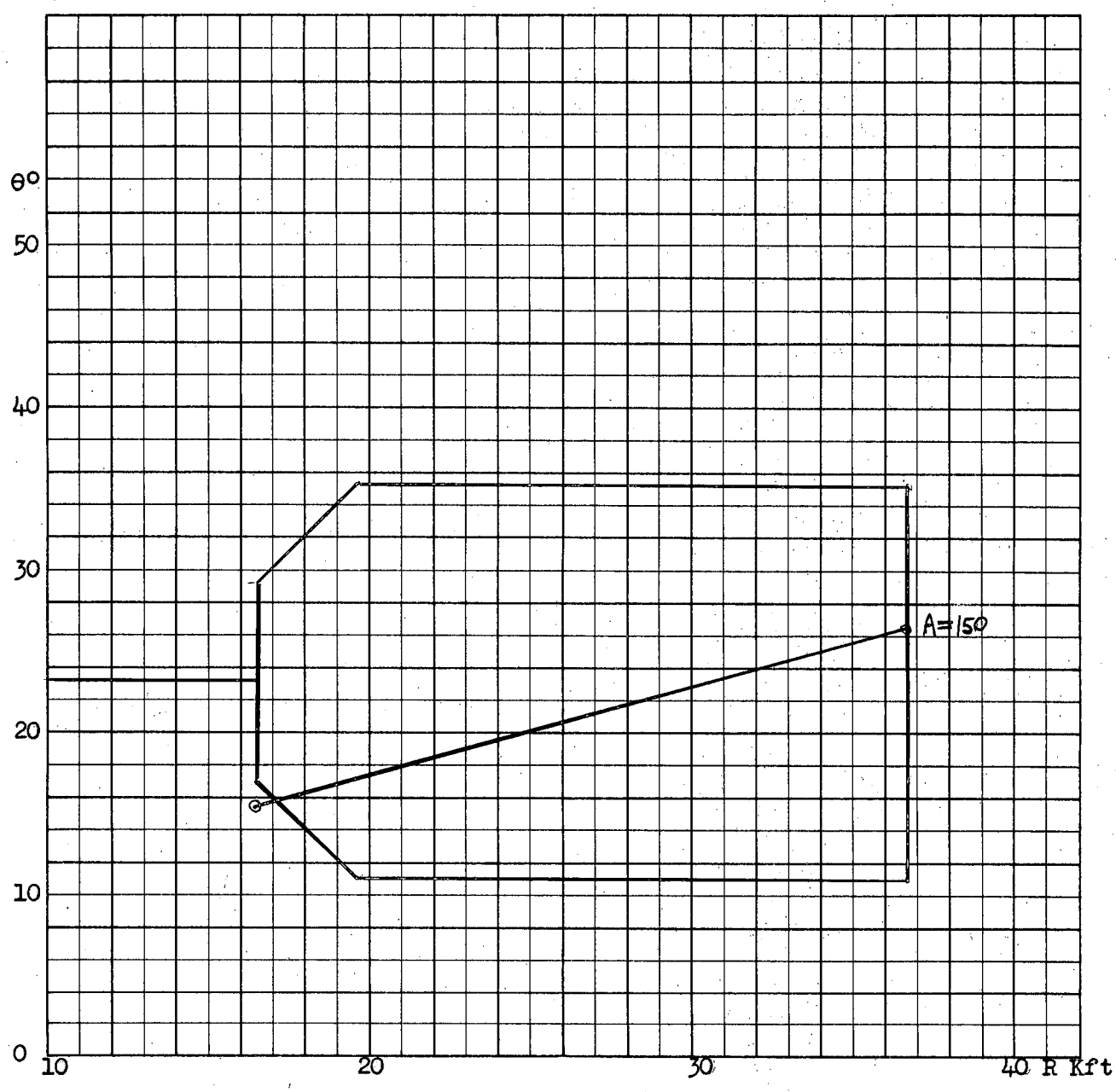

1(d) (ii) A=150

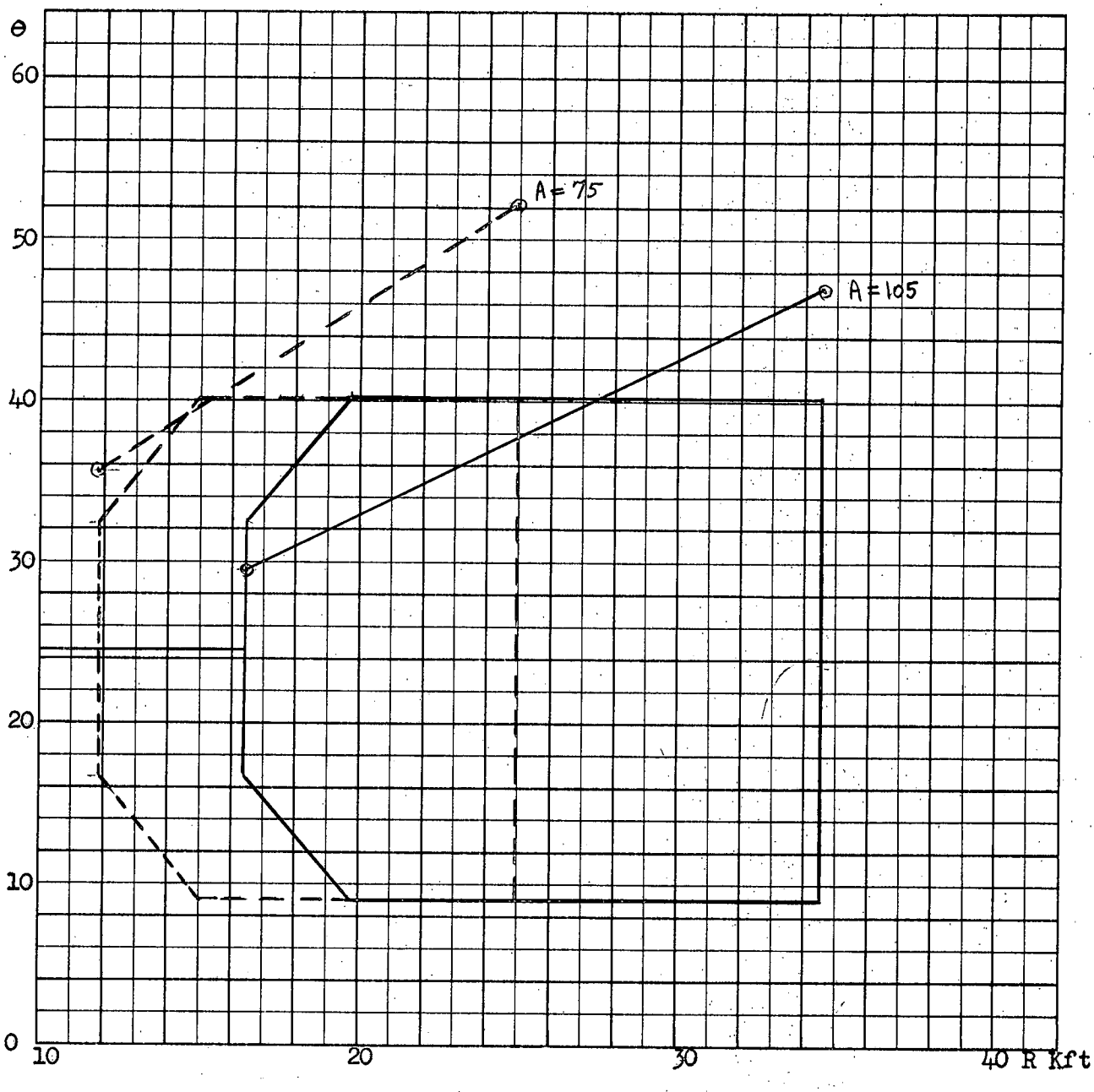

1(e) H=40K (i) A=75, 105 V_T= 825.35 V_F= 893.32

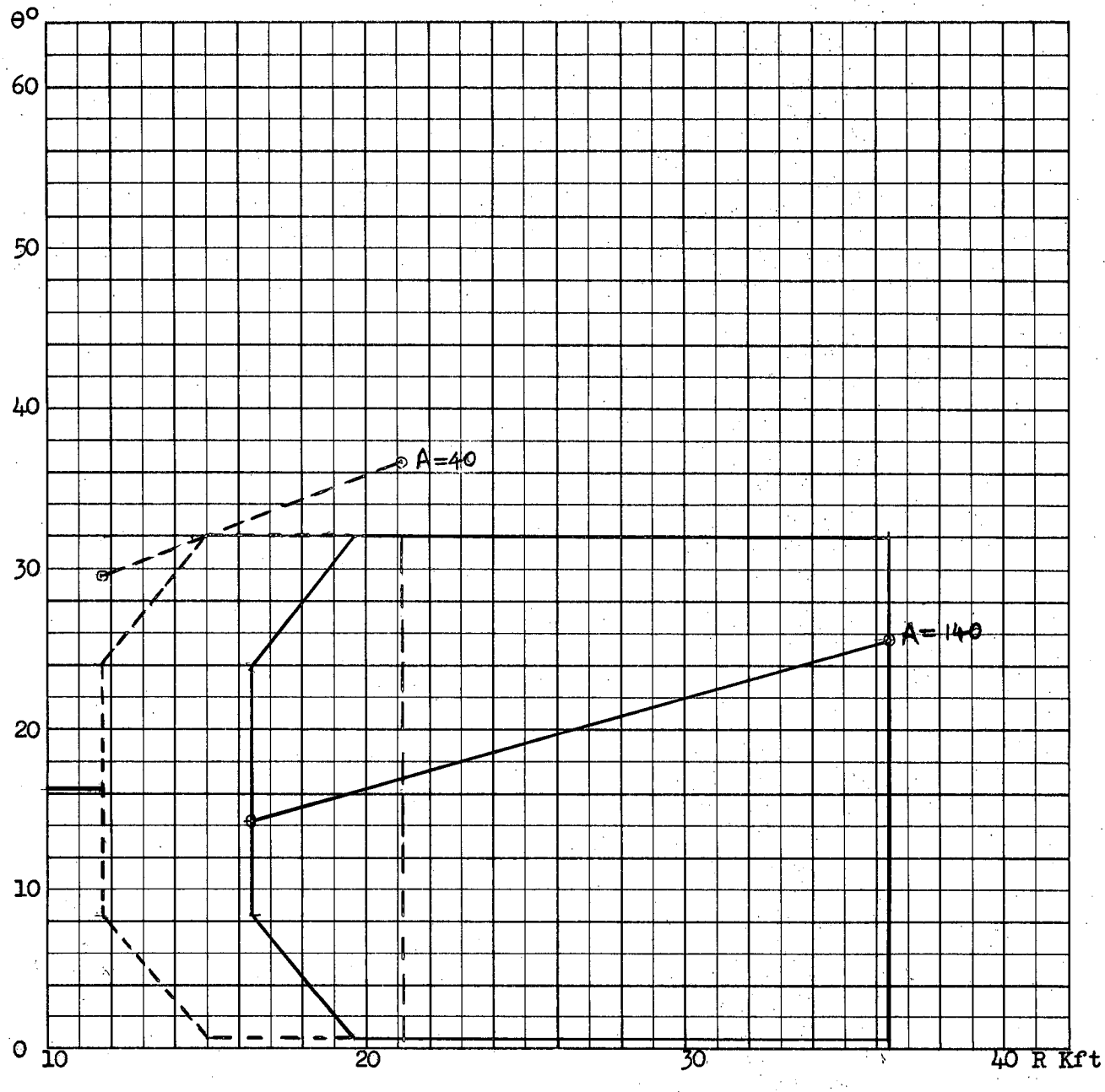

1(e) (ii) A=40, 140

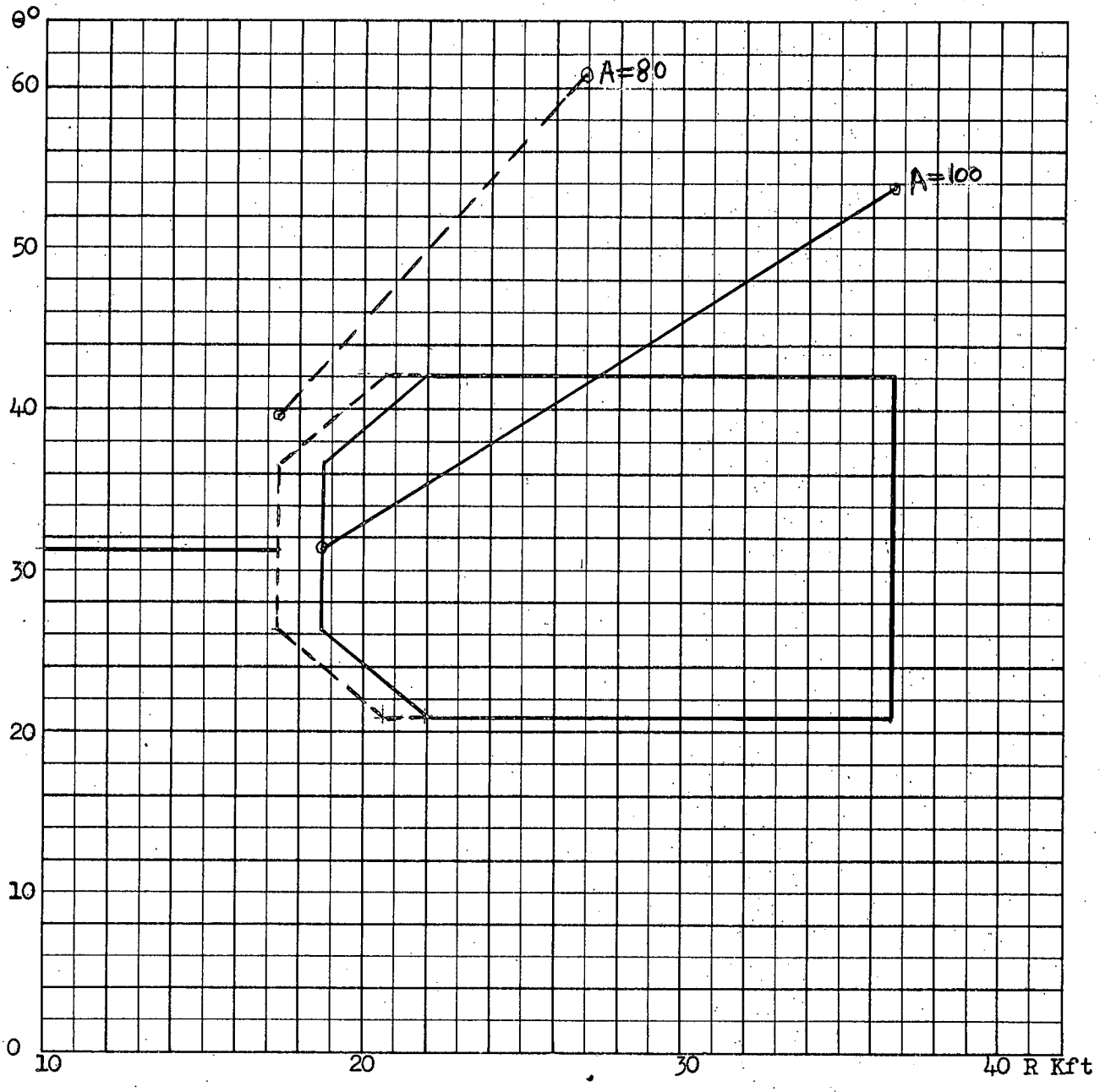

2(a) H=50K (i) A=80, 100 $V_T = 1456.5 = V_F$

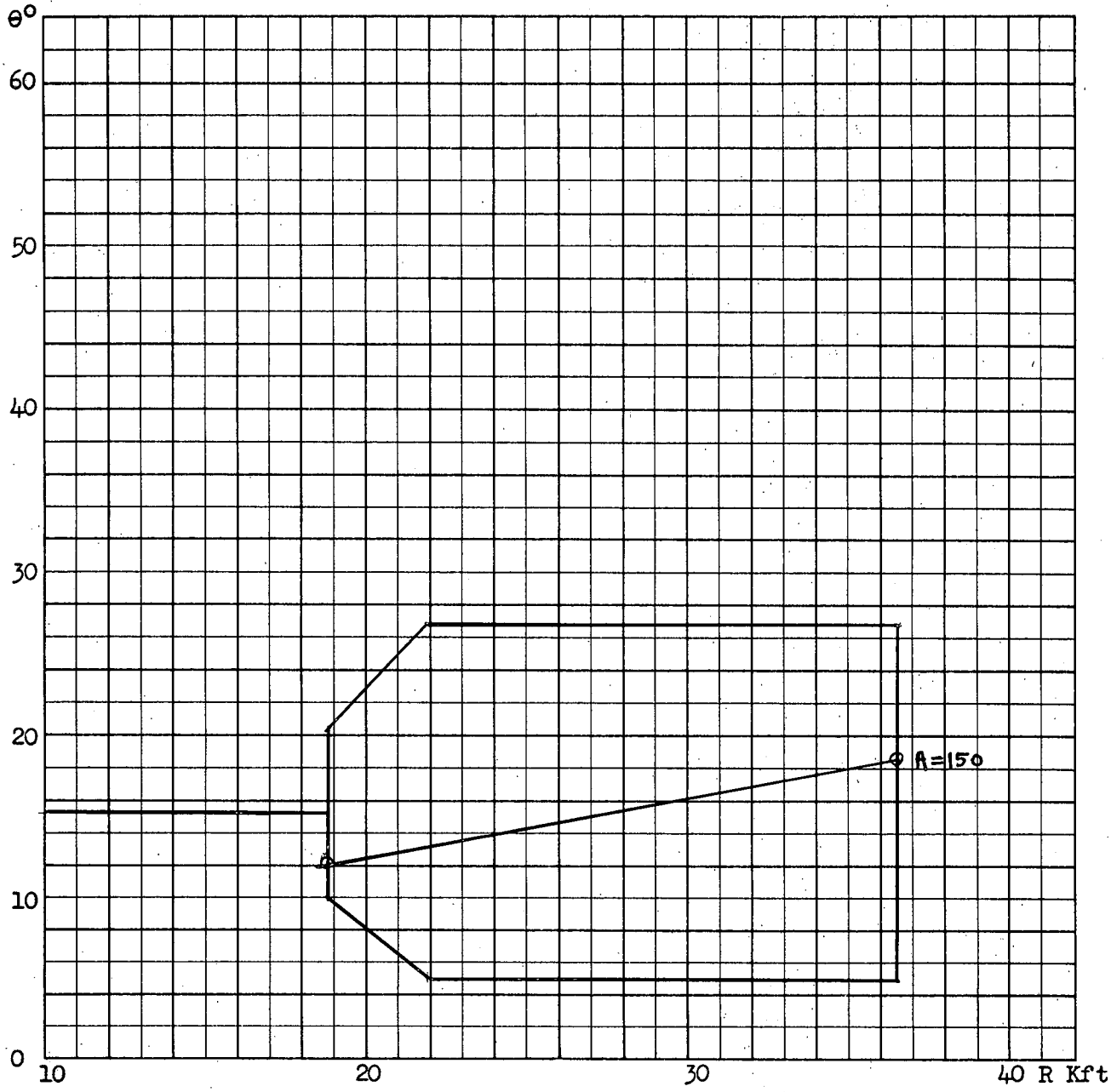

2(a) (ii) A=150

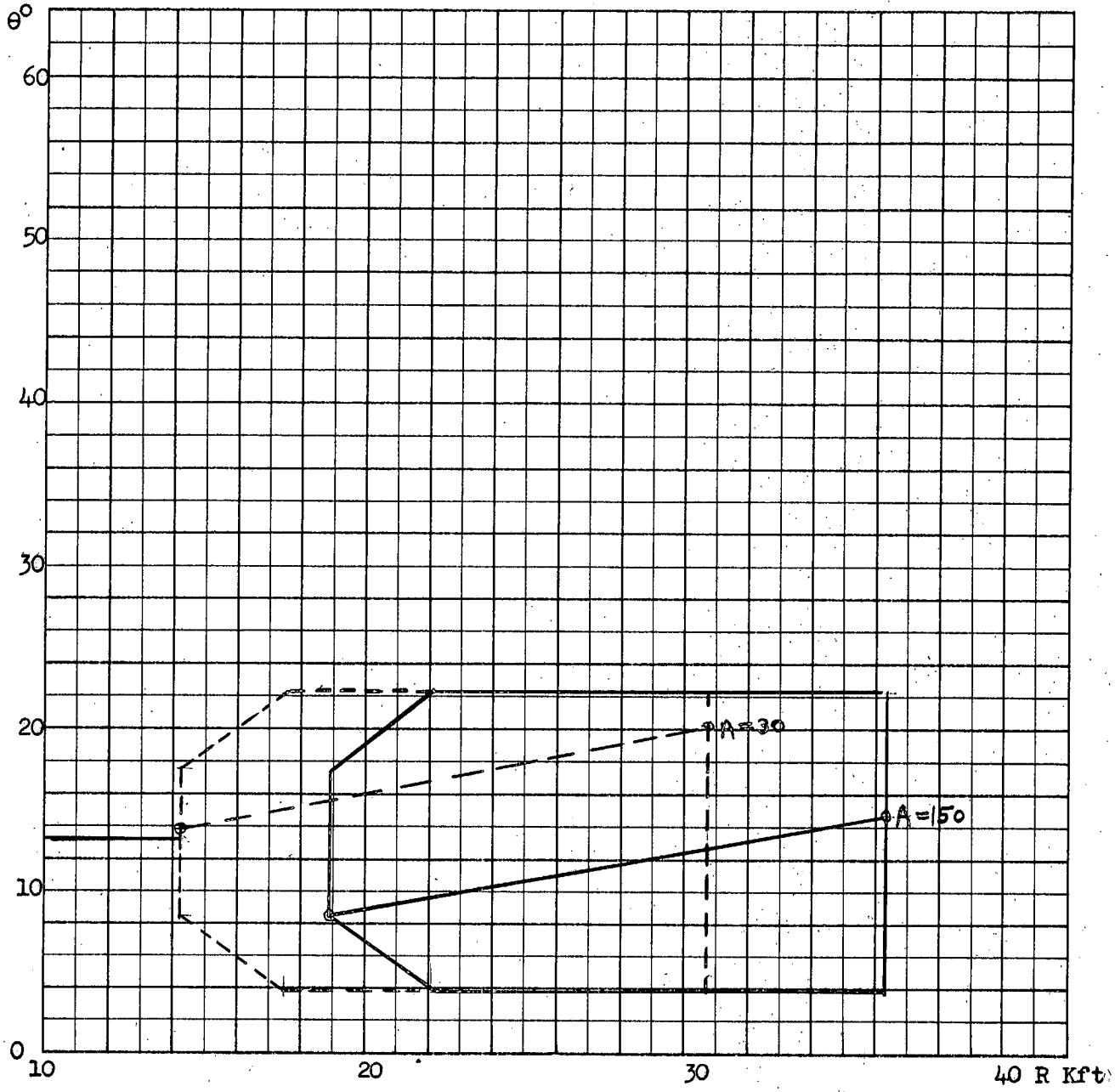

2(b) H=50K (i) A=30, 150 V_T= 1456.5 V_F=1942

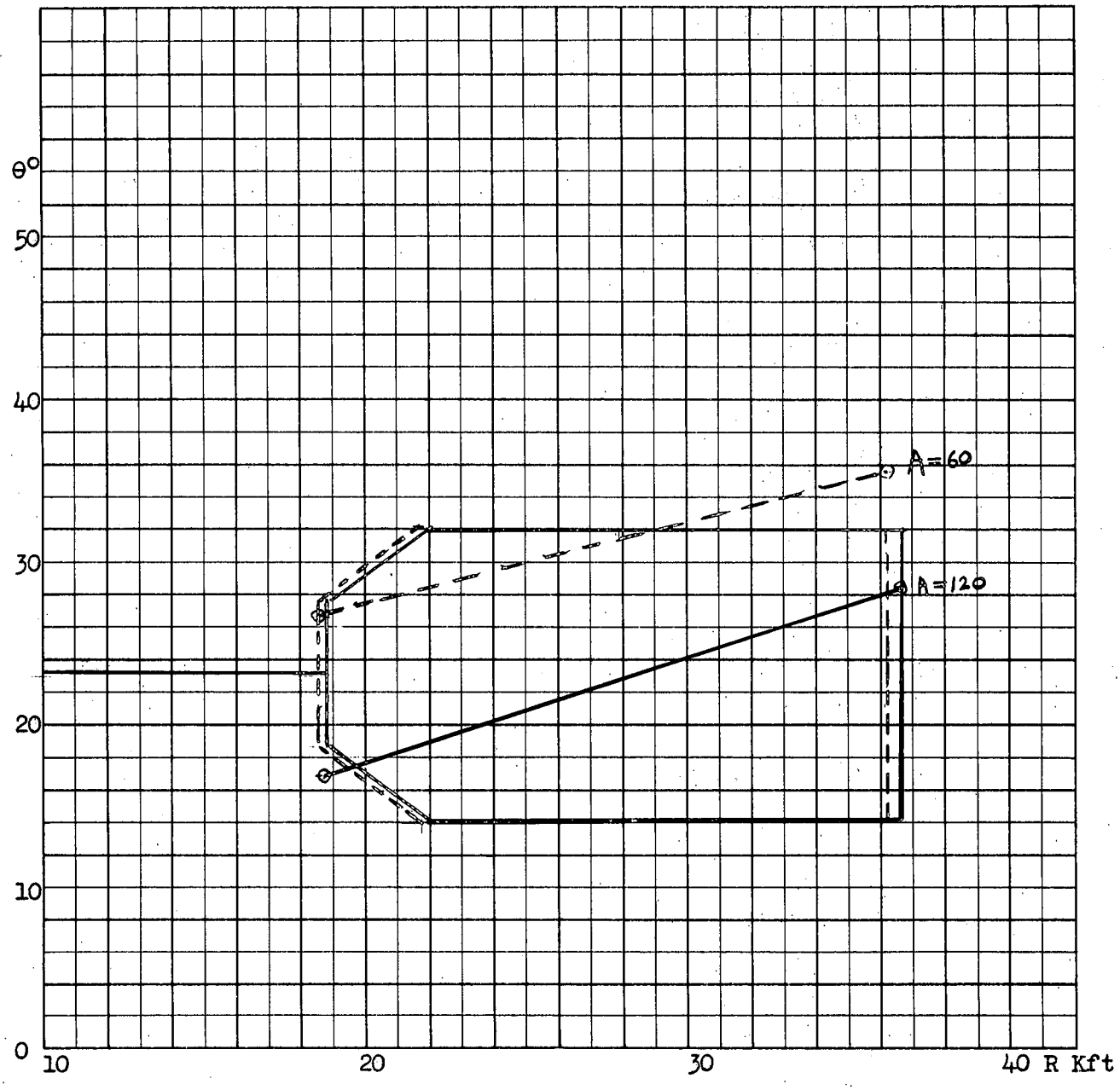

2(b) (ii) A=60, 120

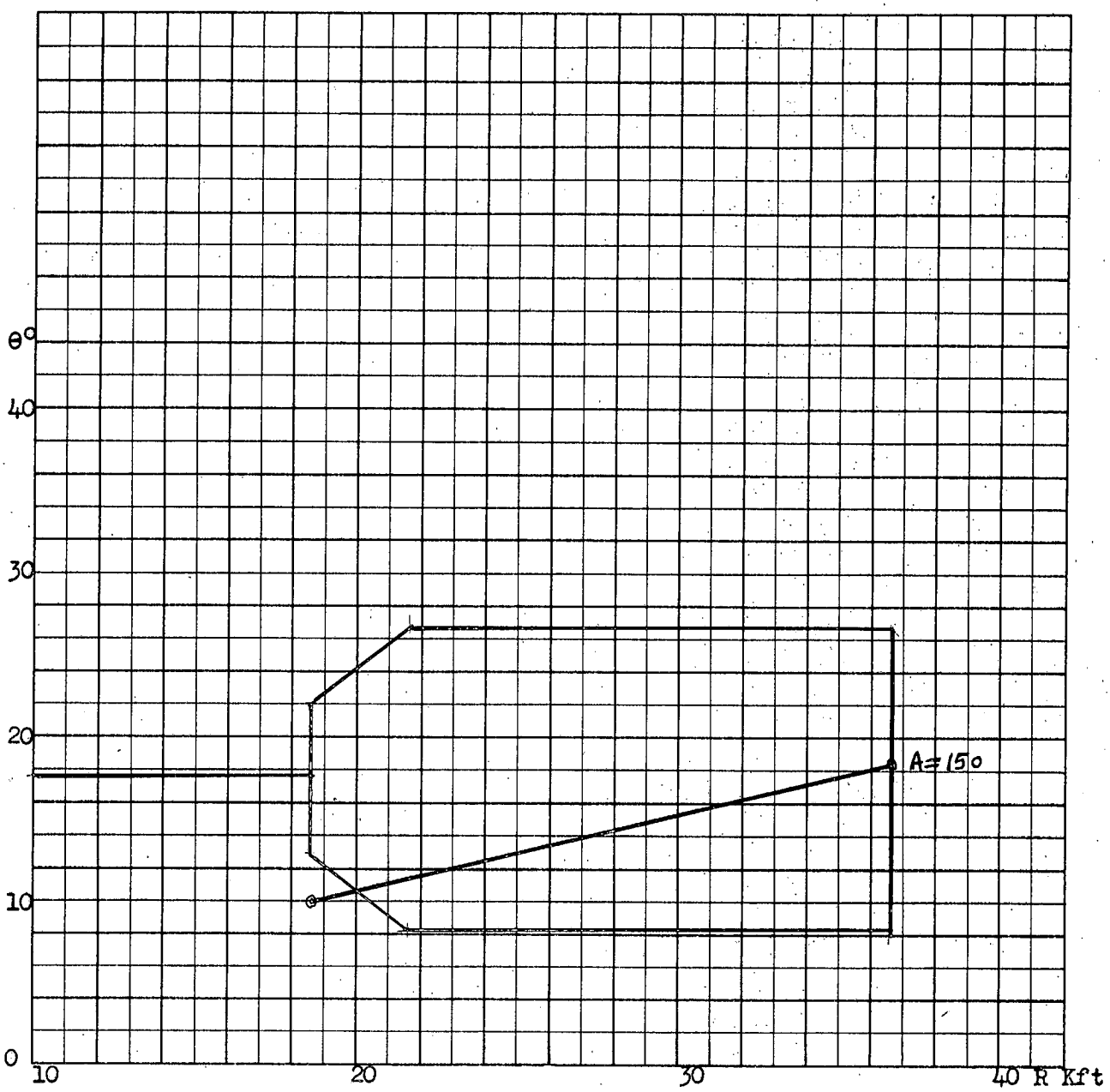

2(c) H=50K (i) A=150 $V_T = 1942 = V_F$

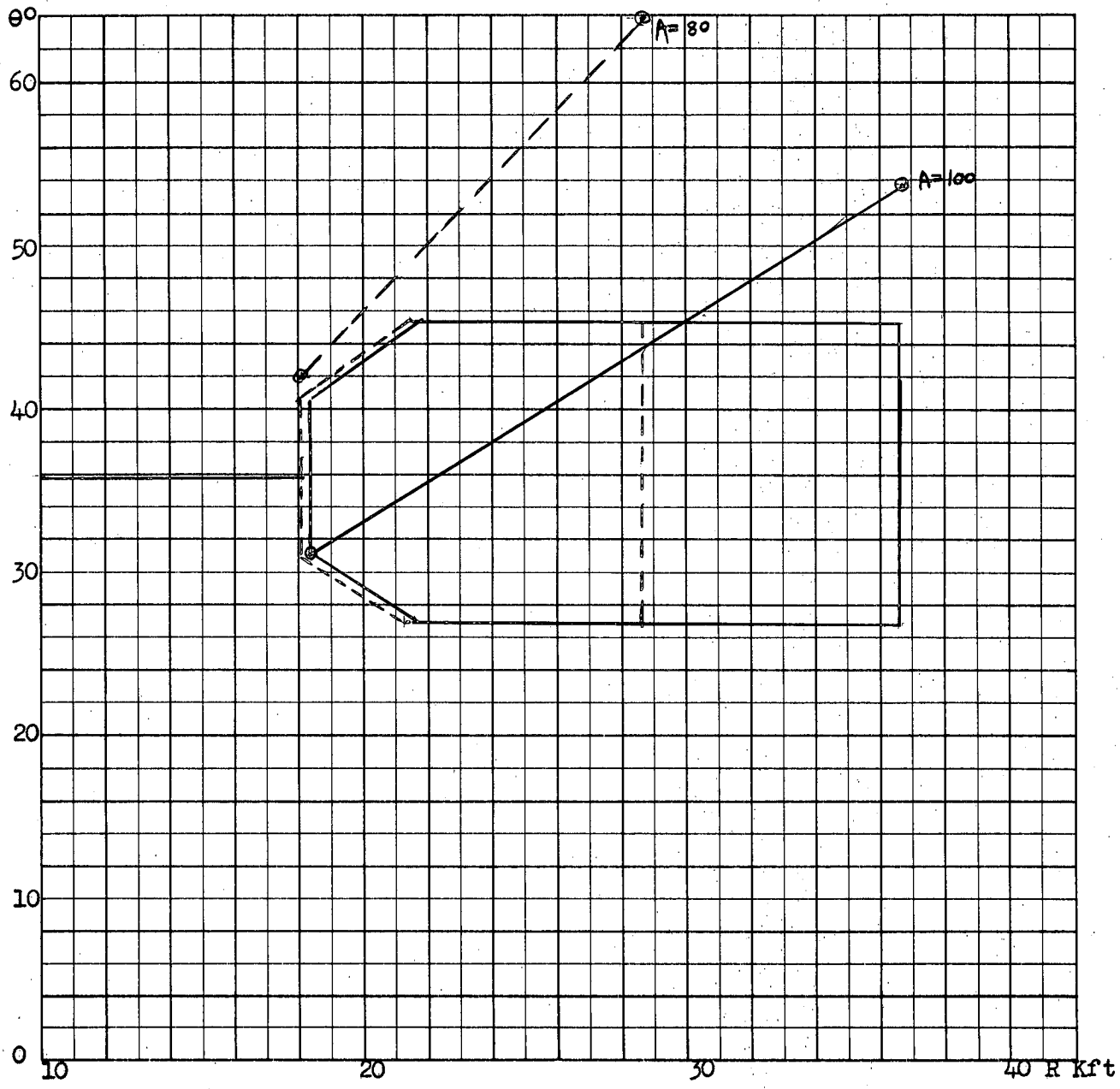

2(c) (ii) A=80, 100

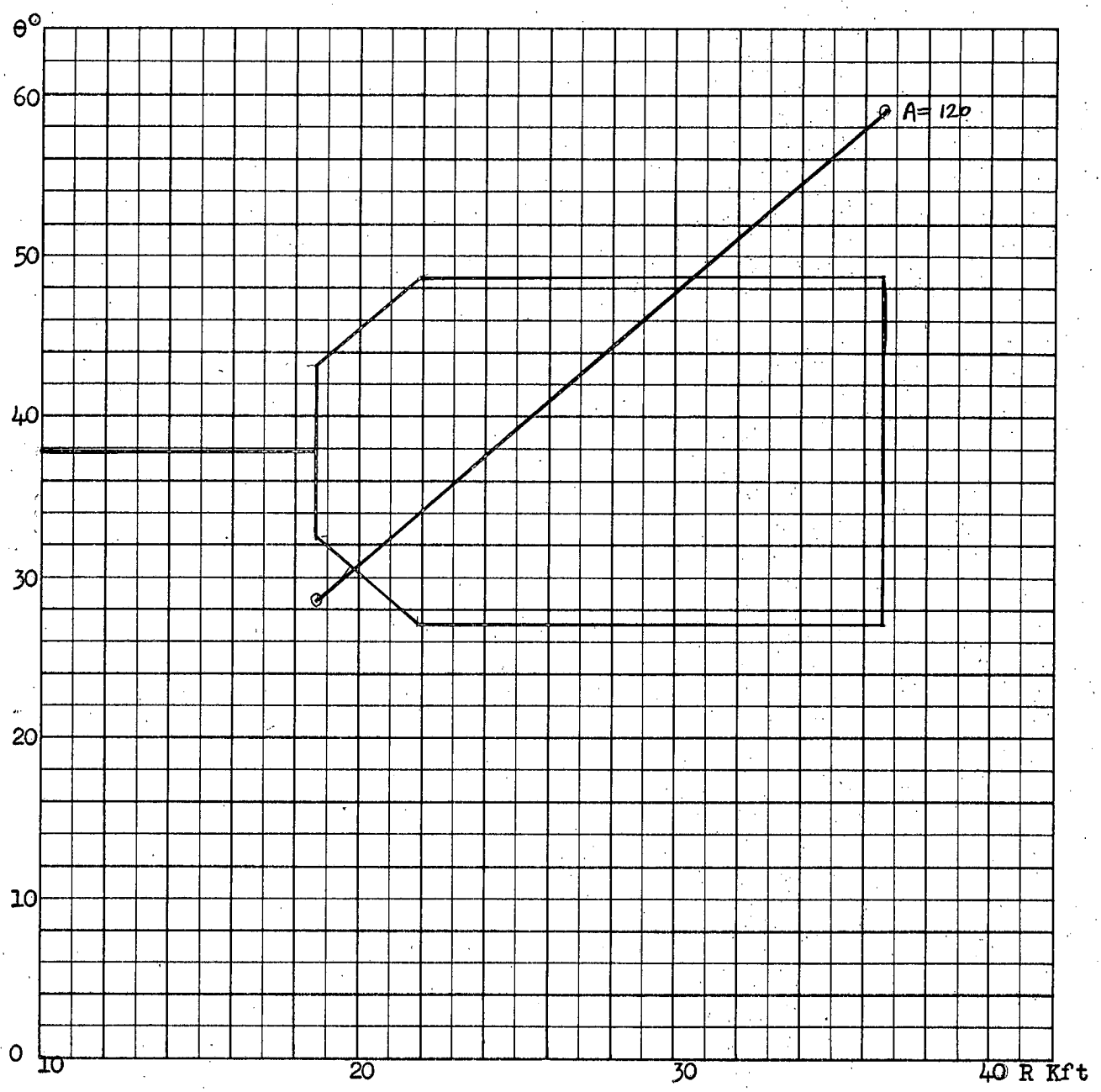

2(d) H=50K (i) A=120 V_T=1942 V_F=1456.5 .

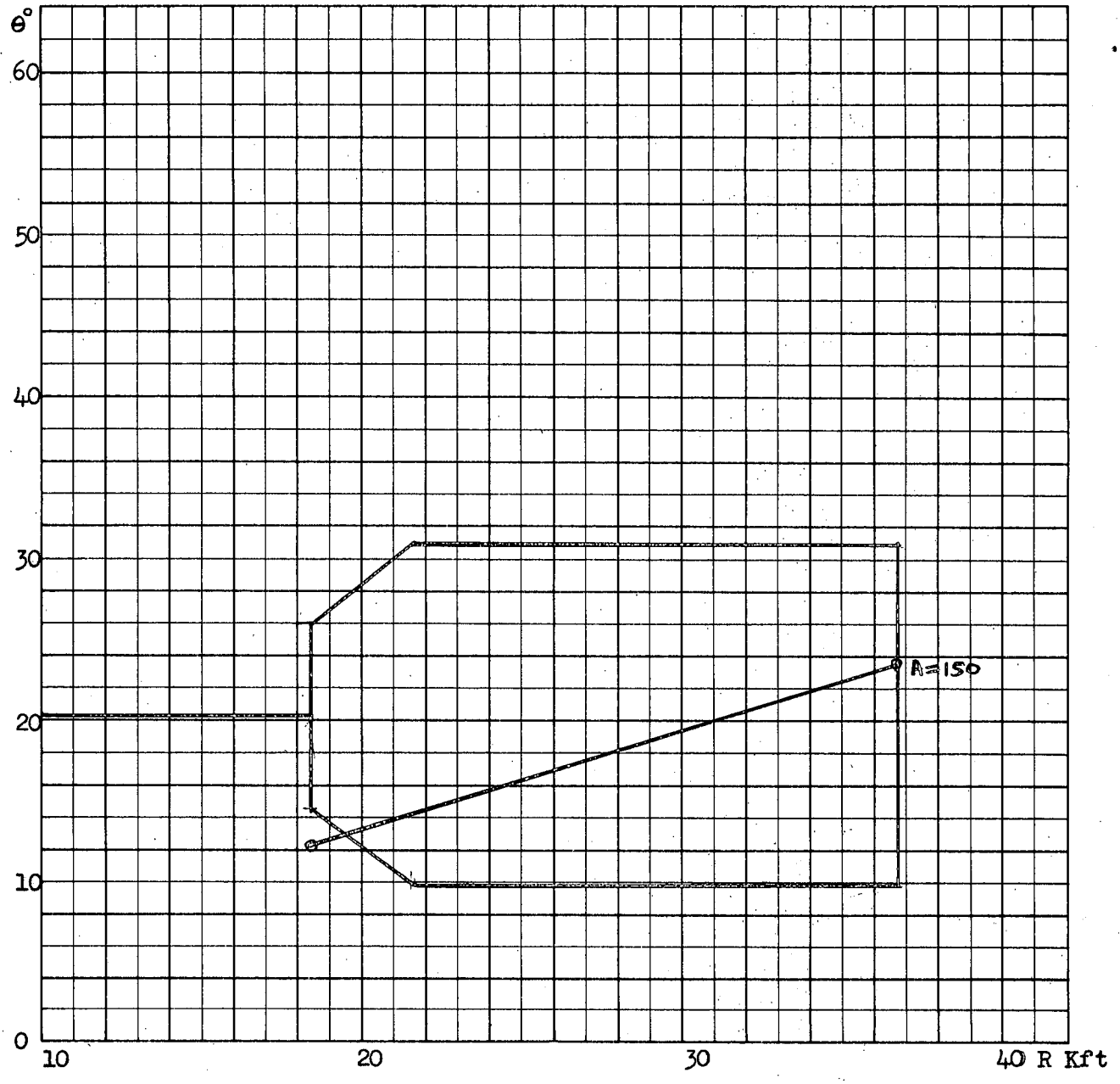

2(d) (ii) A=150

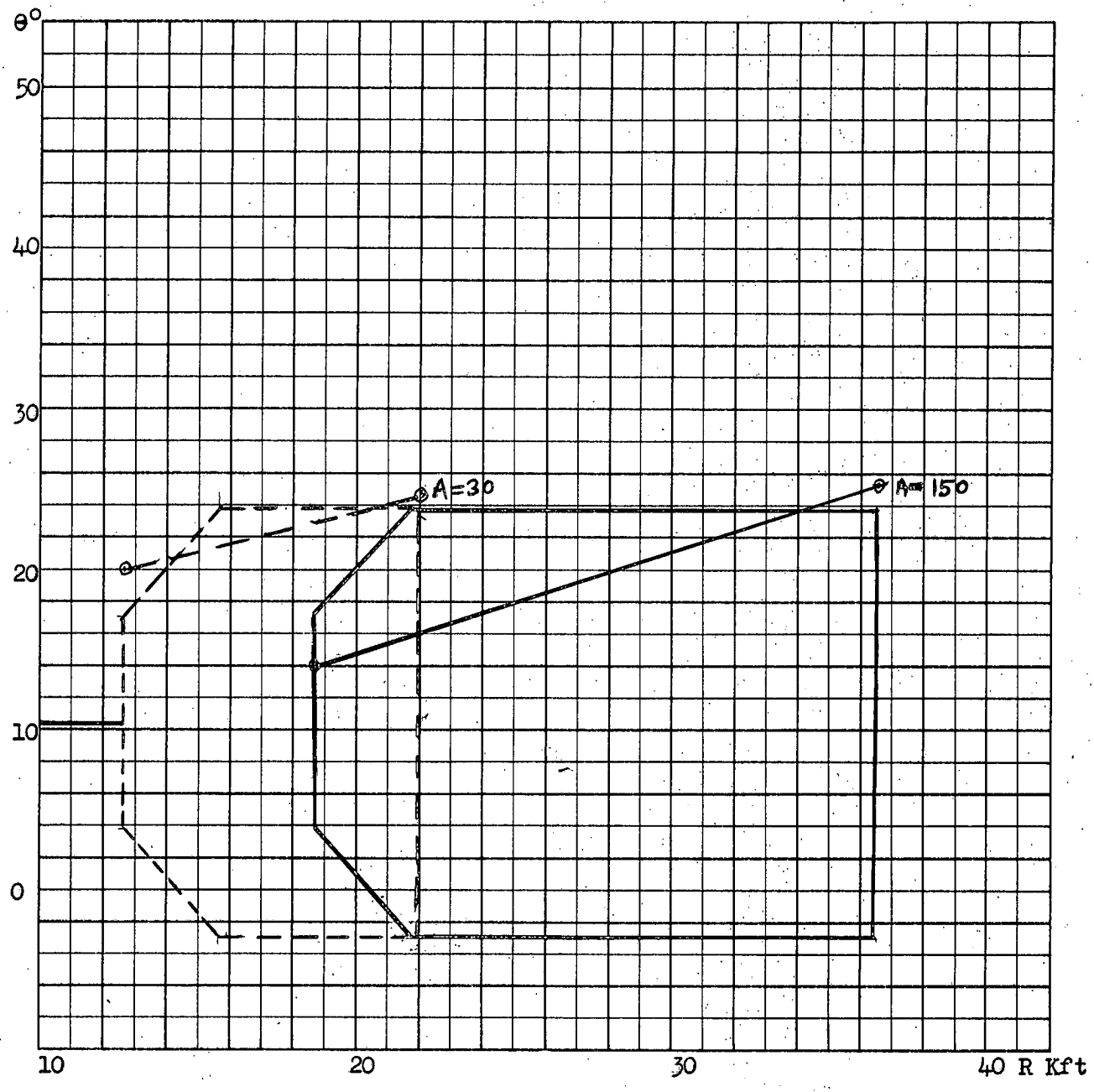

2(e) H=50K (i) A=30, 150 V_T=825.35 V_F= 893.32

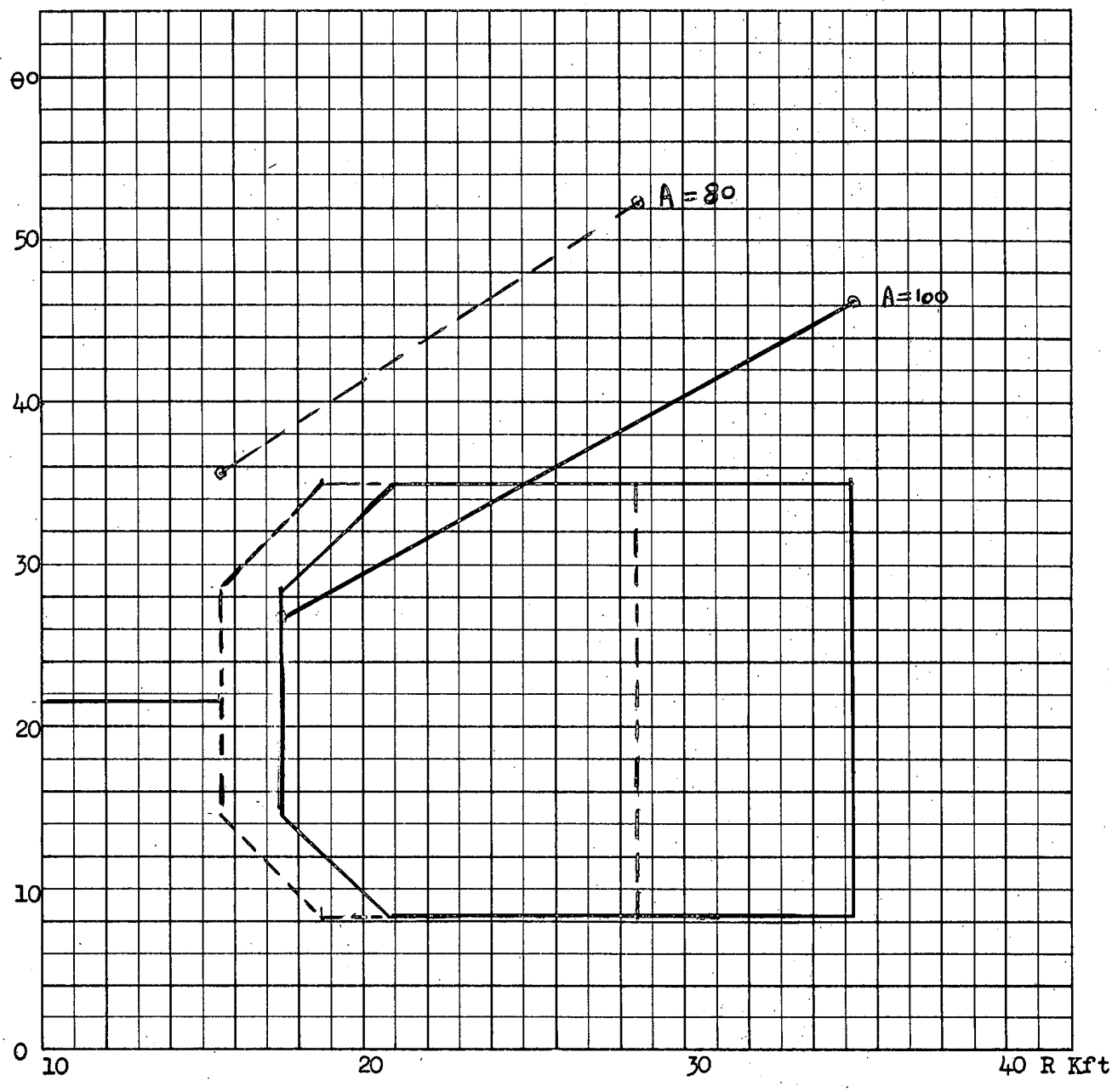

2(e) (ii) A=80, 100

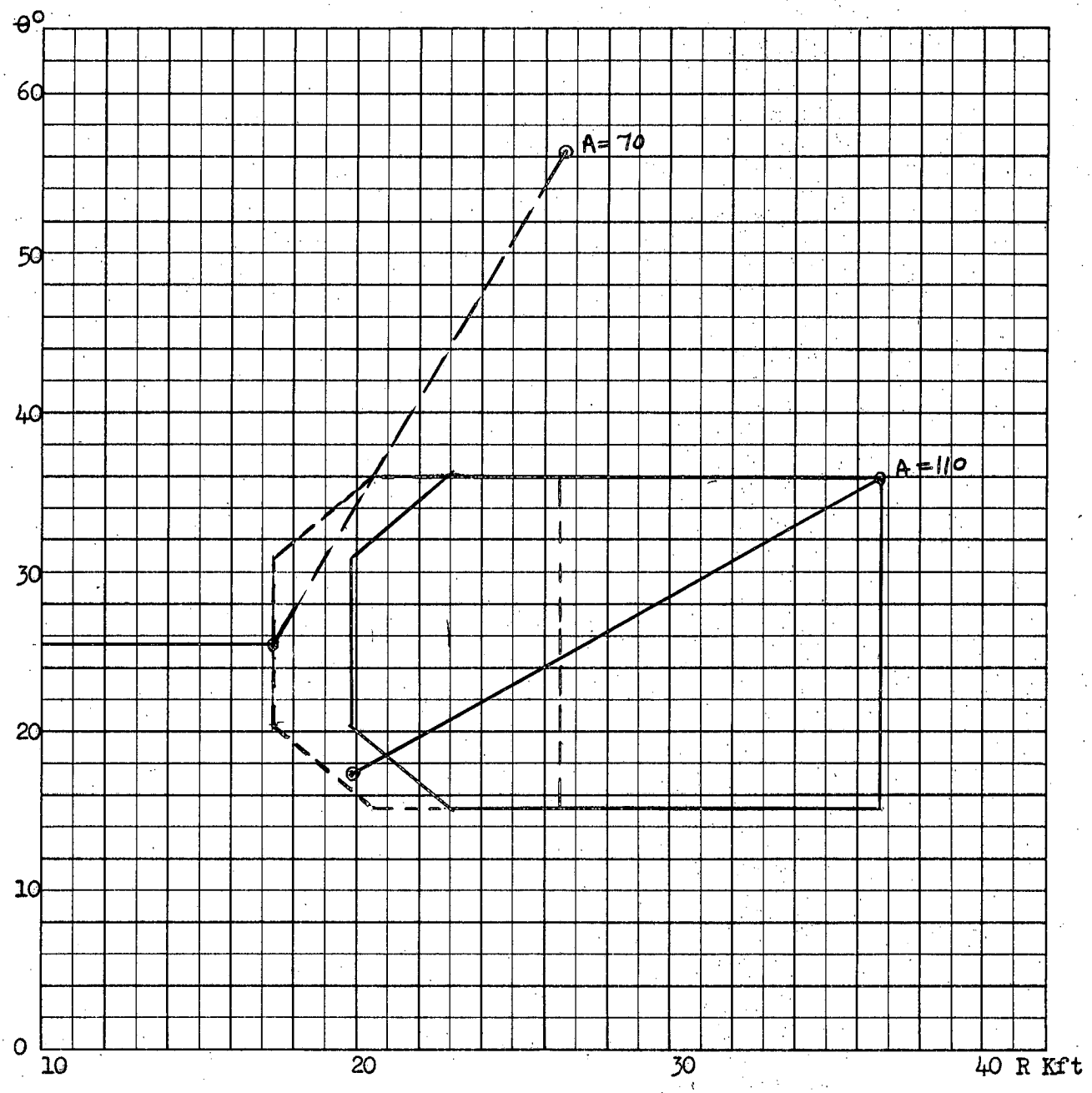

3(a) H=60K (i) A=70, 110 V_T=1456.5 = V_F

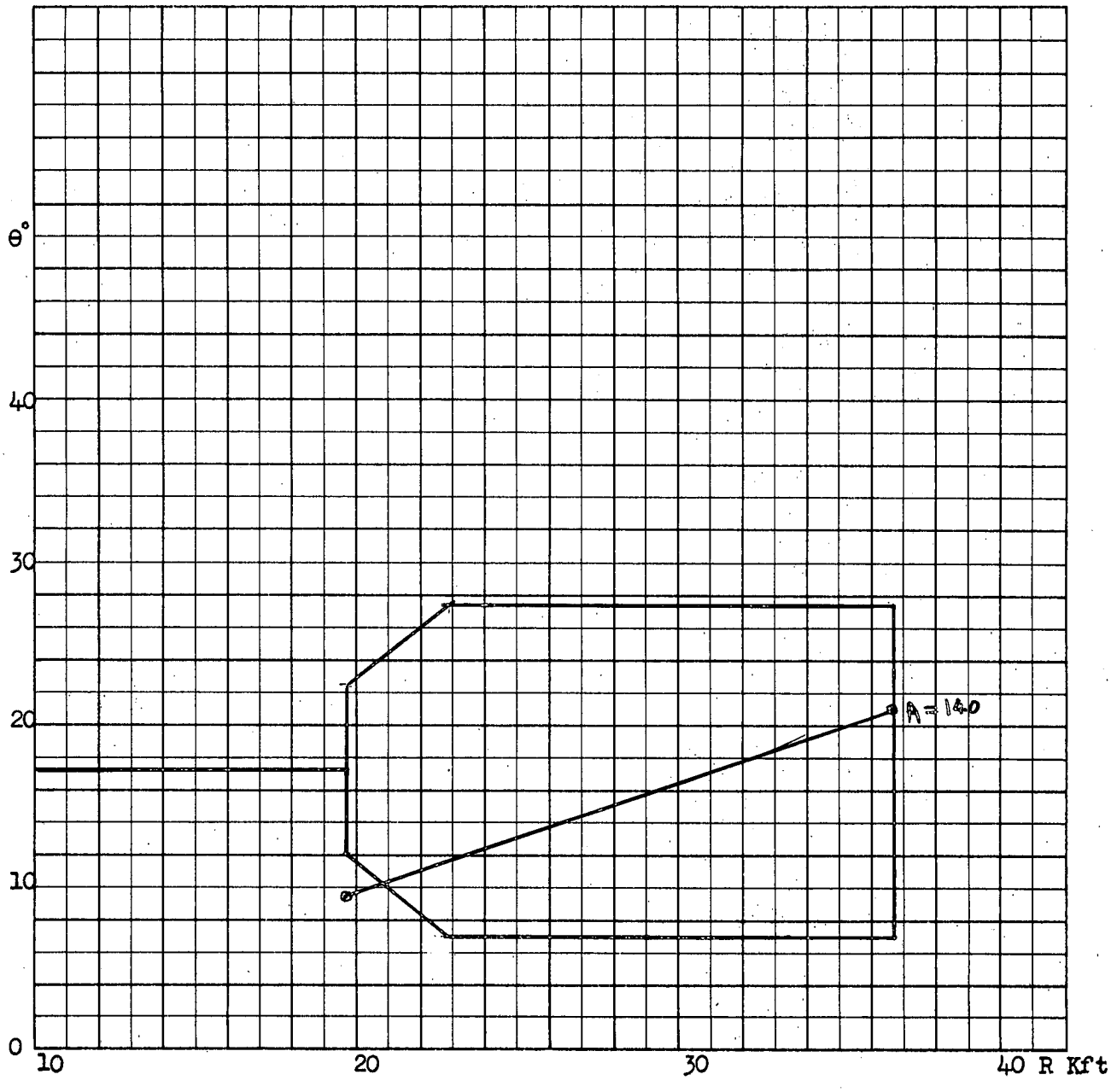

3(a) (ii) A=140

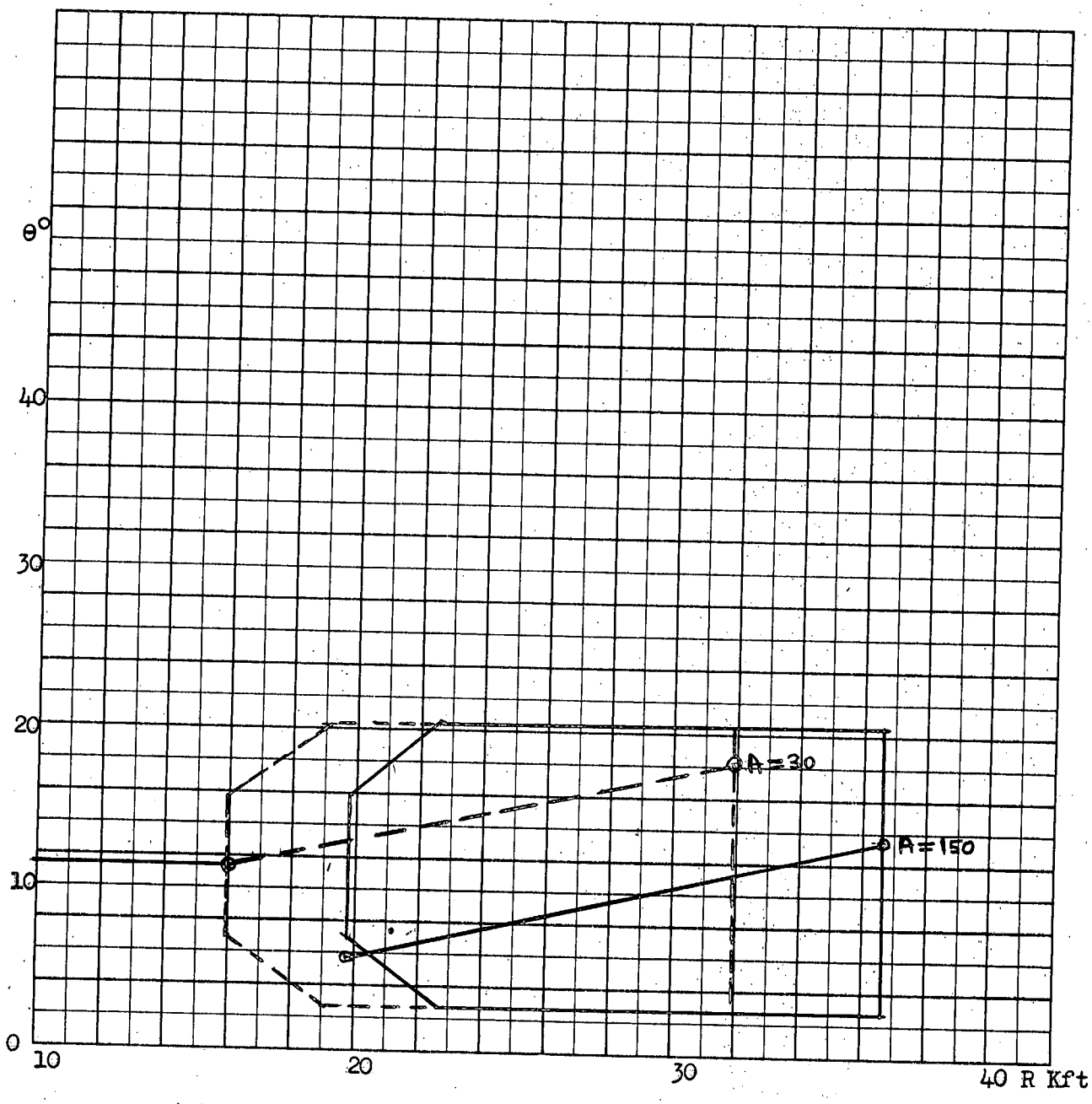

3(b) H=60K (i) A=30, 150 V_T=1456.5 V_P=1942

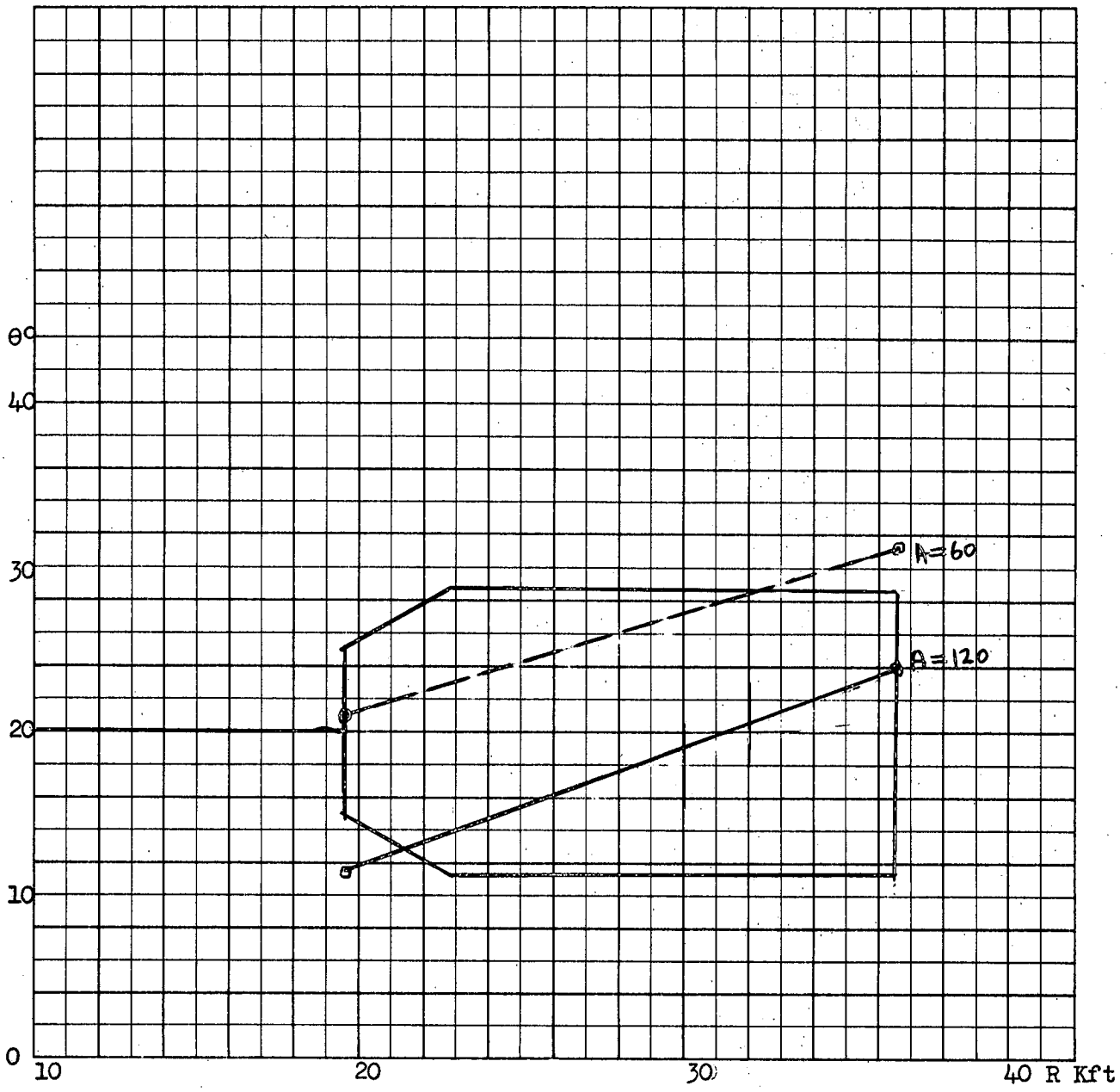

3(b) (ii) A=60, 120

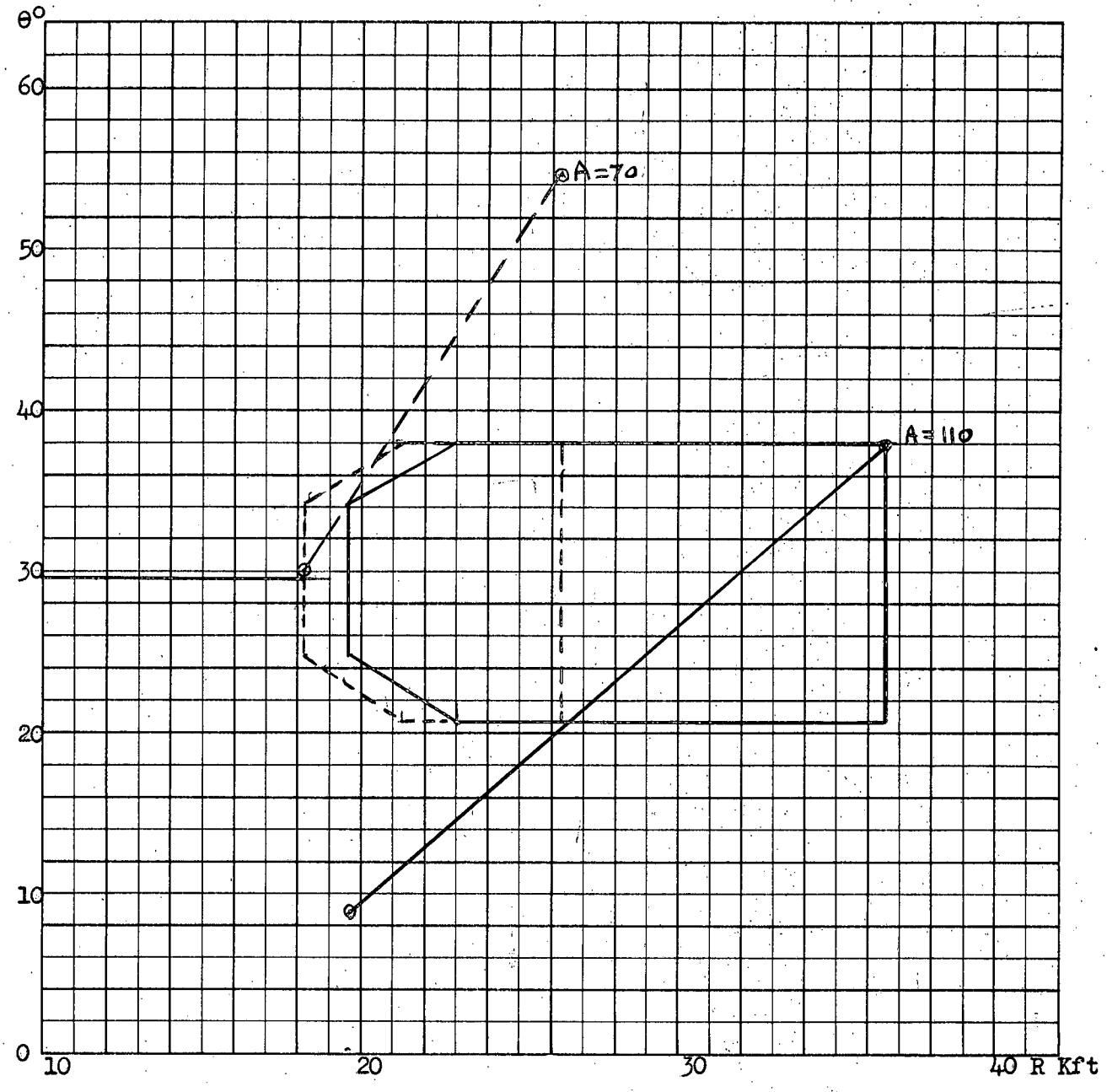

3(c) H=60K (i) A=70, 110 V_T=1942 = V_F

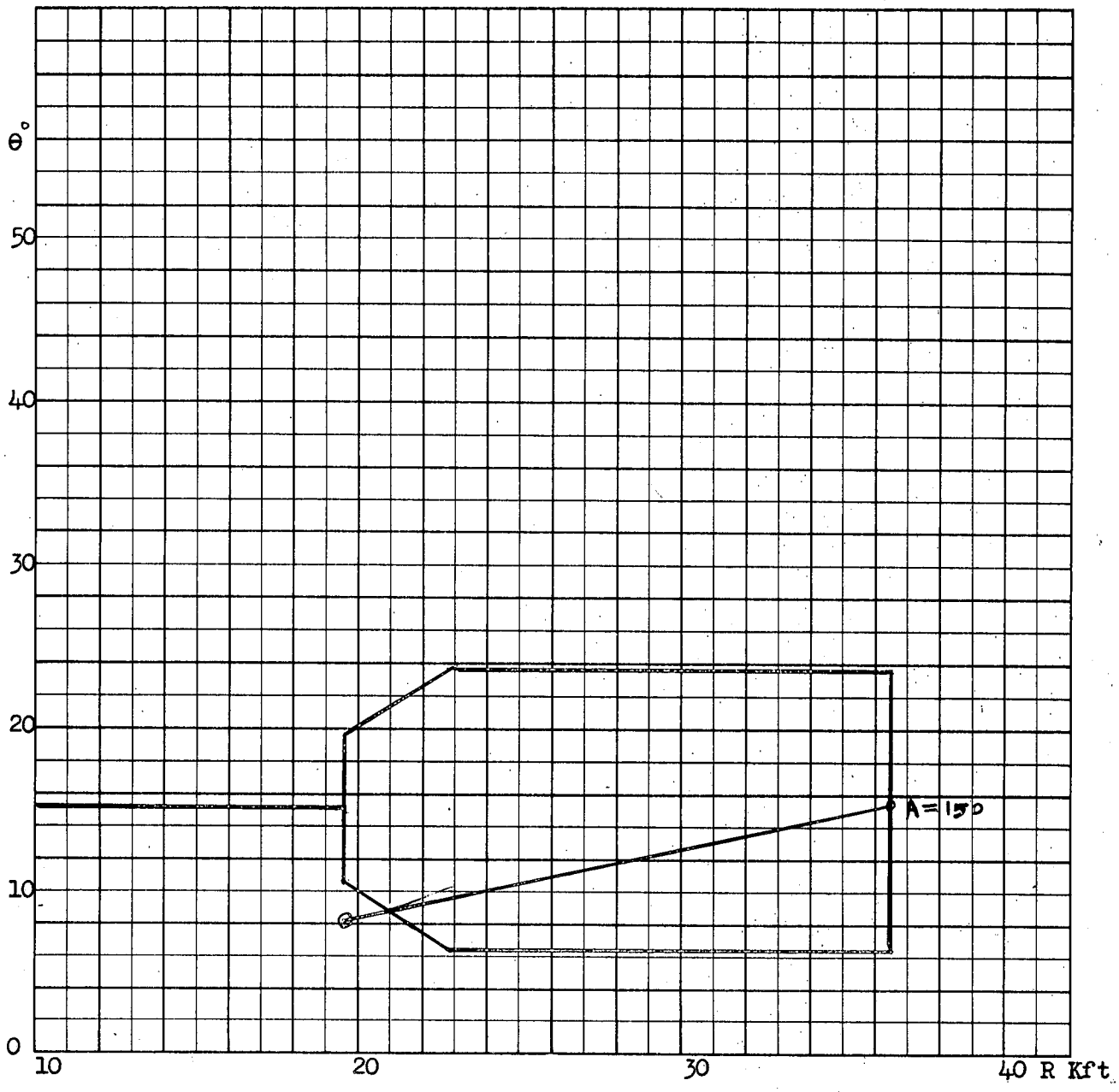

3(c) (ii) A=150

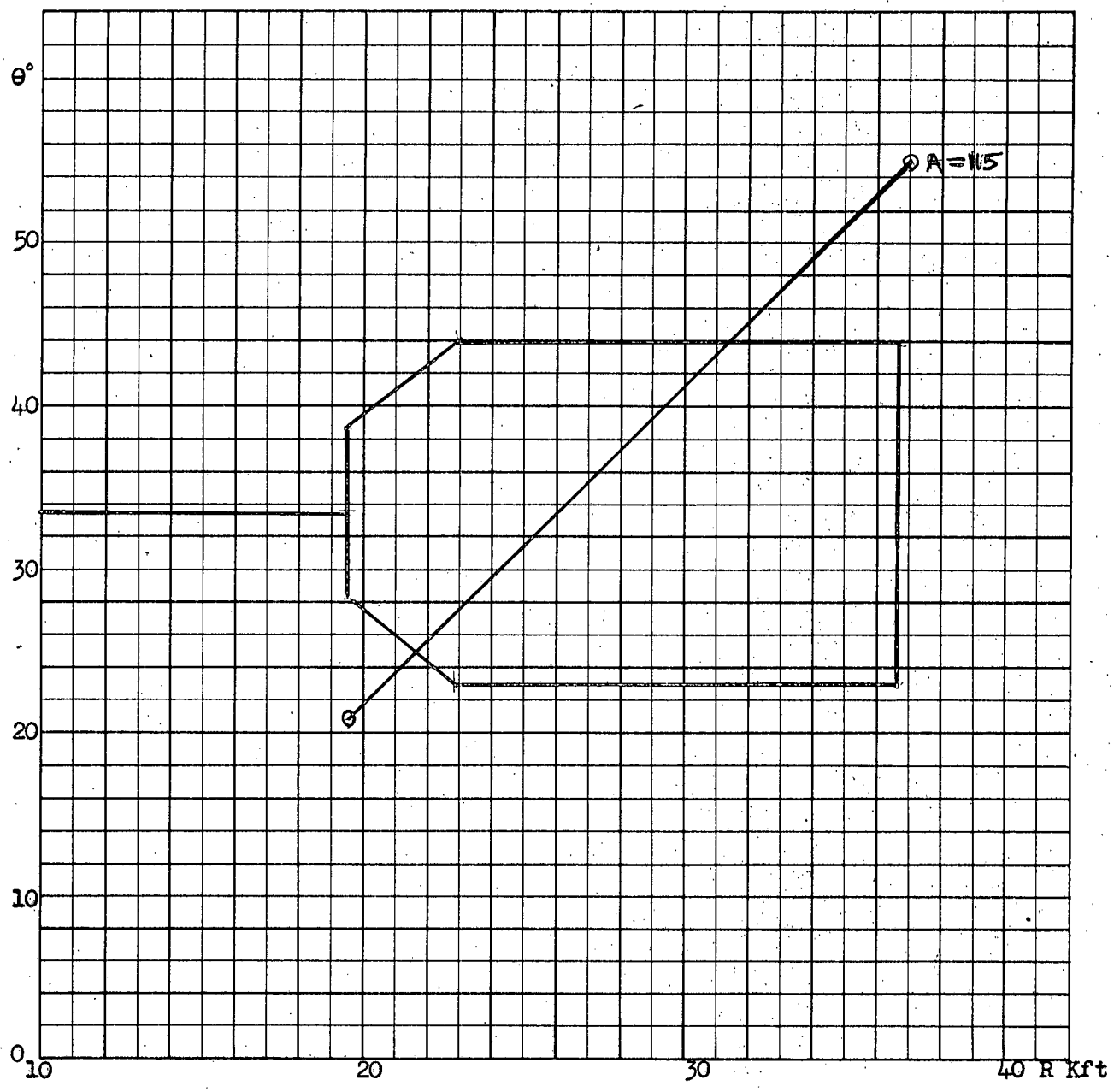

3(d) H=60K (i) A=115 V_T=1942 V_F=1456.5

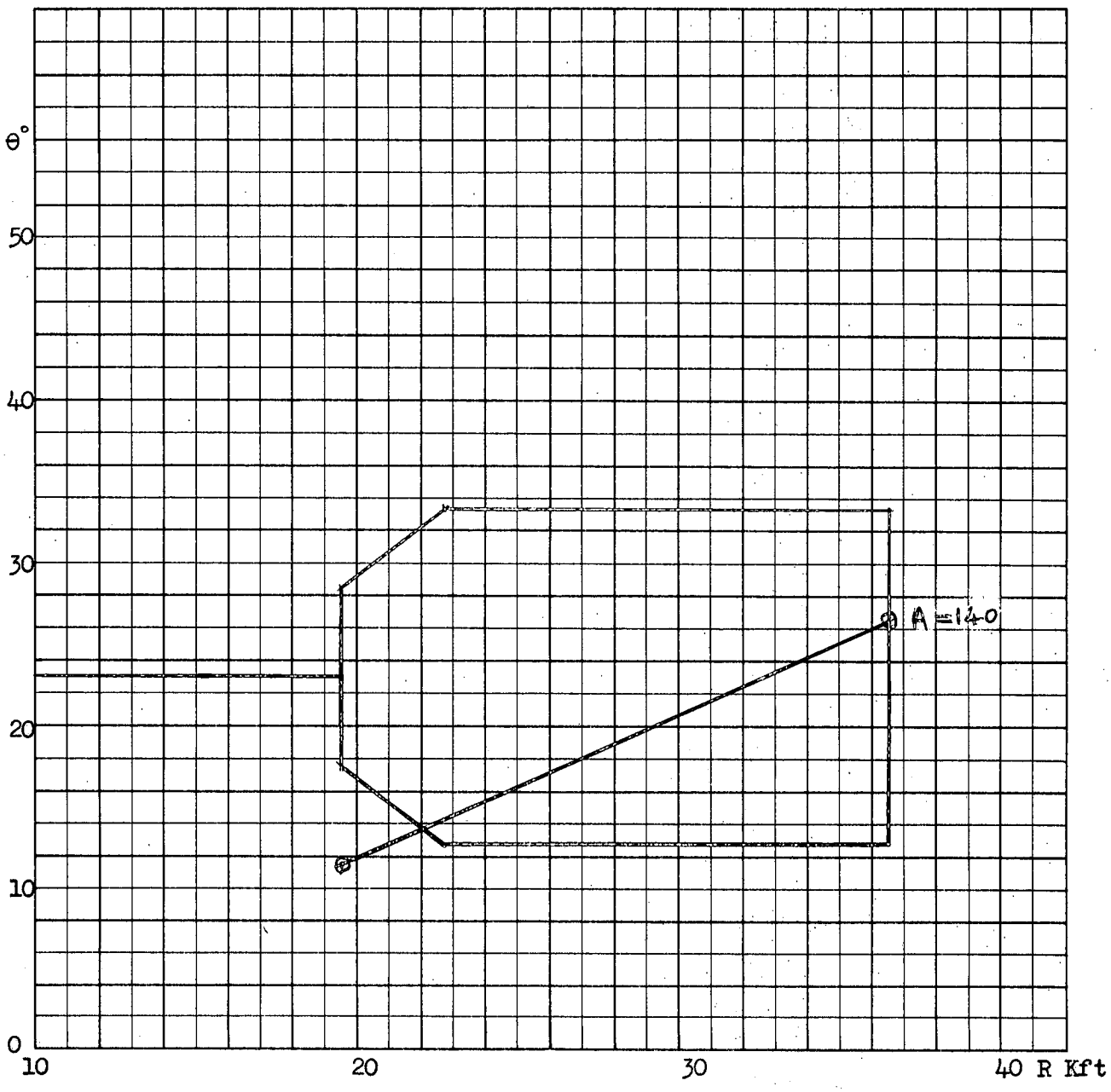

3(d) (ii) A=140

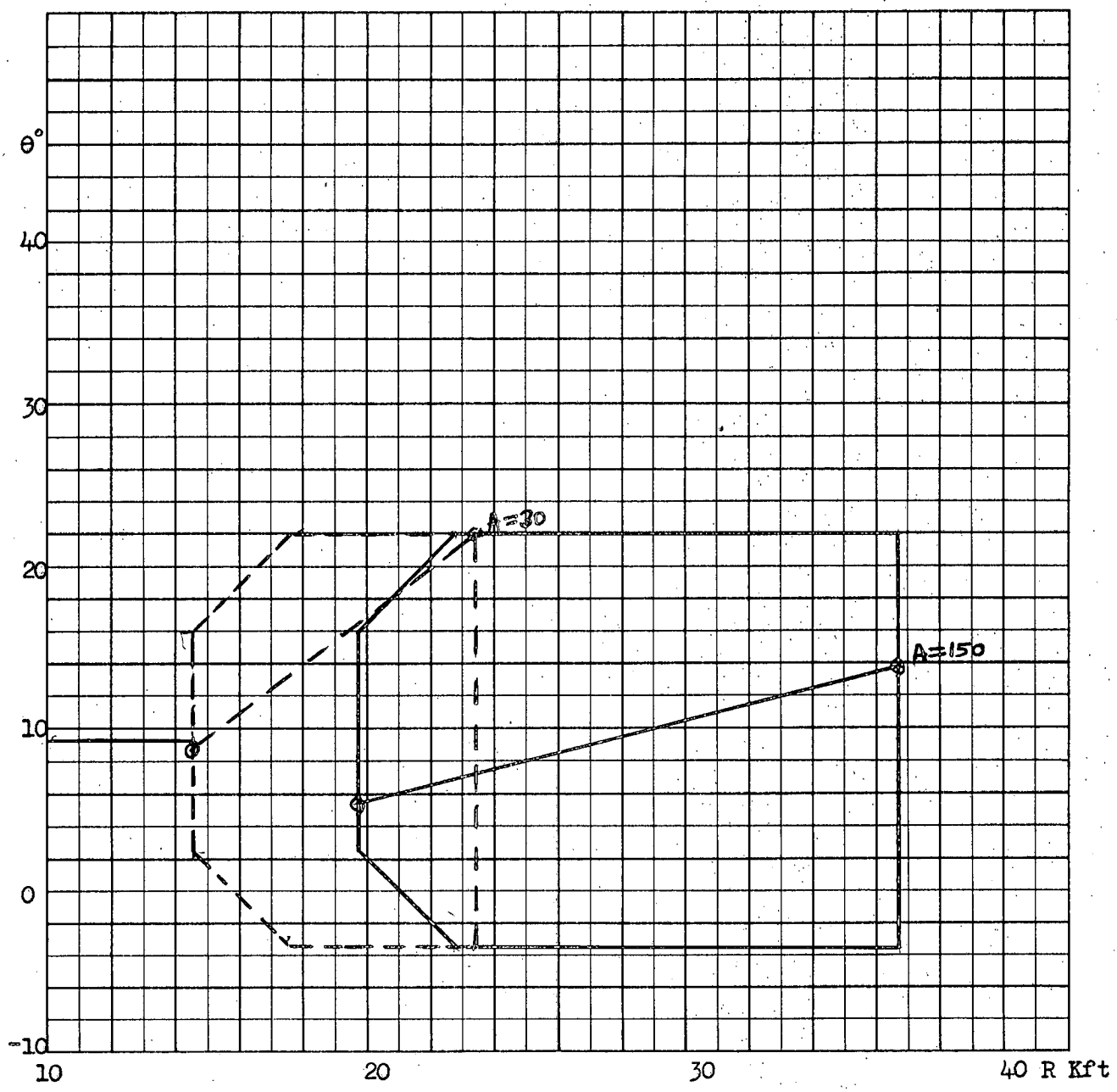

3(e) H=60K (i) A=30, 150 V_T=825.35 V_F=893.32

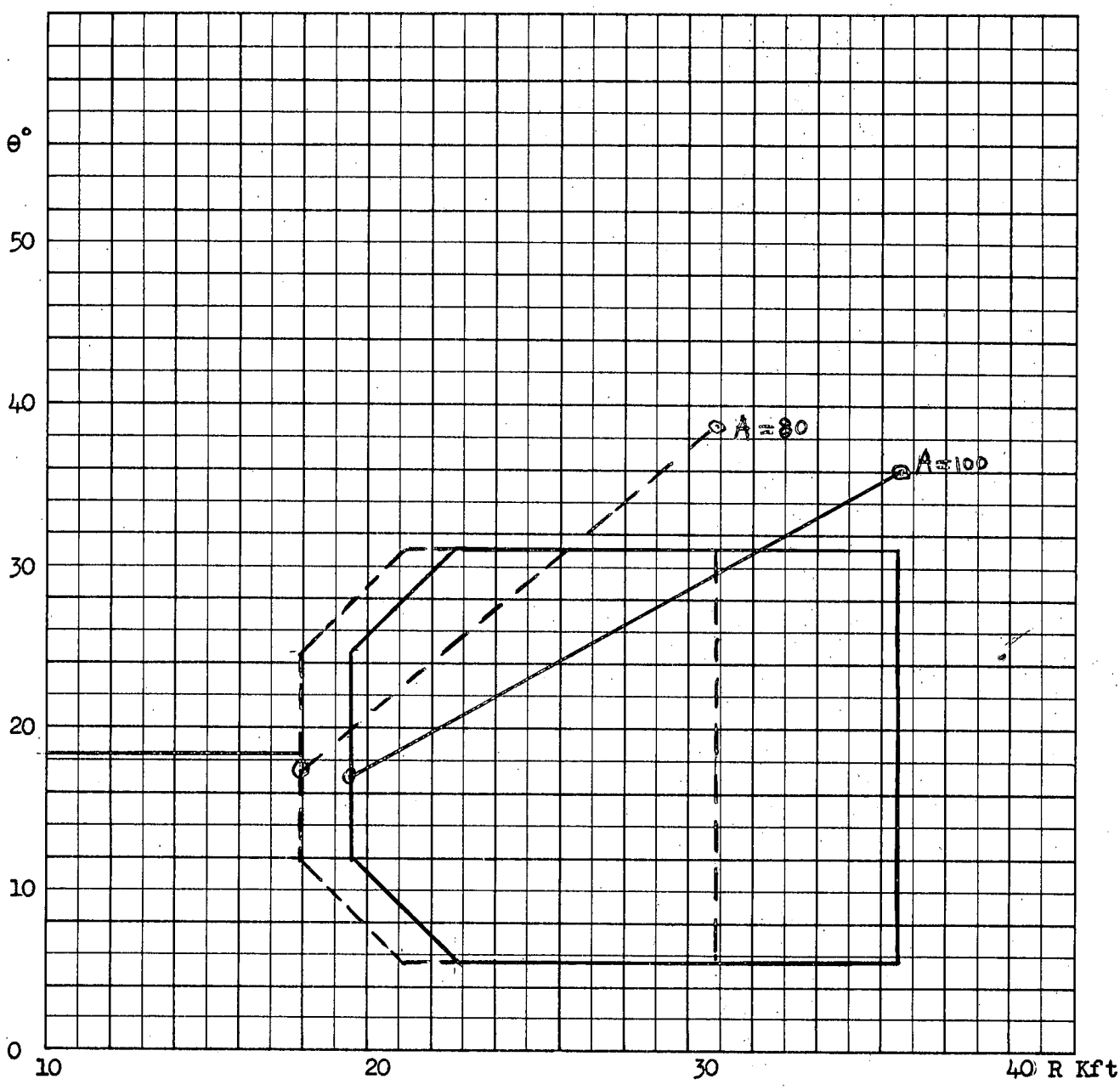

3(e) (ii) A=80, 100

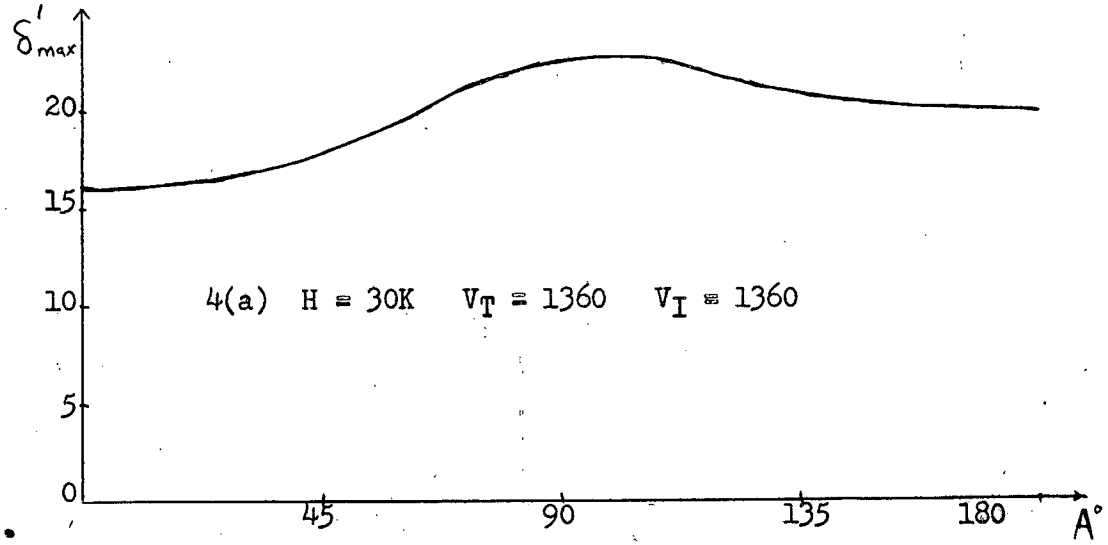

4(a) H = 30K V_T = 1360 V_I = 1360

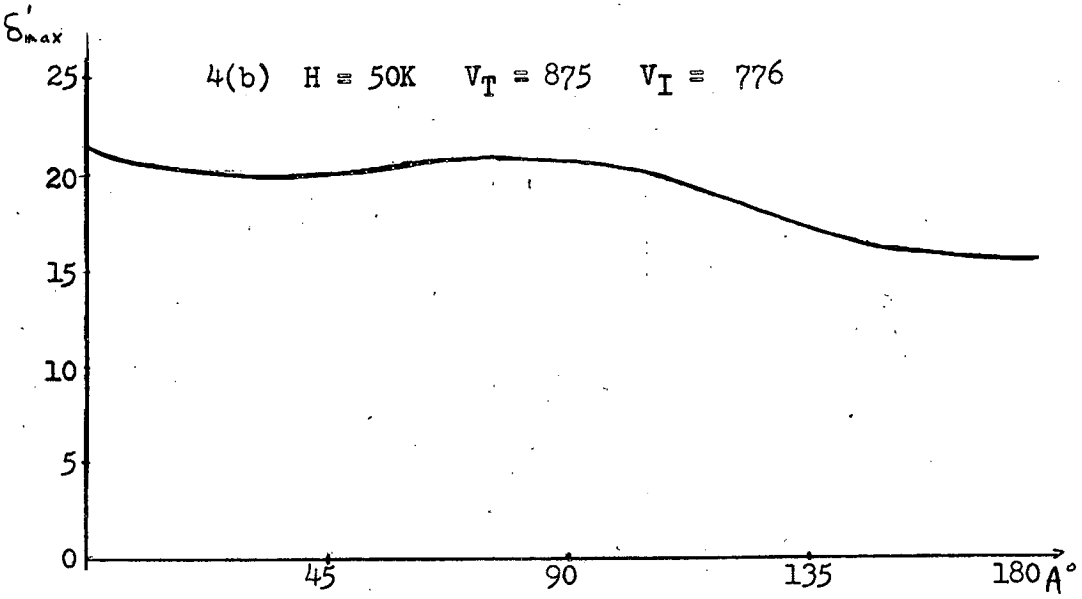

4(b) H = 50K V_T = 875 V_I = 776

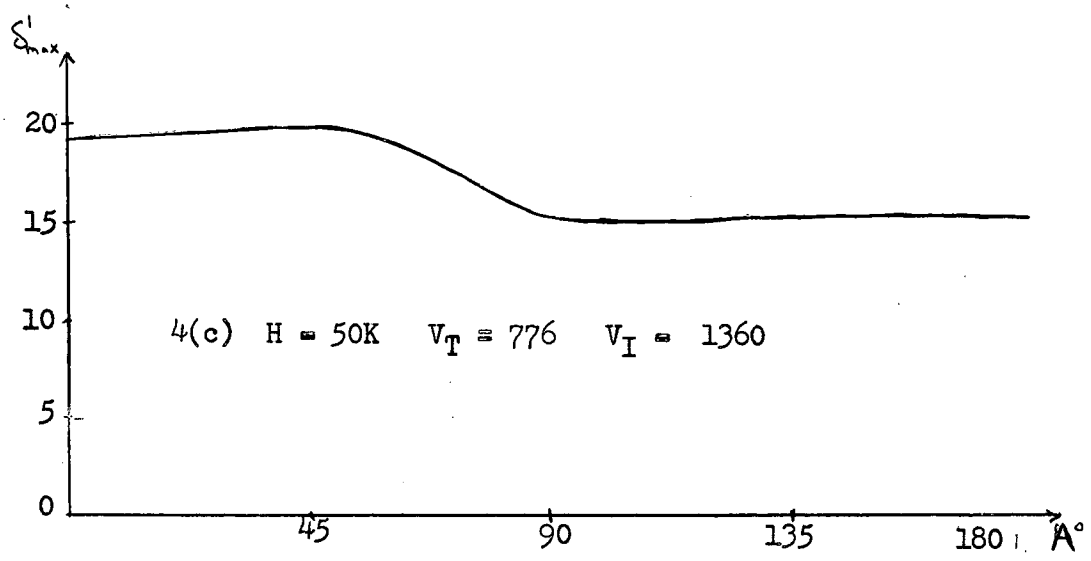

4(c) H = 50K V_T = 776 V_I = 1360

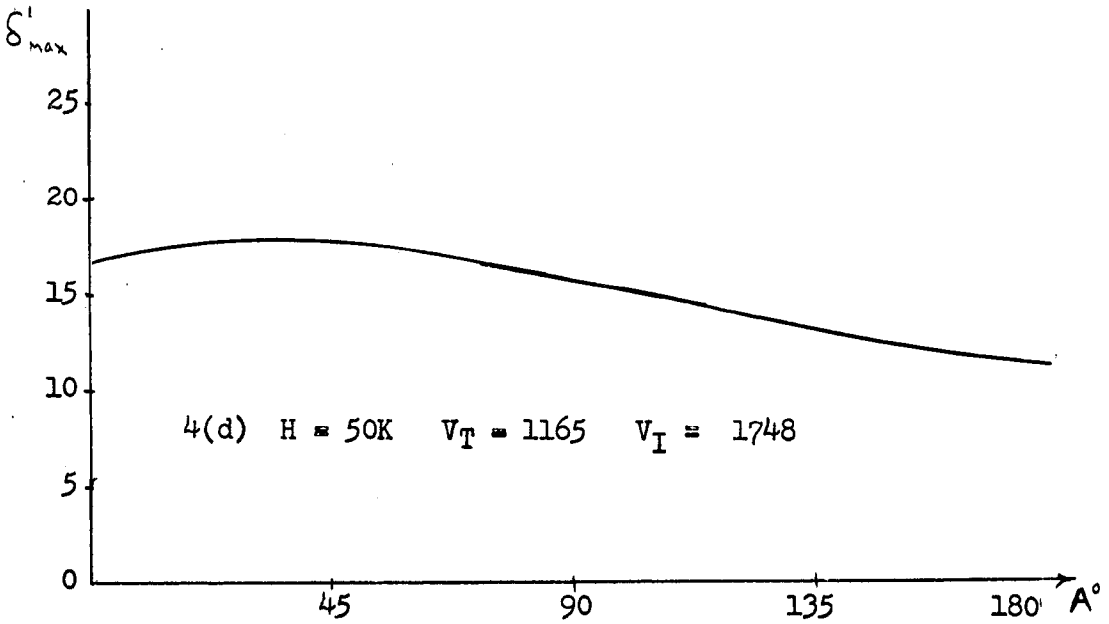

4(d) H = 50K V_T = 1165 V_I = 1748

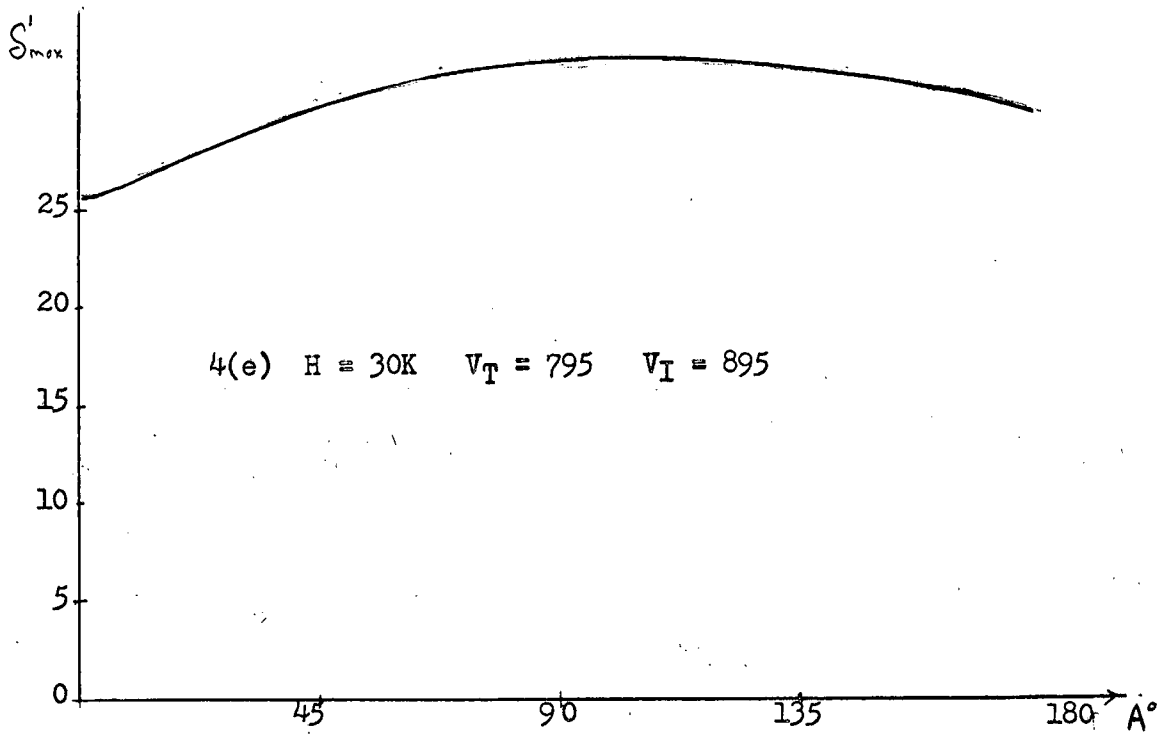

4(e) H = 30K V_T = 795 V_I = 895

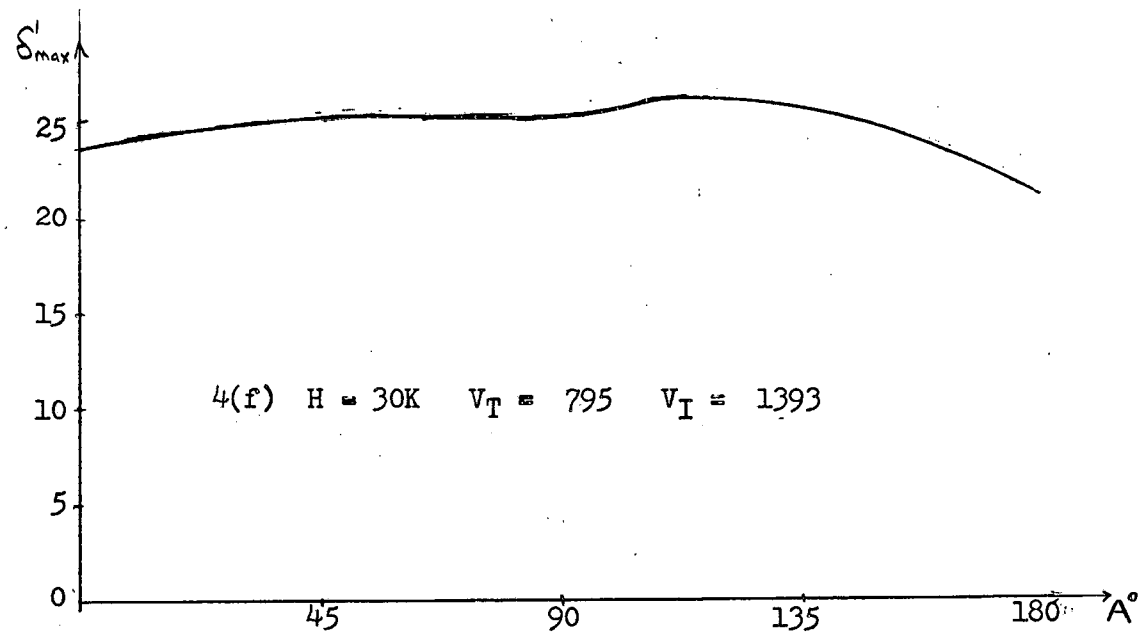

4(f) H = 30K V_T = 795 V_I = 1393

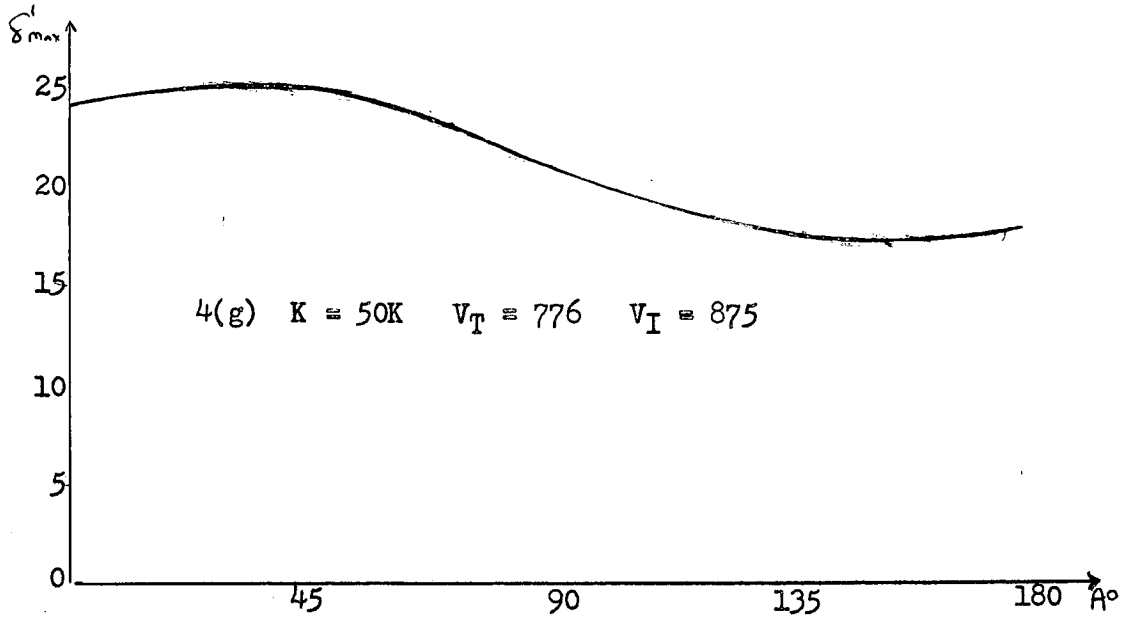
δ'_{max}
25
20
15
10
5
0
45
90
135
180
A°
4(g) K = 50K V_T = 776 V_I = 875

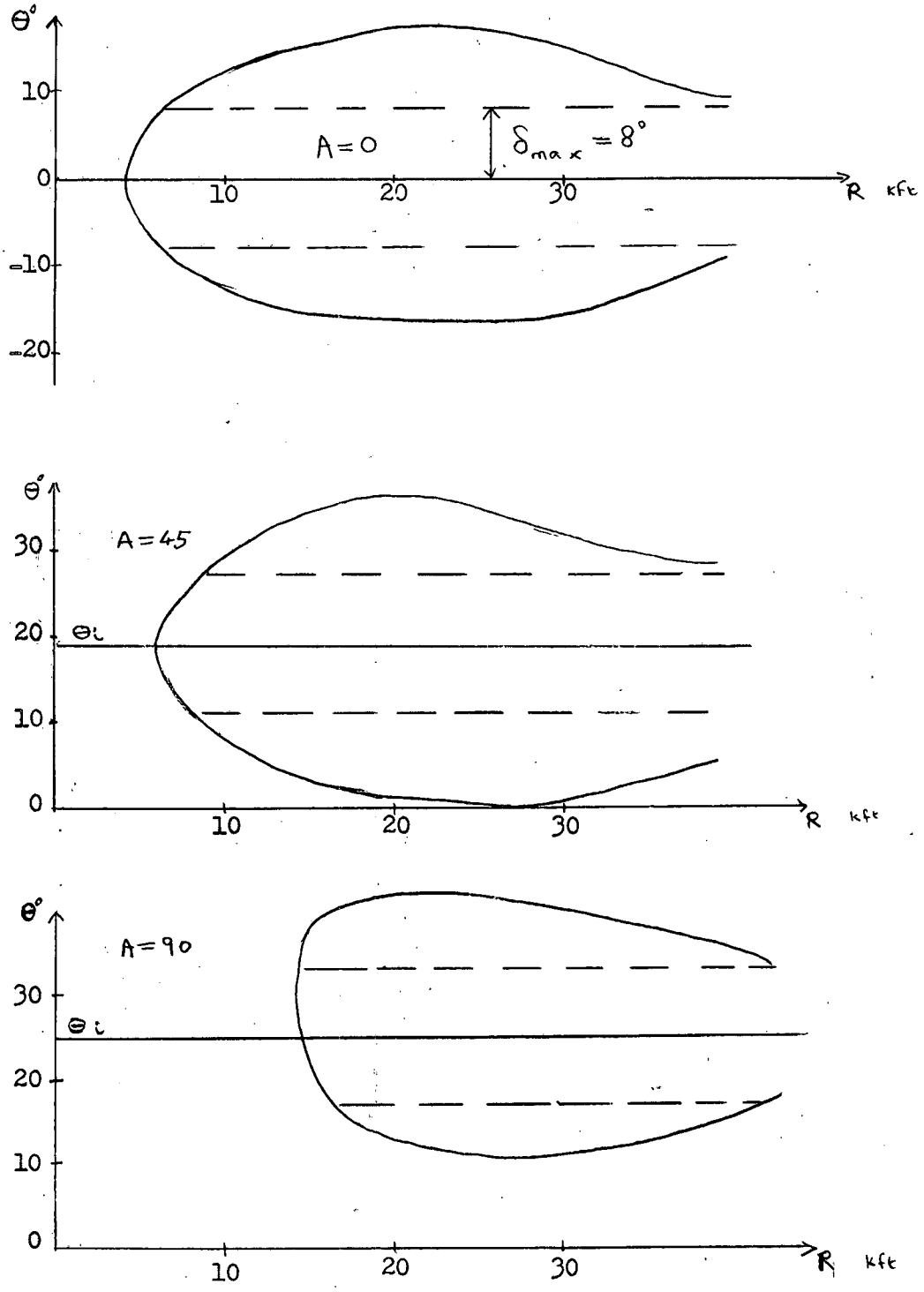

Figure 5. H = 50K V_T = 1165 V_I = 1748 $\delta_{max} = 8^\circ$

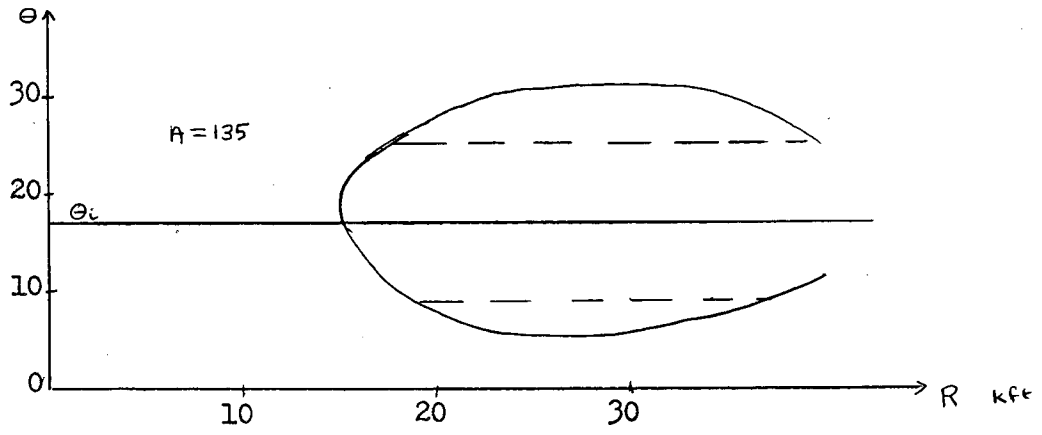

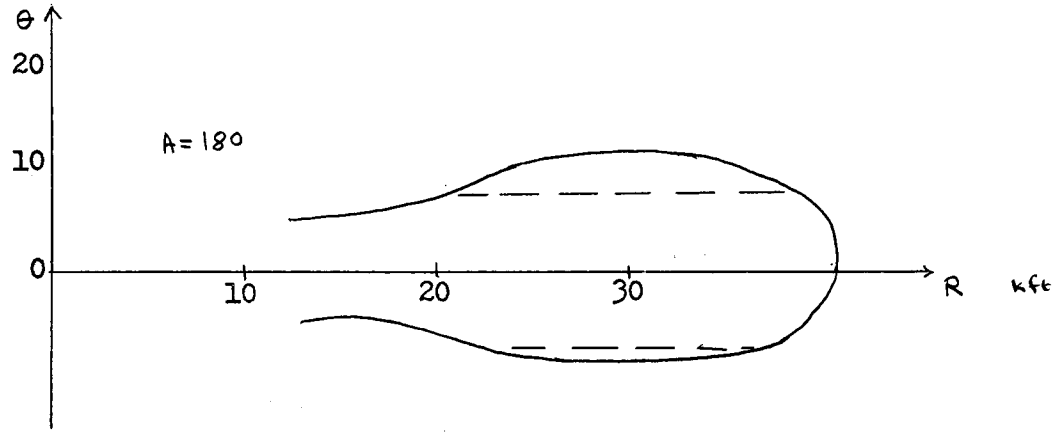

Figure 5. H = 50K V_T = 1165 V_I = 1748 δ_{max} = 8°

Appendix "K"

REPORT OF ECM DISCUSSIONS WITH RCA AIRBORNE SYSTEMS LAB.

by

F. Slingerland,

J.-P. Regniere.

1 INTRODUCTION

This appendix is a report on discussions held at RCA, Airborne Systems Laboratory, Waltham, Mass., on Nov. 18-21, regarding ECM threats and the ECM vulnerability of the Astra I system.

The following RCA representatives were present:

Mr. John Daelhousen	-	Head of A.S.L.
Dr. Werner Sievers	-	A.S.L.
Mr. David Wellinger	-	A.S.L.
Mr. Earl Blanchard	-	A.S.L.
Mr. Earl Masterson	-	Fire Control Engineering, RCA Camden

The Canadian representatives were:

Capt. James Morris	-	USAF/RCAF/DArmEng.
Mr. J.P. Regniere	-	Guidance Group, CARDE.
Mr. F.W. Slingerland	-	Systems Group, CARDE.

Attachment "A" is a copy of the Canadian visit request, and outlines the purpose of the visit in more detail.

2 CCM FEATURES OF ASTRA I

Not all of Astra's anti-jam features were discussed. The following is an outline of the main topics covered:

2.1 A.G.C.

The dynamic range of the Astra AGC is quoted as 120db. 30 db of this is achieved by current-controlled ferrite attenuators in the r.f. section. Camden are confident that they will better the quoted figure of 120 db and expect to achieve approximately 130 db. This dynamic range is required primarily to handle normal target echoes at short range, as can be seen from RCA's estimates of cross-over ranges against various jamming threats.

The AGC sample is taken after the video stage. The problem of obtaining AGC action on CW or pulsed jamming is solved by pre-gating the video input after the second detector, as shown in Figure 1.

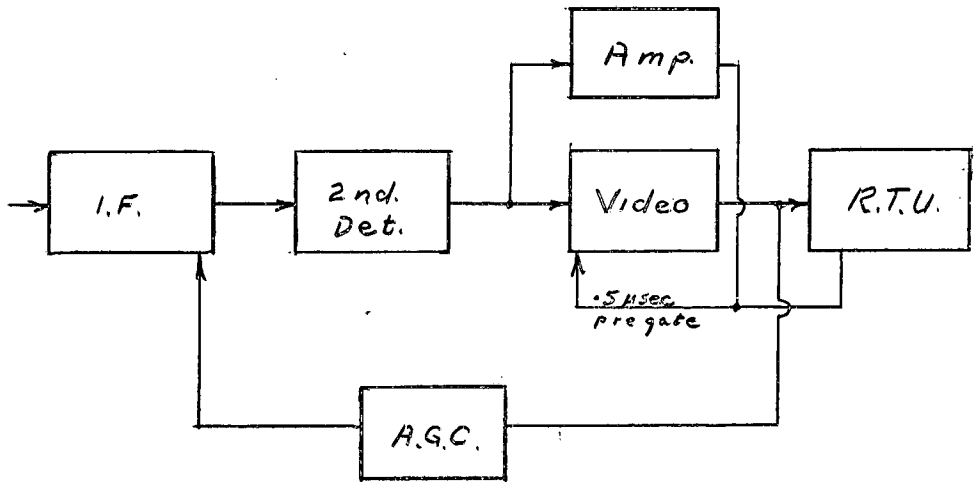

Figure 1 - Pre-gating Circuit.

The loop response of the AGC circuit is approximately as shown in Figure 2.

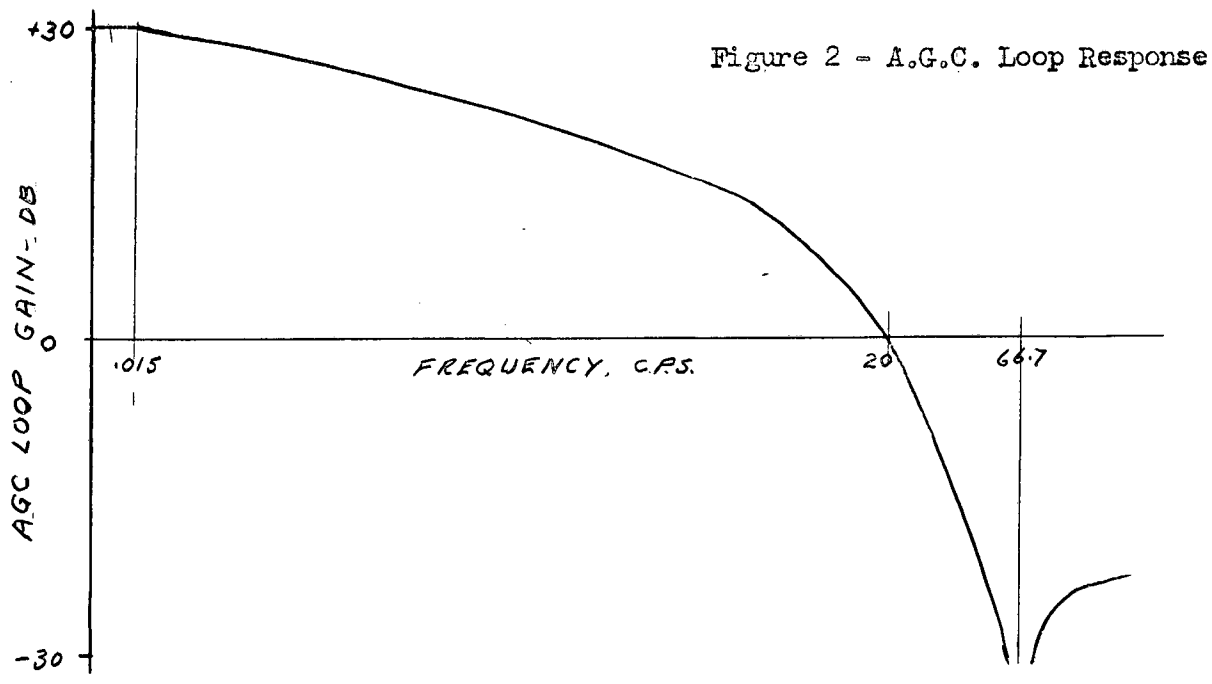

Figure 2 - A.G.C. Loop Response

It will be noted that the loop has relatively fast response for a conically scanning system and it appears that this may nullify the potential advantages of pulse edge tracking. Let it be assumed, for instance, that there is a region near the target's beam in which pulse edge tracking would normally be useful in helping the range rate memory to prevent chaff break lock. In this region the chaff echo becomes relatively large while still within the range gate. At first, video clipping will hold the chaff signal at the same level as the target echo. However, within about 1/20 second the AGC will respond to the growing chaff echo and the true target echo will be depressed into the receiver noise level. The edge tracking circuits will now pull over to the edge of the chaff cloud and carry the range gate off on the cloud. It appears preferable to slow down the AGC response, allowing the IF to saturate if need be until the chaff passes out of the range gate. During the period of IF saturation the range gate would coast on $\dot{R}$ memory, and on IF desaturation would still be locked on the true target. If no saturation occurred, video clipping and pulse edge tracking would prevent break lock.

There may be other more cogent reasons for having relatively fast AGC response, and the process of chaff break lock is not easy to delineate. However, it is suggested that compatibility of pulse edge tracking and "fast" AGC warrants further examination.

2.2 Angle Tracking

The Astra tracking loop is gyro stabilized and rate-aided, with a time constant between one and two seconds. The conical scan frequency will be fixed at 66-2/3 cps for all Arrow aircraft, being obtained by counting down from the 400 cps supply. This renders all Astra systems simultaneously vulnerable to a rather simple form of conical scan foxing as will be discussed in section 3.3.

Camden have achieved successful passive angle tracking of a "White" noise source. No measurements of angular rate noise have been made under such conditions. However, it was believed that angle tracking of a single jammer should be smoother than echo tracking because of the presence of a strong signal, and the absence of angle and amplitude scintillation and a.m. noise from range tracking loop. In multiple target situations passive tracking would probably be poorer than active tracking because of the poorer angular discrimination of the one-way antenna gain pattern in the passive mode.

2.3 Crossover Ranges

RCA assume that a target echo can be seen through white noise on an A scope at 0 db signal-to-jamming ratio. However, a 7db signal-to-jam ratio is needed for lock-on.

2.4 Ranging Methods in ECM

2.4.1 Quasi-passive Ranging

This device was first developed by RCA for WADC and was

described in a report entitled "New Techniques and Components for Air Defence Aircraft" produced by the Airborne Fire-Control Engineering Dept. 580, RCA Camden. It has been described in various Astra progress reports and consists of gating the radar on for 50 millisec, off for 2 sec. with random frequency shift during the off period. The technique is effective against present day spot jammers and may also be effective against repeaters which normally are held off for 50 - 100 ms. when painted to avoid triggering on searching radars. It is also effective in preventing passive analysis by such search receivers as the APR-9. It is obviously not effective against wide-band barrage jamming. Some independent means of angle tracking is required since the active angle track circuits cannot operate on such a low duty cycle. As originally developed for ADC, the system acquired the target by sampling seven 1-μsec gates, and acquisition ranges were comparable with those of normal acquisition. However, the Astra system will use a single wide gate to avoid complexity and in so doing will sacrifice acquisition range because of the higher noise levels involved. The learning of $\dot{R}$ has been achieved by feeding in an arbitrary initial $\dot{R}$ which is then corrected during the 50 ms. transmission period. Quasi-passive ranging adds an estimated 15 yds. range noise to the normal range tracking errors.

It appears advisable for the navigator to transfer directly from search to QPR on every attack because of the potential advantages in deception gained thereby. The price paid may be a reduction in AI lock-on range, though not in detection range. This can be offset by corrective turns initiated by the navigator before lock-on.

2.4.2 Range Extrapolation*

RCA believe there may be situations in which an initial range is obtained on the jammer before it transmits, with no range thereafter. They have developed a passive ranging computer which extrapolates this range using the equation

$$\frac{d}{dt}\left(R^2 \omega_{los} \right) = - V_i \omega_i \cos L$$

Where ω_{los} = angular rate of the line of sight

ω_i = interceptor's turning rate

V_i = interceptor velocity

L = lead angle

Note that this equation is invalid if the target does not fly straight. The computer has been breadboarded and provides range information correct to 400 ft. if fed with one range input at about 50 miles.

* Planar Simulation of a Passive Ranging Computer (S)
RCA 588-SP7-TM206
R.C. Blanchard

2.4.3 Ground Echo Correlation.

RCA mentioned work done by Fairchild on the "Padar" system which determines the delay between direct jamming signals and the signal forward-scattered from the ground. This, combined with a knowledge of interceptor altitude and line-of-sight elevation angle will provide range. Correlation is difficult because of the multi-path noise on the ground echo. It is achieved by feeding the direct signal to the x plates and the echo to the y plates of an oscilloscope and delaying the direct signal so as to produce a straight line on the scope.

It is difficult to see how this device will work against a continuous jamming signal since it would be somewhat difficult to separate the direct and echo signals so as to correlate them. Also, even if separation is achieved, it is unworkable against anything approaching white noise, which is uncorrelatable. It is CARDE's guess that the system was designed for bomber defence against pulsed signals in which separation and correlation are relatively easy. There is no intention to install such a system in Astra I.

2.4.4 Passive-Active Switching.

Against an unattended responsive jammer there may be some hope of inducing the jammer to shut off by shutting off the AI. By turning on the AI again range information might be obtained during the short period before the jammer again turns on. Such systems would require additional development and there is no intention of providing Astra I with this feature.

2.4.5 Power Measurements.

The equation $\frac{2P}{\dot{P}} = -\frac{R}{\dot{R}}$ where P = power received,

was discussed as a means of measuring a pseudo time-to-go. RCA had rejected the method believing it was excessively vulnerable to jammer antenna pattern variations and low-frequency a.m. CARDE's work on the subject was discussed and it was agreed the idea should be re-examined.

2.4.6 Ranging Manoeuvres.

RCA have considered ranging by a turn from a collision course to some non collision course, or vice versa, as described in Lamplight and CARDE TL N-47-12. The range equation is as follows:

$$R \doteq \frac{V_i}{\omega_1} (\text{Sin } L_1 - \text{Sin } L_c)$$

Where subscript $_1$ indicates the non collision course, $_c$ the

collision course, other symbols as before. The formula would be exact if the turn were instantaneous and is within 10% for representative turn rates and ranges. The practicality of the procedure depends critically on the amount of noise on ω_1 which can be square-wave filtered if oscillating manoeuvres are used.

2.5 Variable Polarization

RCA agreed that variable polarization is not intrinsically a good CCM since it is quite feasible to omni-polarize a jammer by polarization switching approximately every 100 usec or by installing multiple jamming antennas of different polarizations. However, it is necessary to distinguish between possible and probable jamming threats. No American jammer has yet been provided with omni-polarization.

There are other problems in the Astra I polarization system since it is not space stabilized, and break-lock may occur every time the aircraft is rolled. Also, it is believed by the Missile Electronics Section at CARDE that variable polarization may cause serious changes in the antenna beam pattern which could reverse the error slope of the conical scan pattern. This point will be further discussed with RCA shortly.

2.6 Decoy Radar

It has been suggested by AFHQ that the space and weight allocated to the Sparrow III CW injection systems could be utilized to provide a decoy or range-only pulsed radar of about 250 KW peak power operating at high X band frequencies. A very simple system could be installed with only a few months development time. However, the radar could be made somewhat more useful CCM-wise if more complexity and weight were added, and no decision has yet been taken as to whether it will be installed or what form it will take. It would be useful against spot and repeater jammers but ineffective against barrage or sequential spot jammers.

2.7 CCM Attack Course

A temporary decision has been made by ASL for the programming of a course to steer when jamming denies range. It will be a fixed lead angle course with four choices of lead angle, depending on whether target speed is greater or less than 1.2 Mach and altitude greater or less than 30000 ft. It was understood that Camden would incorporate the fixed lead anti-ECM course into Astra I.

An alternative suggestion considered by RCA was to achieve a collision course by nulling ω_{LOS}, measure the lead angle, L_c, then turn to a new fixed lead angle L_1 defined by the following relation:

$$\text{Sin } L_1 = \frac{4}{3} \left[\frac{V_i}{V_i + V_m} \right] \text{Sin } L_c$$

Where V_i = interceptor velocity

V_m = missile velocity increment

$\frac{4}{3}$ = an empirical factor.

This provides a more intelligent choice of fixed lead angle. However, once the fixed lead course is set up, target aspect angle will change and the lead angle chosen will no longer be correct. This argues for making the turn from collision to fixed lead comparatively late in the interception if GCI can supply rough range information.

Another CCM course discussed consisted of achieving a true collision course, then decelerating and reaccelerating in a controlled fashion so as to drop behind the true collision position by a distance equal to the missile's relative travel (F-pole). The fighter would then be on a correct lead collision course, and furthermore could triangulate range using the lead angles before and after the manoeuvre and the known deceleration distance as a base line. The procedure could be fairly accurately carried out using integrating accelerometers and the known acceleration characteristics of the fighter. However, it requires that the target fly a straight course.

2.8 Aural Presentation as a C.C.M.

RCA have proposed to furnish the navigator with an aural presentation of the radar signals. This idea was first investigated at MIT in 1954, in Project Buzzsaw, whose main purpose was the aural identification of propeller-driven aircraft. Dr. Elkind of ASL presented a tape recording which indicated the following:

(a) The sound of propeller aircraft was very similar to that of the same aircraft heard flying overhead. Propeller modulation was clearly readable but not very useful for identification.

(b) The Doppler from jet engine compressor intake and turbine blades could be faintly heard within 30° of the nose and tail regions, respectively, of a jet aircraft.

(c) When aircraft flew through ground clutter a Doppler beat between the aircraft and ground echoes was heard, together with propeller modulation, interspersed with periods of silence when presumably a strong ground echo drove the AGC to low gain.

(d) The dispensing of a chaff bundle was clearly marked by a Doppler whistle of rising tone *

(e) Aircraft flying through a chaff cloud caused a steady Doppler note.

---

* A velocity difference of 1 kt produces a 30 cps Doppler note at S band or a 90 cps note at X band, hence chaff detection is positive even on target beam.

(f) Most of the records were taken on an S band 10000 prf ground-based tracking radar (Porcupine); one was taken from an AI which was equal in quality.

(g) Attempts were made to aurally range track using an APG 33 but were not too successful. However, successful aural angle tracking was achieved by disabling the conical scan.

The recordings were made by passing the output of the boxcar detector through a 500-1000 cps bandpass filter to eliminate conical scan and pulse repetition frequencies.

Possible CCM uses of aural techniques include:

(a) Identification of jammers by aural "signature" - most jammers emit some low frequency hum.

(b) Detection of chaff drops or missile release.

(c) Possibly, tracking of aircraft through area sown chaff.

(d) Possibly, manual angle tracking of a scan inverter by searching for maximum conical scan hum. This would require better low frequency response than is provided by the audio amplifier and earphones presently planned for Arrow. RCA plan to do lab. tests of aural effects early in 1958.

3 COUNTERMEASURE THREATS

Discussion centered on chaff and repeater jammers of various types.

3.1 Chaff

Chaff is considered by RCA to be a growing threat since development of nylon and glass fibres for this purpose have increased the echoing area per pound by a factor of 10. Blossoming speeds will increase with target speeds. SAC now has dispensers capable of laying one-pound bundles at 8 per second. A chaff rocket has also been developed which weigh 25 lb. and lay a 600 ft. corridor composed of 5 chaff bursts at 120 ft. intervals. Area-sown chaff appears the worst threat; break-lock chaff can be countered at most target aspects by Astra's range rate and angular rate memory, video clipping and pulse edge tracking (but see section 2.1). It was agreed that Astra was not vulnerable to a single burst of gravity launched chaff since in the critical beam region the slow angle tracking response would prevent break-lock. However, dispensing rates of about 2 per second are sufficient to provide a continuous angular error signal and in such a case rate-aided angle tracking only delays break-lock.

RCA had made chaff analyses similar to those reported in DRTE/EL report R-5086-1 and their findings are in substantial agreement, indicating a break-lock area on the target's beam.

3.2 Range Gate Stealers

It was noted that Astra I uses prf jitter only during search, to clean up ground returns, and removes the jitter during tracking. Hence it is vulnerable to simple range gate stealers. Also it may well be impossible for the navigator to detect gate stealing before break-lock since the AGC will be controlled by the jamming pulse and the target echo will be depressed into the noise level. Gate stealing can be fully effective with imperceptible departures from true range rate.

A variable o-15 usec delay circuit has been developed by ATTC for S-band jammers which is applicable to X-band with some additional development. The circuit is shown in Figure 3.

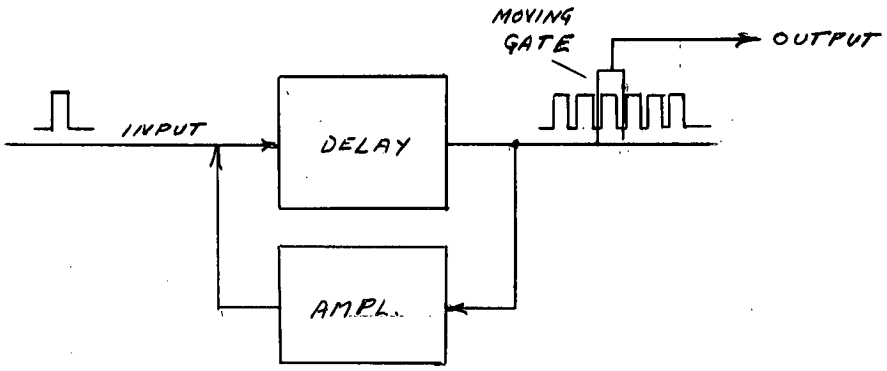

Figure 3 - Variable RF Delay.

The regenerative circuit delivers a train of closely spaced pulses. With each succeeding input pulse the gate selects the next successive output pulse as a response so as to produce a gradually increasing delay. The system is now designed with a delay between input and initial transponded pulse of .1 usec and a similar delay between this and succeeding pulses in the train. This type of delay circuit is not countered by prf jitter since it operates on each input pulse independently. The major design problem has been the build-up of noise in the regenerative circuit.

3.3 Angle Track Breakers

RCA estimates that a false conical scan modulation of 50% (presumably at normal echo signal level) existing for over one second is necessary to break Astra's angle tracking. The false modulation must be within "one or two" cps of the true scan frequency to pass the filter of the phase sensitive detector

and pull off the rate-aided tracking loop. There are several ways of introducing false conical scan modulation, such as the classical inverse gain repeater developed by Stanford University, spot or barrage jamming with low frequency amplitude modulation. These latter types retain their effectiveness in the confused multiple target-multiple fighter situation. However, their modulation efficiency is low. RCA estimated that a 2 w/mc barrage jammer having random a.m. from 50 to 70 cps could only produce 10% conical scan modulation in Astra since the a.m. power had to be spread over such a wide band. If one uses a single frequency of a.m. it must be swept very slowly - about 1 cycle per 20 seconds in order to remain in the conical scan bandwidth for a sufficient time. The optimum jammer lies between these two methods.

The spot jammer with wide band low frequency a.m. may be effective in breaking angle track. A study of jammer powers and modulation densities should be made to determine the relative effectiveness of these various types of angle track breakers. The unintelligent barrage jammer with wide band low frequency a.m. is certainly the enemy's best weapon in a multiple aircraft situation if adequate power is available.

The fact that Astra's conical scan frequency is fixed makes it possible for a barrage jammer to defeat all attacking Astra systems at once by tuning narrow band a.m. to their common conical scan frequency.

The tactical "fix" to angle track breaking is to leave the AI on search, so as to retain angle (and, for the pulsed scan inverter, range) information. The navigator must then become the fire-control computer. Project Sprint tests indicate that a navigator can do a satisfactory job of steering to a launch condition suitable for a guided missile.

4 OPERATIONAL ECM ANALYSIS

RCA are attempting to develop methods of determining Astra's probability of success in various ECM situations. This can be expressed as

$$P_{\text{success}} = \sum_{n} P_n \text{ not encountered} + P_n \text{ encountered} \times P_n \text{ countered}$$

where the right hand side involves probabilities of encountering and countering ECM situations of various types n.

4.1 Probability of Occurrence of ECM

RCA stated that most American authorities estimate a probability of 98% that some type of jamming will be encountered. RCA have used the following breakdown:

Countermeasure	Probability of Occurrence
Chaff	80%
Barrage	80%
Scan Inverters	60%

Scan inverters were rated lower because of the difficulty of operating them in multiple aircraft situations. No estimates were given for spot jammers, range gate stealers or decoys, but these would certainly have some non-zero probability. The method of using these probabilities was discussed, in view of the fact that they add up to more than 100%. If probability of occurrence is defined as the probability that one or more aircraft in a formation is using this type of countermeasure then the overlapping probabilities are valid. This is not the definition required in an analysis of a fighter's chance of success in an ECM environment. Any given target aircraft may carry both chaff and electronic jamming for a given radar band. However, within a single aircraft, the various types of electronic jamming are mutually exclusive. Thus although a single bomber may carry one equipment capable of spot and barrage jamming, it will operate in one or other of those modes at a given time. Similarly barrage and repeater jamming are mutually exclusive in operation. Hence the probabilities of a fighter encountering various types of X band electronic jamming from a single target must sum to 100%, with chaff and decoys as independent overlapping occurrences. However, it is still possible to encounter combinations of jamming types in a formation because the AI may simultaneously receive different types of jamming from different aircraft. This factor must be taken into account because the probability that the fighter will defeat a given combination of jamming signals depends strongly on the specific combination, and, to make matters worse, on the relative strengths of the individual jamming signals in the combination. This latter depends on the geometrical arrangement of the target and fighter formations and the AI antenna patterns. The only possible simplification is to determine a weighted average strength ratio for a given jamming combination, where the weighting accounts for the various relative ranges of the two (or more) jammers and their relative positions in the AI antenna pattern. Thus the P encounter model for a given rf band should be roughly as shown below:

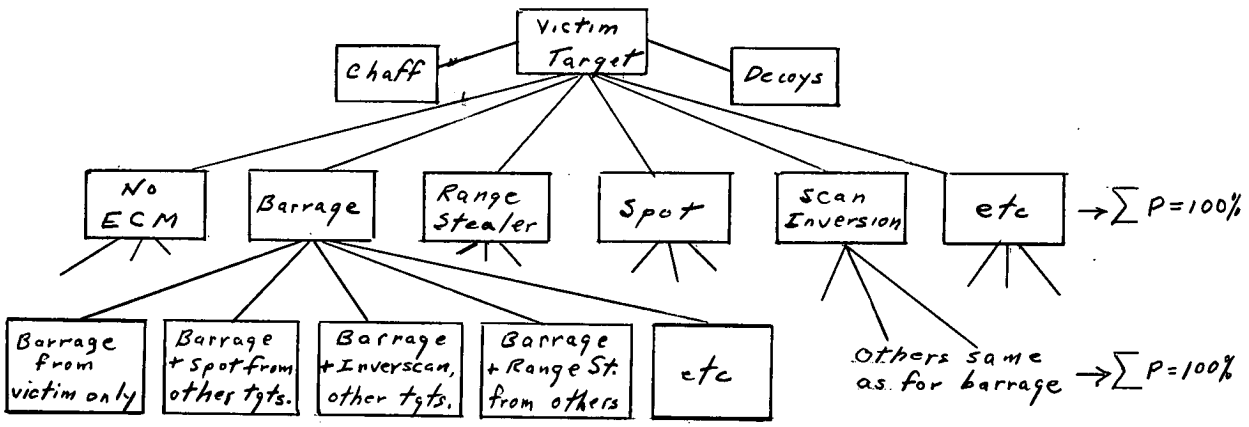

P ENCOUNTER MODEL

Once such a model is formed, a P counter must be determined for each square in the lowest row, and the series summed to give P success. The task is difficult but not impossible.

4.2 Probability of Countering Specific ECM

There was a brief discussion of RCA methods for determining P counter in specific jamming situations.

4.2.1 Chaff

For break-lock chaff, an angular zone near the target's beam was computed within which the AI broke lock. Attacks which entered this zone were counted as failures. The probability of an attack initiating at a given target aspect angle was obtained from previous GCI analyses of the marshalling point concept. It is CARDE's understanding that this curve, with its chaff gaps was then multiplied by the normal non-chaff placement probability, and integrated over all aspects to give P counter.

There seemed to be no allowance made for the fact that attacks initiated at a given aspect angle might terminate at a much different aspect because of GCI placement errors. CARDE's method appears preferable in this respect, but it does not allow for the probability distribution of initial aspects.

4.2.2 Barrage Jamming

RCA were primarily concerned with obtaining a useful crossover range against these jammers. An attack was considered successful if a lock-on crossover was achieved 2 seconds beyond the minimum missile launch range. The jammer was assumed to have fixed polarization, but this polarization could be right or left circular or plane polarized in any plane with equal likelihood. The AI navigator was allowed the best of the four polarization choices at his disposal. These assumptions led to probability contours of crossover range, with a probability of 1 at the crossover range for no polarization rejection and other contours at lower probability at increasing ranges. This set of contours was then superimposed on the non-ECM manoeuvre barriers to determine P counter. This is an approximation and is likely optimistic since the manoeuvre barriers are degraded when ECM homing modes have to be used and these homing modes sometimes result in angular chunks being cut out of the available launch zone.

RCA to date have not included ranging methods other than crossover in their P counter analysis.

5 RECOMMENDATIONS

It will be noted that not all the queries of Attachment "A" were answered during the visit, since on some topics - e.g. lab. tests of Astra vs jammers, RCA has no information as yet. On

certain topics further information or study is required:

5.1 The effect of AGC loop response on pulse edge-tracking should be further examined.

5.2 Tests should be made of passive angle-tracking noise and accuracy in simulated multiple aircraft situations.

5.3 A program for investigating aural CCM should be specified.

5.4 An analysis should be made of the angular errors producible by various jamming power densities with various types of low frequency a.m.

5.5 More information is required on the effect of variable polarization on antenna patterns.

5.6 The desirability and feasibility of providing Astra with varying conical scan frequency should be examined.

5.7 It appears feasible to develop realistic methods of assessing Astra's effectiveness against ECM but much further study is required in the formulation of ECM models.

Attachment "A"

Visit Request

SECRET

9736-21

5 Nov 57

Chief of Air Staff,
Air Force Headquarters,
Ottawa, Ont.

Attention: D.S.E.

CARDE Visit to RCA to Discuss ECM

1. CARDE is presently carrying out a fairly extensive operational study of the effectiveness of the Arrow - Astra I system in the presence of ECM. This has primarily been concerned with:

a) The simulation of various attack courses which utilize angular information only.

b) Determination of placement probability for these courses.

c) Determination of probability of launching the missile within its acceptable range and heading zone, using five different methods of passive ranging.

The study has presumed certain capabilities in the radar, fire control system and crew. It is proposed to check these by a series of flight trials using CF100s. A copy of the project proposal was transmitted to W/C Bernstein by Mr. Mitchell of CARDE Systems Group during his recent visit. The project is nick-named End Run. Jamming will be simulated within the fighter using circuits which interfere with the normal radar display. Breadboarded circuits have been tested successfully on the MG-2 which simulate the display of jamming during auto-search and during passive angle track or hand control.

2. In general CARDE wishes to gain both technical and operational information on the Astra I's reaction to and use in ECM which will permit realistic theoretical evaluation and ECM simulation. In

particular CARDE seeks answers to the following queries:

2.1 What jamming threats do RCA consider realistic during the operational life of the Arrow System?

2.2 What further work has been done on the study of detection of ECM and choice of ECCM by the navigator beyond that shown in progress report 3?

2.3 CARDE has devised ways of determining the probability of interception success against ECM and wishes to compare their methods with those in use at RCA.

2.4 What specific tactical measures (as opposed to technical) do RCA envisage as a counter to the ECM threat?

2.5 CARDE has done studies of the effectiveness of chaff against Astra I which indicate that it is not vulnerable to any of the normal chaff-dispensing techniques. However further information is required on effective time constants of the range and angle tracking circuits.

2.6 What are the technical characteristics of the AGC in Astra and how well is it expected to operate against various jammer noise distributions?

2.7 There are indications that an effective crossover against the scan inverter jammer can be achieved at about twice the range calculated by the normal crossover formula. CARDE wishes to discuss the effect of this jammer on Astra I. In particular we are interested in the effect of random amplitude modulation at or near the conical scan frequency.

2.8 CARDE wishes to simulate for flight trials the semi-passive ranging mode of Astra and more information is required on its technical characteristics.

2.9 One range finding technique which has received considerable attention at CARDE is the use of cyclic fighter manoeuvres about a collision course. The feasibility of the technique is wholly dependent on the amount of noise on the angular rate signals generated during passive angle track. What noise spectrum is expected during passive radar tracking? During IR tracking?

2.10 It is believed that RCA have developed a range computer which, given one value of range and range rate during an intercept, will continuously compute a reasonably accurate range and time to go. CARDE wishes to obtain details on the design and performance of this computer. There is some doubt at CARDE as to whether the required initial values will ever be available and we would like to discuss this from an operational standpoint.

2.11 The Guidance Group at CARDE has made an experimental study of the effects of various CM conditions on an MG-2 radar. CARDE would be willing to discuss the methods of proceeding and the results obtained in view of their application to the Astra system. The experiments consisted mostly of CW or swept-frequency jamming; conditions of receiver saturation were observed and some degradation in range and angle tracking ability was determined. Some experimentation with noise jamming was also made; however this was somewhat limited because of a shortage of equipment and manpower.

2.12 If time permits CARDE would like to discuss RCA's methods of determining navigation accuracy requirements in the non-ECM case. This work is analogous to our placement studies, but there appear to be some differences in our concepts of navigation accuracy and GCI vectoring error.

3. It will be noted that the questions are both technical and operational, and for this reason visits have been requested to both Waltham and Camden. Mr. F.W. Slingerland, CARDE Systems Group, and Mr. J.P. Regniere, CARDE Guidance Group propose to visit Waltham on Nov 19 and Camden on Nov 20.* Could W/C Bernstein be requested to inform the relevant R.C.A. personnel of our visit and queries.

(Dr. L.J.L'Heureux)
Acting Chief Superintendent
CARDE

* The Camden visit was cancelled and a Camden representative was sent to Waltham.

DISTRIBUTION

Recipient	Copy No.
Chief Supt. & D/Chief Supt.	1
A/Chief Superintendent	2
Superintendent "B" Wing	3
Superintendent "C" Wing	4
Superintendent "D" Wing	5
Superintendent "E" Wing	6
Superintendent "F" Wing	7
Superintendent "G" Wing	8
Document Library	9 - 23
Systems Group	24 - 26
Dr. G.V. Bull	27
Mr. C.J. Wilson	28
Dr. W.J. Surtees	29
Mr. D.P. Fleming	30
Mr. J.P. Regniere	31
DRB HQ: Ch. of Establish'ts	32
Ch. Scientist	33
DWR	34 - 35
D Eng R	36
D Phys R	37
DSIS for circulation	38 - 40
Director/N.A.E.	41
S/ORG	42
S/DRTE EL	43
S/DRTE RPL	44
DRM, London	45 - 46
DRM, Washington	47 - 48
DRB Liaison Officer Lincoln Lab MIT	49
RCAF, HQ: ATTN COR/DSE	50 - 51
ATTN S/L Peek	52 - 54
ATTN C ArmE	55 - 57
ATTN SACAS	58
ATTN TSO, RCA Camden, N.J.	59 - 60*
RCA Airborne Systems Lab., Waltham, Mass. Attn: Mr. Daelhousen	61 - 62*

---

*Copies 59-60 and 61-62 are to be addressed S/L Peek, DSE, for distribution to: - TSO, RCA, Camden, N.J.
- RCA Airborne Systems Lab., Waltham, Mass. Attn: Mr. Daelhousen

UNCLASSIFIED

#298448